APPLYING ACTIVITY-BASED PROTEIN PROFILING TO IDENTIFY POTENTIALLY DRUGGABLE SERINE HYDROLASE ENZYMES IN LEISHMANIA SPP

JAIME ARIEL ISERN

APPLYING ACTIVITY-BASED PROTEIN PROFILING TO IDENTIFY POTENTIALLY DRUGGABLE SERINE HYDROLASE ENZYMES IN LEISHMANIA SPP

A thesis submitted in partial fulfilment of the requirements for the degree of Doctor of Philosophy from Durham University

Jaime A. Isern

Supervised by Prof. Patrick G. Steel

Co-Supervised by Prof. Ehmke Pohl

Department of Chemistry

April 2022

Abstract

Leishmaniasis is a poverty related and one of the most important tropical diseases in the world with more than 12 million infected people, 0.9 to 1.6 million new cases each year, between 20000 and 30000 deaths per year, and 350 million people at risk of infection. Available drugs face problems with toxicity, administration and resistance which challenge their effectiveness. Consequently, the identification of new drug targets and the development of new treatments are imperative. Although serine hydrolases have been demonstrated to participate in crucial roles in the life cycle of the parasite and its virulence, these have not been yet characterized and the Leishmania serinome remains surprisingly neglected. This project attempts map and explore therapeutic targets within SHs present in the *Leishmania* proteome using an activity-based protein profiling (ABPP) strategy in the quest to find new protein drug targets for drug discovery. Initial experiments using commercial fluorophosphonate (FPs) probes revealed significant differences between the SH expression levels throughout their life cycles and between different *Leishmania spp*. As these probes are only effective for *in vitro* labelling, a suite of cell permeable probes has been synthesized and applied to study the Leishmania serinome in whole cells. Following proteome labelling and enrichment, the mass spectrometry-based tagging method, iTRAQ, led to the identification of two serine proteases: Carboxypeptidase LmxM.18.0450 and prolyl oligopeptidase (POP) LmxM.36.6750. Using a competitive ABPP approach, we were able to identify small molecule inhibitors for these enzymes which did showed activity against both *L. mexicana* promastigotes and axenic amastigotes. Collectively, these findings suggest that the serinome is a valuable source of new drug targets and that ABPP is a reliable approach for target discovery.

Acknowledgments

During this amazing journey that was my PhD, I had the privilege to get to know and share experiences with many great people. First, I would like to thank my supervisor Professor Patrick Steel for his continued guidance, patience, and support throughout the project. Second, I would like to thank the NTD Network for funding my research which without, I could not have fulfilled my dream of achieving a doctorate.

I would also like to thank those who had a direct impact to my thesis: My co-supervisor Professor Ehmke Pohl, Dr Exequiel O. J. Porta who I worked with in this project, for his unconditional support and friendship, Dr Angelo De Lira Machado, Dr Douglas Escrivani, Dr Kalesh Karunakaran. The PGS group who I shared great experiences with, in particular Dr Jonathan Reuven, Dr Vanessa Lyne, Dr Michaela Buerdsell and Victor Agostino.

Finally, I want to thank my friends and family, in particular my parents, grandparents, and brothers. Your infinite love and support made this dream come true.

Declaration

The work presented in this thesis was carried out in the Department of Chemistry at Durham University between October 2018 and March 2022. All work is the author's own except for collaborative which is acknowledged where appropriate. No part of this work has been submitted for any other degree at this, or any other University.

Statement of Copyright

Table of contents

List of abbreviations

AA	Amino acid
ABP	Activity-based probe
ABPP	Activity-based protein profiling
α-CT	α chymotrypsin
ADME	Absorption, distribution, metabolism, and excretion
AIBN	Azobisisobutyronitrile
Am.	Amastigote
AOMKs	Acyloxymethyketones
APS	Ammonium persulphate solution
ASPP	Active site peptide profiling
ATP	Adenosine triphosphate
ATR	Attenuated total reflection
B	Biotin
BME	2-mercaptoethanol
Boc_2O	Di-tert-butyl dicarbonate
CBr_4	Carbon tetrabromide
cc	Concentration
CCl_4	Carbontetrachloride
CDC	Centres for disease control and prevention
$CHBr_3$	Bromoform
CL	Cutaneous leishmaniasis
DALY	Disability-adjusted life year
DAST	Diethylaminosulfur trifluoride
DCC	*N,N´*-dicyclohexylcarbodiimide
DCM	Dichloromethane
DIPEA	*N,N*-diisopropyletyhylamine
DMAP	4-dimethylaminopyridine
DMF	Dimethylformamide
DMSO	Dimethylsulfoxide

DTT	Dithiotreitol
eD	Electron donating
EDC.HCl	N-(3-Dimethylaminopropyl)-N′-ethylcarbodiimide hydrochloride
EDTA	Ethylenediaminetetraacetic acid
eN	Electron neutral
ES^+	Electrospray
ESI	Electrospray injection
Et_2O	Diethyl ether
Et_3N	Triethyl amine
EtOAc	Ethyl acetate
EtOH	Ethanol
eW	Electron withdrawing
FDA	U.S. Food and drug administration
FP	Fluorophosphonate
GSK	GlaxoSmithKline
Hex	Hexane
HRMS	High resolution mass spectrometry
IC_{50}	Half maximal inhibitory concentration
IR	Infra-red
iTRAQ	Isobaric tag for relative and absolute quantification
KOAc	Potassium acetate
LCMS	Liquid chromatography mass spectrometry
m/z	Mass to charge ratio
MALDI	Matrix-Assisted Laser Desorption/Ionization
mCPBA	meta-chloroperoxybenzoic acid
MeOH	Methanol
MS	Mass spectrometry
MudPIT	Multidimensional protein identification technology
MW	Molecular weight
N.R.	No Reaction

NaAsc	Sodium ascorbate
NADP	Nicotinamide adenine dinucleotide phosphate
NBD	4-Chloro-7-nitrobenzofurazan
NBS	N-bromosuccinimide
NMR	Nuclear magnetic resonance
NTD	Neglected tropical disease
$P(OEt)_3$	Triethyl phosphite
PAGE	Polyacrylamide gel electrophoresis
PBS	Phosphate buffer saline
$Pd(OAc)_2$	Palladium Acetate
$Pd(PPh_3)_4$	Tetrakis palladium
PDB	Protein data bank
PEG	Polyethylene glycol
POP	Prolyl oligopeptidase
PPh_3	Triphenylphosphine
Prom.	promastigote
RFU	Relative fluorescence units
Rh	Rhodamine
rt	Room Temperature
SA-PMPs	Promega Streptavidin MagneSphere Paramagnetic Particles
SAR	Structure-activity relationship
SDS	sodium dodecyl sulphate
SH	Serine hydrolase
SILAC	Stable isotope labelling by/with amino acids in cell culture
S_N1	Unimolecular nucleophilic substitution
S_N2	Bimolecular nucleophilic substitution
S_NAr	Aromatic nucleophilic substitution
SPhos	2-Dicyclohexylphosphino-2',6'-dimethoxybiphenyl
spp	species
st	Stationary

TBAI	Tetrabutylammonium iodide
TBTA	Tris((1-benzyl-4-triazolyl)methyl)amine
TCEP	tris(2-carboxyethyl)phosphine
TEAB	Triethylammonium bicarbonate
Tf	Triflate
THF	Tetrahydrofuran
TLC	Thin-layer chromatography
TOF	Time of flight
VL	Visceral leishmaniasis
ZPP	Z-ProProlinal

1. INTRODUCTION

1.1 Project Introduction

Leishmaniasis, a poverty related disease, is one of the seven most important tropical diseases in the world with more than 12 million infected people, with 0.9-1.6 million new cases each year. 350 million people are currently at risk of infection, making it a major public health issue and if left untreated, it can lead up to 30000 deaths per year. Although some treatments are available, these are limited and problems with toxicity, administration, resistance as well as other factors such as climate change and forced migrations challenge their effectiveness. Consequently, the identification of new drug targets and the development of new treatments are imperative. This project will focus on the quest to find new protein drug targets for drug discovery in *Leishmania* using the technique of activity based proteomic profiling (ABPP). In particular, it will focus on enzymes containing serine in their active sites as targets.

Chapter 1 will provide the background to the project; the general aspects of leishmaniasis and the different strategies for target identification and drug discovery with the available tools for this purpose. Subsequently, the specific technique for target identification, ABPP, will be reviewed. An introduction to enzymes with serine as a catalytically active residue present in biological systems, and more specifically serine hydrolases and their relevance in *Leishmania* will then be presented before the chapter concludes with the project hypothesis. Chapter 2 will present the in-gel labelling of serine hydrolase profiles obtained in different *Leishmania spp* throughout their different life stages using commercially available activity-based probes as well as gel free target discovery proteomics. Chapter 3 will discuss the synthesis of novel activity-based probes and the biological assays conducted with these. Finally, overall

conclusions and future work needed will be discussed in Chapter 4, whilst Chapter 5 will provide the detailed experimental methodologies used.

1.2 Leishmaniasis

Leishmaniasis is a vector borne parasitic disease transmitted by about 30 species of phlebotomine sandflies and caused by about 22 morphologically indistinguishable species of obligate intracellular protozoa of the genus *Leishmania* (Figure 1.1).[1–3] This disease is relevant in humans and other mammals such as dogs or wild rabbits,[4–8] and presents a variety of clinical manifestations that range between self-curing cutaneous lesions to life-threatening visceral disease, according to the species of *Leishmania*.[9,10]

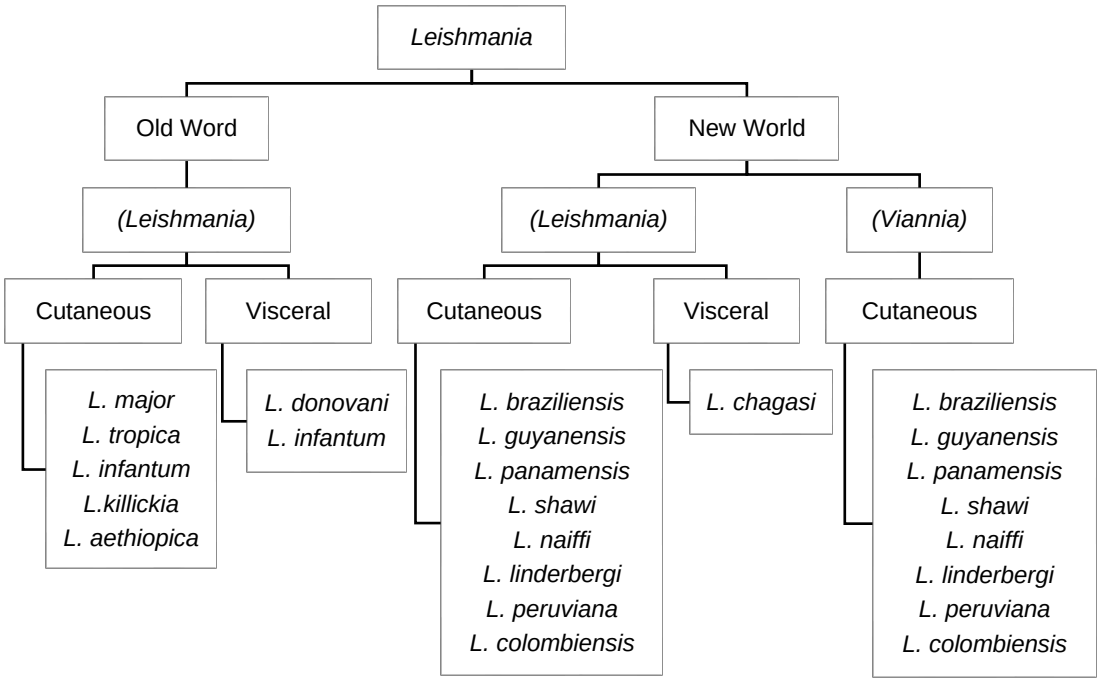

Figure 1.1 The *genus Leishmania* and its species.[1,4,9,11]

The most common is cutaneous leishmaniasis (CL). The parasites responsible for CL are normally divided in two major groups: old world species and new world species (Figure 1.1). CL can go from self-healing ulcers to scarring, disfigurement and ultimately more serious manifestations such as diffuse cutaneous leishmaniasis (DCL) and disseminated cutaneous leishmaniasis (DL), where non ulcerative lesions are distributed around the body, or the rarest form, mucocutaneous leishmaniasis (MCL), produced by *Viannia* subgenus strain, which produces a highly disfiguring and potentially life-threatening condition as result of late-stage destruction of oronasopharyngeal mucosa and cartilage.[1,4,9,11]

On the other hand, the most severe form is called visceral leishmaniasis (VL) which if untreated, can progress to death in 90% of the cases.[12] It compromises the mononuclear phagocytic system, normally involving the spleen, liver, lymph nodes and bone marrow. [13] Furthermore, after recovering from VL, up to 20% of the patients can develop post kala-azar dermal leishmaniasis (PKDL). These infected patients serve as a parasite reservoir, playing an important role in the transmission of the disease and impede its eradication.[14]

In addition to the physical manifestations, mental illnesses, psychosocial morbidity including depression, anxiety, and social stigma have been associated with all types of leishmaniasis leading to reduced quality of life (QoL).[15]

1.2.1 Epidemiology

Present in about 90 countries, and endemic to Asia, Africa, America and Europe,[4,5] the latest figures show that the number of infected people globally exceeds 12 million, with 0.9 to 1.6 million new cases each year, and between 20000 and 30000 deaths

yearly,[12] causing a loss of an estimated 981000 disability-adjusted life years (DALYs).[16] In 2017, 94% of new cases reported were concentrated in only seven countries: Brazil, Ethiopia, India, Kenya, Somalia, South Sudan and Sudan.[17] With this epidemiological importance, coupled to the lack of effective measures to counter this situation has led the World Health Organization (WHO) to declare this disease as neglected by both public and private organizations.[4,5,17,18] Furthermore, several factors of different natures such as drug resistance and immunosuppression by HIV, or the increasing levels of travel to endemic areas, forced migrations or wars, in addition to global warming and the progressive destruction of the vectors' natural habitats contribute to the spread of leishmaniasis and the adaptation of vectors to urban and semi-urban environments, making more people at risk of infection.[4,5,19]

The WHO estimates there are between 0.6 and 1M new cases of CL worldwide (Figure 1.2). This number has increased considerably due to forced migration, leading to cases being reported in non-endemic areas.[9,20,21] Most cutaneous leishmaniasis cases are in the Americas, the Mediterranean basin, the Middle East, and Central Asia. In 2020, over 85% of new cases occurred in 10 countries: Afghanistan, Algeria, Brazil, Colombia, Iraq, Libya, Pakistan, Peru, the Syrian Arab Republic, and Tunisia, whilst more than 90% of mucocutaneous leishmaniasis cases occur in Bolivia, Brazil Ethiopia, and Peru.[10]

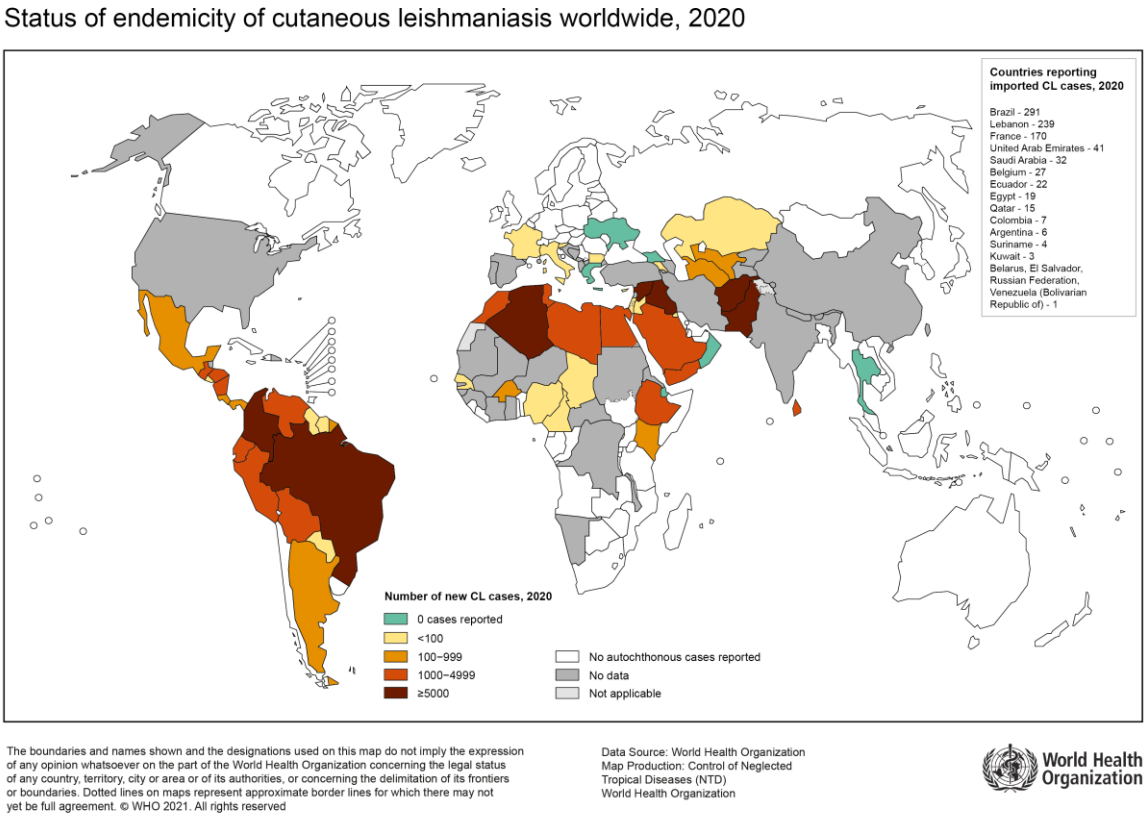

Figure 1.2. Status of endemicity of cutaneous leishmaniasis worldwide, 2016.[17]

On the other hand, although VL is endemic in 60 countries, in 2017, more than 95% of the new cases were concentrated in 10 countries (Bangladesh, Brazil, China, Ethiopia, India, Kenya, Nepal, Somalia, South Sudan and Sudan).[10] Efforts made in several countries such as India, Nepal and Bangladesh have resulted in a 75% decrease of the global incidence. Despite this, countries from east Africa and South America have not seen any improvements in treatment (Figure 1.3).

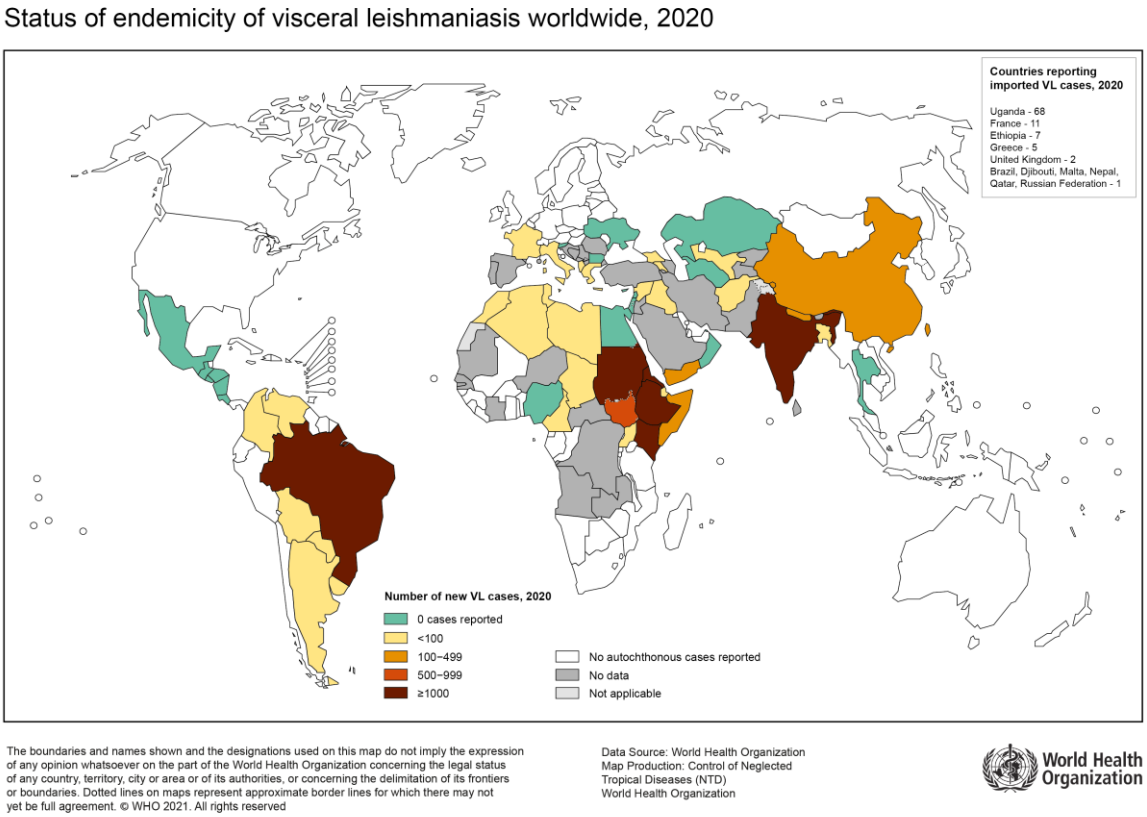

Figure 1.3. Status of endemicity of visceral leishmaniasis worldwide, 2020.[10]

1.2.2 Life cycle

As depicted in Figure 1.4, *Leishmania* has a “digenetic” life cycle. The bite of an infected female phlebotomine sand fly leads to parasite transmission to the mammal host. During a blood meal, it deposits infectious metacyclic promastigotes from their proboscis by regurgitation (**1**). Once inside the human body, the promastigotes are phagocytized by macrophages and other mononuclear phagocytic cells (**2**). Inside these cells, they establish in compartments known as *Leishmania* parasitophorous vacuoles (LPVs) to protect themselves from degradation.[22] Inside the LPVs, they transform into amastigotes (**3**) and multiply by simple division until the membrane ruptures releasing the amastigotes and allowing them to infect more mononuclear

phagocytic cells (**4**). Different factors such as the host immunological response and the parasite species, will determine the nature of the disease. Sand flies get infected by feeding on infected cells during a second blood meal (**5**, **6**). The amastigotes ingested then transform into procyclic promastigotes which develop in the gut (**7**), multiply, and then migrate to the proboscis (**8**) as metacyclic promastigotes to continue the life-cycle.[23]

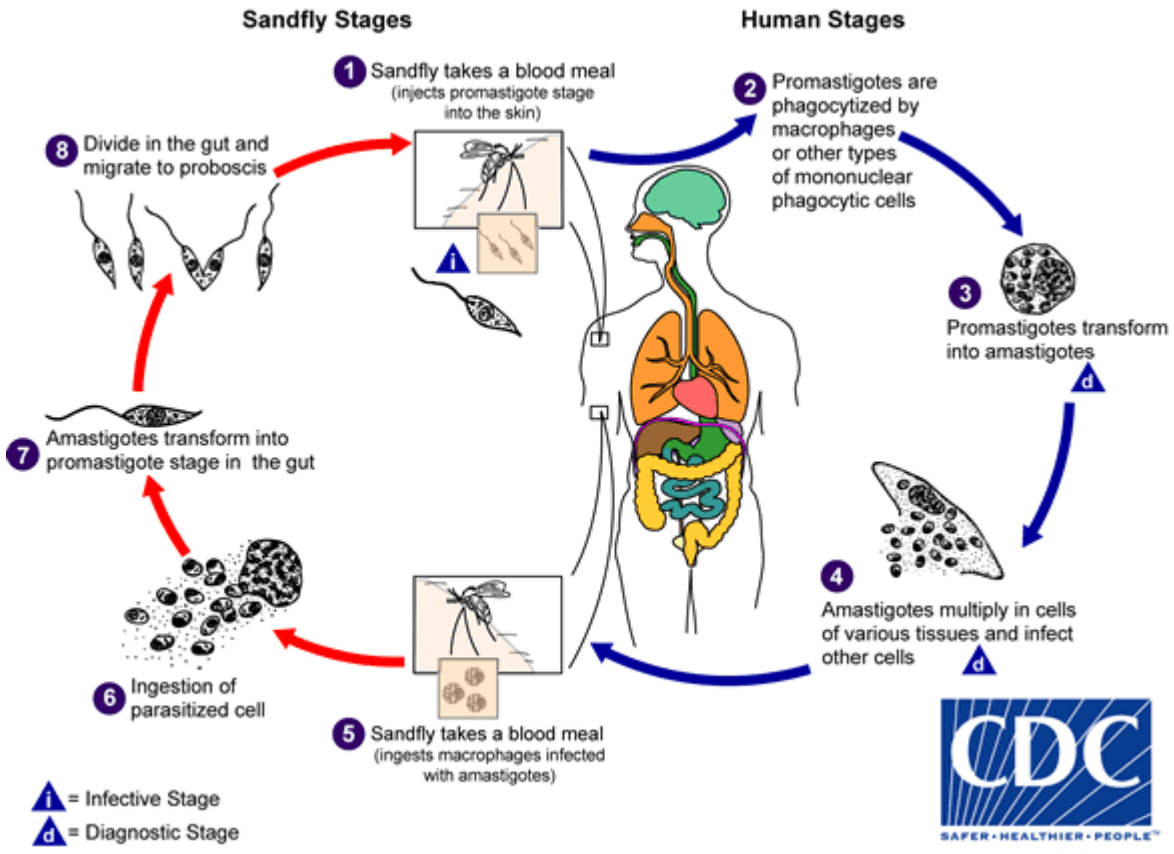

Figure 1.4. Life cycle of leishmaniasis.[23]

1.2.3 Available therapies

Although after recovering from leishmaniasis most people become immune to further infection, providing a good rationale for vaccine development research, no vaccine is yet available.[9,24,25] Instead, since the 1920s, chemotherapy has been the main treatment for the different clinical manifestations of leishmaniasis. In contrast with other NTDs (e.g., praziquantel in schistosomiasis and ivermectin for lymphatic filariasis), mass drug administration for prevention is not possible due to the zoonotic nature of the disease, the toxicity of the available drugs or parenteral administration.[26,27]

Pentavalent antimonial monotherapy, such as sodium stibogluconate and meglumine antimoniate (Figure 1.5) have been the main treatments available for VL and CL for several decades. This is despite their narrow therapeutic windows, administration complexity and toxicity with side effects such as local irritation, anorexia, nausea, vomiting, myalgia, arthralgia, increases in hepatic enzymes, urea, and electrocardiographic alterations.[4] In addition, drug resistance and general treatment failure have been observed with antimonials.[4,9,25] Although its mechanism is still unknown, an accepted theory is that they induce apoptosis by increasing the cell susceptibility to oxidative stress.[28] The combination of intralesional pentavalent antimonial compounds with cryotherapy has been used as treatment with cure rates up to 91%. Despite this effectiveness, this is not widely available in endemic areas, where the monotherapy treatment still prevails. In addition, long and painful treatment schemes are required.[9,29–31]

Pentamidine (**3**) (Figure 1.5), has also been used to treat CL in South America, but the extended treatment times, and narrow timelines are causative of high failure rates,[32] making it not a good option as a first therapy option.

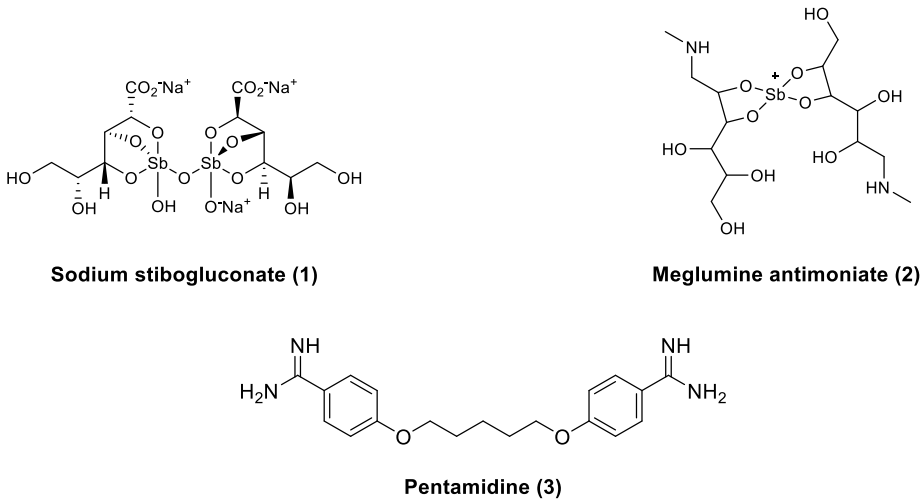

Figure 1.5. Current pentavalent antimonials and pentamidine used to treat CL.

In the case of VL, pentavalent antimonial drugs are still used in many regions, but due to their increasing ineffectiveness, other drugs are used instead.

Different formulations of Liposomal Amphotericin B (**4**) have been used to treat VL. It is thought to induce cell death by increasing the permeability of the cell membranes.[33,34] It possesses a high cure rate (more than 90%), but it has important and potentially lethal side effects. In addition, the high cost, parenteral administration, and drug resistance cases observed in *L. donovan*i clinical isolates also remain as issues.[25,26]

Miltefosine (**5**) is the only oral drug available to treat VL. Its mechanism of action is not well understood, but it is known that it inhibits phosphatidylcholine, and affects the mitochondrion.[35] Although the administration type is more convenient and its side

effects milder, after 10 years, the efficacy of miltefosine has dropped considerably.[25,26,36,37]

Paromomycin (**6**) is a broad-spectrum antibiotic, also used to treat parasitic diseases that has been used to treat both VL (intramuscular injection) and CL (ointment). This drug works by inhibiting translation on ribosomes. Advantages like good efficacy, low cost and shorter treatment make this drug a good alternative.[38] However, its parenteral treatment is long and painful, and it has hepatic toxicities and ototoxicities as side effects.[39]

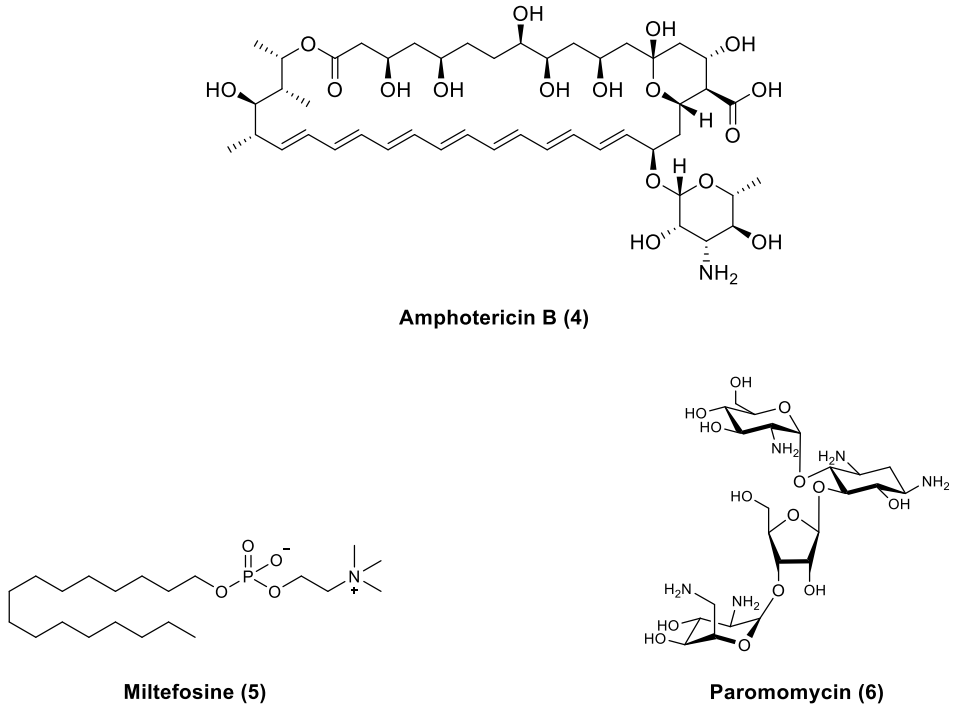

Figure 1.6. Drugs used to treat VL.

As discussed above, the current antileishmanial drugs and treatments available for both CL and VL are no longer attractive and safe options to treat these diseases, due to their high toxicity, difficult parenteral administration, and emergence of resistance.

In consequence, the development of new, better, and friendlier drugs with known modes of action is of great necessity to overcome the current challenges. The next section presents the basic concepts of the early stages in the drug discovery pathway.

1.3 Strategies for target identification and validation

1.3.1 Introduction

The process of drug discovery in which new targets and drugs are discovered and optimized to treat disease is a linear pathway that involves four main steps: first, an early stage that involves the identification of a target, the search for a lead compound and the validation of this target. The optimization of the lead compound in terms of activity and selectivity defines the second stage. Subsequently, the pre-clinical development stage comprises *in vivo* studies such as pharmacokinetics and pharmacodynamics and toxicological studies, following the final stage, which is the clinical trials in humans (Figure 1.7).

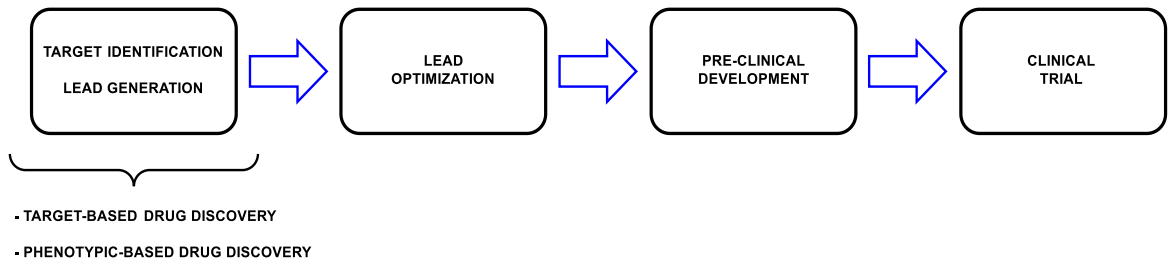

Figure 1.7. Stages of the drug discovery process.

The early stage of the drug discovery pathway can normally be considered to follow one of two approaches (Figure 1.8): phenotypic-based or target-based drug discovery.

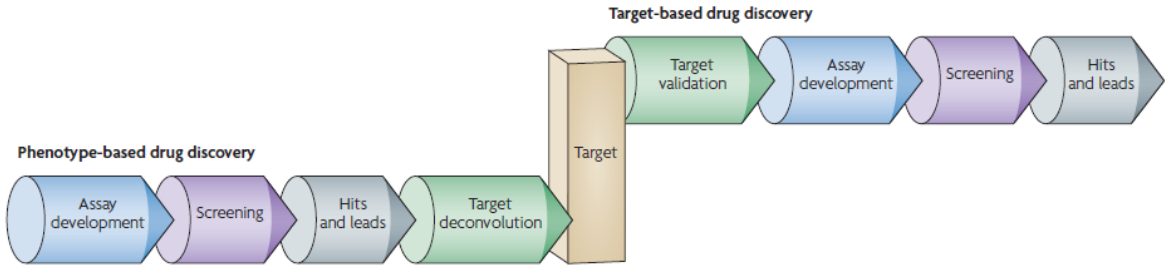

Figure 1.8. Phenotype-based versus target-based drug discovery. In the first approach, lead molecules are identified first, followed by target deconvolution to identify the molecular targets involved in the pharmacological response. In contrast, target-based strategy starts with the identification and validation of a specific target before the search for lead compounds.[40]

1.3.2 Phenotype-based drug discovery

This strategy begins with an assay in which the exposure of a candidate molecule to a whole organism exerts the desired effect, based on an observable change in phenotype. The compound can then be optimized for efficiency to produce the desired outcome. Subsequently, the target is identified retrospectively.[41] A classic example of this pathway is the discovery of the β-lactam antibiotics such as penicillin, which were discovered and optimized without knowing *a priori* the molecular targets. Instead, optimization was led by bactericidal and bacteriostatic effects. Subsequently the target was identified as a transpeptidase enzyme crucial for the proper formation of the cell wall.

1.3.3 Target-Based drug discovery

The target-based drug discovery process starts with the identification and selection of a specific protein target. The next step is verifying that the target selected is vital for

the disease and its modulation is beneficial for the disease treatment, a step known as target validation. Subsequently assays are developed to enable the screening of chemical libraries of small molecules to identify compounds showing high affinity interaction with the selected target. Once suitable hits have been found, optimization of the hit compounds leads to progression along the drug discovery pathway. As an example, the discovery of the reverse transcriptase enzyme of HIV and its function led to the development of many effective antiretroviral drugs such as azidothymidine (AZT), used to treat AIDS.[41,42]

1.3.4 Target based vs. phenotypic based drug discovery

Whereas phenotype-based drug discovery used to be the main strategy used, advances in genomics and proteomics have made target-based screening the favoured approach for the pharmaceutical industry. From 1999 and 2013, 70% of the 113 first-in-drugs approved by the FDA were identified using this strategy. The major advantage of the target-based approach is that knowing the mechanism of action accelerates research, due to easier and faster optimization. Additionally, it is less expensive than a phenotypic approach when generating a drug with suitable physicochemical properties. For example, a well-defined target structure allows efficient structure-activity relationship (SAR) studies. The more the understanding and knowledge of a disease, the greater the benefits of a target-based approach.

However, target-based approaches could lead to the design of compounds that having been engineered in simplified cell-based assays can fail or have different behaviours in more complex environments like a living organism. Also, a challenge in a target-based approach relies on the fact that despite the target being known and its

mechanism described, a specific compound could be acting on more than one target. This can create confusion about the real target and mode of action of the drug, sometimes making the validation process more complex.[42]

In contrast, a phenotypic drug discovery process directly reports on the effectiveness of a compound in a relevant cellular environment instead of a purified target providing immediate evidence of the ability to deliver the desired effect. Also, phenotypic assays can pick up the intricacy of biological systems exploiting synergistic effects. Moreover, the deconvolution phase can lead to the identification of new targets and mechanisms, potentially providing an understanding of complex modes of action. On the other hand, the optimization of compounds without knowledge of the target presents potential difficulties for cell-based phenotypic screens.[41,42]

In summary, how do we decide which drug discovery strategy is best? In general, depending on the previous knowledge of a disease, in some cases a drug target is so clearly validated that the advantages of a target-based approach are compelling. In other cases, when the targets are not clear an approach using phenotypic assays could be beneficial. Ultimately, each specific drug discovery challenge requires its own unique solution, using the best of both approaches whenever possible.[42]

In the particular case of *Leishmania spp*, high-throughput screening assays conducted by Peña *et al*.[43] revealed only 351 hits when using the GSK set of 1.8 million compounds. This corresponds to a mere 0.0195% of the set, suggesting that a phenotypic approach might not be the best option and a target-based drug discovery path should be encouraged.

1.4 Activity Based Protein Profiling (ABPP)

1.4.1 Introduction

In all drug discovery programmes a major challenge is to identify and validate the molecular target by demonstrating a functional role in the disease phenotype.[44] Even though genomic information can provide some ideas about a protein function[45–47] and techniques such as genetic knockout and overexpression have been very useful, most proteins are regulated by post-translational events that cannot be predicted in the gene expression signature.[45,48] The same problem is observed with available proteomic methods such as LCMS,[45,49,50] yeast two-hybrid methods (Y2H)[45,51] and protein microarrays,[45,52] which fail to address protein activities in their native state.

As the role of a protein is determined by its activity rather than its expression level, methods to address this activity of natively expressed protein families amongst a background of high biological complexity have been developed. One of these techniques, named activity-based protein profiling (ABPP), has become a common and strong tool for the functional characterization and identification of proteins in native and complex proteomes.[45,53–57] The keystone, is the design of active-site directed small molecule probes capable of covalent protein modification. These activity-based probes (ABPs) target proteins with similar catalytic features. After this covalent modification, a reporter group present in the probe is used for visualization and/or separation of the probe-protein system, making the fractionation of a proteome based on catalytic activity the main purpose of the technique (Figure 1.9 A).

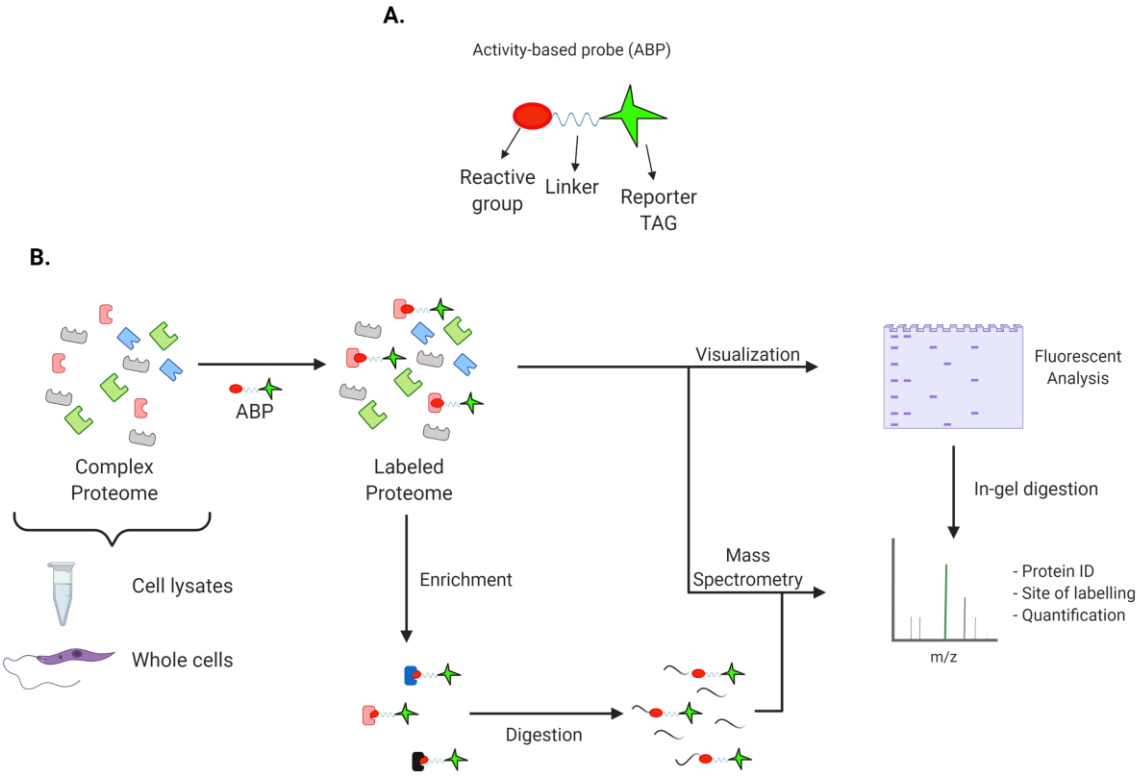

Figure 1.9. General aspects of ABPP process: After designing and synthesizing the probes (**A**), they react with the proteome. Subsequently, gel-based and mass spectrometry-based analyses can be used to visualize, identify, and quantify the labelled enzymes. The former is used to visualize the complex using fluorescent TAGs while the latter uses avidin enrichment and protease digestion followed by Multidimensional Protein Identification Technology techniques for Identification and quantification purposes (**B**).[58]

1.4.2 Principles of ABPP

The ABP, which consists of a binding group, also called a warhead, a linker, and a reporter group, is incubated with the crude cell, tissue, or other sample of interest. The warhead interacts specifically with the enzyme active site, and bonds covalently with it. After the proteome has been labelled, it can be analysed using several techniques such as in-gel visualization or mass spectrometry identification (Figure 1.9 B).

Importantly, as the proteins are identified using a small molecule binding interaction, the targets addressed by this technique are potentially druggable, a prerequisite for further medicinal considerations.[45]

1.4.3 Probe and Tag design

The crucial part of any ABPP experiment is the correct design of specific probes.[45]The warhead is the reactive part that binds covalently to the protein, modifying enzymatic active sites in the proteome (Figure 1.10 A). This moiety ideally exhibits reactivity that results in a small subset of proteins being labelled.[45,59–61] Different warheads have been used to design ABPs. Some of these warheads' present high selectivity towards the hydroxy nucleophile group present in serine enzymes, like sulfonyl fluorides derivatives,[62] or contain electrophilic fluorophosphonates, as used by Liu *et al.*[63] to label, identify and characterize serine hydrolases present in rat tissue using probes **7** and **8** (Figure 1.10 A). Additionally, variations of fluorophosphonates with biotin and different linkers were used to label serine enzymes present both in soluble and membrane proteomes. This allowed and accelerated the characterization and identification of active site serine enzymes.[64] Other reactive residues such as threonine, cysteine and lysine can be addressed too. For example, β-sultams derivatives are used to bind threonine enzymes[65] while acyloxymethyketones (AOMKs) such as probe **9** have demonstrated notable reactivity and selectivity towards cysteine proteases[66] (Figure 1.10 B) and ABPs based on ATP (**10**) are used to target the conserved lysine that protein kinases possess (Figure 1.9 C).[45]

A.

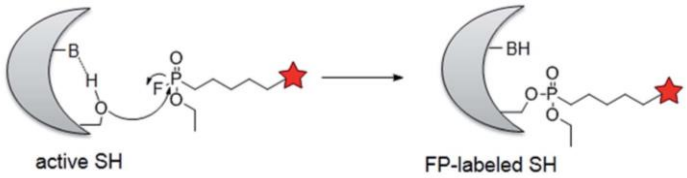

Tipical fluorophosphonate probes

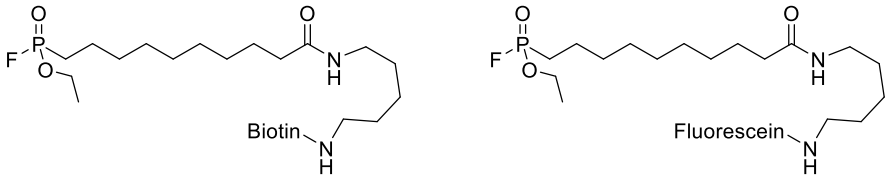

7 **8**

B. **C.**

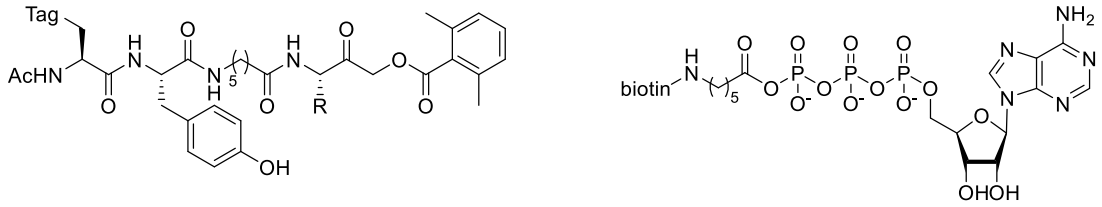

9 **10**

Figure 1.10. A) Covalent interaction between an active-site serine hydrolase and a fluorophosphonate ABP and common structures of biotinylated (**7**) and fluorescent (**8**) fluorophosphonate ABPs.[58,62] **B)** Acyloxymethyl ketone probe **9**.[66] **C)** ATP based kinase probe **10**.[45]

One challenge with the highly reactive residues can be a lack of selectivity. This can be solved by the addition of a binding group. This group, which displays particular characteristics in terms of size and hydrophobicity, is part of the warhead, and guides the probe with noncovalent interactions to specific enzymatic active sites.

The second part of the probe, the tag, is used to visualize and/or separate the ABP-enzyme complex from the proteome. Normally, fluorophore groups such as NBD or different types of rhodamines are used to visualize the probe while biotin is commonly

used to purify the complex from a whole protein extract. Sometimes multi-functional reporters are used combining a visualization moiety, biotin, and cleavable groups for purification purposes.

As the tags often present charged groups and/or large sizes, they may interfere with the warhead-active site interaction and/or its cell permeability. To cope with this challenge a linker, is commonly used to put “distance” between the warhead and tag so they do not interfere with the ABP-probe interaction. For this, chains with different chemical moieties and lengths such as aliphatic and polyether chains, are normally used. To avoid affecting the cell permeability, the use of benign groups such as an alkyne or azide has been used to bind with the tag by simple and effective bioorthogonal reactions such as click chemistry[45,67–69] or Staudinger ligation.[45,70,71] This allows separating the tag from the probe, minimizing possible interferences (Figure 1.11).

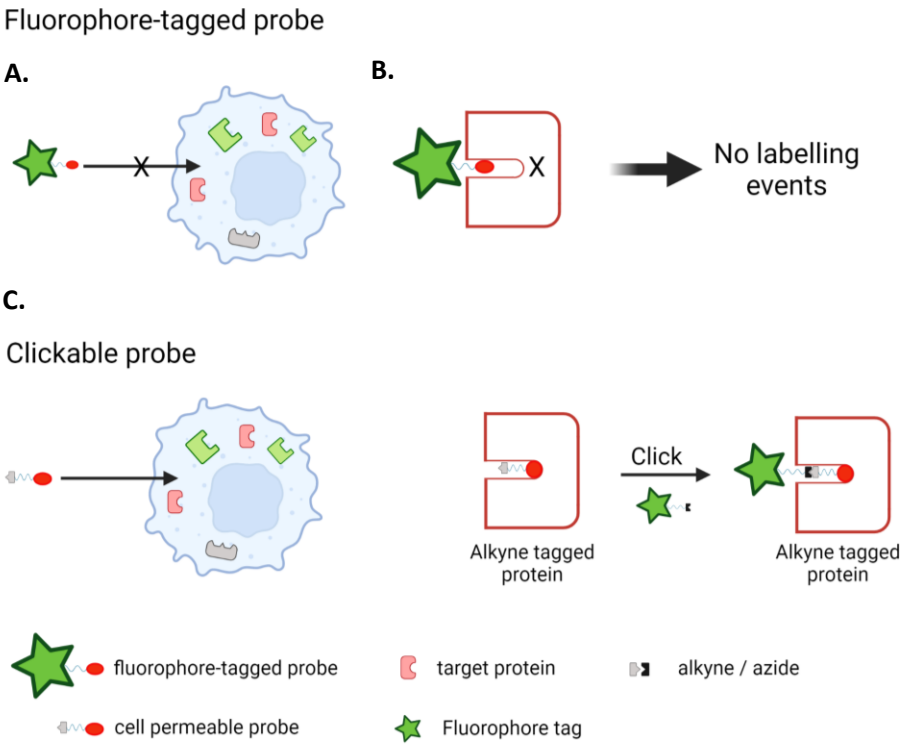

Figure 1.11. Advantages of applying click chemistry to ABPP. Non labelling outcomes are observed if **A**) Pre-tagged probe is not cell permeable or **B**) The size of the tag inhibits engagement with the target site. **C**) A probe with an alkyne handle is cell permeable and can engage target. Subsequent click reaction leads to the labelled proteins.[45]

Additionally, the linker is often used to provide the probe with the proper physicochemical properties needed to interact in a biological environment such as enough permeability to move through membranes and hydrophobicity.

ABPP probes fall within two broad categories: directed and nondirected.[45,56] Directed probes, which are designed to target a mechanistically related family of enzymes, require some insight about the mechanism, structure or ligand preferences of the enzyme.[45,54] Two approaches can be used in this category; one is using mechanism-based inhibitors as reactive groups with a high preference over specific enzyme

classes.[45,56] As examples for directed probes, fluorophosphonates (**6** and **7**, Figure 1.10 A) and acyloxymethyl ketones probes have been designed as mechanism-based probes targeting serine and cysteine enzymes, respectively (**10**, Figure 1.10 C), [45,56] or phenyl vinyl sulfonates and sulfones, which interact with the family of protein tyrosine phosphatases.[72] The other option is incorporating specific high-affinity binding groups specific to shared enzymatic features, although in this case, knowledge of the mechanism is needed.

In contrast, nondirected probes consist of molecules that contain a mild electrophile, such as sulfonate esters or Michael acceptors, or a photoreactive group such as benzophenone, with non-specific interactions capable of interacting with many enzyme classes. They also possess a binding group responsible for target selection. The advantage of these probes is that enzymes that lack affinity labels can be addressed.[45] As no previous knowledge is required of the enzyme structure or active site, these probes are useful for extending ABPP to less well-characterized enzymes.[45,73] Examples of these probes are alkyl/aryl sulfonate ester warheads **11** and **12** which have been shown to bind several mechanistically different enzyme classes such as epoxide hydrolases, thiolases, NAD/NADP dependent oxidoreductases and aldehyde dehydrogenases (Figure 1.12).

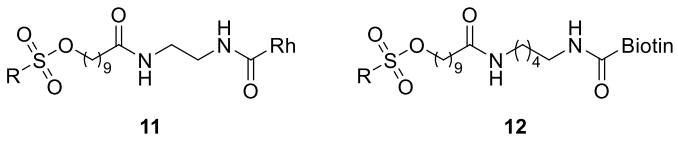

11 **12**

Figure 1.12. Non-directed sulfonate esters probes.

1.4.4 Analytical Tools for ABPP

The other part of the ABPP process involves the identification of the ABP-labelled protein from a complex proteomic mixture. To achieve this, several analytical tools are available. Each of them presents advantages and disadvantages in relation to sensitivity, target identification and amount of sample needed, that need to be accounted for at the time of deciding which method to use. Some of the most common methods are discussed below.[45]

1.4.5 Gel-Based Platforms

This method is the most standard and highly developed technique used in ABPP since it is simple, fast, robust, and amenable to high-throughput analysis of many proteomes a day.[45] The basis of the method is applying a proteome to an SDS polyacrylamide gel and resolving it by one or two dimensional electrophoresis. Readout can be by either in-gel fluorescence scanning or avidin blotting, for fluorescent and biotinylated ABPP probes, respectively. To reveal the identity of the labelled enzymes, the bands observed in the gel are cut, digested with trypsin, and analysed by tandem mass spectroscopy (MS/MS). To reduce background levels of non-target proteins, biotin-(strept)avidin enrichment is often needed before applying the labelled proteomes to the gel. The major challenges with the technique are its low resolution, meaning the capability to separate enzymes with similar molecular weight, and sensitivity, of around 10 pmol/mg proteome, which is higher than the natural abundance of many target enzymes.[45,74,75]

Finally, as mono-dimensional PAGE separates according to molecular weight and the fact that homologous proteins sometimes have similar masses, enzymes of the same

family interacting with an ABP could co-migrate on the gel, affecting the subsequent MS analysis, problem that can be partially solved by doing 2D-PAGE analysis.

Despite there being evident disadvantages of gel-based platforms, their advantages are significant enough to make this tool very useful and commonly employed.[45,74,75]

1.4.6 LC-MS-Based Platforms

1.4.6.1 Multidimensional Protein Identification Technology (MudPIT)

Several LC-MS strategies have been developed to improve the poor resolution of gel-based platforms and the identification of labelled proteomes. The simplest of these strategies is known as multidimensional protein identification technology (MudPIT)-ABPP.[45,49,76] Here, biotinylated ABPs are used to label proteomes which are then incubated with (strept)avidin beads and the supernatant filtered off. Subsequently, the enriched proteome is digested, and the resulting peptides are analysed by multidimensional LC-MS/MS (Figure 1.13). The identification of the proteins is achieved by an algorithm that analyses the data obtained from the fragments to reconstruct the sequence of each enzyme and compares it with a data base.

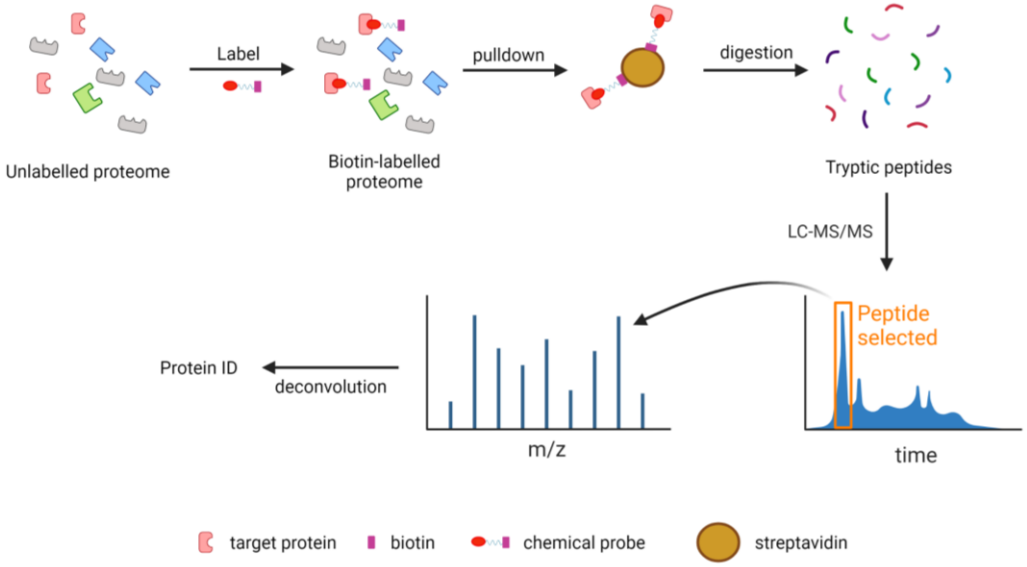

Figure 1.13. Basic MudPIT ABPP.[45]

The main benefits of this technique include superb resolution, sensitivity (1 pmol/mg proteome) and target identification. However, it does not give information regarding the specific site of probe labelling. To obtain this, a complementary technique named active site peptide profiling (ASPP) is used. The main difference between this analysis and (MudPIT)-ABPP is the moment at which the tryptic digestion occurs. In ASPP this happens before the biotin-(strept)avidin enrichment.[45,77,78] The ABP-peptides are then enriched using either (strept)avidin or antibody resins for biotinylated or fluorescent probes, respectively. Analysis by LC-MS/MS and subsequent data processes provides insights about the labelling site. (Figure 1.14). One disadvantage that this technique possesses is its inability to test multiple samples at the same time and conduct relative quantification analysis.

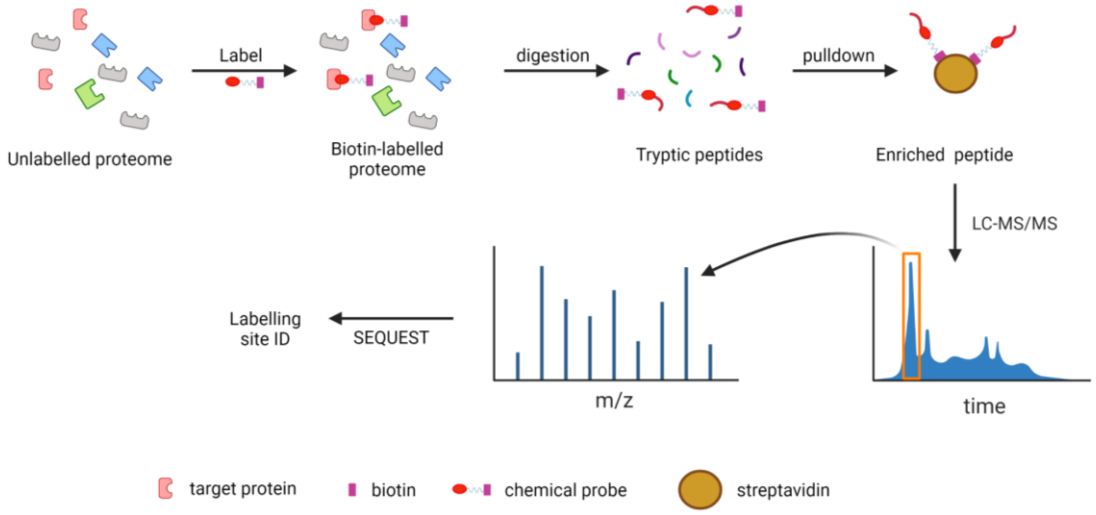

Figure 1.14. Active site peptide profiling (ASPP) After the proteome is labelled, the sample is digested prior to isolation by pulldown. Consequently, only the peptides that contain the active site-ABP complex are enriched and identified.[45]

1.4.6.2 Stable Isotope Labelling by Amino acids in Cell culture (SILAC)

This mass spectrometry-based technique uses isotopic labelling to obtain accurate, relative, and quantitative information about the expression levels of proteins between different samples. The technique consists of growing a pool of cells in a regular medium (light) containing regular amino acids and another pool with similar medium, but with a heavier isotopically labelled amino acid, ideally essential, such as lysine-$^{13}C_6$ or Leu-d3. These labelled amino acids are incorporated into all proteins as they are synthesized. After enough cell division cycles, the degree of incorporation is evaluated by LC-MS/MS to confirm its completion. Subsequently, equal amounts of light and heavy samples are mixed, the cells are lysed and then, the homogenates can either be digested and analysed by LC-MS/MS or separated using a gel-based technique, followed by excision, digestion, and LC-MS/MS analysis to obtain the

identification of the peptides and determination of their relative abundance based on the ratio of heavy and light peptides present in the sample (Figure 1.15). Some disadvantages of SILAC include that the preparation phase can be time consuming, as many cell cycles are needed until the heavy amino acids are incorporated. Another disadvantage is that as the number of labelled amino acids is limited, the number of cellular states that can be compared is also limited. Nevertheless, SILAC is considered as one of the best methods available for quantitative proteomics.[79–81]

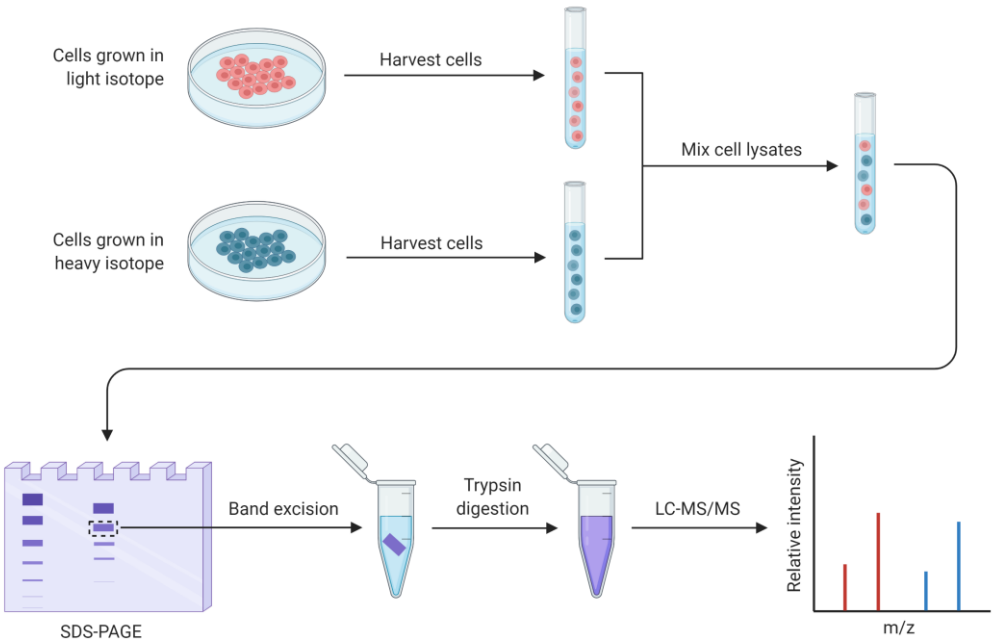

Figure 1.15. SILAC quantitative differential protein expression Method. Cells are cultured in different media containing isotopic labelled essential amino acids. After incubation, the cultures are mixed, lysed and analysed by LC-MS/MS. Identification and quantification of the labelled proteins are obtained from the heavy/normal labelled amino acids ratio.

1.4.6.3 Isobaric tag for relative and absolute quantitation (iTRAQ)

This technique is a tandem mass quantitative proteomics method which uses isobaric (same mass) labelling for the identification and quantification of proteins from different samples simultaneously. The principle relies on the use of several tags with the same mass, but with different isotope distributions throughout their structure which bind covalently to proteins and subsequent mass spectrometry analysis. The isobaric tags are formed by 3 main groups: I) a reporter group, based on N-methylpiperazine, for relative quantification upon MS/MS, II) a balance group, needed to maintain the isobaric nature of the tag. To differentiate the tags, these two fragments possess heavy isotopes alternately distributed along the groups so that the total mass of both remains constant, and III) the peptide reactive group *N*-hydroxysuccinimide, to bind covalently to the peptides through lysine side chains and N-termini via free amines (Figure 1.16 A). Once the samples are labelled with the tags, they are combined and initially, the same peptides from the different samples appear at the same mass in MS. However, after the fragmentation of these peptides, the fragments enable peptide identity to be established, and the iTRAQ tag fragments release the reporter ions whose ratios are proportional to the relative quantity of the peptides in each sample (Figure 1.16 B).[82,83]

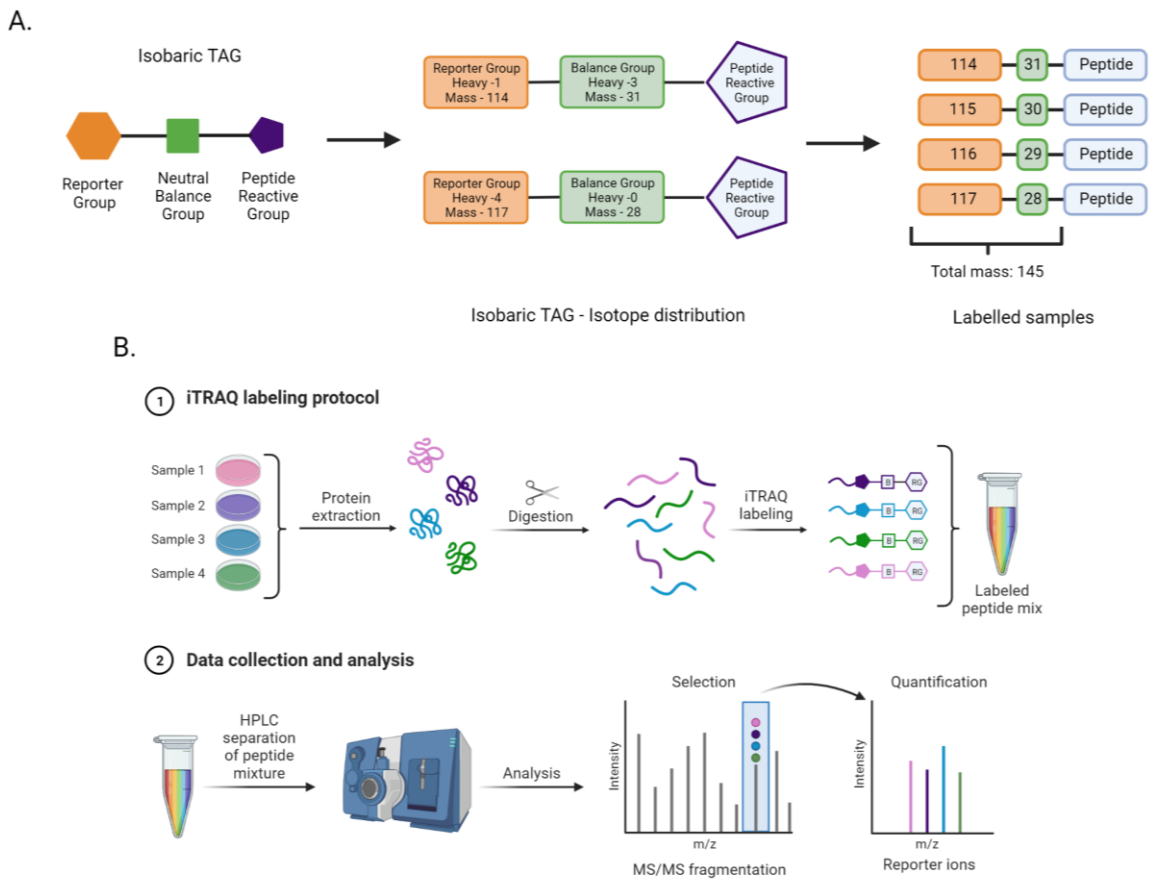

Figure 1.16. A) Isobaric tag building blocks. **B)** Normal iTRAQ workflow.

1.5 Serine Hydrolases

1.5.1 Introduction

One of the largest and diverse family of enzymes is the serine hydrolase family. This include esterases, proteases, lipases, and peptidases, all with important roles in different processes in several diseases. Their function is to catalyse the hydrolysis of ester, thioester, and amide bonds in different substrates. This is achieved due the presence of a highly nucleophilic and conserved serine residue present in the active site, that attacks the carbonyl group present in substrates, followed by the cleavage of the adduct by a water molecule, restoring the serine (Figure 1.16).[45] The heightened reactivity is normally achieved as a result of the interaction of three amino acid

residues: serine or cysteine (as nucleophile), histidine or lysine (as base) and aspartate or glutamate (acidic residue acting as a base) that together form the "catalytic triad". In a catalytic triad, the basic residue interacts with the hydroxy group present in serine, polarizing it and giving the correct orientation, at the same time as the acidic residue stabilizes the basic residue (Figure 1.17).[84] This interaction makes the serine residue of the active site different to other serine residues present. It is this enhanced reactivity that ABPP exploits for the study of serinomes.[45,85]

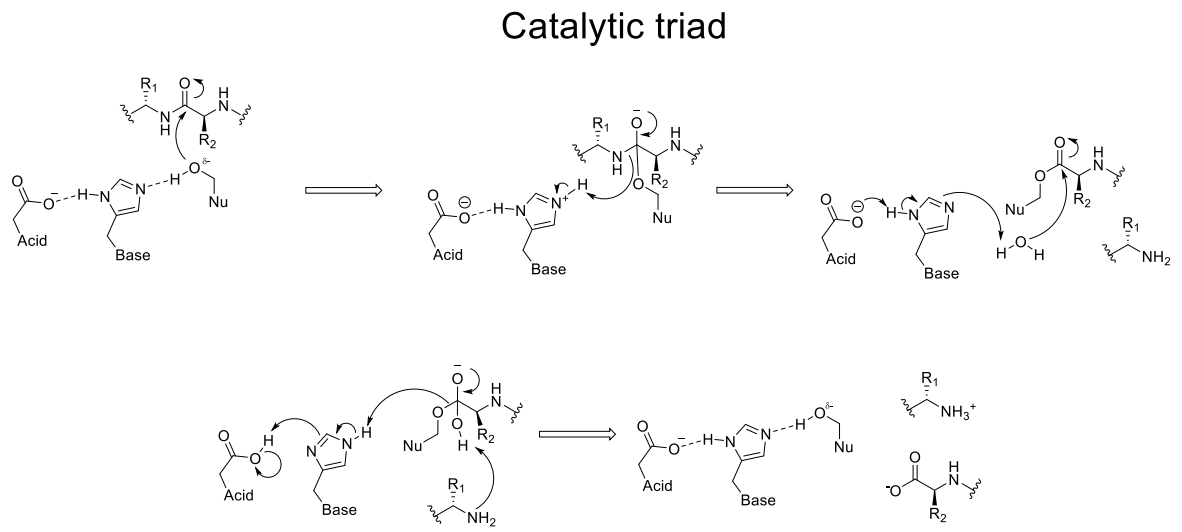

Figure 1.17. Mechanism of action of serine hydrolases: The activated serine residue attacks the carbonyl group of the substrate, cleaving the peptide chain and releasing the first reaction product. Subsequently, a water molecule attacks the intermediate and releases the acyl group from the enzyme restoring the catalytic triad.[58]

Fluorophosphonate probes have been the most used probes to profile serine hydrolases. This moiety is a known inhibitor of serine hydrolases which was first developed and used as a chemical weapon working as a powerful inhibitor of acetylcholinesterase, a crucial enzyme of the nervous system.[86] This group is not

selective for any particular class of serine hydrolase as it does not resemble an ester substrate or peptide enabling the profiling of the whole enzyme family. Also, it shows very low reactivity towards other classes of hydrolases like metallohydrolases, cysteine hydrolases and aspartyl hydrolases. In addition, they are only reactive with the active serine hydrolases and not with their zymogen.[45,87] Also, by modifying or adding different binding groups it is possible to modulate the affinity of this warheads to specific members within the enzyme superfamily.[45,88]

Other ABPs have been developed to target serine hydrolases ranging from poor to high selectivity towards active serine residues and hydrolase affinity (Figure 1.18).[89]

Warhead Scaffold	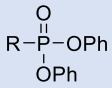			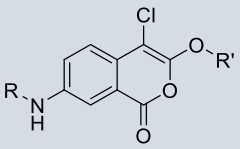	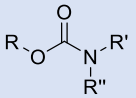
Warhead	Diphenyl phosphonate	Sulfonyl fluoride	β-lactam β-lactone	4-chloro isocoumarin	Carbamate
Serine Selectivity	High	Poor	Poor	High	Moderate
Affinity	Proteases	Proteases	b-lactamases	Broad	Lipases

Figure 1.18. Structures of other reactive warheads used to target serine hydrolases.

1.5.2 Serine hydrolases in *Leishmania spp*

A comparison of sequence similarity and putative biological activity in *Leishmania spp* proteases showed that among this group, serine proteases represent between 10 and 16% of the protease genes and most of these proteins are endoproteases. As these enzymes are involved in the transition from promastigotes to amastigotes, have roles as virulence factors and participate in the degradation of the extracellular matrix, needed for the dissemination of the parasite in the host, they are key in all steps of the

life cycle of the parasite making them perfect targets for treating the disease.[84] Given these roles, the SH superfamily represents a resource to explore for new drug targets and whilst this has been done in many systems such as humans,[90] rice (*Oryza sativa L.*)[91] or *Plasmodium falciparum*,[92] the *Leishmania* serinome remains surprisingly neglected.

1.6 ABPP in *Leishmania spp*

Although not widely used, ABPP has been applied in *Leishmania spp,* either for the exploration of specific targets such as *N*-myristoyltransferase, an enzyme responsible for protein lipidation considered a potential drug target in *L. donovani*,[93] or to unveil the role of deubiquitination enzymes (DUBs) from the proteasome of *L. mexicana*.[94] In other cases, it was applied to find the target of a potent antileishmanial drug like the chalcone-based probe developed by Escrivani et al.[95] which allowed the identification of peroxidase cTXNPx as a potential drug target.

Despite these applications, ABPP has not yet been applied to explore the serinome for new drug targets. Consequently, this project aims to map and explore therapeutic targets within SHs present in the *Leishmania* proteome using an activity-based protein profiling (ABPP) strategy. The initial in-gel labelling of serine hydrolase profiles obtained in different *Leishmania spp* using commercially available activity-based probes, as well as gel free target discovery proteomics are described in the next chapter.

2. Profiling Serine Hydrolases

2.1 Introduction

In chapter 1 the necessity for developing new drugs with new mechanisms of action, and that serine hydrolases (SHs) could potentially be good candidates as molecular targets were discussed (section 1.5.2). In consequence this project attempts to provide the first comprehensive profile of active SHs present in *Leishmania spp* during the different life stages of the parasite. As an initial approach, the use of commercially available fluorophosphonate probes was explored to develop techniques and verify the strategy. These probes possess either a fluorophore tag (**13**) for in-gel visualization of labelled enzymes, or a biotin handle (**14**) for enrichment and identification by mass spectrometry (Figure 2.1 A)[96] using a typical ABPP workflow with *in vitro* labelling of different *Leishmania spp* homogenates (Figure 2.1 B).

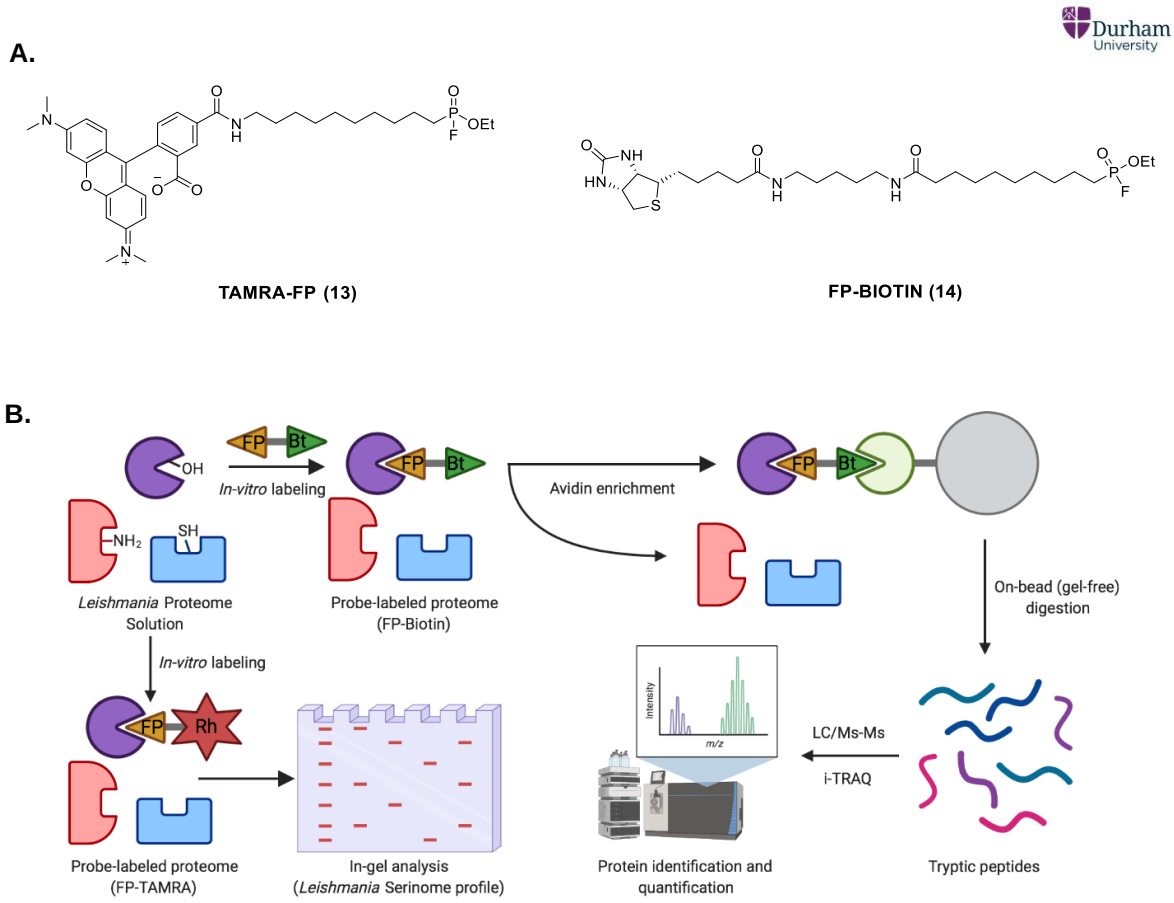

Figure 2.1 A) Structures of commercial probes TAMRA-FP and FP-Biotin. **B)** ABPP workflow used with *in vitro* conditions: Cell lysates were incubated with the ABPs. The labelled proteomes were separated and visualised using in-gel fluorescence using probe **13**. Enrichment, digestion, and protein identification using LC-MS/MS analysis was carried on using probe **14**.

2.2 Optimization of conditions

2.2.1 *Leishmania spp* promastigote growth curves

Leishmania spp are characterized by having a dimorphic life cycle, developing into promastigotes in the sandfly, and intracellular amastigotes in the mammalian host (section 1.2.2). Moreover, the promastigote stage can be further sub-divided into two distinct stages; an initial non-infective procyclic promastigote stage in which the parasites divide and, the non-dividing and infective metacyclic promastigote form at the end of the promastigote stage.[97,98] As these forms present very distinctive roles in the promastigote life, it was hypothesised that the serinome expression probably

would vary as well. In order to answer this hypothesis, we require access to biological models from each stage of interest which in turn required an understanding of parasite growth. Consequently, it was necessary to construct the respective growth curves for each species.

L. mexicana and *L. amazonensis* (New-World strains), and *L. major* (Old-World strain) promastigotes were adjusted in triplicate to 1×10^5 parasites/mL in fresh Schneider media in a 24-well plate and incubated at 26 °C. For 10 days, parasites were counted daily, and data was analysed using GraphPad Prism 9 (Figure 2.2 A). As observed, the growth of all 3 species is similar, reaching the stationary phase between days 7 and 10. Finally, the morphologies of the promastigote phases were analysed by microscopy. Promastigotes in log phase were rounder in shape and visually dividing (Figure 2.2 B), whilst stationary-phase parasites were more elongated (Figure 2.2 C).[99]

A.

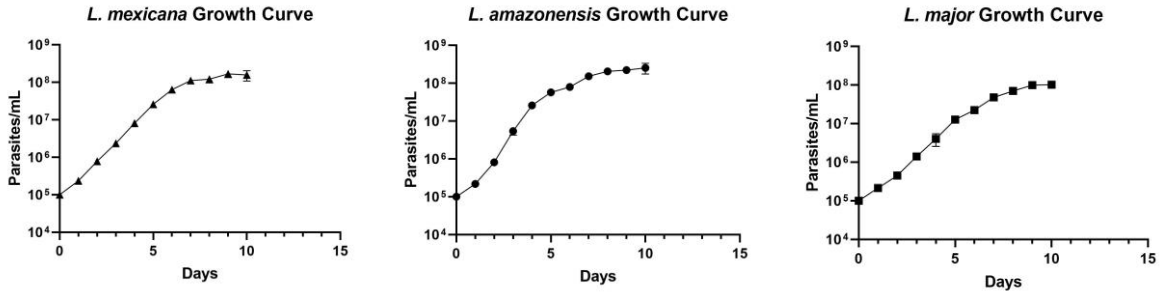

B.

Procyclic promastigotes

C.

Metacyclic promastigotes

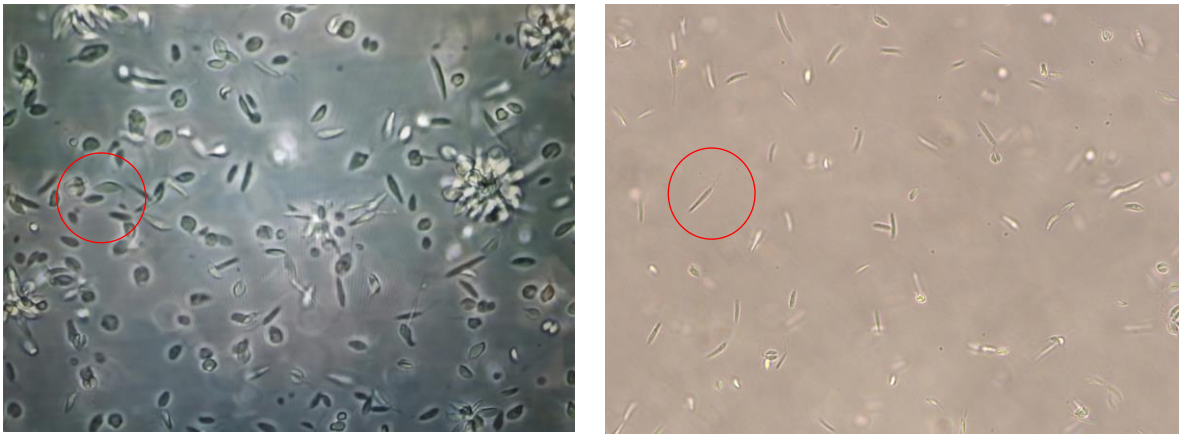

Figure 2.2 A) Growth curves of L. *mexicana*, L. *amazonensis* and L. *major* parasites were constructed by counting the parasites/mL during 10 day and plotted using GraphPad Prism 9. The standard deviation values were obtained from the triplicate measurements. Optical microscopy of **B)** procyclic and **C)** metacyclic L. *mexicana* parasites (40X augmentation). The red circles enclose parasites with the typycal morphology of each stage.

2.2.2 *Leishmania spp* axenic amastigote cultures

Once the mammalian host is infected, metacyclic promastigotes enter the second life cycle stage and differentiate to amastigotes (section 1.2.2). Analysing the serinome in the intracellular amastigote stage of the parasite is important not only because is the more clinically significant form, but also because it is known that the parasite expresses different proteins depending on the life stage.[100]

Amastigotes are normally obtained from infection assays of animal tissues or *in vitro* cells, and are normally more difficult to handle than promastigotes. As this is not possible at Durham University, an alternative option, in which promastigotes are differentiated *in vitro* into so called axenic amastigotes was adopted. Whilst these axenic amastigotes do not reflect the real intracellular parasite, comparative proteomic studies indicate that it is a good approximation model.[101,102] In addition, protocols for the generation of axenic amastigotes have been well established for *L. mexicana* parasites.[99] Following this precedent, promastigotes were incubated initially at pH 7 and 26 °C, followed by succesive passages that included changes in the culture media composition, pH and temperature. The morphologies of the parasites were analysed by microscopy, and it was confirmed as observed in figure 2.3, that the parasites possess the characteritic non-flagelated round form of amastigotes.

Figure 2.3. Optical microscopy of *L. mexicana* axenic amastigotes (40X augmentation). The red circle enclose parasites with the typycal morphology for amastigotes. To obtain axenic amastigotes, log stage parasites were incubated at 26 °C for 3 days in Schneider's medium, 15% FCS, pH 7.0, seeded at 5 × 10^5 parasites/ml. On day 3, they were transferred to Schneider's medium, 20% FCS, pH 5.5, seeded at 5 × 10^5 parasites/ml and incubated for 6 days at 26 °C. On day 9, metacyclic parasites were transferred to Schneiders medium, 20% FCS, pH 5.5, seeded at 5 × 10^5 parasites/ml and incubated for further 5-7 days at 32 °C.

2.2.3 Lysis conditions

There is no universal procedure for obtaining cell homogenate, with reported methods varying according to particular circumstances such as cell type or location of the target proteins. Consequently, once the parasite cultures in their different life stages were successfully obtained, attention was focused on obtaining lysates that would preserve the integrity and activity of the target proteins. Moreover, as many serine hydrolases are proteases, commonly used protease inhibitor cocktails cannot be used posing an

aditional challenge. Consequently, different commercial lysis buffers such as RIPA,[103] or IP Pierce,[104] as well as additional lysis buffers prepared, containing SDS, protease inhibitors, and including sonication, were then tested. *L. mexicana* promastigotes parasites were lysed with the different buffers, and the extracts obtained were then incubated with TAMRA-FP (1 μM) for 15 min at room temperature (rt), and analysed by fluorescence imaging after SDS-PAGE separation. Initially the commonly used commercial lysis buffers ThermoFisher Pierce IP and RIPA were compared. As shown in figure 2.4 A (lanes 1 and 2), when using Pierce IP, bands with good intensity and resolution were observed. In contrast, fewer bands, and lower intensities and resolution were observed when RIPA was used, suggesting that lower amounts of active enzymes were present in the lysate. Subsequent tests using sodium dodecyl sulfate (SDS) as detergent, with or without metalloprotease inhibitor EDTA or cysteine protease inhibitor E-64, in addition to sonication, failed to produce better labelling than Pierce IP. Additionally, protein degradation was observed using coomassie blue protein stain since loss of band resolution was observed, suggesting that using the SDS-sonication conditions were more harsh (lanes 3-5). In contrast, similar results were observed when using modified Pierce IP lysis buffer (LyBA), in which the detergent was switched to commercial Triton X-100 instead of ND-40 (present in Pierce IP), and without EDTA (Figure 2.4 C). These conditions were then compared with the previously described methods. Both Pierce IP and its variation with Triton X-100 (LyBA) produced more fluorescent bands than that observed previously. This indicated that more active enzymes are present in the homogenate. This conclusion was supported by the protein stain gels, which showed more and better resolved bands consistent with lower protein degradation. Consequently, Pierce IP lysis buffer was chosen for further experiments.

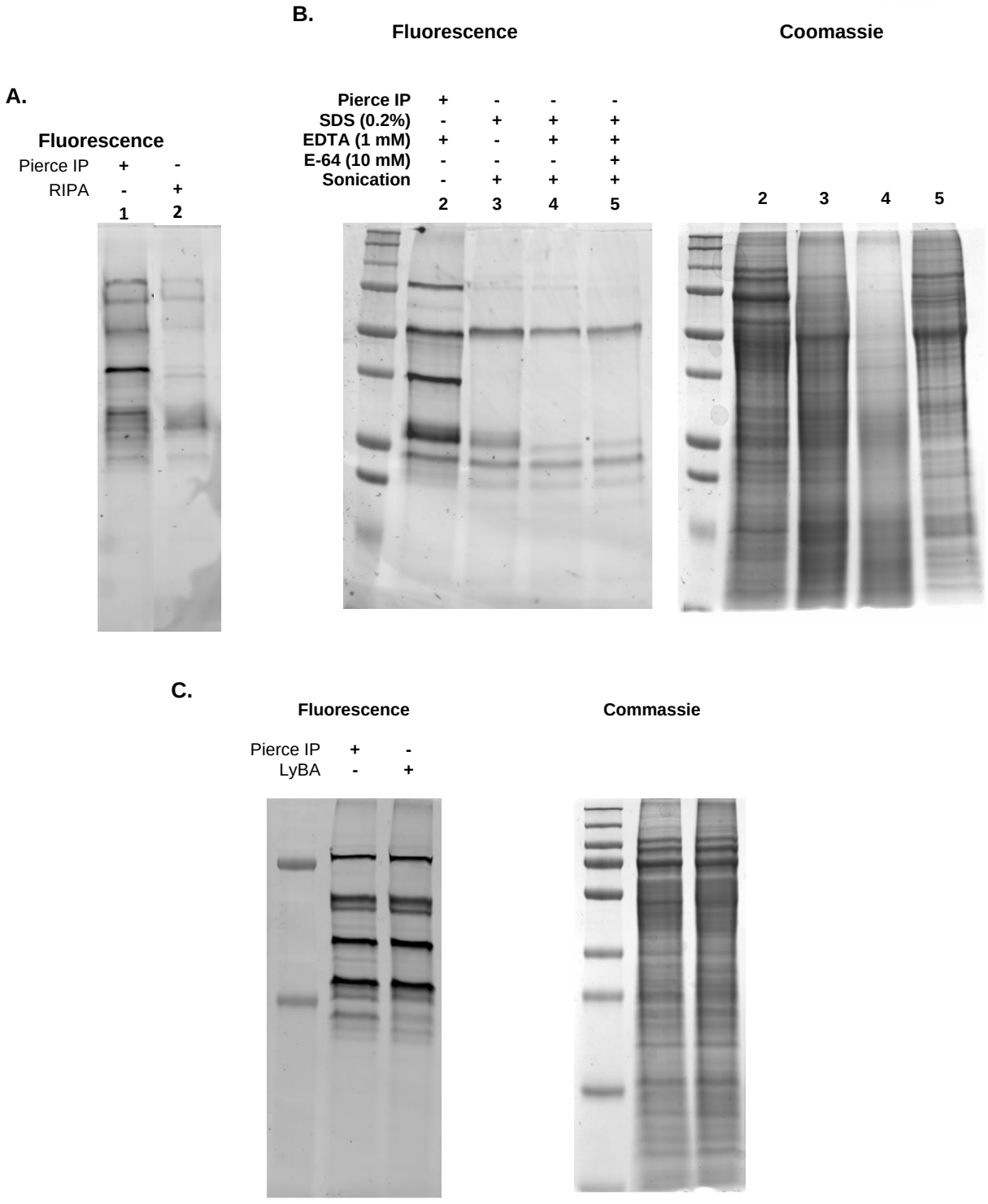

Figure 2.4 In-gel comparison between different lysis conditions. **A)** Pierce IP vs RIPA lysis buffers. **B)** Pierce IP lysis buffer was compared against SDS + sonication based lysis buffers with and without protease inhibitors. **C)** Pierce IP vs Lysis buffer A (LyBA). The lysates were obtained as follows: *L. mexicana* promastigote parasites were centrifuged at 1000 × *g* for 5 min to pellet the parasites, and washed 3 times with PBS prior to addition of the lysis buffer. Finally, after 5 minute incubation on ice, the homogenates were centrifuged at 13000 × *g* for 10 min to pellet cell menbranes (general procedure

5.2.1.5). In all cases the lysates were incubated with TAMRA-FP (1 μM) for 15, and proteomes were separated by SDS-PAGE. Labelled bands were observed by fluorescence imaging.

2.2.4 TAMRA-FP specificity

One of the most important characteristic of ABPP is the capacity of the probes to only interact and covalently label specific enzymes (section 1.4). Despite TAMRA-FP having been widely validated as an ABP, a set of contols was necessary to confirm this hypothesis and validate it in the biological context of these experiments. Consequently, a set of negative controls was performed in which *L. mexicana* lysates were exposed to denaturing conditions (95°C for 5 min) prior to incubation with probe TAMRA-FP (1 μM) for 15 min at rt (lane 5, Figure 2.5). Additionally, normal and denatured lysates were also incubated with DMSO. The absence of fluorescent bands in either the denatured lysates and the normal ones treated with DMSO confirmed that there are no endogenous fluorescent enzymes present (lanes 2-3, Figure 2.5) and that the probe only interacts with active enzymes (lane 4, Figure 2.5).

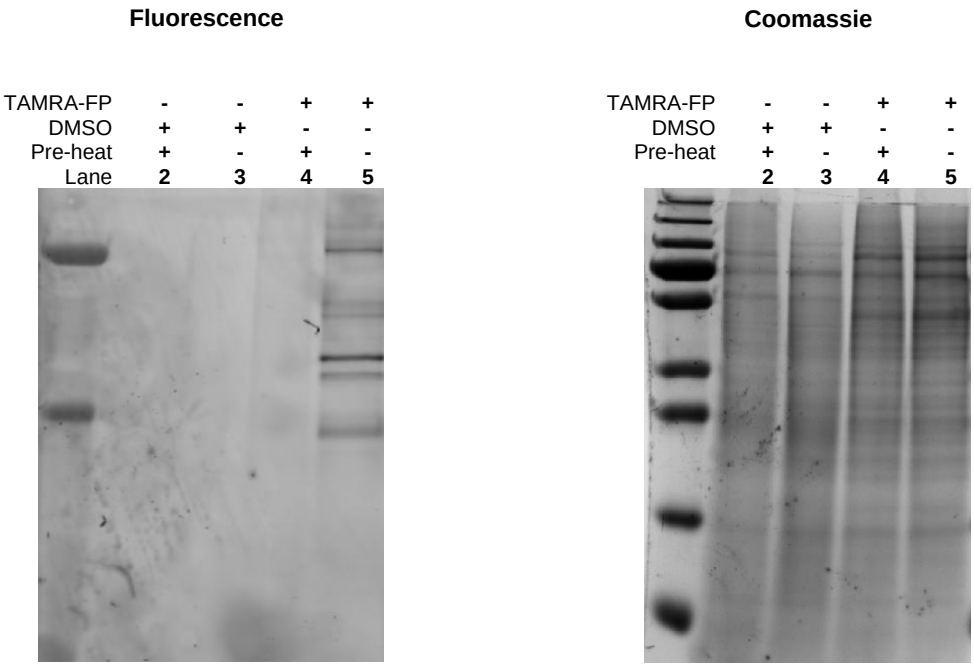

Figure 2.5. Negative controls and validation of TAMRA-FP as an ABP in *L. mexicana* promastigote lysates. Parasite homogenates were treated with DMSO (lanes 2-3) and TAMRA-FP (1 μM, lanes 4-5) under normal (lanes 3 and 5) and under denaturing conditions (lanes 2 and 4). Proteomes were resolved by SDS-PAGE and visualised by fluorescent imaging.

Additionally, to confirm that the FP probe does not interact with cysteine proteases, a competition assay using commercially available E-64 (Figure 2.6 A), a known and commonly used cysteine protease inhibitor, was carried out. As showed in figure 2.6 B, no decrease in the fluorescence of any bands is observed confirming that none of the labelled enzymes are cysteine enzymes. In contrast, an increase in fluorescence was observed in all the major bands (85, 60, 40 and 30 kDa) (Figure 2.6 B, lane 3). This could be explained by the decreased proteolytic activity, due to the inhibition of the cysteine proteases present in the proteome.

A.

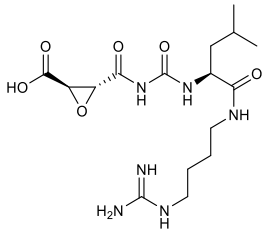

E-64 (15)

B.

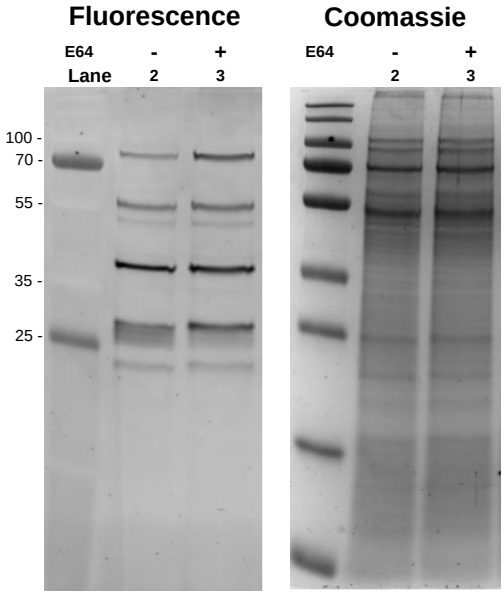

Figure 2. 6. A) Structure of E-64. **B)** The non-interaction between TAMRA-FP and cysteine proteases was confirmed conducting a competitive ABPP assay between cysteine protease inhibitor E-64 and TAMRA-FP. Here, *L. mexicana* lysates were preincubated with E-64 (500 μM) for 1 h prior the addition of TAMRA-FP (1 μM). The samples were then incubated for a further 15 min. Finally, the proteomes were resolved by SDS-PAGE and analysed by fluorescent imaging.

2.2.5 TAMRA-FP incubation time

Once the lysate conditions and negative controls were satisfactorily obtained, attention was focussed on obtaining the optimal probe incubation time. Knowing that different enzymes may interact with different selectivities towards the probe, their labelling rate

may also differ. In addition, as it is not possible to use protease inhibitors, using the lowest incubation time is important to reduce protein degradation by protease action. In order to address this challenge, biological replicates of *L. mexicana* promastigote lysates were incubated with TAMRA-FP (1 μM) for 15, 30 and 60 min at room temperature before being analysed by fluorescent imaging (Figure 2.7). This revealed that the labelling pattern and integrity of the bands is similar and does not increase in time. Therefore, a 15 minute incubation time of TAMRA-FP was chosen as optimal for further experiments.

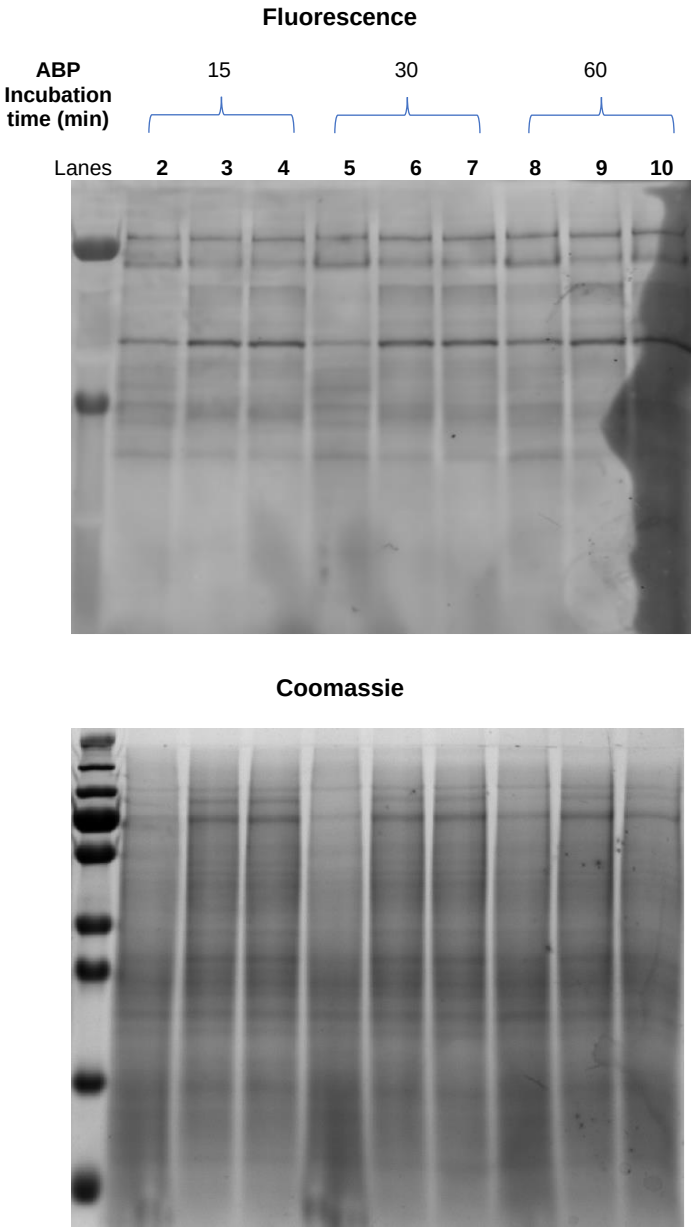

Figure 2.7. TAMRA-FP labelling rate assay. *L. mexicana* lysates were incubuated with TAMRA-FP (1 μM) for 15 (lanes 2-4), 30 (lanes 5-7) and 60 (lanes 8-10) minutes. Proteomes were resolved by SDS-PAGE and analysed by fluorescent imaging.

2.2.1 *Leishmania spp* serinome labelling with TAMRA-FP

Having succesfully determined the optimal labelling conditions, we focused our attention on profilling the serinome of different *Leishmania spp* at key stages of their life cycles. We hypothesize that different old- and new- world species may possess

different enzyme expression profiles due to their geographical divergence. This is supported by the fact that available treatments present different efficacies depending on the species.[11] In addition, different parasite roles, such as cell division or infectivity, are more relevant depending on the life stage of the parasite (sections 2.1.1 and 2.1.2), therefore, there could be a correlation in the expression levels of specific enzymes. Consequently, serine hydrolase profiles from New-World (*L. mexicana* and *L. amazonensis*) and Old-World (*L. major*) species were obtained using *in vitro* labelling with TAMRA-FP. Here, biological replicates from the different parasite lysates (1 mg/mL protein) were incubated with TAMRA-FP (1 μM) for 15 min at room temperature and analysed with fluorescent imaging. In all cases, DMSO was used as negative control, and pre-heated (5 min at 95 °C) proteomes were used to determine TAMRA-FP probe specificity towards active enzymes. The results obtained are described in the following sections.

2.2.1.1 *L. mexicana* serinome

Following incubation of non-infective log phase *L. mexicana* promastigotes with TAMRA-FP and processing as described above, labelled proteins were detected in the proteome with 4 strong signals observed at approximately 85, 60, 40, and 30 kDa (Figure 2.8 A, lane 2) in addition to a number of weaker signals. Overall, labelled enzymes were observed throughout a 20-80 kDa range. A similar pattern was observed for stationary phase promastigotes, although an increase in fluorescent intensity in some of the bands was observed, suggesting a variation of the expression level of the enzymes (Figure 2.8 A, lane 3, Figure 2.8 B). The fingerprint obtained for axenic amastigotes presented new signals at 70 kDa and between 40 and 55 kDa

(Figure 2.8 A, lane 4). In addition, a decrease in the expression levels of the 55, 40 and 30 kDa bands was also observed (Figure 2.8 B).

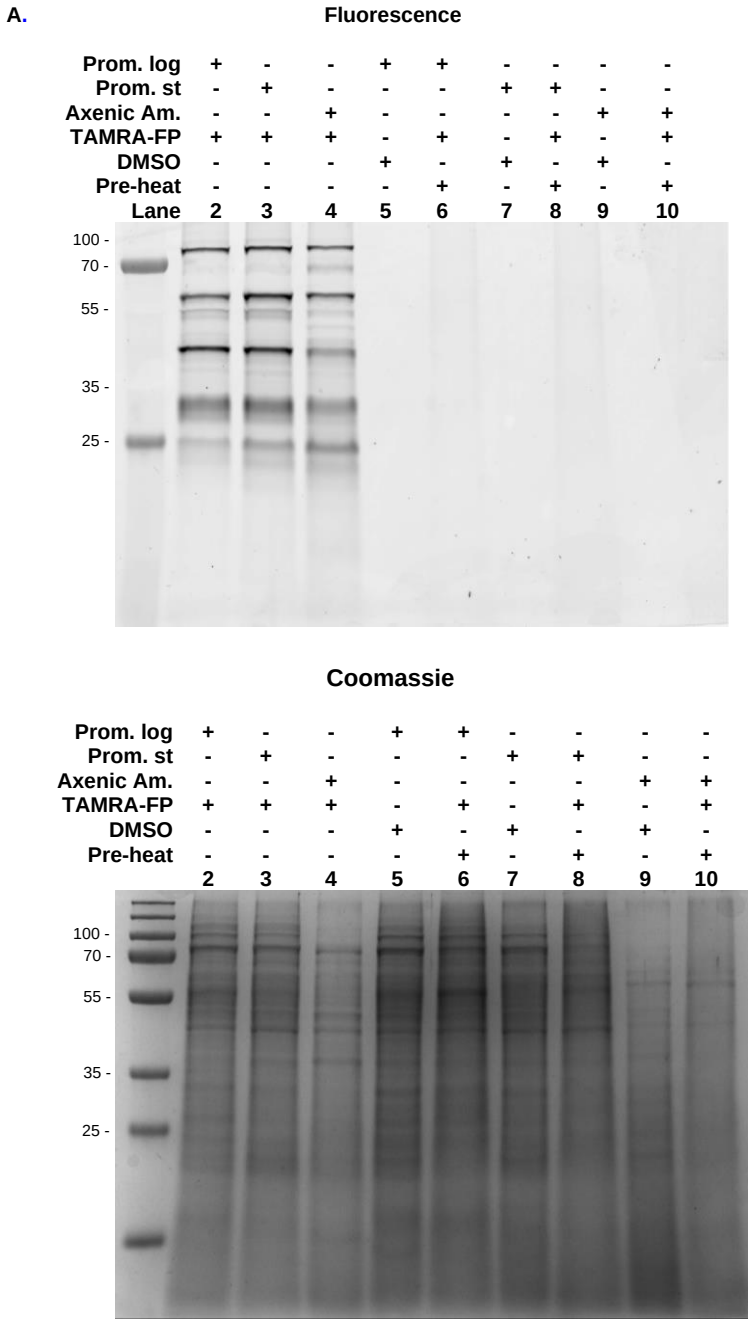

B.

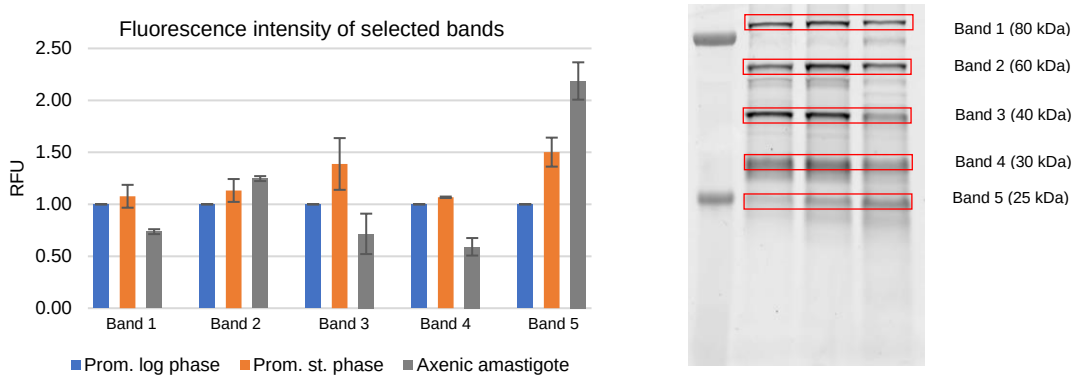

Figure 2.8. A) Serinome in-gel visualization with TAMRA-FP (1 μM) of *L. mexicana* log (lane 2), stationary (lane 3) promastigotes and axenic amastigote (lane 4) lysates (1 mg/mL). Lanes 5-10 show the negative controls (with and without TAMRA-FP and in denaturing conditions). **B)** Changes in expression levels of labelled enzymes expressed as relative fluorescence units (RFUs). The values for each band from stationary and axenic amastigotes are relative values to the early promastigote stage. The fluorescense intensities were obtained from volumes using ImageLab 6.1.

2.2.1.2 *L. amazonensis* serinome

A comparable pattern to *L. mexicana* was observed for *L. amazonensis* log promastigotes, with more intense bands at approximately 80, 55, 40, and 30 kDa (Figure 2.9 A, lane 2). When moving from log to stationary phase, loss of bands in the 40-55 kDa region was observed. In contrast, new bands were present below 20 kDa (Figure 2.9 A, lane 3), and a decrease in fluorescence in bands 3 (40 kDa) and 4 (30 kDa) was also observed (Figure 2.9 B).

A.

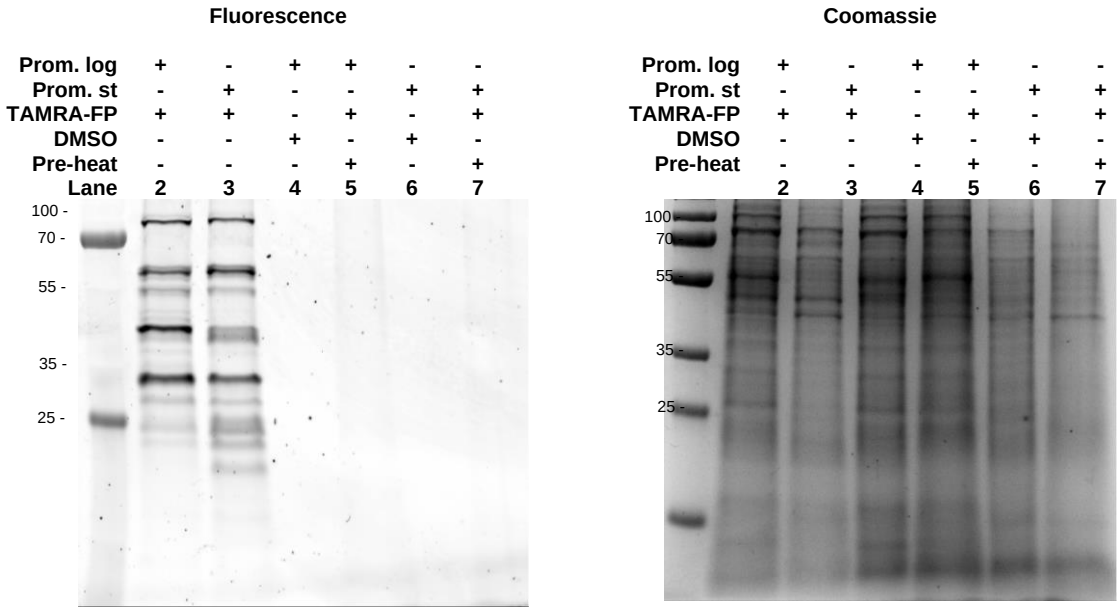

B.

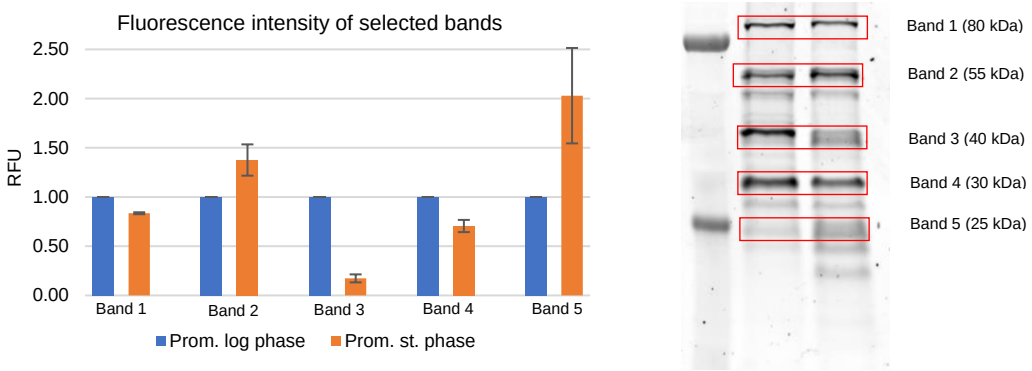

Figure 2.9. A) Serinome in-gel visualization with TAMRA-FP (1 μM) of *L. amazonensis* log (lane 2) and stationary (lane 3) promastigote lysates (1 mg/mL). Lanes 4-7 show the negative controls (with and without TAMRA-FP and in denaturing conditions). **B)** Changes in expression levels of labelled enzymes expressed as relative fluorescence units (RFUs). The values for each band from stationary and axenic amastigotes are relative values to the early promastigote stage. The fluorescense intensities were obtained from volumes using ImageLab 6.1.

2.2.1.3 *L. major* serinome

Having studied New-World species, it was of interest to compare the output obtained from an Old-World species. Compared with *L. mexicana* and *L. amazonensis*, more high intensity bands were observed in the *L. major* log phase fingerprint. Here, six bands were detected at approximately 80, 60, 50, 42, 40, and 30 kDa, along with other signals of lower intensity (Figure 2.10 A, lanes 2-3). In stationary *L. major* promastigotes, an increase in the level of expression was observed in almost all bands (Figure 2.10 B).

A.

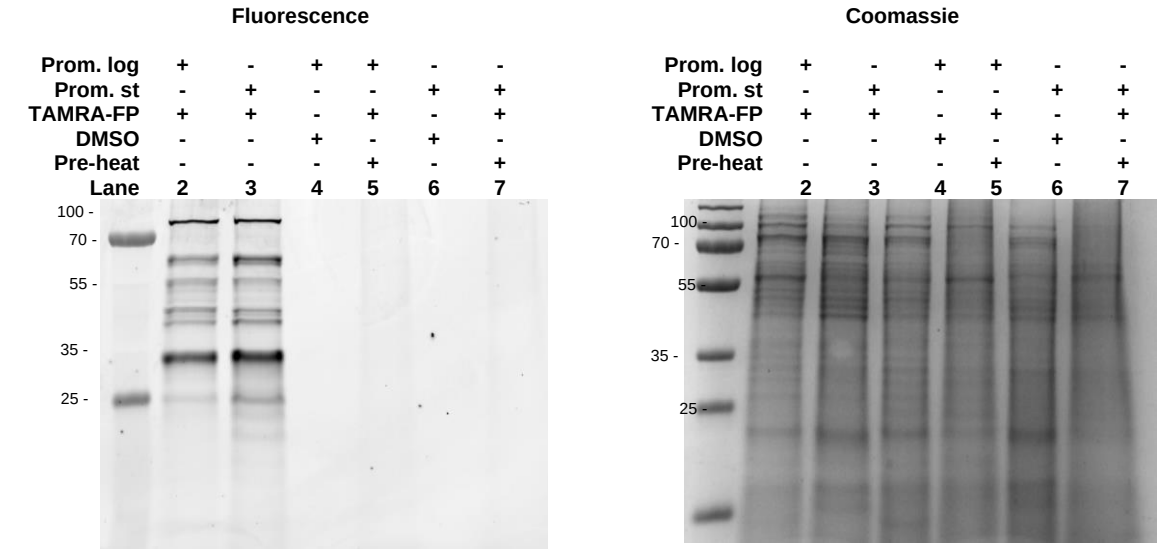

B.

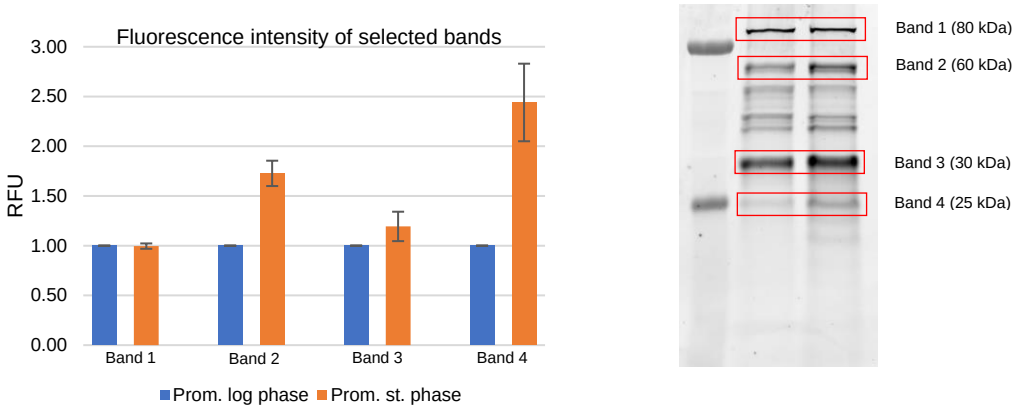

Figure 2.10. A) Serinome in-gel visualization with TAMRA-FP (1 μM) of *L. major* log (lane 2) and stationary (lane 3) promastigote lysates (1 mg/mL). Lanes 4-7 show the negative controls (with and without TAMRA-FP and in denaturing conditions). **B)** Changes in expression levels of labelled enzymes expressed as relative fluorescence units (RFUs). The values for each band from stationary and axenic amastigotes are relative values to the early promastigote stage. The fluorescense intensities were obtained from volumes using ImageLab 6.1.

2.2.1.4 Discussion

As discussed above, and observed in figure 2.11 A, both New-World species possess similar fingerprint in their log phases (Figure 2.11 A, lane 2, 4). In contrast, a different landscape was discovered for Old-World *L. major* in both promastigotes' stages, suggesting that the evolutionary divergence between *Leishmania* drastically affects the parasitic proteome of the species (Figure 2.11 A, lane 3, 7). In general, moving from log phase to stationary phase did not produce significant changes in the pattern. Although new bands were observed in the low molecular weight range, it was not possible to confirm whether these were new enzymes or the product of degradation by active proteases.

The expression differences observed in the serinome fingerprints of the different life stages of the parasite supports the hypothesis of the dynamic role and importance of enzymes in each life stage. This idea was reinforced when the distinct fingerprints obtained from *L. mexicana* promastigotes and axenic amastigotes were taken into consideration.

A.

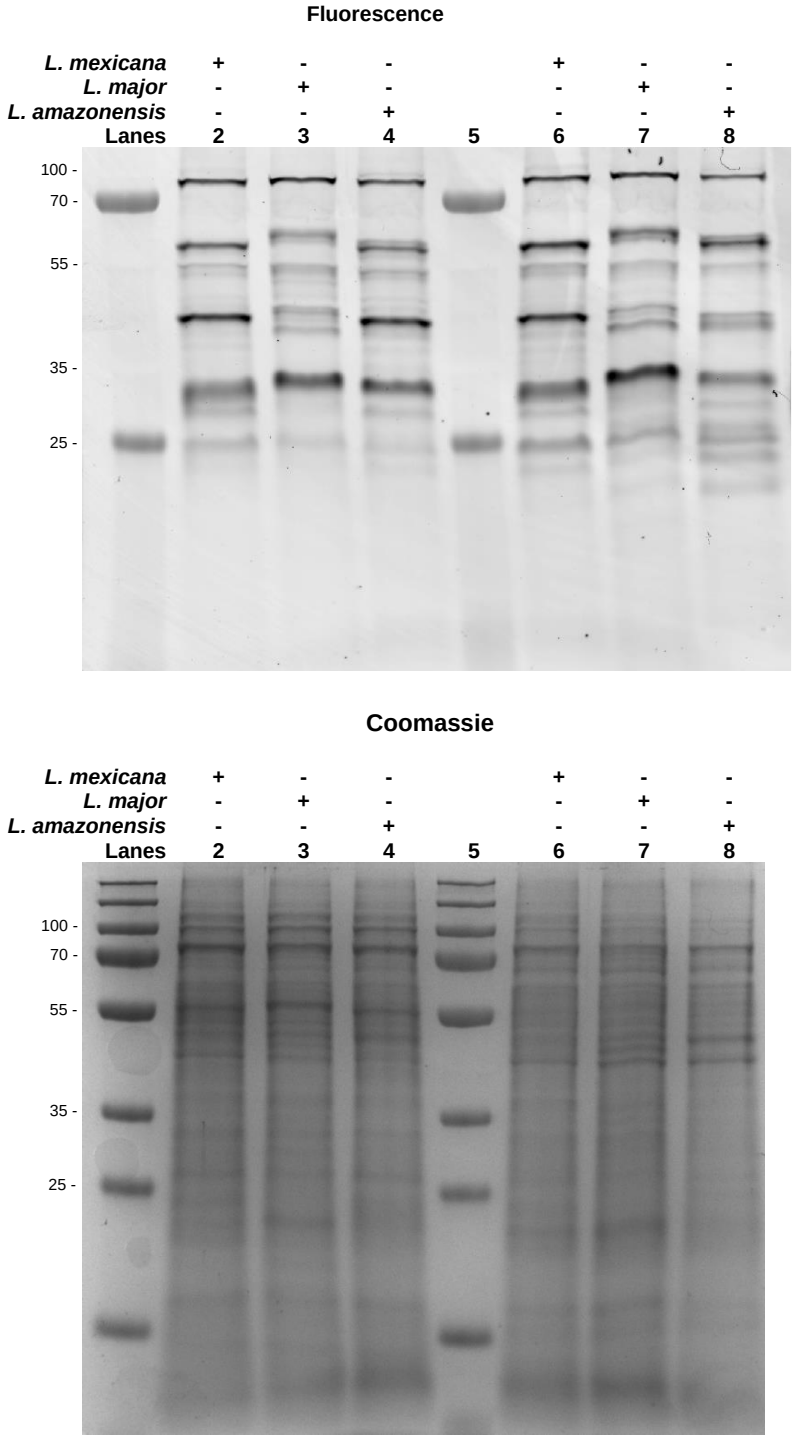

Figure 2.11. Serinome comparison between *L. mexicana*, *L. amazonensis* and *L. major* in their promastigote log (lanes 2-4) and stationary(lanes 6-8) phases using TAMRA-FP (1 μM).

At this point, the nature and identity of the labelled bands cannot be assigned and further gel-free mass spectrometry experiments, as well as competitive ABPP assays are needed for the identification and characterization of the labelled bands. These are detailed in the next sections of this chapter.

2.3 Gel-free mass spectrometry proteomics for target discovery

As mentioned in section 1.4.6, in-gel visualisation does not provide information about the identity of the enzymes labelled. To obtain these insights, as discussed in chapter 1, gel-free MS approaches are used. Since iTRAQ enables the analysis of simultaneous samples at the same time and conducting comparative studies; this was selected as the MS method of choice. Moreover, it also provides further benefits including the fact that it possesses a large dynamic range, analyses are faster, and it offers the ability to obtain relative quantification of the peptides identified.[82,83]

Consequently, to identify the previously in-gel labelled enzymes, *L. mexicana* was chosen as a model species and analysed in its log, and stationary promastigote forms as well as axenic amastigote. The respective lysates were incubated with FP-biotin (**15**) (Figure 2.12 A, AdooQ Bioscience, CAS: 259270-28-5) at a concentration of 4 mM (per mg/mL of protein), for 1 h at rt and a sample with DMSO was used as negative control. The biotinylated enzyme-ABP complexes were then enriched using NeutrAvidin-Agarose beads, followed by TCEP on-bead reduction of the disulfide bridges and subsequent alkylation of cysteine residues with chloroacetamide. Finally, the samples were digested with trypsin and desalted on Pierce C-18 Spin columns. Once the preparative steps were done, the samples were labelled with the iTRAQ reagents and pooled followed by a desalting step. Finally, the samples were analysed

on LC-MS/MS and proteomics analysis was then carried out as discussed in section 1.4.6.[a]

Confirmation of the integrity of the samples were obtained from in-gel labelling with TAMRA-FP (1 μM) revealing the same band as observed previously (Figure 2.12 B). In addition, pre-treating the lysate with FP-Biotin before the addition of TAMRA-FP led to complete inhibition of all labelling events verifying that these probes bind the same enzymes. (Figure 2.12 C).

A.

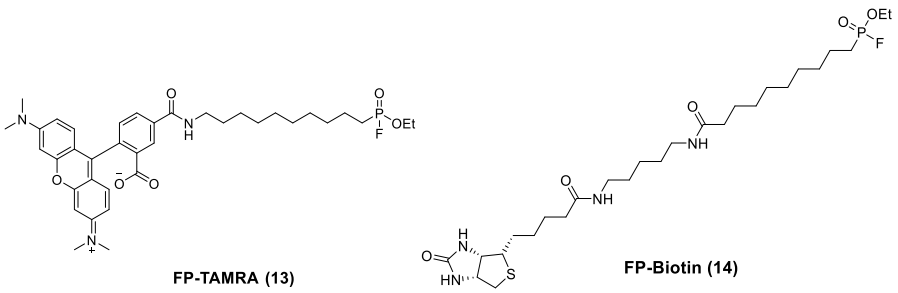

FP-TAMRA (13) FP-Biotin (14)

B.

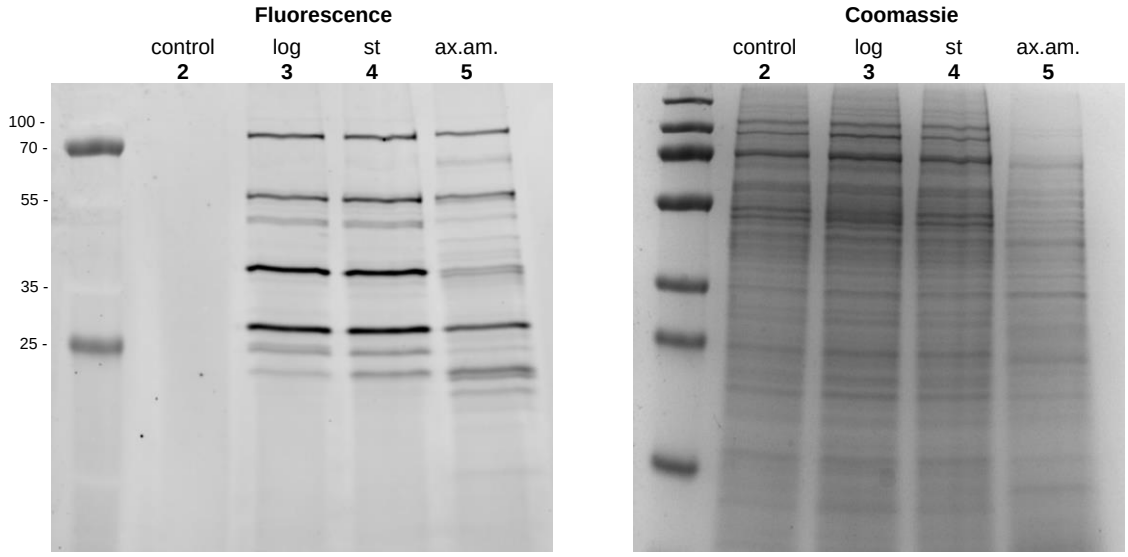

[a] Dr Kalesh Karunakaran carried out the affinity enrichment, iTRAQ proteomics and data analysis.

C.

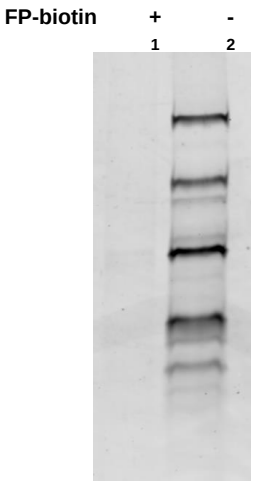

Figure 2.12 A) Structures of TAMRA-FP (**13**) and biotinylated probe FP-biotin (**14**)**. B)** In-gel controls of the enriched *L. mexicana* lysates in their log (lane 3), stationary (st) (lane 4) and axenic amastigote (ax. am.) (lane 5) phases using TAMRA-FP (1 μM). **C)** Competitive ABPP conducted to compare affinity. FP-biotin (2 μM) was incubated in a L. *mexicana* promastigote lysate (1 mg/mL) for 60 min at rt. Subsequently, TAMRA-FP (1 μM) was added, and the mixture was incubated for a further 15 minutes followed by SDS-PAGE and fluorescent imaging.

Once the controls were finished, after analysis and deconvolution of the data obtained, 4 proteins were identified that selectively bound to probe **15** (fold change > 2). After subtracting the background protein Acetyl-CoA carboxylase LmxM.30.2970, a naturally biotinylated enzyme, we observed 3 SHs from which 2 are the proteases: prolyl oligopeptidase (POP) LmxM.36.6750 (77 kDa) and carboxypeptidase LmxM.18.0450 (51 kDa); and the other one is the lipase lysophospholipase LmxM.24.1840 (30 kDa).

The prolyl oligopeptidase family is a group of serine proteases which cleaves the C-terminal side of proline residues present in peptides with less than 30 AA. In humans, they are considered important drug targets as they are associated with diseases such as amnesia, depression, and diabetes among others.[105,106] Based on sequence

homology, POP (697 AA) has at least one human ortholog, the *Hs*POP (PDB: 3DDU, 710 AA) with which it shares 44% identity and 63% similarity and it possesses orthologs between the different members of the *Trypanosomatidae* group. In the context of leishmaniasis, POP has been reported to be involved in the host invasion process of *L. infantum* in murine macrophages and therefore could be considered a virulence factor.[107] Similar results have been found for its *Trypanosoma cruzi* orthologue POP Tc80, which suggest that this enzyme may be important for degrading the extracellular matrix and thus allowing host-cell invasion.[108]

Carboxypeptidases are proteases that catalyse the hydrolysis of a single C-terminal amino acid residue from the C-terminus of a protein. They are often involved in post-translational modification processes. Carboxypeptidase (462 AA) would have homology with *Hs*Cathepsin A (apoprotein, PDB:4CI9, 455 AA), sharing 30% identity and 43% similarity. The only previous report on serine carboxypeptidase is in *T. cruzi* (a LmxM.18.0450 ortholog), where there is no conclusive information on the biological function of this enzyme and its roles in the parasite.[109]

Lysophospholipase is an esterase involved in lipid catabolism that belongs to the phospholipase B family which catalyses the hydrolysis of the acyl group present in 2-lysophosphatidylcholine. Human lysophospholipase (278 AA), possesses homology with thioesterase (LYPLA2), sharing 29% homology and 50% similarity. Homologs have also been found in trypanosomastids, where in *T. brucei*, Tb927.8.6390 was found sharing 55% identity 74% similarity. Whilst there have not been any reports of its function in *Leishmania spp*, it has been identified as an ortholog of lipase TbLysoPLA (Tb927.8.6390), present in Trypanosoma brucei, and which its main function is still not fully understood.[110]

Having identified these potential proteins of interest, it was then of interest to see if selective inhibitors could be identified to better understand their function. One approach to do this is competitive ABPP which is described in the following section.

2.4 Competitive ABPP

Competitive ABPP is a widely used variation of ABPP useful to determine target engagement and selectivity profiles of enzyme inhibitors in complex proteomes. The main difference relies on pre-incubation with a potential competitor prior to the addition of the ABP (Figure 2.13). This not only allows the identification of inhibitors for a particular enzyme, but it can also reveal and validate unknown targets or modes of action of a potential drug.[90,111] These compounds compete with the ABPs for the active site of the enzymes and the competition is confirmed by a decrease or loss of a fluorescent signal. For example, different serine protease inhibitors such as PMSF were used by Dului *et al.*[91] in a competitive fashion to identify proteases within the serine hydrolases visualized with TAMRA-FP in a specific rice bran (*Oryza sativa L.*). Following this precedent, competitive ABPP approaches were adopted to find inhibitors that interact with the enzymes found in the MS experiment (prolyl oligopeptidase LmxM.36.6750, carboxypeptidase LmxM.18.0450, and lysophospholipase LmxM.24.1840). In consequence, to identify potential proteases within the labelled proteome, commercially available and known serine protease pan-inhibitors were selected as competitors against TAMRA-FP. Each competition experiment was carried out as follows. Competitors were preincubated in increasing concentrations (0-500 μM) with *L. mexicana* promastigote lysates (1 mg/mL) for 60 minutes before addition of TAMRA-FP (1mM) probe and incubation for further 15 minutes. Subsequently, the samples were run on SDS-PAGE and the gels analysed

by fluorescence imaging. The experiments were done with biological replicates (x3) and fluorescent curves were constructed analysing the intensity volumes of the bands and standardized with values relative to the control measurement (no competitor).

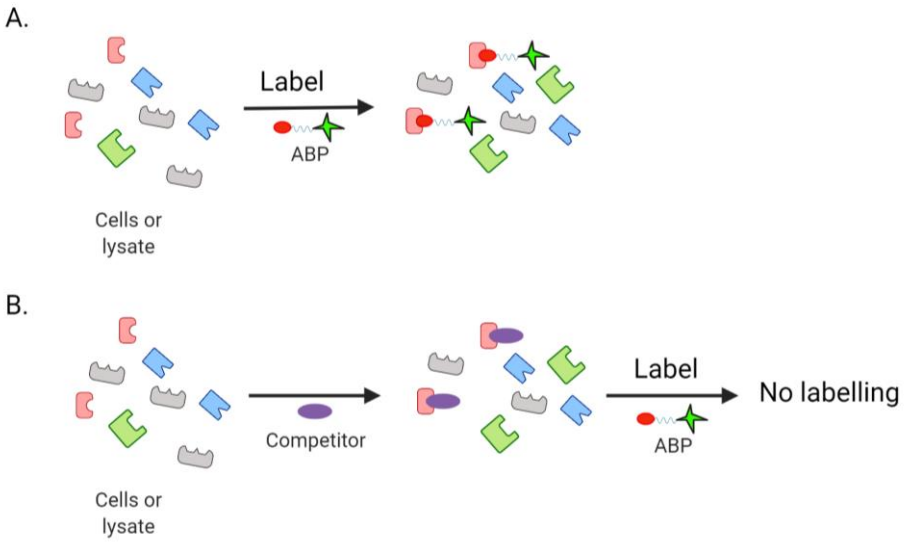

Figure 2.13. Traditional ABPP labelling (A) and competitive ABPP (B). In a competitive fashion, a potential competitor is added to the whole cells or tissue homogenates and incubated for a specific amount of time prior to the addition and further incubation of the ABP. Competition is confirmed by a decrease in the fluorescent intensity of the labelled bands.

2.4.1 Competition with chymostatin

Chymostatin (Figure 2.14 A) is a reversible inhibitor of several proteases, including chymotrypsin, papain, chymotrypsin-like serine proteinases and chymases. In mammalian cells, it is effective at a final concentration of 10 to 100 μM. Interestingly, when we used chymostatin as a competitive agent, we observed a significant reduction in two important signals present in the *L. mexicana* promastigote serinome at approximately 80 and 55 kDa (Figure 2.14 B, bands 1 and 2, lanes 2 to 7). These

findings reinforce the hypothesis discussed in section 2.3.2, where we suggested that these bands correspond to proteases POP and carboxypeptidase.

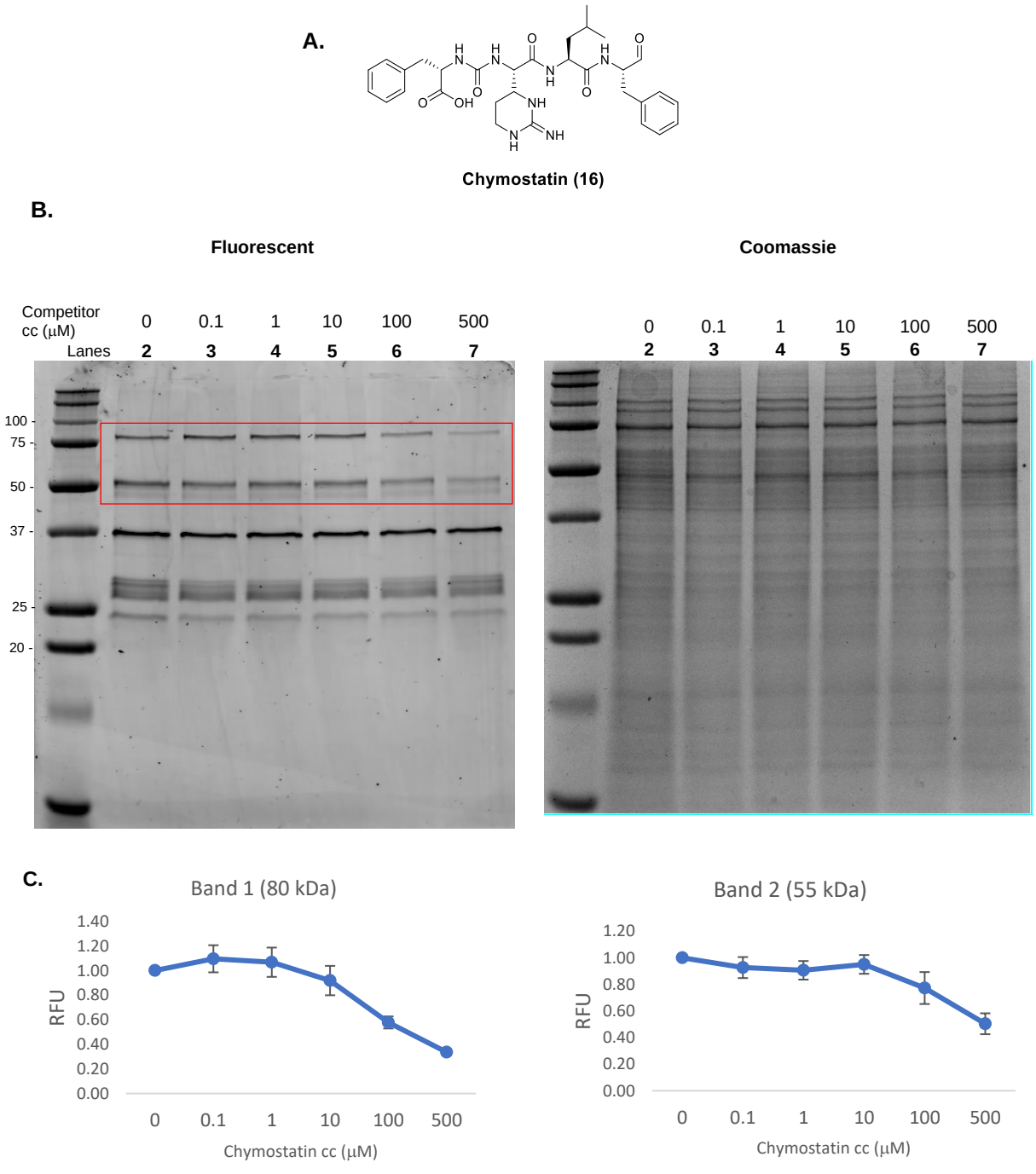

Figure 2.14. A) Structure of Chymostatin (**16**). **B)** Competitive ABPP between serine protease inhibitor Chymostatin and TAMRA-FP. *L. mexicana* lysates (1 mg/mL) were incubated for 1 h with increasing

concentrations of chymostatin (0-500 μM) (lanes 2-7) prior the addition of TAMRA-FP (1 μM) and further 15 min incubation. **C)** Relative fluorescence units (RFU) vs competitor concentration inhibition curves of bands 1 (80 kDa) and 2 (55 kDa).

Competition using other known commercially available serine inhibitors such as Dabigatran BIBR 953 (CAS 211914-51-1) which inhibits proteases like thrombin, trypsin, plasmin, among others; Antipain (CAS 37691-11-5) which interacts with trypsin-like proteases or Camostat mesylate (CAS 59721-29-8), with similar affinity as dabigatran (figure 2.15 A) failed to modify the labelled enzymes suggesting that these do not interact with the serine hydrolases labelled with TAMRA-FP (figure 2.15 B).

A.

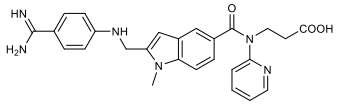

Dabigatran (17)

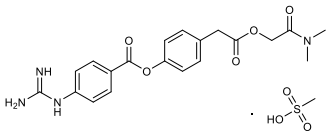

Camostat (18)

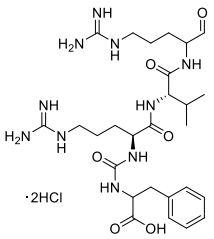

Antipain (19)

B.

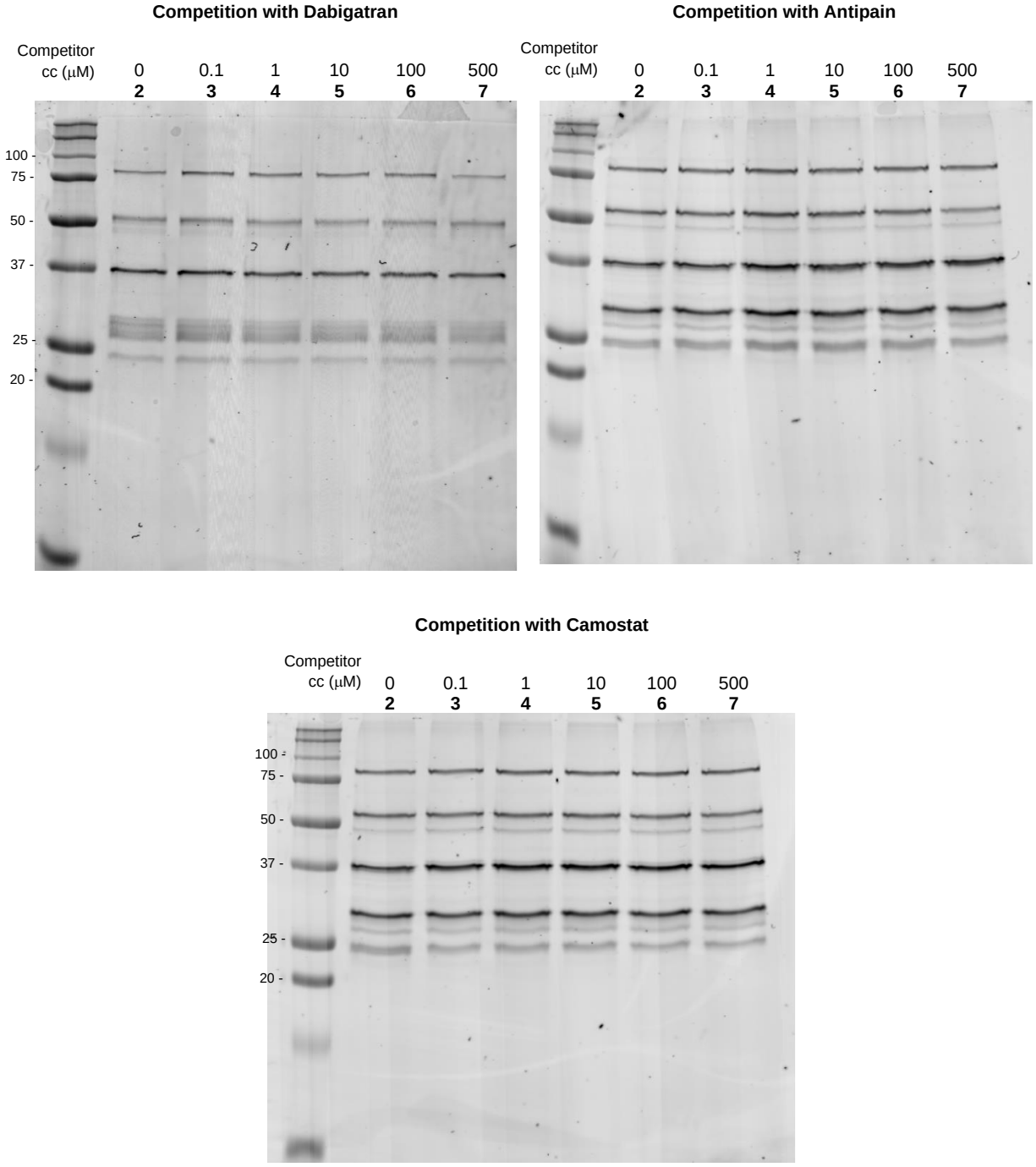

Figure 2.15. A) Structures of protease inhibitors Dabigatran BIBR953 (**17**), Antipain (**18**) and Camostat (**19**). **B)** In-gel fluorescence analysis of the competitive ABPP between increasing

concentrations of serine protease inhibitors (0-500 μM) and TAMRA-FP (1μM) in *L. mexicana* promastigote lysates (1 mg/mL).

2.4.2 Competition with Z-ProProlinal

After identifying POP from the gel-free experiments, it was decided to explore inhibitors of prolyl oligopeptidase (POP) LmxM.36.6750. Z-ProProlinal (ZPP) (**20**) (Figure 2.16 A), a protected modified dipeptide, is a potent, and known reversible inhibitor of POP.[112] It was recently used by Lasse *et al.*[107] to inhibit recombinant prolyl oligopeptidase of *L. infantum* (rPOPLi) expressed in *Escherichia coli*. Consequently, when ZPP was used in a competitive fashion to test its inhibition capacity in a proteome, complete inhibition was observed at 10 pM (Figure 2.16 B, lane 3), confirming a high specificity towards POP LmxM.36.6750 even in a complex protein environment. As previously mentioned in section 2.3, ZPP was previously proven to impair infection of murine macrophages by *L. infantum* (IC_{50} 4.2 nM),[107] making POP a potential druggable therapeutic target.

A.

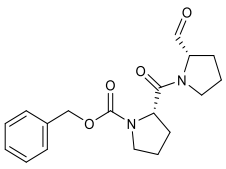

Z-Pro-Prolinal (20)

B.

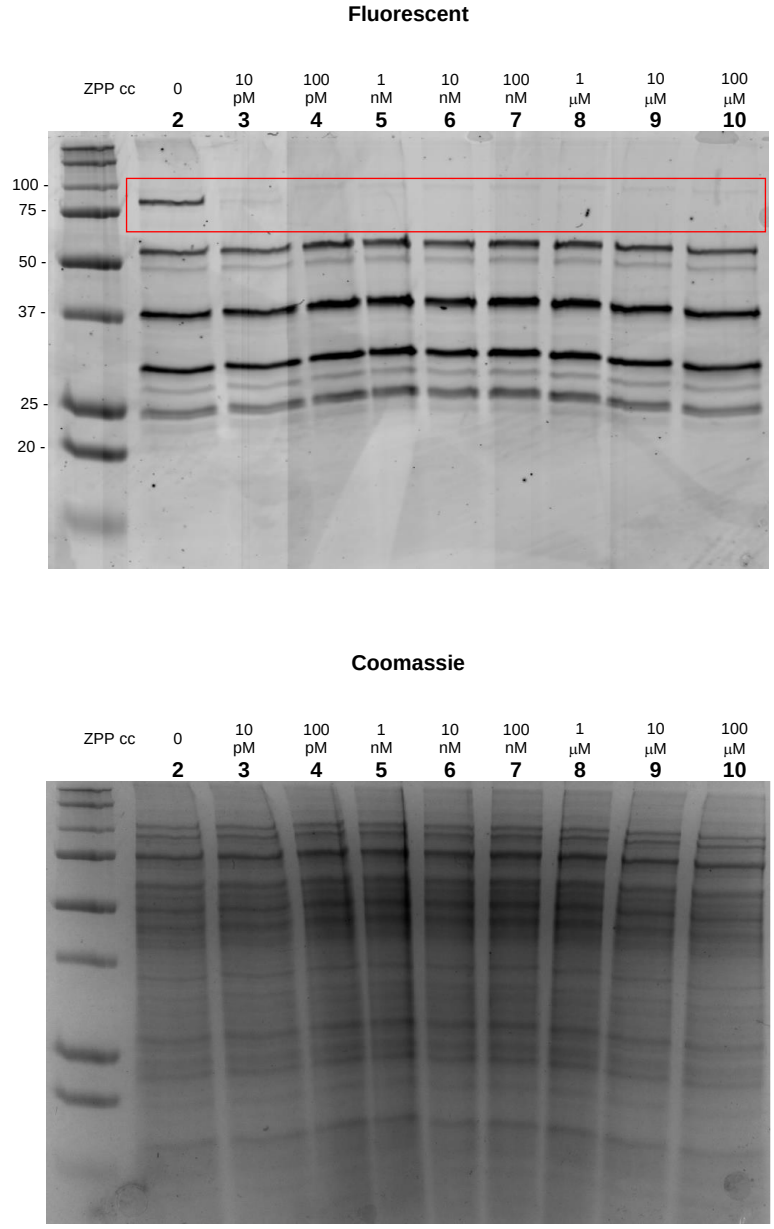

Figure 2.16. A) Structure of ZPP **B)** In-gel fluorescence analysis of the competitive ABPP between increasing concentrations of POP inhibitor ZPP (0-100 μM) and TAMRA-FP (1μM) in *L. mexicana* promastigote lysates (1 mg/mL).

2.5 Cell viability to serine protease inhibitors

Having successfully inhibited POP and carboxypeptidase using chymostatin and ZPP, we decided to further explore whether these enzymes are essential for the survival of

the parasites (both promastigotes and axenic amastigotes) as well as the inhibitors' capacity to compromise parasite survival. For this, we performed the Resazurin cell viability assay, which allows us to determine the 50% inhibitory concentration (EC_{50}) of selected inhibitors. Resazurin is metabolized by the mitochondria into resorufin, which is fluorescent thus allowing indirect viability calculations. Consequently, *L. mexicana* parasites (1×10^5 promastigotes /1×10^6 axenic amastigotes) were added per well to a 96-well plate and incubated with increasing concentrations of each inhibitor for 44 h at 26 ºC. This was followed by addition of Resazurin and incubation for a further 4 h at 26 ºC. Cell viability was measured by fluorescence, and EC_{50} values were obtained by GraphPad data analysis (General procedure 5.2.1.17) with clemastine[113] used as a positive control.

When *L. mexicana* promastigotes and axenic amastigotes were dosed with ZPP (0-100 μM), no biological activity nor morphological changes were observed. In contrast, when chymostatin was used, the calculated EC_{50} was 28 ± 5 nM, which demonstrates this compound to be highly potent against this species. Compared to the competitive assay previously described (Figure 2.14 C, section 2.4.1), where POP and carboxypeptidase were inhibited with chymostatin (over 1 and 10 μM respectively), the EC_{50} value obtained here is significantly lower. Therefore, it was hypothesized that chymostatin may be acting on other essential proteases that are not revealed with the TAMRA-FP probe. Additionally, when the experiments were repeated using *L. mexicana* axenic amastigotes, similar results were obtained for both chymostatin (EC_{50} 23 ± 5 nM), and ZPP (no effect) (Figure 2.17).

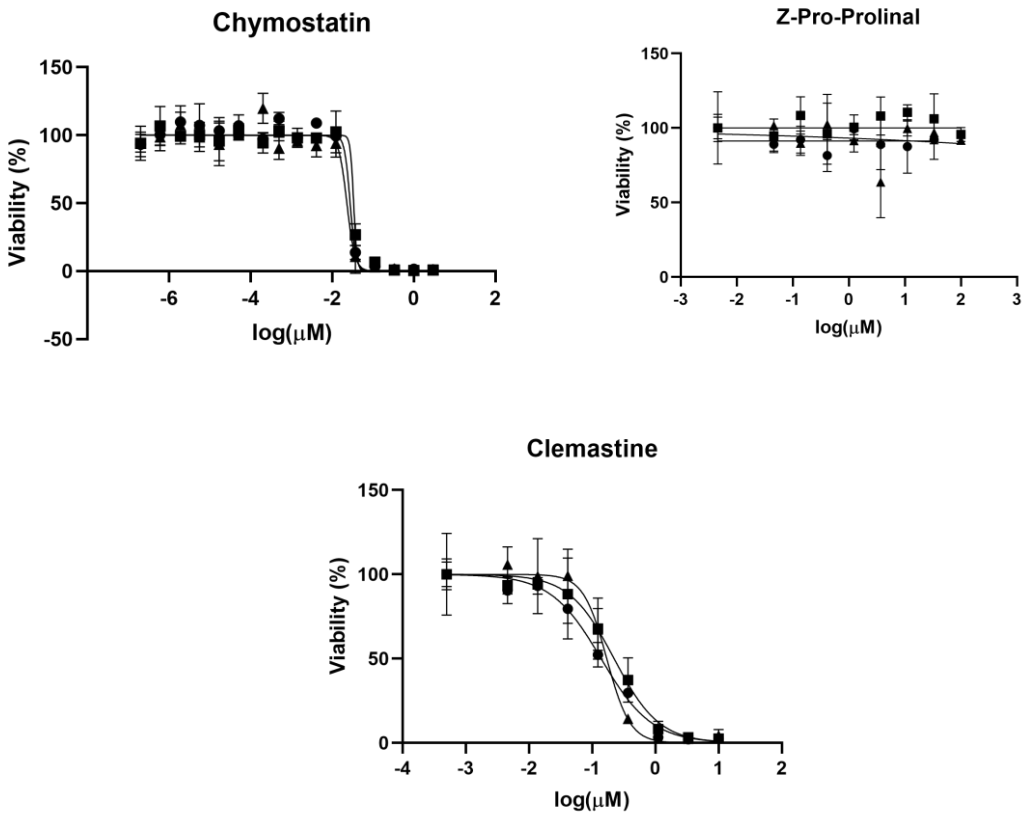

Figure 2.17. EC_{50} curves of chymostatin (EC_{50} 28 ± 5 nM for promastigotes and 23 ± 5 nM in axenic amastigotes), ZPP and clemastine (EC_{50} 177 ± 42 nM for promastigotes and 66 ± 13 nM in axenic amastigotes) against *L. mexicana* promastigotes. These results are the mean and standard deviation of three independent experiments (● (X1), ■ (X2) and ▲ (X3), which are shown individually in each graph. For each species, clemastine was used as a positive control.

The high potency observed with chymostatin, is a promising result as it suggests that it might be targeting an enzyme vital for the parasite survival. Moreover, chymostatin EC_{50} values in HeLa cells were reported to be over 3 orders of magnitude higher than for *L. mexicana* parasites (a concentration of 100 mM produced 10 ± 4 % of cytotoxicity).[114]

2.6 Conclusions

The results presented demonstrated how ABPP can be successfully used to profile enzymes of interest for target discovery. Using the commercially available probe TAMRA-FP, comprehensive first serinome profiles of Old-World *L. major* and New-World *L. mexicana* and *L. amazonensis* species throughout different stages of their life cycle were obtained using fluorescent in-gel visualization. The plasticity and divergence of the proteome becomes evident when comparing the SHs landscapes obtained between the *Leishmania spp*, particularly if the comparison is made between New-World and Old-World species. Moreover, these enzyme fingerprints provided insights on how the expression levels of these enzymes change as they progress through their life cycle.

Target discovery using iTRAQ, allowed the identification of serine proteases carboxypeptidase LmxM.18.0450, prolyl oligopeptidase LmxM.36.6750 and serine lipase lysophospholipase LmxM.24.1840. Although in-gel labelling does not provide information about the integrity of the labelled enzymes, a comparison between the results obtained between both in-gel and gel-free ABPP, suggests that probably more enzymes should had been identified using a MS approach. This hypothesis is supported since several defined bands were observed in-gel using TAMRA-FP, and no labelling was observed after competition with FP-biotin. In consequence, the experiment should be repeated.

Competitive assays identified chymostatin as an inhibitor of POP and carboxypeptidase. In addition, cell viability assays demonstrated its high potency and capability to compromise parasite survival in *L. mexicana* promastigotes (EC_{50} 28 ± 5 nM) and axenic amastigotes (EC_{50} 23 ± 5 nM). These values are surprisingly lower

than those reported from current available drugs such as miltefosine on *L. amazonensis* promastigotes (47.0 ± 3.9 μM)[115] or with antimonials on *L. major* ([Sb(III)] EC_{50} 4.3 ± 0.3 μM, [Sb(V)] EC_{50} 44 ± 6 μM)[116]. Altogether, in addition to the low EC_{50} values reported in HeLa cells, these results could position chymostatin as a potential hit compound. Although, to validate it as a hit compound, additional assays such as cytotoxicity determination and intracellular amastigote tests are needed. More importantly, new probes should be developed to use in competitive assays to determine the target enzyme. Finally, due to its peptidic nature, its metabolic stability could pose a concern. In consequence, pharmacokinetics and pharmacodynamics profiles need to be further addressed.

When the *L. mexicana* promastigote serinome was treated with ZPP, a very high selectivity was observed at 10 pM against prolyl oligopeptidase (POP) LmxM.36.6750. When compared to the TAMRA-FP labelling, selectivity was confirmed by the fact that no other bands were inhibited even at higher concentrations such as 100 μM, albeit interaction with other enzymes not labelled by TAMRA-FP cannot be discarded. In addition, it has been reported that ZPP prevents the invasion of *L. infantum* in murine macrophages meaning that this serine protease could be acting in the host invasion processes. Hence, prolyl oligopeptidase could be considered a virulence factor that could offer a potential access port for the design of new drugs against this protozoan.

Despite these promising results, there are limitations with the TAMRA-FP probe. As most ABPP workflows are carried out using tissue homogenates, where proteins are removed from their native cellular environments. As the function of an enzyme is often tied to the presence of inhibitors/activators as well as protein-protein interactions, the alterations produced during cell lysis could produce inactivation of enzymes and loss of binding affinity between the probes and the target enzymes. Therefore, *in vitro*

proteomic preparations can only approximate the functional state of proteins in a living cell or organism. As TAMRA-FP contains a bulky and charged tag, it cannot go through membranes, making it unfit for *in vivo* labelling.

Moreover, in this biological context, its affinity was shown to be not as broad as expected, as in-gel labelling revealed fewer enzymes than the predicted by *in-silico* studies conducted in this group where 28 SPs were identified,[b] in addition to the competitive ABPP assay, where TAMRA-FP failed to label all the chymostatin target enzymes, suspected to be serine proteases. To address this challenge, cell permeable probes are required, containing warheads with different reactivities to fine tune their affinities towards SHs and capable to be used in *in vivo* conditions. These studies will be addressed in the following chapter.

[b] The *in-silico* studies were conducted by Dr Exequiel O. J. Porta.

3 Expanding the Serine Hydrolase universe

3.1 Introduction

As discussed above, the use of the commercial probe TAMRA-FP presented limitations when attempting to label the serine hydrolase family. It has been known as a common limitation when using ABPs with large and bulky reporter tags, that limit probe uptake and distribution in cells.[117] This has been successfully addressed by replacing the tag with an alkyne handle in the probe with subsequent attachment of the tag using bioorthogonal Cu catalysed cycloaddition (click chemistry). [67,69,117]

Another limitation we observed, was the low binding affinity observed in our biological context. Consequently, to address these issues and with the objective of fine tuning the affinity of fluorophosphonate probes in an attempt to target new enzymes not labelled with TAMRA-FP, new activity-based probes need to be devised. Therefore, it was decided to focus on 3 sets of probes: aromatic fluorophosphonate (aryl-FP), alkyl fluorophosphonate (alkyl-FP) and benzylic fluorophosphonate (benzyl-FP) probes with the objective of varying the electrophilic character of the phosphorus as well as the global electronic and steric environments of the warheads.

3.2 Activity-based Probes strategy

Simple modular synthetic pathways were devised for these probes consisting of the synthesis of the warhead, the synthesis of the linker and its attachment to the warhead and then concluding with the fluorination of the linker-warhead intermediate. The fluorination of the warhead was conducted last as the reactivity of the fluorophosphonate would interfere with the other synthetic steps (Figure 3.1).

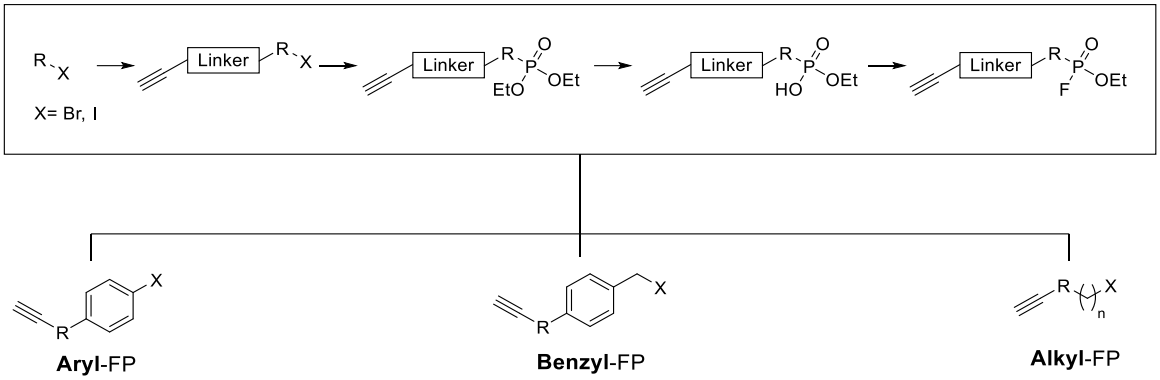

Figure 3.1. General synthetic strategy ABPs. Initially, linkers are attached to the warhead, prior or after the conversion of the alkyl, benzyl or aryl halide to the phosphonate moiety followed by sequential phosphonate hydrolysis and fluorination to produce the desired probes.

3.2.1 Warhead synthesis

3.2.1.1 Aryl FPs

The initial set of FP probes prepared contained an aryl phosphonate. As shown in figure 3.2, three main options with electronically different patterns were proposed: fluorophosphonates with an aromatic electron donor group; with an aromatic neutral group and with an aromatic electron withdrawing group. The objective of this set was to analyse the effect in specificity of the warheads when changing the electrophilicity of the phosphorus atom.

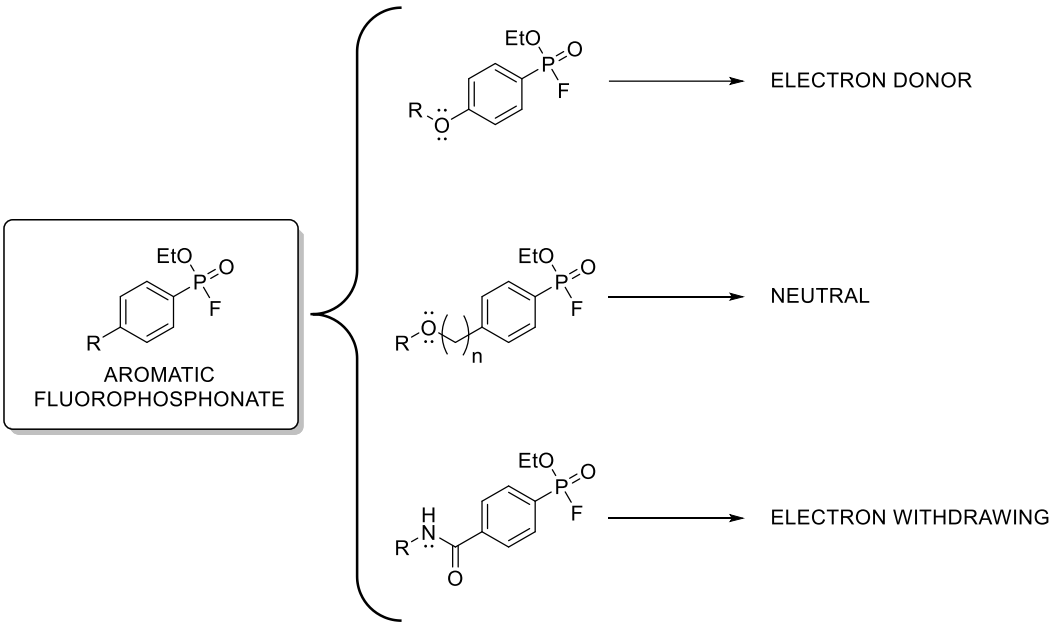

Figure 3.2. Aryl fluorophosphonate warheads with different electronic character provided by electron donor, neutral and electron withdrawing binding groups.

Initially a simple tolyl moiety was used as a model substrate. A search of the literature revealed the possibility to form the C-P bond using a Michaelis-Arbuzov type reaction (Scheme 3.1).[87]

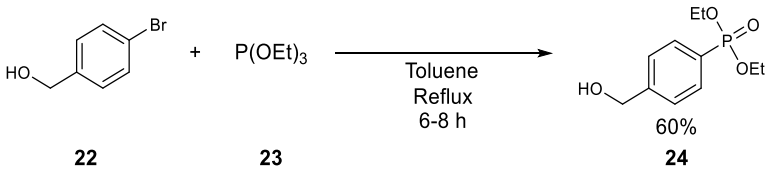

Scheme 3.1. Michaelis Arbuzov type reaction reported by Suresh Reddy *et al*.[118]

Whilst attractive as a single step process, this report was unusual as it is mechanistically improbable that the reaction could proceed through a standard S_N1, S_N2 or S_NAr nucleophilic substitution pathway. Consequently, the exact literature

conditions were repeated (Scheme 3.2) and as suspected, all attempts to reproduce this transformation failed to deliver any of the desired product **26**.

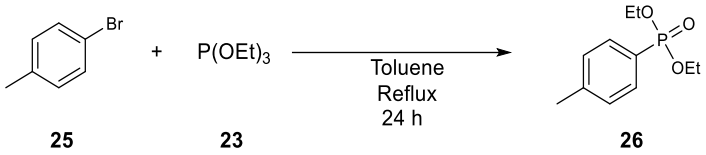

Scheme 3.2. Synthesis of diethyl 4-methylphenylphosphonate **26** via Arbuzov reaction.[118]

To verify the Arbuzov conditions, a similar reaction was then attempted starting with the commercially available benzyl halide **27** which afforded the expected benzylic phosphonate in good yield (72%). Evidence of formation of **28** was confirmed from analysis of the ^{1}H NMR spectrum in which the 2 benzylic protons were observed as a doublet at 3.07 ppm with a $^{2}J_{H\text{-}P}$ coupling constant of 21.7 Hz instead of the singlet observed at 4.44 ppm of **27** and the proton decoupled ^{31}P NMR spectrum, showing a single signal at 16.3 ppm as a singlet, instead of the characteristic signal at 138.76 ppm of **23**. In addition, the LCMS spectrum contained the peaks m/z= 307.1 [M(^{79}Br)+H]$^{+}$ and 309.1 [M(^{81}Br)+H]$^{+}$; consistent with a benzylic phosphonate (Scheme 3.3).

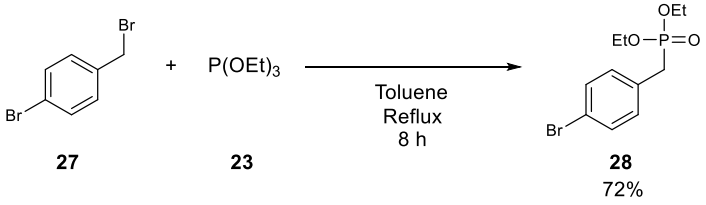

Scheme 3.3. Synthesis of diethyl (4-bromobenzyl)phosphonate (**28**).

With the failure of the Arbuzov approach to deliver an aromatic C-P bond, alternative methods to generate the desired C-P bond were carried out.

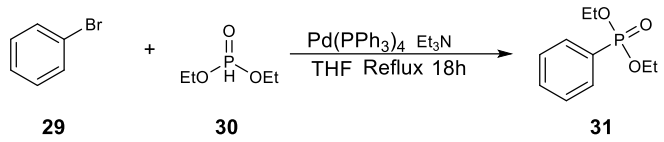

29 **30** **31**

Scheme 3.4. Palladium catalysed cross-coupling reaction reported by Stawinski *et al.*[119]

Based on a report by Stawinski *et al.* (Scheme 3.4), using similar aryl bromide starting materials, a Hirao palladium catalysed cross-coupling reaction was attempted.[119] Here, aryl bromide **25** was treated with diethyl phosphite **30** in the presence of $Pd(PPh_3)_4$ and Et_3N in dry THF at reflux temperature for 18 hours, however, little product formation (**26**) was observed (Scheme 3.5).

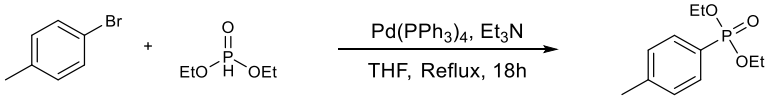

25 **30** **26**
N.R.

Scheme 3.5. Synthesis of the tolyl phosphonate **26**.

Consequently, different conditions to those reported in the literature were tested until the desired product **26**, could be obtained following conditions reported by Goosen *et al.*[120] (Scheme 3.6). This involved using the more polar solvent EtOH, $Pd(OAc)_2$ as a catalyst, PPh_3 as ligand and a sterically crowded tertiary amine i.e., *N,N*-dicyclohexylmethylamine. Evidence for the formation of **26** was confirmed after analysis of the proton decoupled ^{31}P NMR spectrum, which displayed a single signal

at 19.6 ppm while LCMS spectrum contained a peak of m/z= 228.9 $[M+H]^+$, consistent with the molecular mass of **26**.

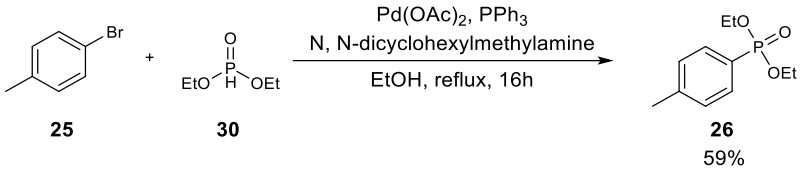

25 **30** **26**
59%

Scheme 3.6. L. Goosen optimized palladium catalysed cross-coupling reaction.

3.2.1.1.1 Synthesis of electron donor phenolic phosphonate probes

With conditions for the C-P cross-coupling reaction enhanced, the synthesis of the first warhead **33**, was attempted starting from commercially available 4-bromophenol **32**. The same conditions were used as for the synthesis of **26**, leading to the phosphonate in 61% yield (Scheme 3.7A). However, when the same reaction was scaled up, lower yields were obtained. A further review of the literature of Hirao cross-coupling conditions suggested that addition of acetate could increase the reaction rate as this anion could prevent the formation of the deactivating complex formed between $Pd(OAc)_2$ and diethyl phosphite and consequently, favour the formation of $Pd^0(PPh_3)_2(OAc)^-$, a reactive species involved in the oxidative addition step.[119] Following this precedent, KOAc was added to the reaction mixture whilst maintaining the other parameters unchanged (Scheme 3.7B). This change in the conditions resulted in an improved yield of 90% being obtained after 86h. Evidence for the formation of **33** was confirmed from analysis of the ^{31}P NMR spectrum where it was possible to observe a single signal at 21.1 ppm supported by the LCMS analysis which

contained the peaks m/z= 231.1 $[M+H]^+$ and 461.2 $[2M+H]^+$ expected for phosphonate **33**.

A.

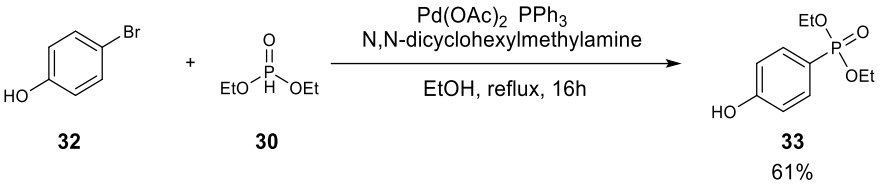

B.

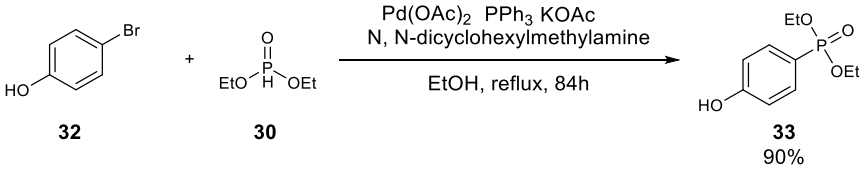

Scheme 3.7. **A)** Synthesis of Diethyl(4-hydroxyphenyl)phosphonate using Goosen *et al.* conditions.[120] **B)** Optimized conditions by addition of KOAc.[119,120]

3.2.1.1.2 Synthesis of electron donor biphenyl phosphonate warhead

Having successfully identified an efficient process to form the phosphonates, it was then decided to use this to generate a biphenyl warhead to explore the effect of steric bulk. This was of interest because it enables further comparison and characterization of ABP-enzyme interactions and affinities of two probes with similar warheads. It was also observed that a variety of biphenyls could be generated through a Suzuki-Miyaura cross-coupling reaction from the corresponding triflate **34** and a phenyl boronic acid **35** (Scheme 3.8).

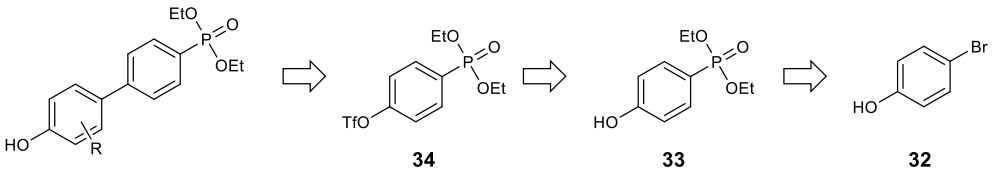

Scheme 3.8. Retrosynthetic path to obtain biphenyls from the aryl halide.

The first requirement was to obtain the triflate. Initial attempts involved the addition of triflic anhydride to a solution of the phenol phosphonate and pyridine in anhydrous DCM at 0°C (Scheme 3.9). These reaction conditions afforded the desired product albeit only in low yield (48%) when compared with similar results reported in the literature by J. Huffman *et al.* (91-99%).[121] Nevertheless, formation of **34** was confirmed by combining the information gathered from the IR spectrum, which did not contain the characteristic signal of the -OH group. In addition, the presence of only one signal in the ^{19}F NMR spectrum at -72.8 ppm and an LCMS spectrum with a peak at m/z= 363.2 $[M+H]^+$ were consistent with the desired product.

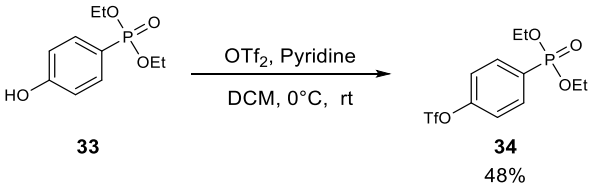

Scheme 3.9. Synthesis of 4-(diethoxyphosphoryl)phenyl (**34**).[121]

Attempts to optimize the yield proved to be surprisingly challenging and ultimately unsuccessful. Notably, different reaction times were tested which revealed that if left

for an extensive amount of time, no product could be observed (LC-MS) suggesting that the product is unstable under the reaction conditions.

With the triflate **34** in hand, the Suzuki reaction to form the biphenyl phosphonate warhead was attempted. As many conditions could be found in the literature, but none with this specific system, general conditions were used. Here, the triflate phosphonate **34** was reacted with phenyl boronic acid **35** in the presence of $Pd(OAc)_2$, SPhos, KF in THF:H_2O (4:1) for 2 h, at rt. Unfortunately, formation of the desired biphenyl **36** was not observed. After some optimization it was found that increasing the reaction temperature to 40°C and extending the reaction time allowed **36** (Scheme 3.10) to be isolated in moderate yield. Confirmation of the product identity was observed from the lack of signals in the ^{19}F NMR spectrum and the presence of peaks at m/z 307.3 $[M+H]^+$, and 613.4 $[2M+H]^+$ in the LCMS consistent with the product molecular mass.

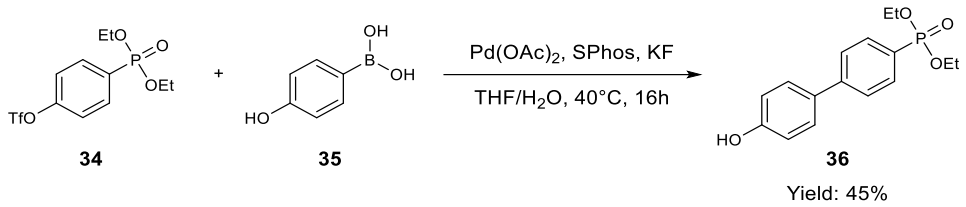

Scheme 3.10. Suzuki cross-coupling reaction to obtain diethyl 4'-hydroxy-[1,1'-biphenyl]-4-ylphosphonate (**36**).[122]

In general, the desired biphenyl phosphonate **36** was obtained in three steps with an overall yield of 19% (Scheme 3.11).

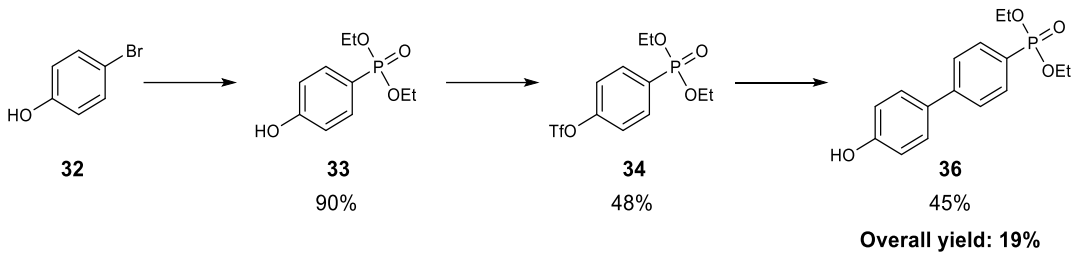

Scheme 3.11. Synthetic pathway to obtain **36**.

An alternative, simpler but less flexible approach to obtain **36** which uses the commercially available biphenyl phenol halide **37** to directly obtain the phosphonate via the Hirao cross-coupling conditions was attempted. Starting from this biphenyl, **36** was obtained in 31% yield (Scheme 3.12). Several attempts to optimize the reaction testing different solvents, reaction times, reactant equivalents and ligands did not improve this outcome. In addition, in most of these attempts about 50% of **37** was recovered indicating that the conversion was very low. The highly conjugated system present in the starting material could be a possible explanation for its low reactivity and poor yield observed.

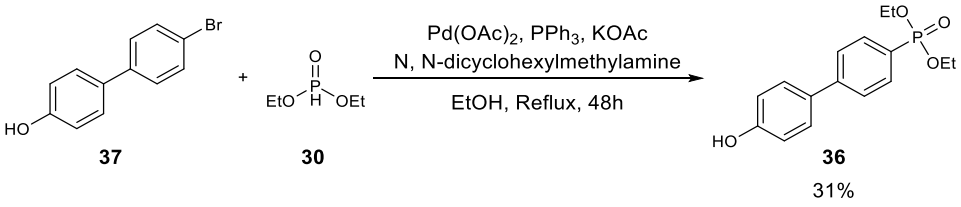

Scheme 3.12. Synthesis of diethyl 4'-hydroxy-[1,1'-biphenyl]-4-ylphosphonate (**36**).

Once the phenyl and biphenyl warheads were obtained, the next step was the attachment of the linker through a Williamson etherification. The reaction conditions

were taken from a literature report by Banday *et al.*[123] as they had described similar reactions using phenols and alkyl halides as starting materials. Consequently, this demanded the use of alkynyl bromide **39**. The synthesis was then explored via two different literature paths. The first, reported by Sharma *et al.*[124] (Scheme 3.13) was a classic bromination in which hexynol **38** was treated with phosphorus tribromide, in anhydrous Et_2O at 0°C for 4 hours. The high volatility of **39** in addition with the fact that different purification methods were attempted until the product was obtained, resulted in a poor yield (6%) in comparison with the reported yield. The second method, an Appel reaction was attempted. **39** was obtained but despite the efforts made to reproduce the results reported by Baughman *et al.*[125] (Scheme 3.13) in which **38** was treated with CBr_4, and PPh_3 in anhydrous DCM, the purification methods failed as it was not possible to separate it from $CHBr_3$ and PPh_3. In best case, evidence of formation of **39** was confirmed after observation of the ^1H NMR spectrum through a triplet being observed at 3.37 ppm, consistent with $-CH_2-Br$ rather than $-CH_2-OH$ protons coupled with the lack of characteristic band for an alcohol in the IR spectrum.

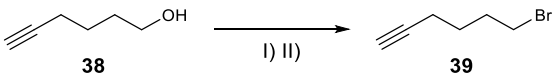

38 **39**

Scheme 3.13. Two different methods to obtain Bromohex-1-yne (**39**): I) Classic bromination using PBr_3 in Et_2O (6%) and II) Appel reaction using CBr4, PPh3 in DCM.

Ultimately, the difficulties in identifying the alkyl bromide **39** by TLC or MS coupled with its volatility and purification difficulties (distillation and chromatography proved to be non-viable) made this reaction a challenge and the tosylate **40** was then considered

as an alternative. This could be simply prepared using the conditions reported by Davison *et al.*[126] (Scheme 3.14).

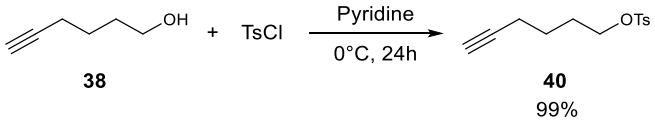

38 **40**
99%

Scheme 3.14. Reported synthesis by Thompson *et al.*[126]

Therefore, alcohol **38** was reacted with TsCl, using pyridine as a base at 0°C. Loss of the -OH band in the IR spectrum and molecular ion peaks at m/z= 253.3 $[M+H]^+$ and 527.3 $[2M+Na]^+$ in the LCMS spectrum were consistent with the proposed structure of **40** (Scheme 3.15).

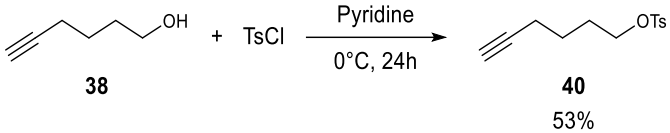

38 **40**
53%

Scheme 3.15. Synthesis of 5-tosylhex-1-yne.

Once the linkers where synthesized, in all cases, the phenols **33** (Scheme 3.16 A and B) and **36** (Scheme 3.16 C) were pre-treated with potassium carbonate as the base in anhydrous acetone with the subsequent addition of the alkyne halides (**39** and **41**) or the tosylate (**40**). As observed in Scheme 3.16 B, the addition of TBAI in catalytic amounts (10 mol%) resulted in a significant yield improvement for the reaction of alkyl phenyl ether **43**.

A.

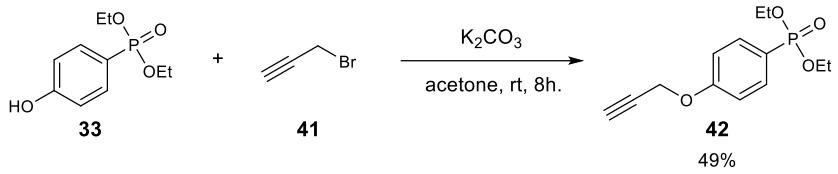

B.

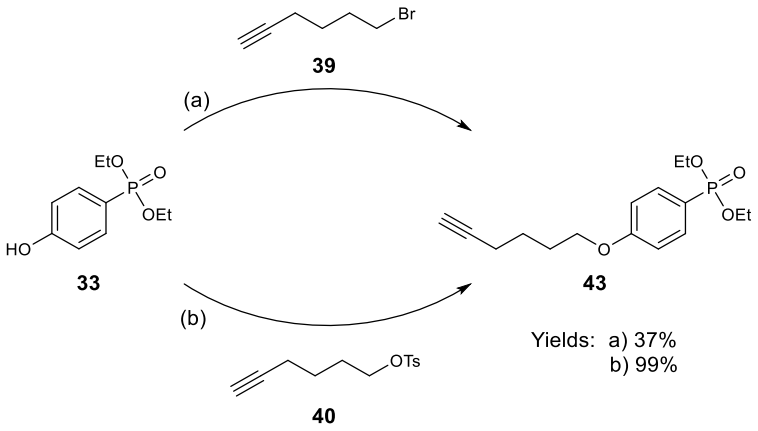

a) K_2CO_3, acetone, rt, 8h.

b) K_2CO_3, Bu_4NI, dry acetone, rt, 36h.

C.

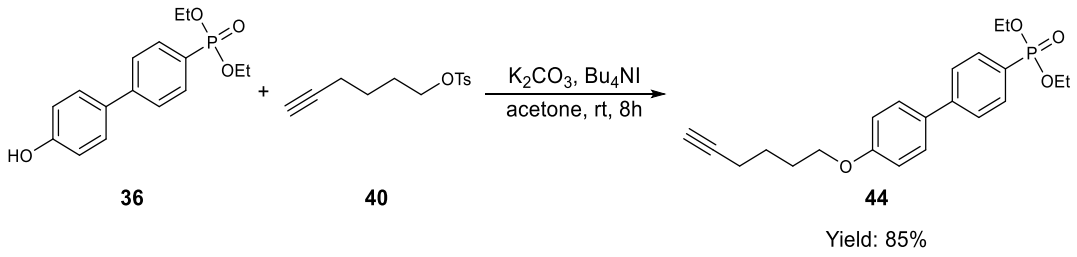

Scheme 3.16. A) Synthesis of diethyl [4-(prop-2-yn-1-yloxy)phenyl]phosphonate (42). **B)** Synthesis of diethyl 4-(hex-5-yn-1-yloxy)phenylphosphonate (43). **C)** Synthesis of diethyl [4'-(hex-5-yn-1-yloxy)-[1,1'-biphenyl]-4-yl]phosphonate (44).

In all 3 molecules, **42**, **43** and **44**, evidence of product formation was confirmed by the loss of the -OH bands in IR spectra, combined with ^{1}H NMR spectra containing the characteristic triplet signals (with relative integrals of 1) for the alkyne protons at δ 2.53 for **42**, δ 1.94 for **43** and δ 1.96 for **44** and ^{31}P NMR spectra contained only single signals consistent with the phosphonate phosphorus atoms: δ 19.2, δ 19.8 and δ 19.2 for **42**, **43** and **44**, respectively**.**

To better explore the effects on specificity and click reaction performance whilst varying the length of the linker, a 3rd probe was devised using warhead **33** in which the linker chain was further extended. The initial synthetic route consisted of amide coupling between 6-amino-1-hexanol (**45**) and 5-hexynoic acid, followed by tosylation of the alcohol as previously described and concluding with the etherification with the phenolic warhead **33**. Amide coupling using general conditions with EDC.HCl and DMAP in DCM failed to deliver the desired product so the sequence of the synthesis was altered. Consequently, **45** was combined with Boc_2O in DCM for 12 h at rt to afford the protected amine **46** in very good yield. From the ^{13}C NMR spectrum it was possible to observe the carbamate carbonyl at δ 156.1, supported by the LCMS analysis which contained the peak m/z 240.38 $[M+Na]^+$ consistent with the product's mass. Using Cerutti *et al.*[127] conditions, **46** was treated with TsCl, Et_3N and catalytic amounts of DMAP in DCM for 12 h at rt which delivered **47** in 78% yield (Scheme 3.17).

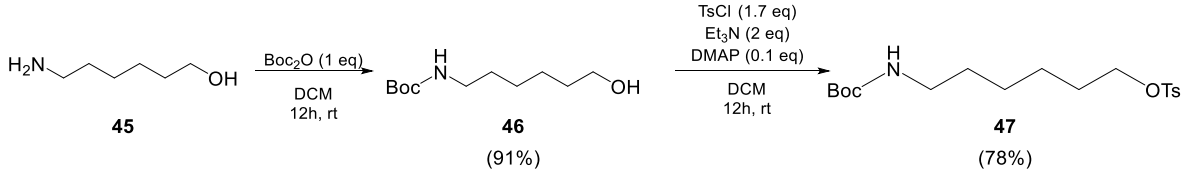

Scheme 3.17. Synthesis of linker **47**.

After, tosylate **47** was attached to warhead **33** as before to afford the desired phenolic ether **48** in 72% yield. Subsequent Boc deprotection using HCl in dioxane followed by amide coupling with 5-hexynoic acid**,** using EDC.HCl as coupling reagent and DMAP in DCM for 24 h at rt afforded the non-activated probe **49** in 31% yield. Evidence of product was observed in ^{13}C NMR spectrum, where the signal corresponding to the carbamate carbonyl group shifted from δ156.1 to δ172.3, a region where carboxylic amides are observed. Additionally, the peaks m/z 424.4 $[M+H]^+$ and 869.6 $[2M+Na]^+$ in the LCMS were present in the spectrum (Scheme 3.18).

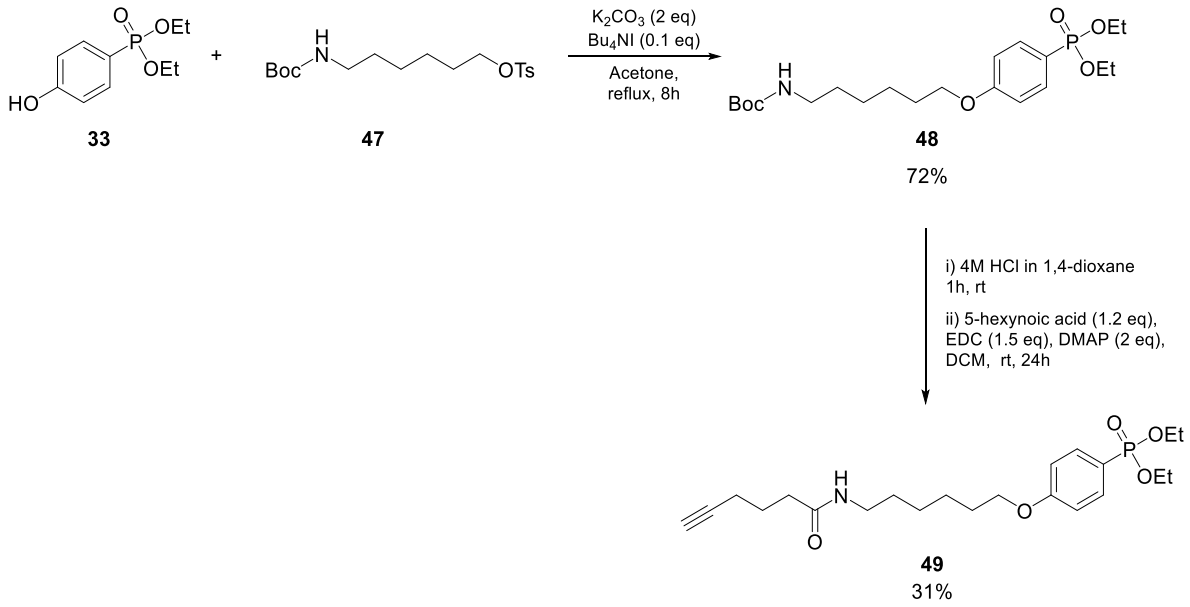

Scheme 3.18. Linker attachment to **33** to afford diethyl (4-{[6'-(hex-5''-ynamido)hexyl]oxy}phenyl)phosphonate (**49**).

3.2.1.1.3 Synthesis of a neutral aryl phosphonate warhead

To generate a neutral warhead, we reasoned that aryl phosphonate **50** could be selectively obtained from 4-bromobenzyl bromide (**27**), while keeping the benzyl halide position available for subsequent etherification with the linker. Consequently, to test

the selectivity of the Hirao coupling reaction, **27** was treated under the same conditions as before (Scheme 3.19). Unfortunately, this reaction was not viable due to a competing reaction at the sp^3 C-Br site giving undesired by-products (**28** and **51**), as confirmed by analysis of the LCMS spectrum of the crude reaction mixture.

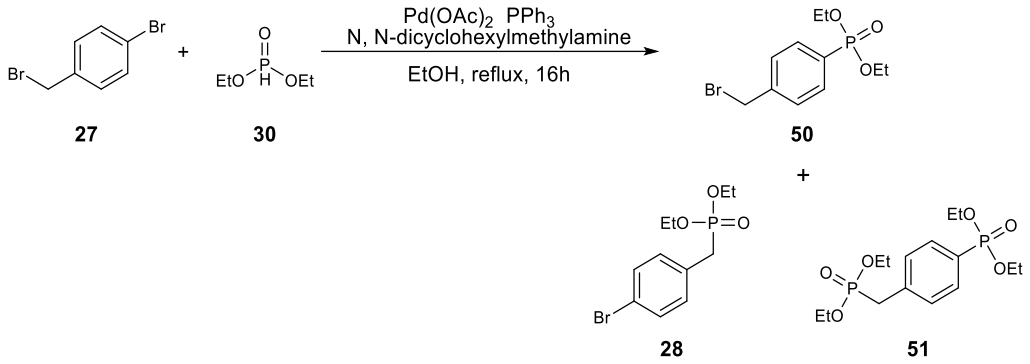

Scheme 3.19. Hirao coupling synthesis of **50**.

Another approach to obtain **50** was to create the benzylic C-Br bond using a free-radical bromination of tolylphosphonate **26**. Consequently, conditions proposed by Ha *et al.*[128] were first tested using **25**, as a simpler starting material which was treated with NBS and AIBN in anhydrous CCl_4 for 4h at reflux temperature (Scheme 3.20). Evidence of formation of **27** was obtained from ^{1}H NMR analysis showing a singlet at 4.4 ppm, characteristic of the benzylic protons in **27**.

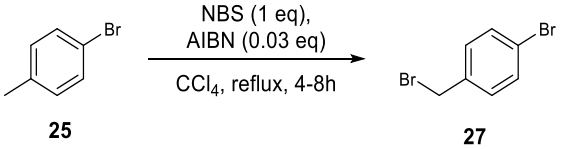

Scheme 3.20. Synthesis of 4-Bromobenzylbromide **27**.

Having tested the conditions, the reaction was repeated starting with the phosphonate **26** and **50** was obtained in 15% yield (Scheme 3.21). Evidence for the formation of **50** was provided by ^{1}H NMR analysis where the spectrum showed a singlet integrating for two protons at 4.46 ppm, characteristic of the benzylic protons in addition to 1:1 molecular ion peaks of m/z 307.2 [M(^{79}Br)+H]$^{+}$ and 309.2 [M(^{81}Br)+H]$^{+}$ consistent with a monobromo derivative in the LCMS spectrum.

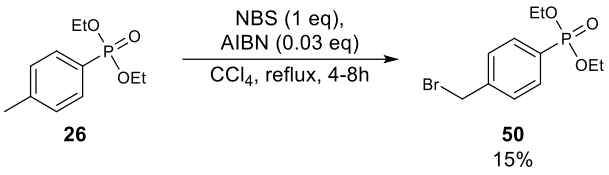

26 **50** 15%

Scheme 3.21. Synthesis of Diethyl(4-bromomethylphenyl)phosphonate **50**.

The low yield suggested this to be a poor starting point for the warhead synthesis. Consequntly, an alternative route starting with 4-bromobezyl bromide in which the order of the synthesis is reversed was proposed. Here, initial attachment of the linker via a Williamson etherification would be followed by the Hirao coupling reaction to generate the aryl phosphonate.

As a proof-of-concept, 4-bromobenzyl bromide and 1-hexanol were coupled using general Williamson etherification conditions. As a result, the desired product **51** was obtained in good yield (86%) proving the strategy to be a valid starting point. Evidence of product formation was found in the IR spectrum which lacked the characteristic -OH stretching signal as well as in the ^{13}C NMR spectra where the benzylic signal shifts from 32.5 ppm to 72.0 ppm because of the vicinal oxygen atom (Scheme 3.22).

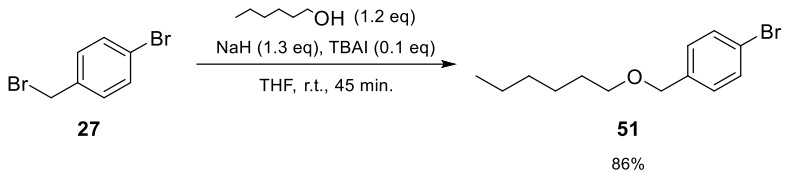

Scheme 3.22. Synthesis of 1-bromo-4-[(hexyloxy)methyl]benzene (**51**)

Initial attempts using 3-(Boc-amino)-1-propanol (**52**) were unsuccessful. Different general conditions were tested but no product was obtained in neither case. Further literature research revealed that under the reaction conditions, this molecule could undergo an intramolecular cyclization to form 1,3-oxazinan-2-one (Scheme 3.23).[129]

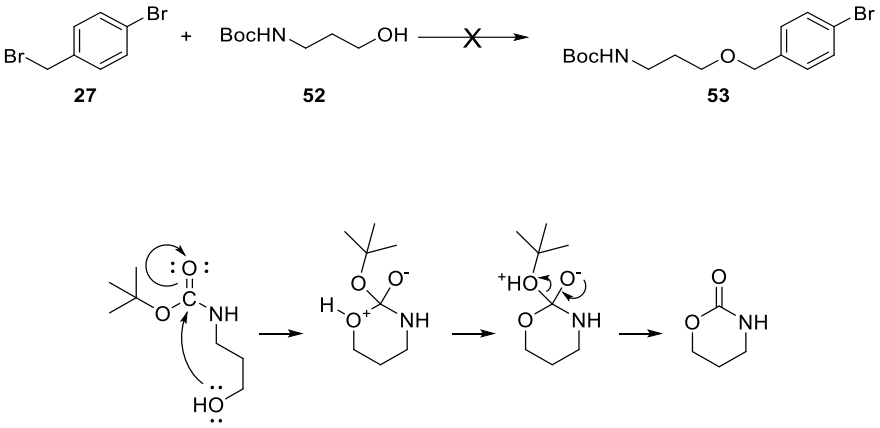

Scheme 3.23. Williamson etherification using 3-(Boc-amino)-1-propanol and proposed intramolecular cyclization mechanism.

To tackle this issue, it was decided to increase the number of carbons in the alkyl chain to disfavor the cyclization. In consequnce, **55** was synthesized as before to prevent the amine acting as an internal nucleophile (Scheme 3.24 A) and same conditions were applied using 5-(Boc-amino)-1-pentanol, NaH and TBAI in THF to afford **56** in 69% yield. m/z (ES^-) 416.1 [M (^{79}Br)–H+H-COOH]$^-$; 418.1 [(^{81}Br)-H+ H-COOH]$^-$ peaks

present in LCMS spectra were used as confirmatory evidence. Subsequent Hirao coupling reaction afforded the phosphonate **57** in 61% yield. Evidence for **57** was obtained from analysis of the ^{31}P NMR spectrum where it was possible to observe a singlet signal at δ 18.9 as expected. Finally, Boc deprotection with 4N HCl in dioxane produced **58** followed by amide coupling with 5-hexynoic acid provided **59** in 65% yield. Evidence of products was based on the disappearance of the signal corresponding to *tert*-butyloxy protons in ^{1}H NMR of **58** and subsequent shifting of the carbamate carbonyl carbon signal from δ 155.9 to δ 172.1 in ^{13}C NMR spectrum of **59** (Scheme 3.24 B).

A.

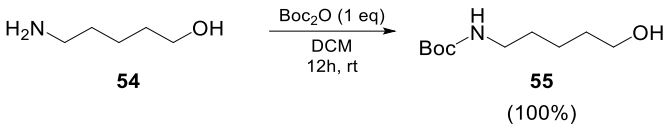

B.

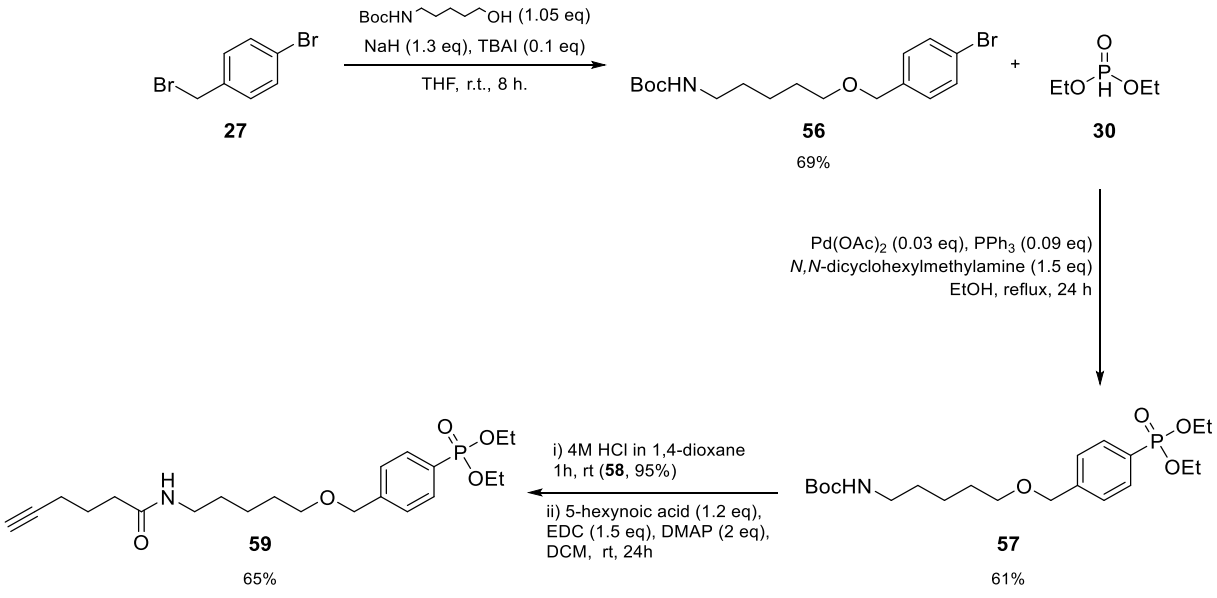

Scheme 3.24. **A)** Boc protection of 5-amino-1-pentanol. **B)** Synthesis of neutral aryl probe diethyl [4-({[5´-(hex-5´´-ynamido)pentyl]oxy}methyl) phenyl] phosphonate (**59**).

3.2.1.1.4 Synthesis of electron withdrawing aryl phosphonate warhead

As shown in Figure 3.3, to complete the aromatic set, a probe with an electron withdrawing effect was devised following a simple synthetic route starting from an aryl ester halide, then introducing the phosphonate with a Hirao cross coupling reaction. The ester group in the *para* position of the aromatic ring would suffice as an electron withdrawing group, but as it is prone to metabolic degradation, a more resistant group such as an amide is more suitable. Therefore, the next step would be the conversion of the ester into an amide followed by linker attachment, concluding with the fluorophosphonate synthesis.

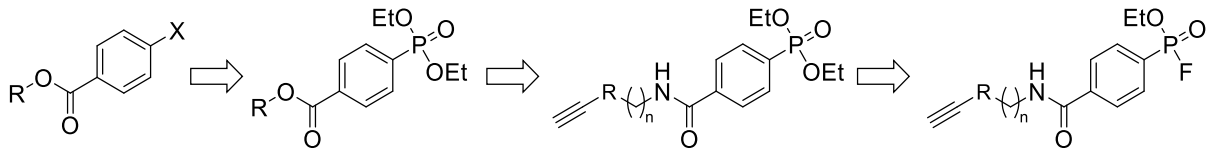

Figure 3.3. Strategy proposed for the synthesis of the electron withdrawing probe.

Starting with commercially available methyl 4-iodobenzoate (**60**), the C-P cross coupling reaction was carried out using the same methodology as before which afforded **61** in 82% yield. Evidence was found in the ^{31}P NMR spectrum with a singlet signal at δ17.0 corresponding to the phosphonate. (Scheme 3.25).

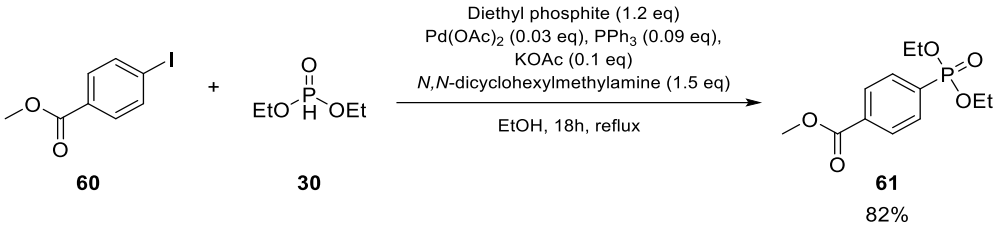

Scheme 3.25. Synthesis of Methyl 4-(diethoxyphosphoryl)benzoate (**59**).

The next proposed step was the conversion of the ester into an amide. A literature search revealed the posibility of obtaining **64** in a single step via a aminolysis reaction, following a nucleophilic addition-elimination mechanism. Normally, this reaction is not a very efficient route, as the alkoxy group is not a good leaving group despite being better than the conjugate base of an amine but, the good yields obtained by Zradni *et al.*[130] in the conversion of alkyl and allylic esters into amides using a microwave reactor in neat conditions (Scheme 3.26 A) worthed further exploration. Therefore, the same conditions were applied to **61** and ethylenediamine in presence of *t*BuOK. Unfortunately, no evidence of product was observed in LCMS spectra. Different reactant equivalents, reaction times, and temperatures were tried but resulted in equally unsuccessful outcomes. A possible explanation could be the decreased electrophilicity of the carbonyl group alpha to an aromatic ring in comparison with an alkylic ester.

A.

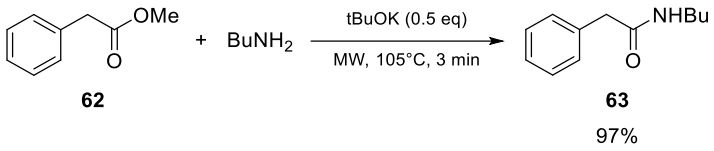

62 **63**

97%

B.

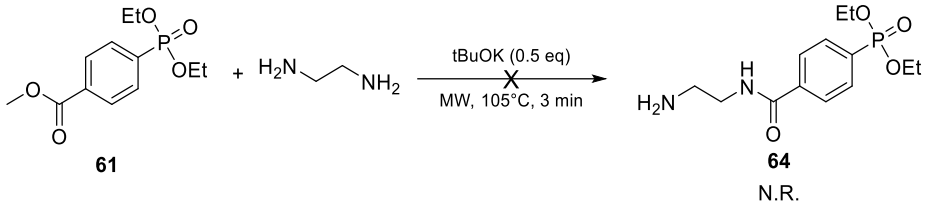

61 **64**

N.R.

Scheme 3.26 A) Amide synthesis using microwave irradiation reported by Zradni *et al.*[130] **B)** Failed synthesis of diethyl {4-[(2-aminoethyl)carbamoyl]phenyl}phosphonate using Zdrani *et al.* conditions.

As this route proved to be ineffective, an alternate route albeit with more synthetic steps was proposed. Consequently, the starting material was switched to 4-iodobenzoic acid (**65**) and Hirao coupling afforded **66** in 94% yield. Subsequent amide coupling using general conditions with EDC.HCl (2 eq) and DMAP (2.5 eq) in THF with an excess of ethilenediamine (50 eq) was unsuccesful as no conversion was observed. In consequence, to increase reactivity **66** was treated with oxalyl chloride and catalytic amounts of DMF to afford acyl chloride **67** in quantitative yield. Subsequent attempts of direct mono-coupling using ethylenediamine in excess were not possible; in all cases a double amidation was observed and no product was isolated after workup (Scheme 3.26).

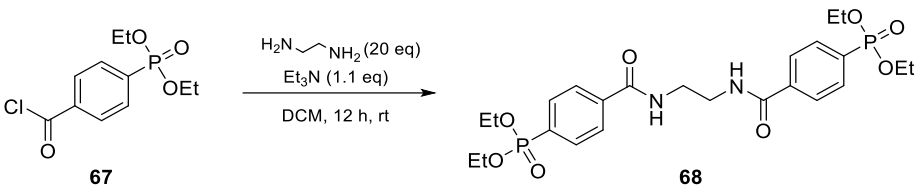

Scheme 3.26. Observation of *bis*-amide formation.

To address this issue, Boc monoprotected ethylenediamine was used instead, in the presence of Et_3N in DCM and **69** was obtained in 79% yield. After removal of the Boc group with HCl 4N in dioxane, the free amine **64** was obtained in 94% yield. Initial attempts to amide synthesis using *in situ* prepared acyl chloride **70** were not succesful due to decomposition. Hence, 5-hexinoic acid was coupled as previously described to afford **71** in 54% yield. Regardless of the addition of synthetic steps to overcome different synthetic challenges, the electron withdrawing probe (before its activation) was obtained using straighforward chemistry which is sumarised in Scheme 3.27.

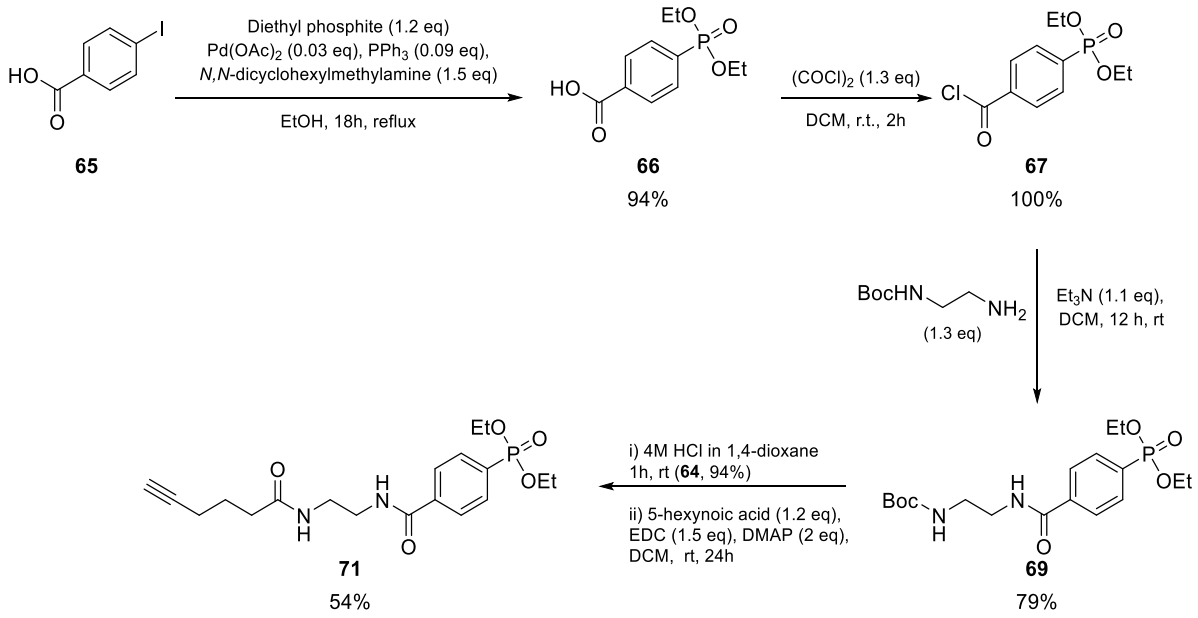

Scheme 3.27. Synthetic route used to obtain electron withdrawing probe precursor **71**.

3.2.1.2 Warhead activation

Having completed the synthesis of the aromatic warheads with their linkers attached the final steps consisted of two sequential reactions: first the activation of the warhead via mono hydrolysis of the phosphonate to form the corresponding phosphinic acid followed by fluorination to obtain the desired fluorophosphonate. Most common procedures for phosphonate hydrolysis are the ones proposed by Kidd *et al.*[64] using $(COCl)_2$ in DCM (Scheme 3.28 A) and the one used by Liu *et al.*[63] using TMSBr instead of $(COCl)_2$ (Scheme 3.28 B).

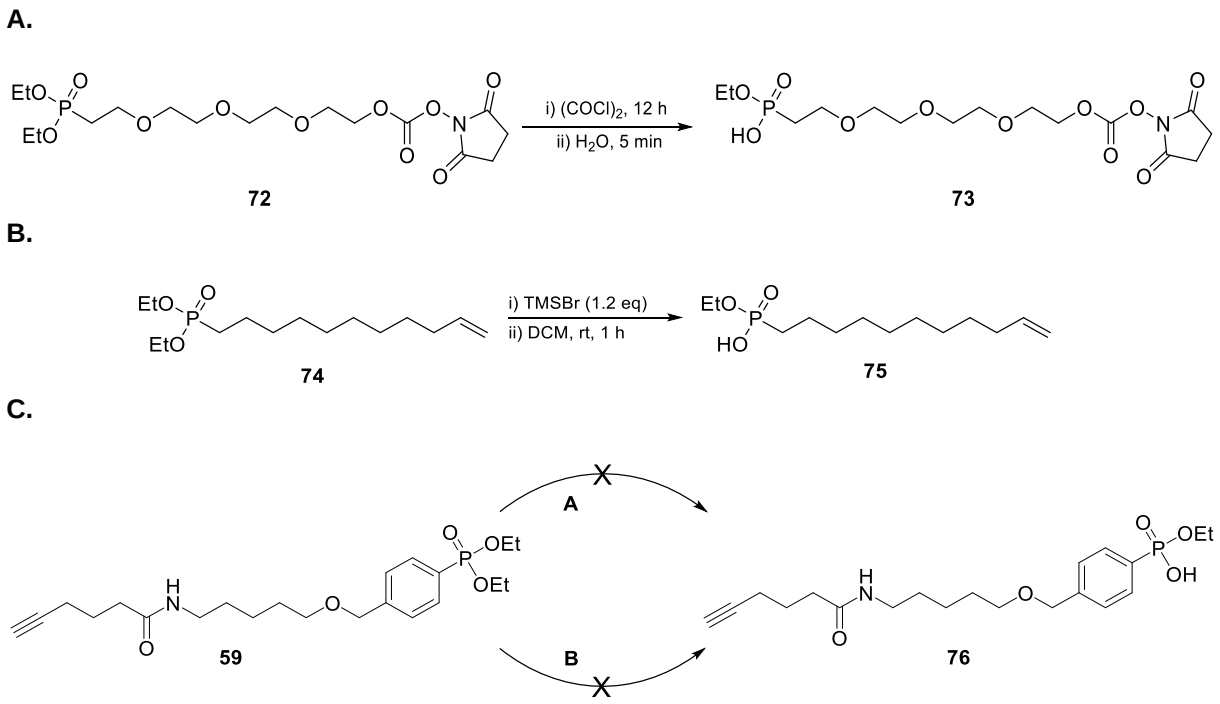

A. i) i) $(COCl)_2$ (3.7 eq), DCM, 0°C to rt, 18 h. ii) H_2O, 5 min
B. i) TMSBr (1.2 eq), DCM, 1 h. ii) $KHSO_4$ (5% p/v), 5 min

Scheme 3.28. Conditions used by **A)** Kidd et al. and **B)** Liu et al. **C)** Hydrolysis of phosphonate **13** using the reported conditions.

Initial attempts to replicate these conditions using phosphonate **59** proved to be unsuccessful. No starting material nor product was present in any case. When TMSBr was used, a peak with mass m/z 368.2 was present in LCMS indicating complete hydrolysis of the phosphonate (Scheme 3.28 C). Additionally, in this case many phosphorus signals were observed in the ^{31}P NMR spectra also suggesting degradation, as shown in figure 3.4.

A.

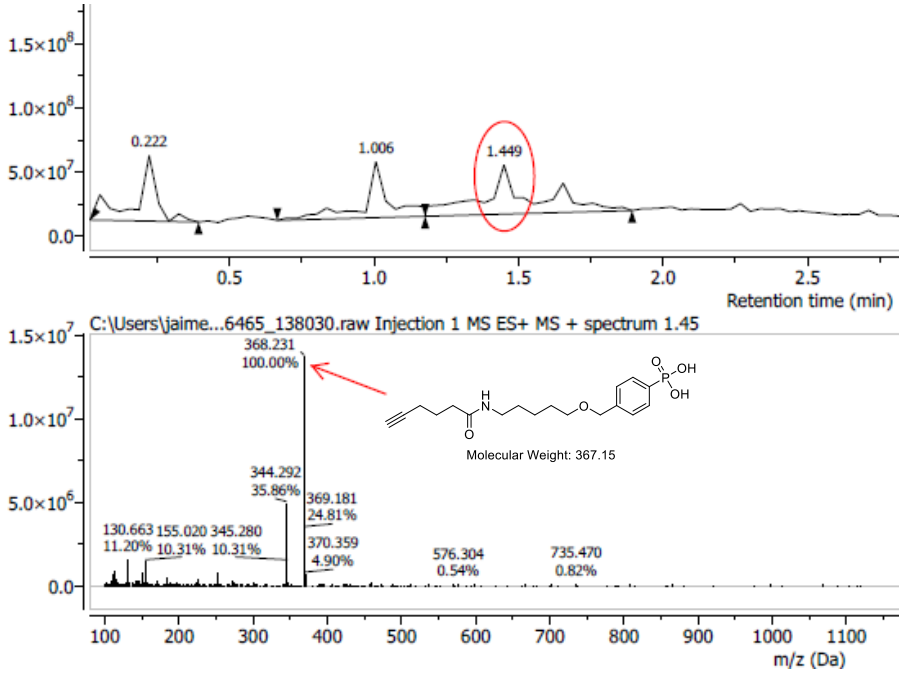

B.

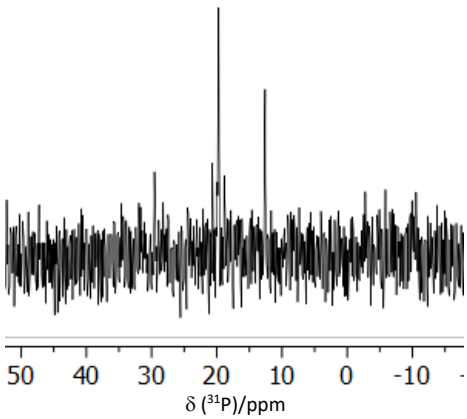

Figure 3.4. A) LCMS (ES^+) and **B)** ^{31}P NMR spectrum indicating degradation of phosphonate.

As the most common conditions used to produce phosphinic acids failed, other conditions were also tested, and the reaction was repeated using different solvents (THF, 1,4-dioxane), but similar results were obtained. After a further literature search, work conducted by Seo *et al.*[131] was found reporting the successful conversion of aryl phosphonates to the desired phosphinic acids using NaOH (2 eq) in H_2O at 80°C. Consequently, these conditions were used on the phosphonate **42**. Fortunately, these conditions delivered the desired phosphinic acid and only mono hydrolysis was observed. Evidence of product was confirmed by LCMS analysis where a m/z 369.4 $[M+H]^+$ peak consistent with the phosphinic acid was present (Figure 3.5).

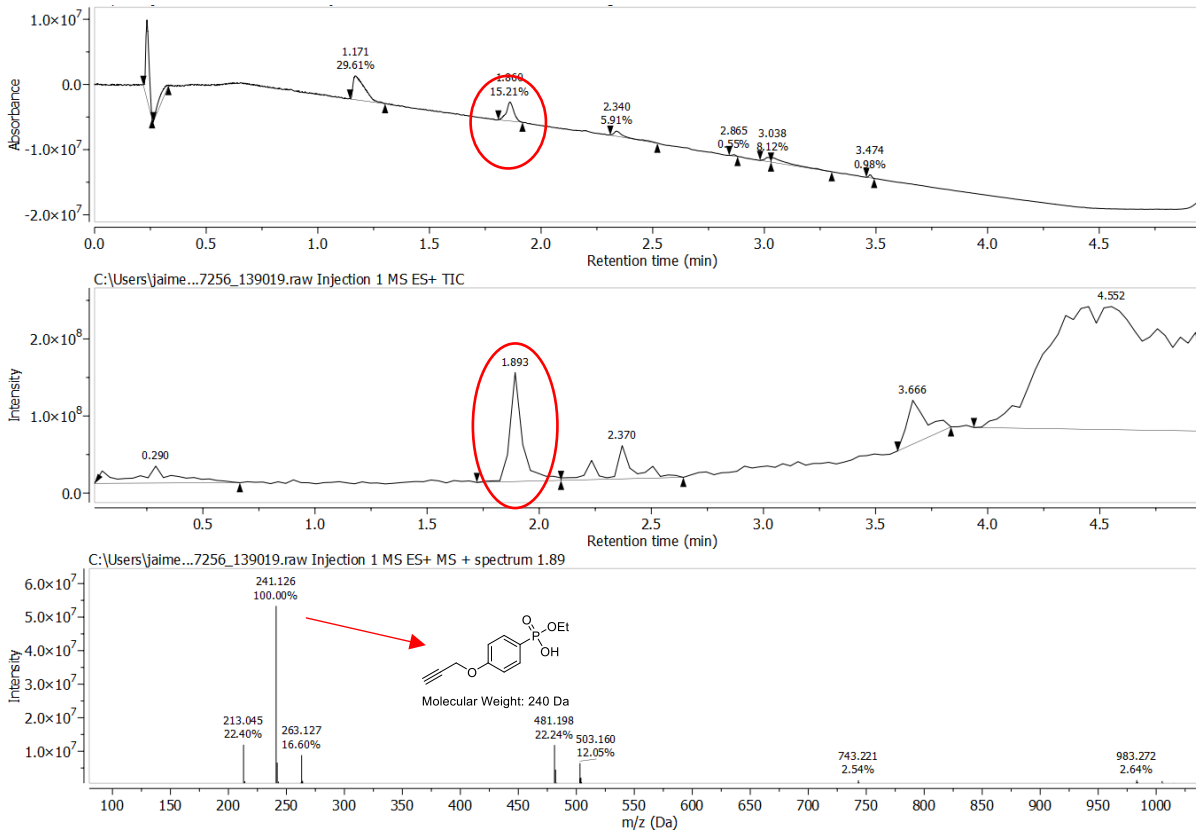

Figure 3.5. LCMS spectra of phosphonate **42** mono hydrolysed compound.

A proposed explanation for the reaction success is the effect of the basic aqueous solution on the mono hydrolysed phosphinic acid; once it is formed, it is present as the conjugated base of the acid, decreasing the overall electrophilicity of the phosphorus atom by delocalization as well as generating a charge repulsion which prevents the second OH^- addition. When the reaction was repeated on the other probes, the reaction time increased as the molecular weight and hydrophobicity of the probes increased to the point of observing no conversion (probes **44**, **49**). Fortunately, after optimizing the conditions, this problem was solved by using a 1:1 mixture of H_2O:EtOH which provided a medium where the starting material was dissolved properly for its hydrolysis. EtOH was selected over other alcohols as it matches the subproduct of the reaction therefore posed less probability of interference. After successfully obtaining the phosphonate hydrolysis conditions, subsequent treatment of the respective phosphinic acid with DAST in DCM afforded the desired aryl fluorophosphonate probe 77. Evidence of product was obtained from analysis of the ^{13}C NMR spectrum, which contained a double doublet signal at δ 116.8 ppm that corresponds to the quaternary aromatic carbon alpha to the phosphorus atom coupled with both P ($^1J_{C-P}$ 209.4), $^2J_{C-F}$ 30.9 and F ($^2J_{C-F}$ 30.9) supported by the doublet present in both ^{31}P (δ 17.7, $^1J_{P-F}$ 1035.1) and ^{19}F (δ -65.5, $^1J_{F-P}$ 1035.1) spectra (Figure 3.6).

A.

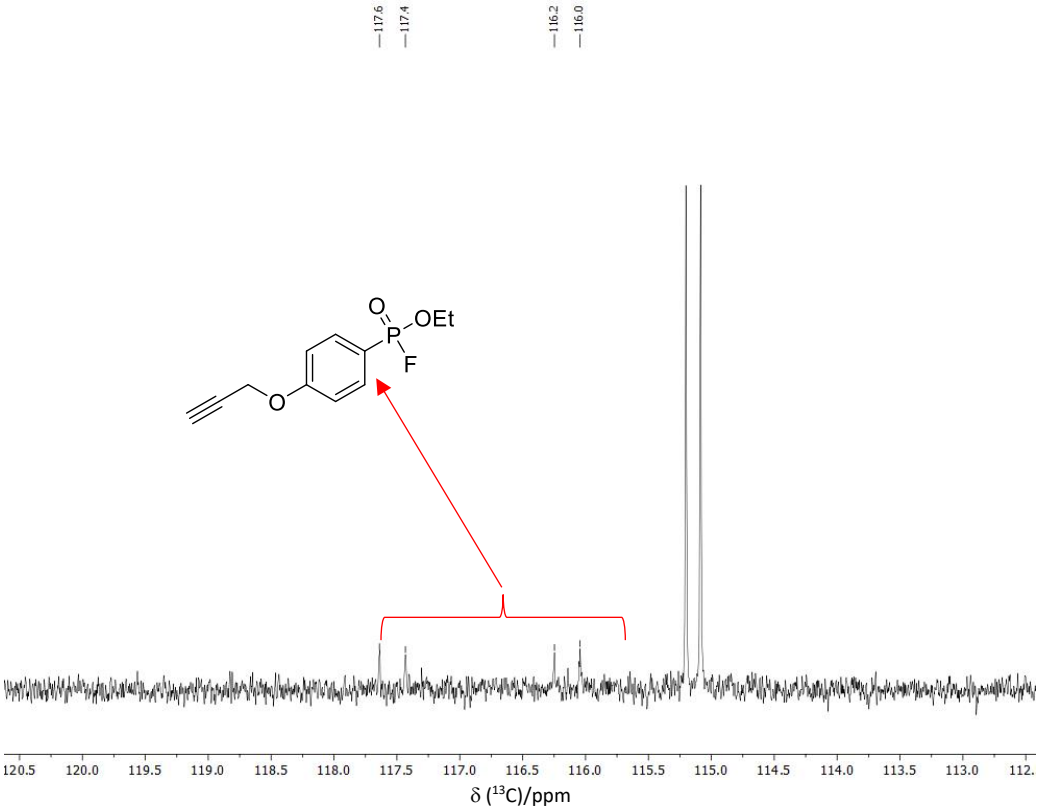

B.

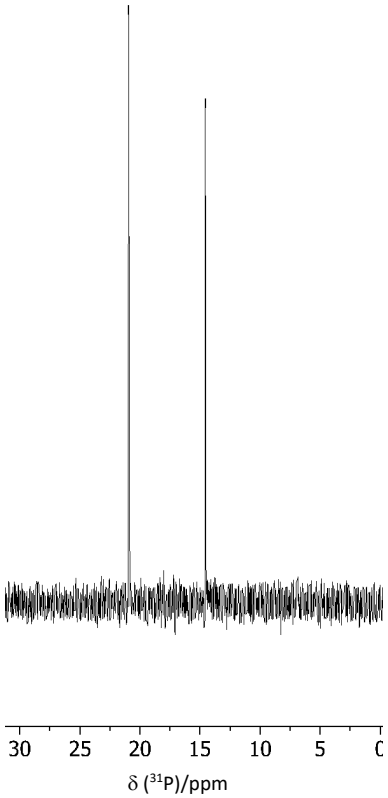

C.

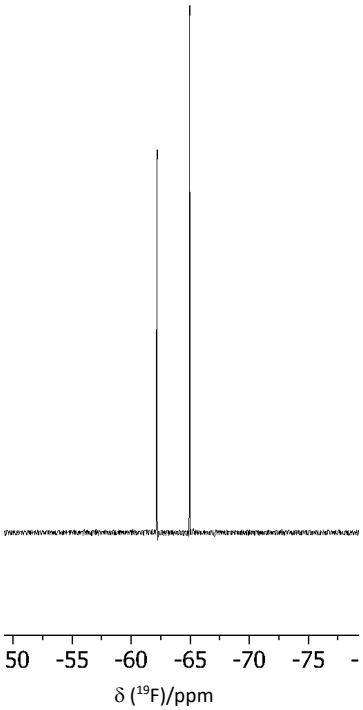

Figure 3.6. Probe **77 A)** ^{13}C NMR double doublet peak of C atom alpha to P atom. **B)** ^{31}P NMR spectra. **C)** ^{19}F spectra.

The table 3.1 summarises the conditions used for the hydrolysis and fluorination of the arylfluorophosphonate probes. In all cases, ^{31}P and ^{19}F NMR spectrums were analysed and used as evidence.

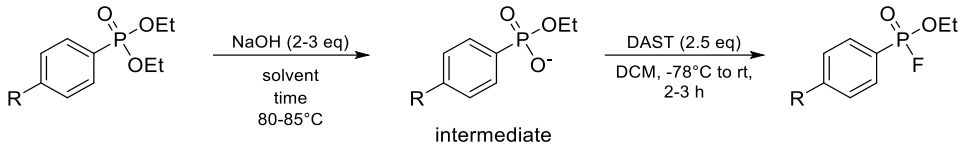

Entry	R=	Solvent	Time (h)	Product	Yield (%)
42	$OCH_2C{\equiv}CH$	H_2O	13	**77**	36
43	$O(CH_2)_4C{\equiv}CH$	H_2O	6.5	**78**	64
49	$O(CH_2)_6NHC(O)(CH_2)_3C{\equiv}CH$	H_2O:EtOH (1:1)	46	**79**	60
44	$(C_6H_4)O(CH_2)_4C{\equiv}CH$	H_2O:EtOH (1:1)	26	**80**	54
59	$(CH_2)O(CH_2)_5NHC(O)(CH_2)_3C{\equiv}CH$	H_2O:EtOH (1:1)	6.5	**81**	64
71	$C(O)NH(CH_2)_2NHC(O)(CH_2)_3C{\equiv}CH$	H_2O	3	**82**	45

Table 3.1. Hydrolysis and fluorinations of synthesized aryl fluorophosphonates.

3.2.2 Alkyl-FP probe

This probe was rationally developed to compare not only the specificity between aryl fluorophosphonates and alkyl fluorophosphonates but also with commercial alkyl fluorophosphonate probe FP-TAMRA. This probe not only contains a long aliphatic linker. We hypothesize that this could be a fatty acid mimic and therefore could help in tuning the affinity of the probe. Thus, reducing the length of the aliphatic linker chain could potentially broaden its specificity. Additionally, substitution of the bulky and charged fluorophore TAMRA for an alkyne handle could provide cell permeability and make it more site accesible.

Attempting the Arbuzov reaction between between propargyl bromide and triethyl phosphite failed to give the desired phosphonate, probably due to the higher reactivity of the molecule on account of the alpha propargyl group. Consequently, 4-bromo-1-butyne was used instead and combined with triethyl phosphite using Arbuzov conditions to afford **84** in 38% yield. Here, $P(OEt)_3$ was used as limiting reactant to improve the purification step. Evidence of product was obtained from ^1H NMR spectra, where signal at δ 2.47 corresponding to the protons in the position alpha to the P atom appeared as a multiplet instead of the triplet expected for the starting material, supported by the LCMS spectrum which contained the peak m/z 191.2 $[M+H]^+$ as expected. Subsequent monohydrolysis of phosphonate **85** using previously described conditions followed by fluorination with DAST afforded alkyl fluorophosphonate **84** in 69% yield (Scheme 3.29). Evidence of the product was obtained from analysis of ^{13}C NMR where a double doublet signal was present at δ 24.2 ($^1J_{C\text{-}P}$ 145.8, $^1J_{C\text{-}F}$ 24.0) corresponding to the C alpha to the P.

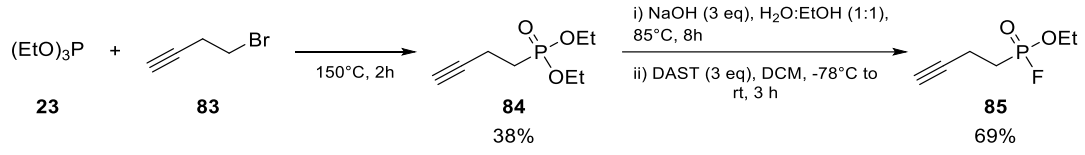

Scheme 3.29. Synthesis of alkylic probe ethyl (but-3-yn-1-yl)phosphonofluoridate.

3.2.3 Benzyl-FP probe

The benzylic fluorophosphonate probe was rationally design to combine features from both alkyl and aryl probes; with a fluorophosphonate with same reactivity as the alkyl warhead, and the bulkiness and electronic character of the aromatic ring, but in this case, beta to the fluorophosphonate which would decrease the warhead rigidity when

comparing with its aryl counterpart. Considering this, the synthesis began with the Arbuzov reaction of commercially available 4-nitrobenzyl bromide (**86**) and $P(OEt)_3$. Initial attempts were not successful leading, instead, to a product producing a peak in the LCMS with a mass consistent with dialkyl *N*-arylphosphoamidate **87** (ES^+ m/z 380.3 $[M+1]^+$) suggesting that these conditions not only produced the desired phosphonate but also promoted the reduction of the nitro group followed by phosphoamidation (Scheme 3.30 A). A literature search revealed that under the conditons used of excess of $P(OEt)_3$ and high temperature (150°C) during 14 hours this reaction had previously been reported (Scheme 3.30 B).[132] Fortunatelly, this problem was overcome by controlling and reducing the reaction time and **90** was obtained in 44% yield (Scheme 3.25 C). Evidence of product was obtained from analysis of the ^1H NMR spectrum where a doublet signal at δ 3.24 and a coupling constant of $^1J_{H\text{-}P}$ 22.4 corresponding to the benzyllic protons coupled with the P atom was present.

A.

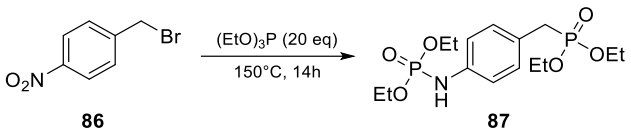

86 **87**

Molecular Weight: 379.3

B.

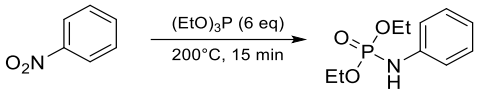

88 **89**

71%

C.

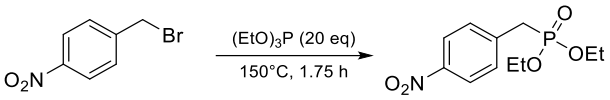

86 **90**

44%

Scheme 3.30. Different products are obtained in Arbuzov reactions in the presence of a nitroarene halide compound with **A)** An extended reaction time to form the *N*-arylphosphoamidate or **B)** synthesis of dialkyl N-arylphosphoramidate reaction reported by Haggam *et al.*[132] **C)** Controlled reaction time reaction time to avoid nitro reduction.

The nitro compound was then reduced with Zn and $NH_4Cl_{(aq)}$ to afford the corresponding aniline **91** which was obtained with 86% yield and evidenced in the IR spectrum by the appearance of a N-H stretching signal at 3344 cm^{-1}. Direct amide coupling between **91** and NHS ester **92** in MeOH afforded the probe precursor **93** in 42% yield. Phosphonate mono-hydrolysis was achieved on basic hydrolysis, but fluorination with DAST failed to afford the desired fluorophosphonate. It was observed that after the addition of DAST, when the temperature was raised from −78°C to rt the reaction mixture changed colour drastically, from yellow to dark brown. As this was not observed in any other successful fluorinations done previously, it was hypothesized that the product was not stable under the elevated reaction temperatures.

Consequently, the conditions were modified. After the addition of DAST the solution was maintained at −78°C and only after complete consumption of the starting material was it quenched with cold water. No colour change was observed in this case and benzylic fluorophosphonate **94** was obtained with 37% yield (Scheme 3.31).

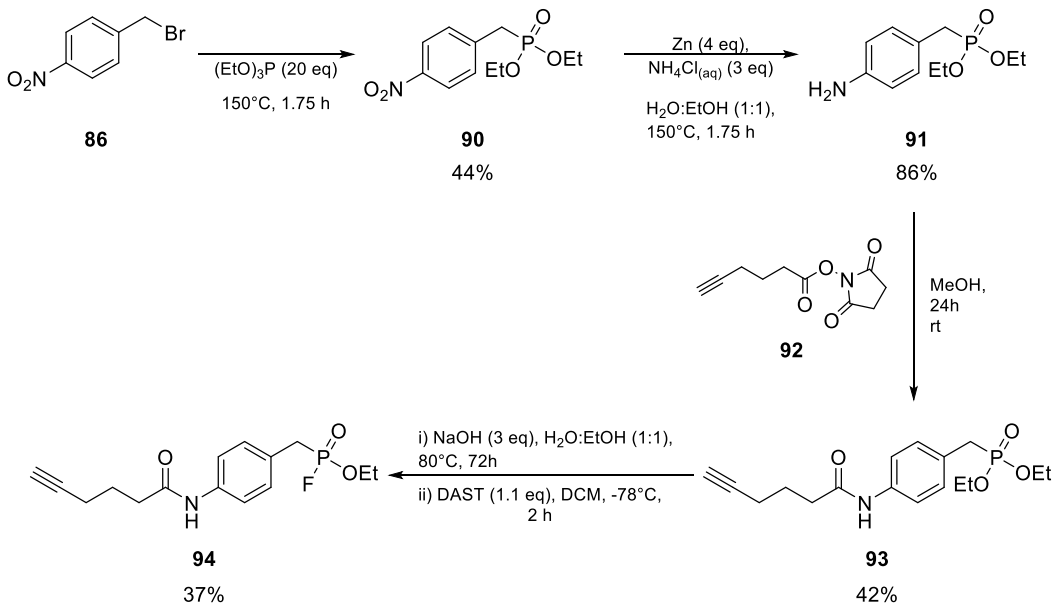

Scheme 3.31. Complete synthesis of benzyl fluorophosphonate probe **94**.

3.2.4 TetraTAG synthesis

3.2.4.1 Introduction

Having developed viable entries to the 3 sets of fluorophosphonate probes, the selection and synthesis of a tag to bind them was required. Commercially available trifunctional tags with a ligation handle, a fluorophore and biotin are available and have been used for tandem labelling, visualization, and enrichment of proteins. Nonetheless, harsh conditions are necessary for the elution of the enriched proteins, in addition to the impossibility of eliminating non-specifically bound endogenous

biotinylated proteins. Another major disadvantage is that after enrichment, the eluted proteins cannot be visualized using fluorescent imaging and the visualization relies on protein staining. To address this issue and to facilitate the enrichment process, cleavable moieties have been used to release the enriched enzymes.[133] These allow the elution under mild conditions of the proteins which can then be digested for subsequent MS identification in a gel-free manner (Figure 3.6).

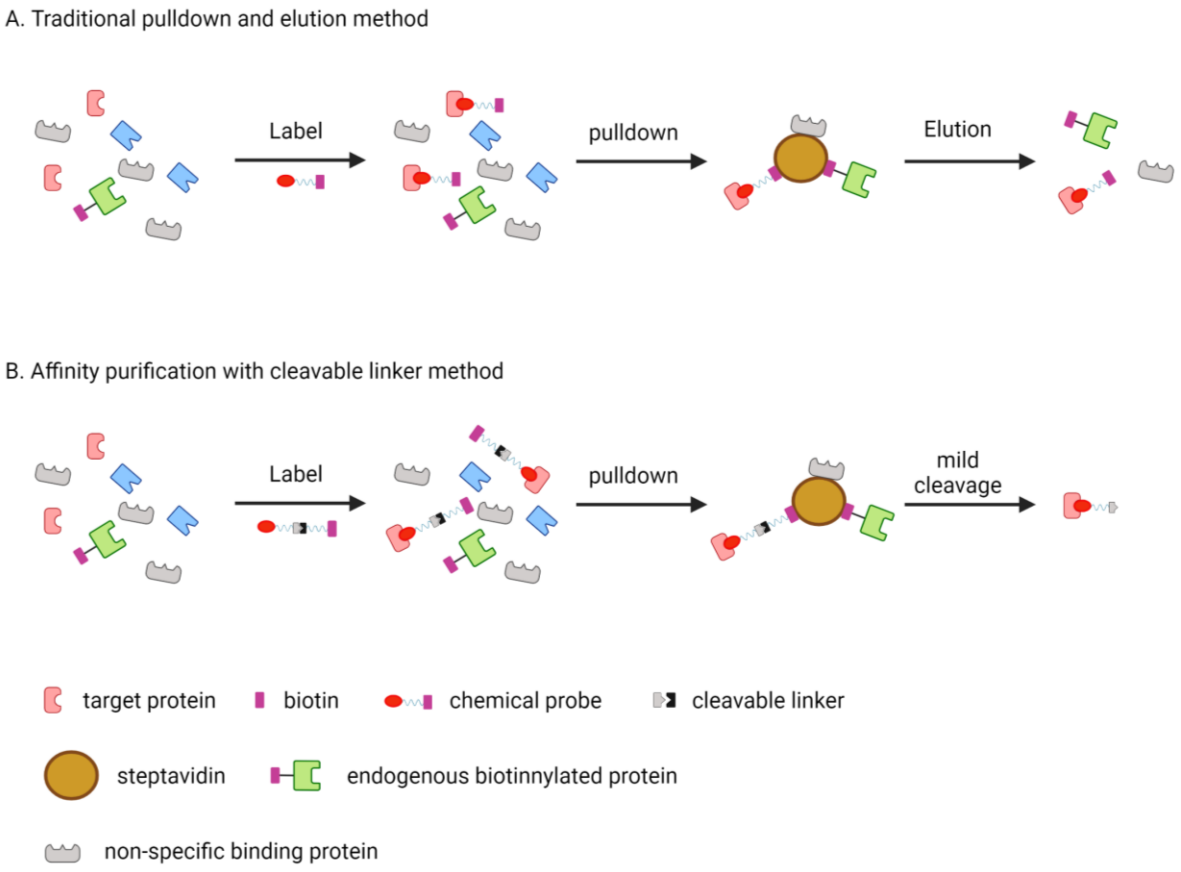

Figure 3.6. Comparison of normal enrichment elution with selective elution using a cleavable linker. In contrast with a traditional elution and pulldown method, linkers with cleavable moieties facilitate elution under mild conditions and allow fluorescent imaging of the captured proteins.

3.2.4.2 Synthesis strategy

The proposed structure to interact with the ABP-enzyme complex would possess an azide handle capable of fishing out the probes using click chemistry, a fluorophore such as Rhodamine isothiocyanate for in-gel visualization, and a biotin end for pulldown connected to a cleavable moiety for subsequent release of the enriched enzyme-ABP-tag complexes. Its synthesis centres on sequentially binding through amide coupling three building blocks previously synthesized on a L-lysine residue. First, an azide-PEG chain followed by the attachment of the biotin cleavable block and finally, addition of rhodamine isothiocyanate fluorophore (Figure 3.7).

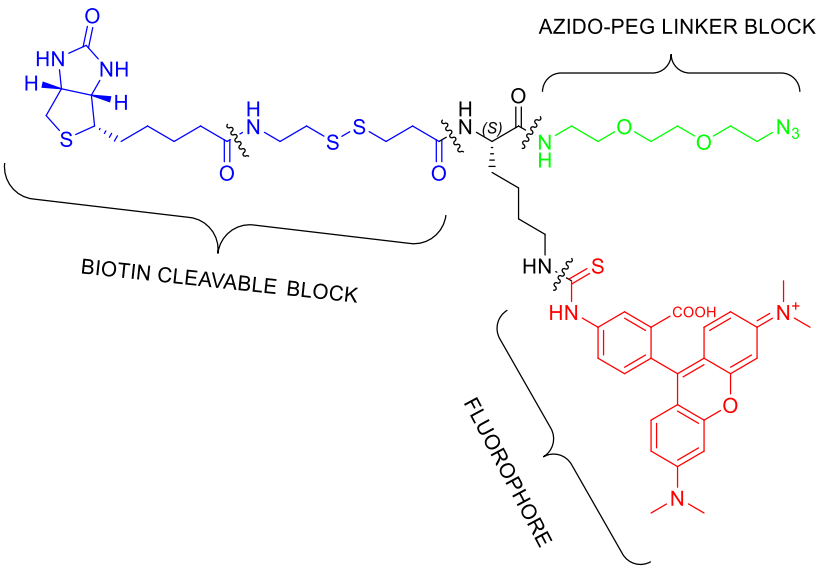

Figure 3.7 Structure of the tetrafunctional tag. 3 building blocks attached to a lysine residue can be observed: in blue, a cleavable biotin fragment used for enrichment; in red, a fluorophore like TAMRA for visualization and in green, an azido peg linker to fish the ABP-enzyme complex.

As a first stage in this process, preparation of the cleavable biotin component was undertaken. This required a source of unsymmetrical disulfide **97**. To obtain it, the

exact conditions reported by Vurgun *et al.*[134] were tested in which **95** was first treated with mCPBA in MeOH at room temperature overnight followed by the addition of 3-mercaptopropionic acid **96**, at room temperature (Scheme 3.32).

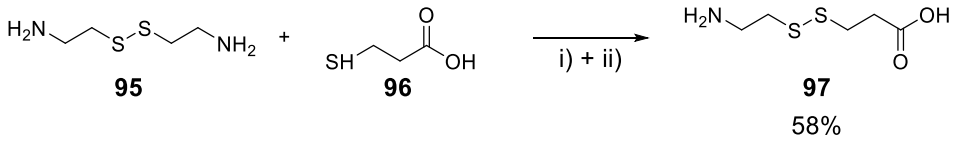

95 **96** **97**

58%

i) MCPBA in DCM, MeOH, rt, overnight and ii) 3-mercaptopropionic acid, EtOH, rt, overnight.

Scheme 3.32. Synthesis of 3-[(2-aminoethyl)disulfanyl]propanoic acid reported by Vurgun *et al.*[134]

Unfortunately, after overnight reaction of the second step (addition of **96**) no product was obtained. Through TLC analysis it was observed that the product was being degraded potentially through extended exposure to the excess of mCPBA present in the reaction mixture. Ultimately, following optimization of the reaction time of the second step and the subsequent purification method, **97** could be obtained in significantly improved yield (82%) (Scheme 3.33). Evidence for formation of **97** was confirmed by HRMS (ES^+) showing a molecular ion of m/z = 182.0 $[M+H]^+$ corresponding to the correct molecular formula ($C_5H_{11}NO_2S_2$).

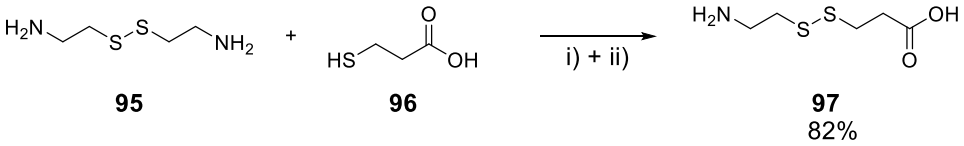

95 **96** **97**
82%

i) MCPBA in DCM,MeOH, rt, overnight and ii) 3-mercaptopropionic acid, EtOH, rt, 2.5h. Purification: Flash chromatography on silica gel. 1st: $CHCl_3$:MeOH and 2nd: EtOAc + (AcOH:H_2O, 2:1) gradient up to 70:30

Scheme 3.33. Synthesis of 3-[(2-aminoethyl)disulfanyl]propanoic acid (**97**) using optimized conditions.

Activation of biotin (**98**) with NHS (**99**) to obtain **100** was first attempted using EDC.HCl as a coupling agent but failed to afford the product with good yield. The reaction was then repeated using conditions reported by Laschewsky and Buller *et al.*[135] Here, **98** was treated with **99** and DCC in DMF at reflux for 20h to afford **100** after recrystallization in 73% yield (Scheme 3.34). Evidence of **100** was confirmed from analysis of the LCMS spectrum which exhibited a molecular ion peak of m/z= 342.3 $[M+H]^+$.

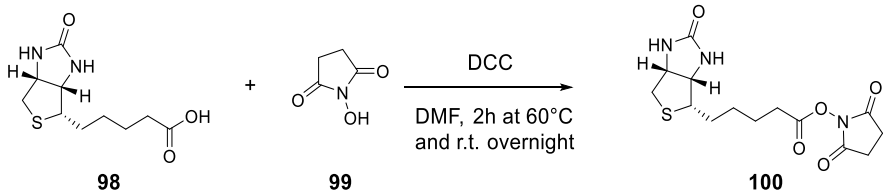

98 **99** **100**
73%

Scheme 3.34. Synthesis of NHS-Biotin (**100**).

With **97** and **100** in hand, coupling conditions used by Marchand-Brynaert *et al.*[136] were considered (Scheme 3.35).

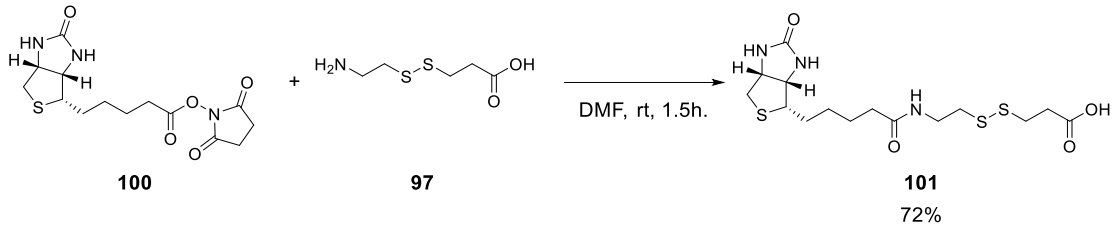

Scheme 3.35. Synthesis of 3-[(2-{5-[(3aS,4S,6aR)-2-oxo-hexahydro-1H-thieno[3,4-d]imidazol-4-yl]pentanamido}ethyl)disulfanyl]propanoic acid reported by Marchand-Brynaert *et al.*[136]

However, when the reaction was attempted, no product formation was observed so it was decided to use general coupling conditions to form the amide bond. Thus, **97** and **100** were combined in the presence of Et_3N in DMF at room temperature and stirred for 2h to afford the desired building block **101** in 50% yield (Scheme 3.36) as supported by a molecular ion peak with m/z= 408.3 $[M+H]^+$ and $[2M+H]^+$ 815.4 in LCMS spectrum.

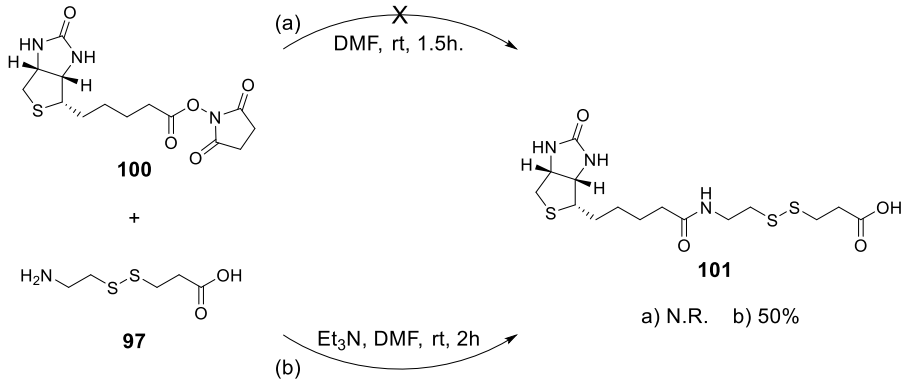

Scheme 3.36. Synthesis of 3-[(2-{5-[(3aS,4S,6aR)-2-oxo-hexahydro-1H-thieno[3,4-d]imidazol-4-yl]pentanamido}ethyl)disulfanyl]propanoic acid **(46)** using (a) Marchand-Brynaert *et al*. conditions[136] and (b) using general coupling conditions.

For the synthesis of the azide-PEG block[c], the methodology reported by Brauch *et al.*[137] was followed. Here, polyethylene glycol **102** was treated with MsCl in the presence of Et_3N in THF at 0°C and brought to rt over 4h to afford **103**. Subsequent substitution with NaN_3 and $NaHCO_3$ in H_2O at 80 °C for 12 h provided the azido-PEG **103**. A Staudinger reaction using PPh_3 and H_3PO_4 in EtO_2 at rt for 18 h then afforded the azido-amine building block **104** (Scheme 3.37 B)**.**

With the building blocks **101** and **104** in hand, attention then turned to assembly of the complete tag. In consequence, **104** was first coupled with the NHS ester of commercially available Fmoc-Lys(Boc)-OH **105,** followed by Fmoc deprotection with piperidine in DMF for 2 h at rt which afforded **107**. Then, amide **108** was obtained as before in good yield (82%) and after boc deprotection, it was coupled with RhSCN in the presence of DIPEA in DCM at rt for 24 h to afford the desired tetrafunctional tag **109** in 43% yield (Scheme 3.37 C). Evidence of product was obtained from analysis of LCMS which contained the peaks m/z 618.9 $[M+H]^{2+}$; and 1236.2 $[M]^{+}$ consistent with the product's mass.

[c] The syntheses of compounds **103**, **104** and **106** were done by Dr Michaela Buerdsell whereas compounds **107** and **108** were carried out by Dr Exequiel Porta.

A.

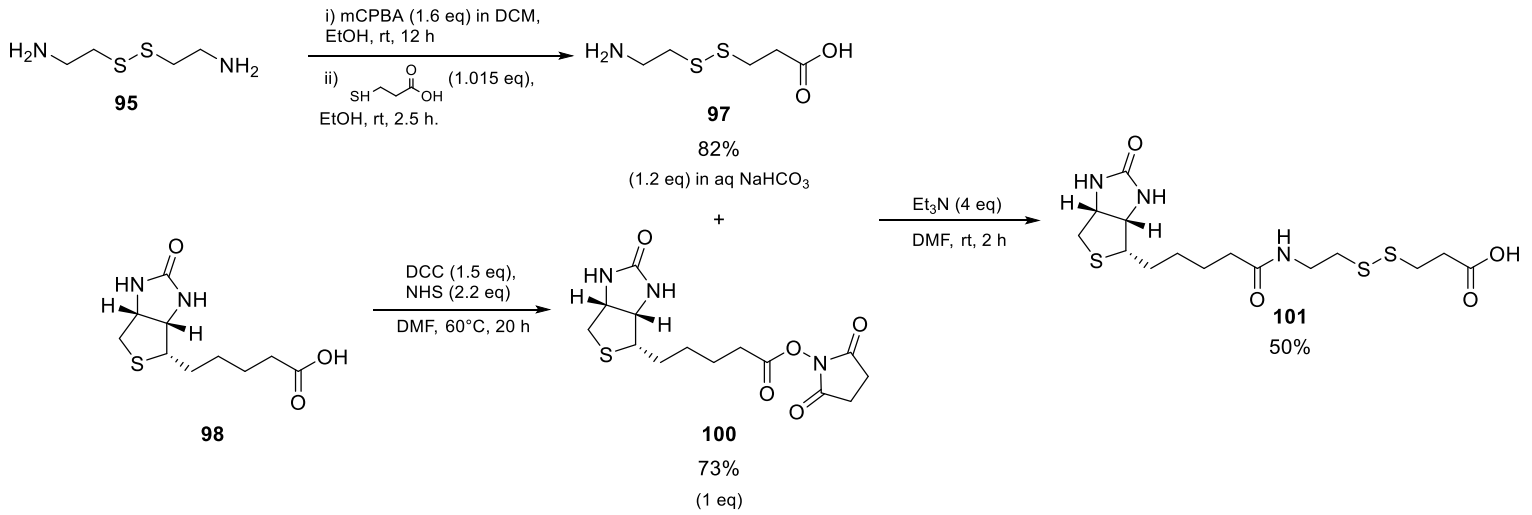
i) mCPBA (1.6 eq) in DCM, EtOH, rt, 12 h
ii) (1.015 eq), EtOH, rt, 2.5 h.
95
97
82%
(1.2 eq) in aq NaHCO3
+
98
DCC (1.5 eq), NHS (2.2 eq)
DMF, 60°C, 20 h
100
73%
(1 eq)
Et3N (4 eq)
DMF, rt, 2 h
101
50%

B.

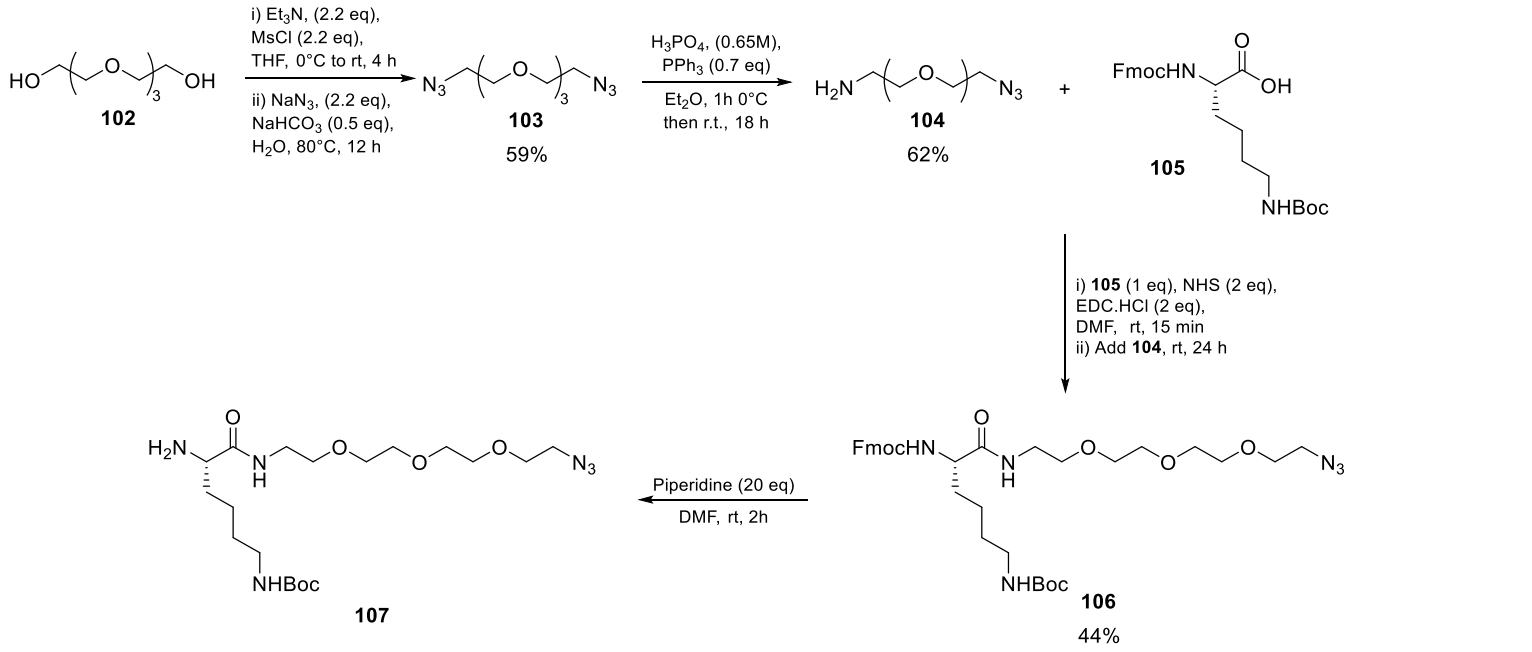
102
i) Et3N, (2.2 eq), MsCl (2.2 eq), THF, 0°C to rt, 4 h
ii) NaN3, (2.2 eq), NaHCO3 (0.5 eq), H2O, 80°C, 12 h
103
59%
H3PO4, (0.65M), PPh3 (0.7 eq)
Et2O, 1h 0°C then r.t., 18 h
104
62%
+
105
i) 105 (1 eq), NHS (2 eq), EDC.HCl (2 eq), DMF, rt, 15 min
ii) Add 104, rt, 24 h
106
44%
Piperidine (20 eq)
DMF, rt, 2h
107

C.

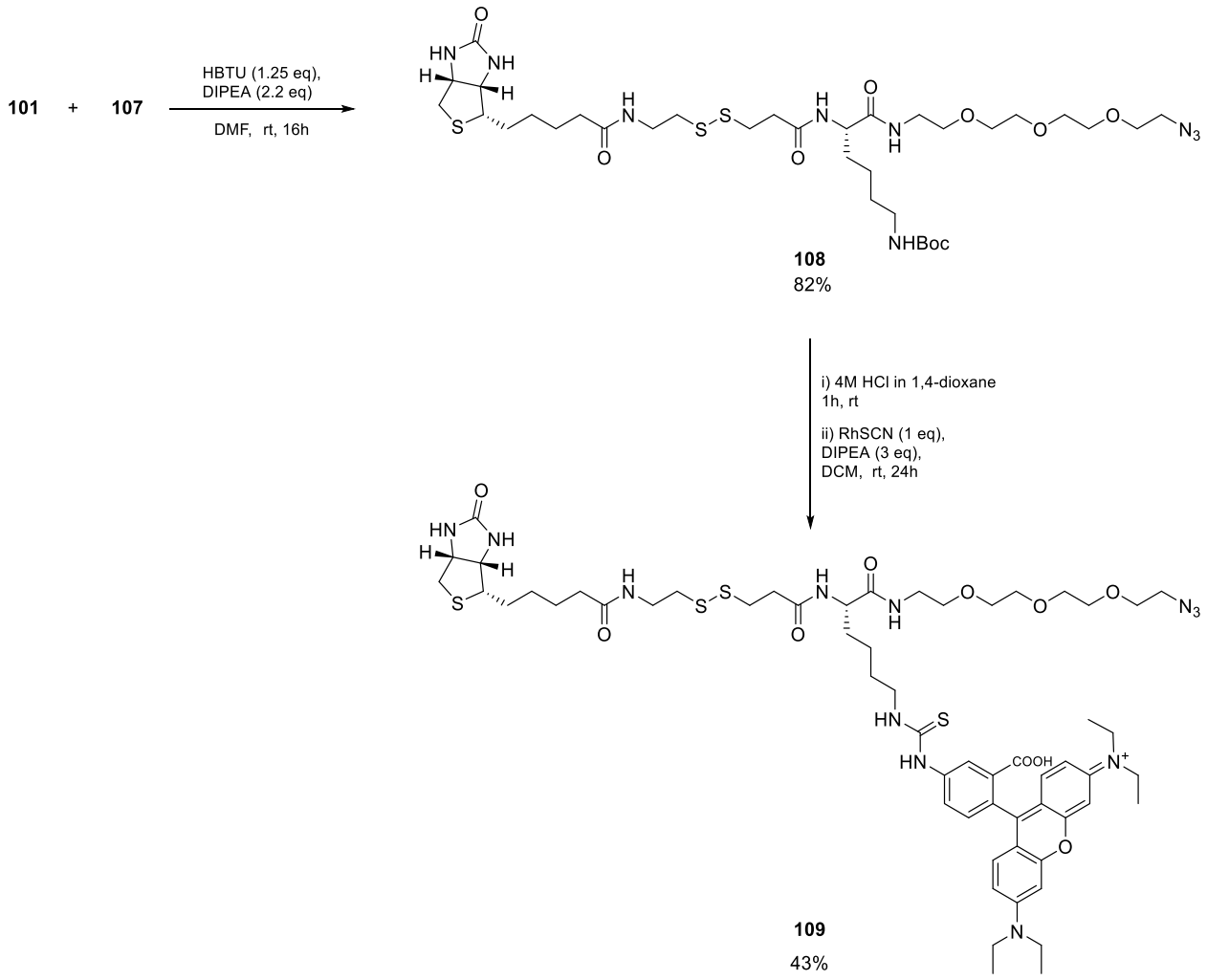

Scheme 3.37. Complete synthesis of tetrafunctional tag **109**. **A)** Synthesis of cleavable biotin block. **B)** Synthesis of azido-PEG block and attachment to lysine residue. **C)** Final coupling with RhSCN to afford the desired tag.[d]

[d] The synthesis of compounds **103**, **104** and **106** were done by Dr Michaela Buerdsell whereas compounds **107** and **108** were carried out by Dr Exequiel Porta.

3.3 In-gel serinome labelling with synthesized probes

With the probes and tags successfully synthesized, attention then turned to their application to study the leishmanial serinome. As mentioned previously, most ABPP workflows are carried out using tissue homogenates or cell extracts where proteins are removed from their native cellular environments. As the function of an enzyme is often tied to the presence of inhibitors/activators as well as protein-protein interactions, the alterations produced during cell lysis can lead to inactivation of enzymes and loss of binding affinity between the probes and the target enzymes. Therefore, *in vitro* proteomic preparations can only approximate the functional state of proteins in a living cell or organism.[54,96,97] As a result, *in vivo* labelling techniques have been developed to address these issues (Figure 3. 8). Examples of this can be observed in the works of both Speers[117] in which different enzyme activities from cancer cells were observed after *in vitro* and *in vivo* labelling using phenyl sulfonate ester probes and Shamshurin[138] who observed similar results on profiling serine hydrolases in *E. coli*.

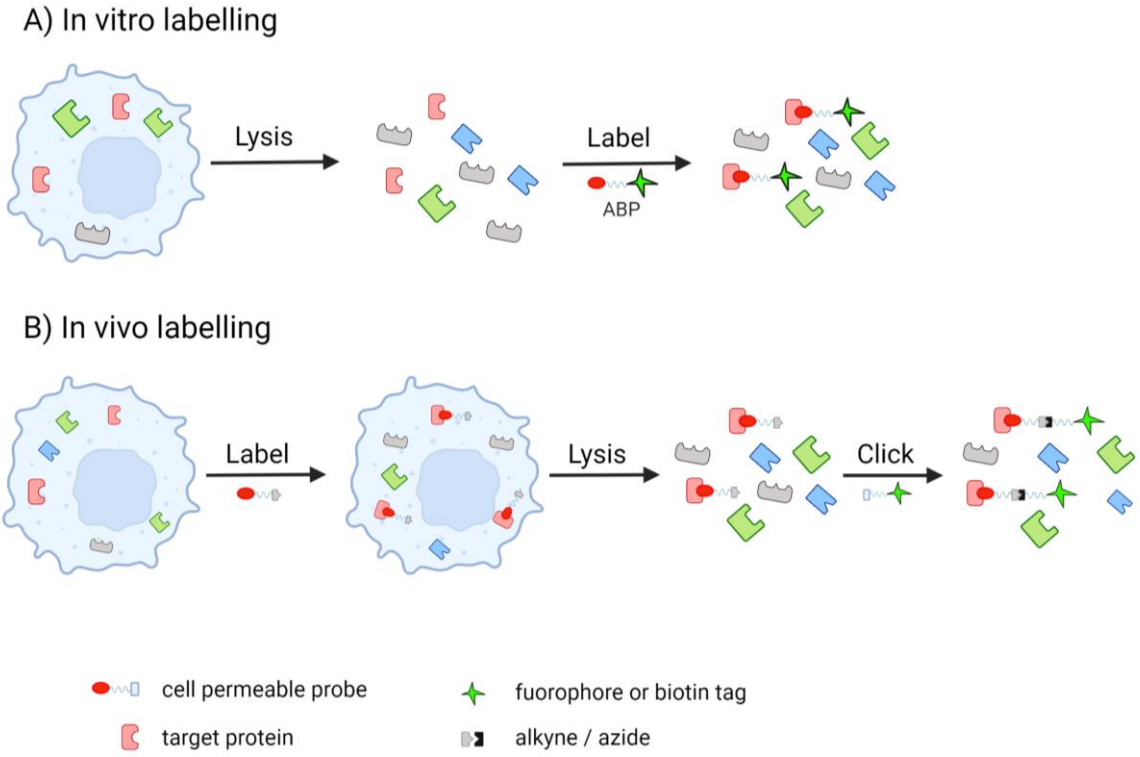

Figure 3.8. *in vitro* and *in vivo* labelling workflows. **A)** *in vitro* labelling: The cell lysate is generated followed by incubation with probes. **B)** *in situ* labelling: cell cultures are incubated with probes and lysed. Subsequently, the tag is attached to the enzyme-probe complex using CuAAC click chemistry.

Consequently, to evaluate and compare the fluorophosphonate probes both *in vitro* and *in vivo* labelling assays were conducted and are described in the following section.

3.3.1 Validation assays

3.3.1.1 Enzyme-ABP binding validation

As discussed above the initial goal of this aspect of the project was to compare probe function between *in vitro* (lysate) and *in vivo* (whole parasite) samples. Despite simple fluorophosphonates having been validated as targets of active serine residues, these did not include aryl FPs probes prepared in this work. Consequently, it was necessary

to validate the aryl fluorophosphonates specificity towards active serine residues. As an initial experiment, aryl-FP **81** (40 μM) (Figure 3.9 A) was chosen as a model aryl FP probe and incubated with commercially available α-chymotrypsin (α-CT) (1 mg/mL), a known serine protease which was selected as a model enzyme. Subsequent TOF-MS ES^+ analysis of untreated α-CT gave a mass of 24448 Da, which is consistent with the mass reported by the manufacturer (CAS 9004-07-3, Sigma Aldrich) (Figure 3.9 B). Following treatment with the probe in equimolar ratio, a new peak with mass 25825 Da corresponding to the mono-labelled protein was observed (α-CT-ABP = [M-1+378]). However, a residual peak of the unmodified α-CT could be observed indicating that the binding was not complete (Figure 3.9 C). This experiment was conducted in pure water, and to better replicate the environment used in the biological assays, it was also repeated using PBS buffer pH 7.2 and lysis buffer (25 mM Tris.HCl pH 7.4, 150 mM NaCl, 1% TRITON, 5% glycerol). In both cases, after dialyzing the samples and subsequent LCMS analysis, the same results were observed confirming the activity of the probe for future experiments with more complex proteomes instead of a model enzyme.

A.

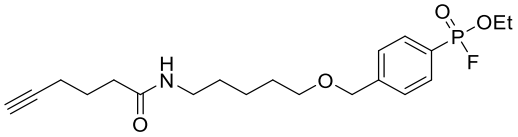

81

Molecular Weight: 397 Da

B.

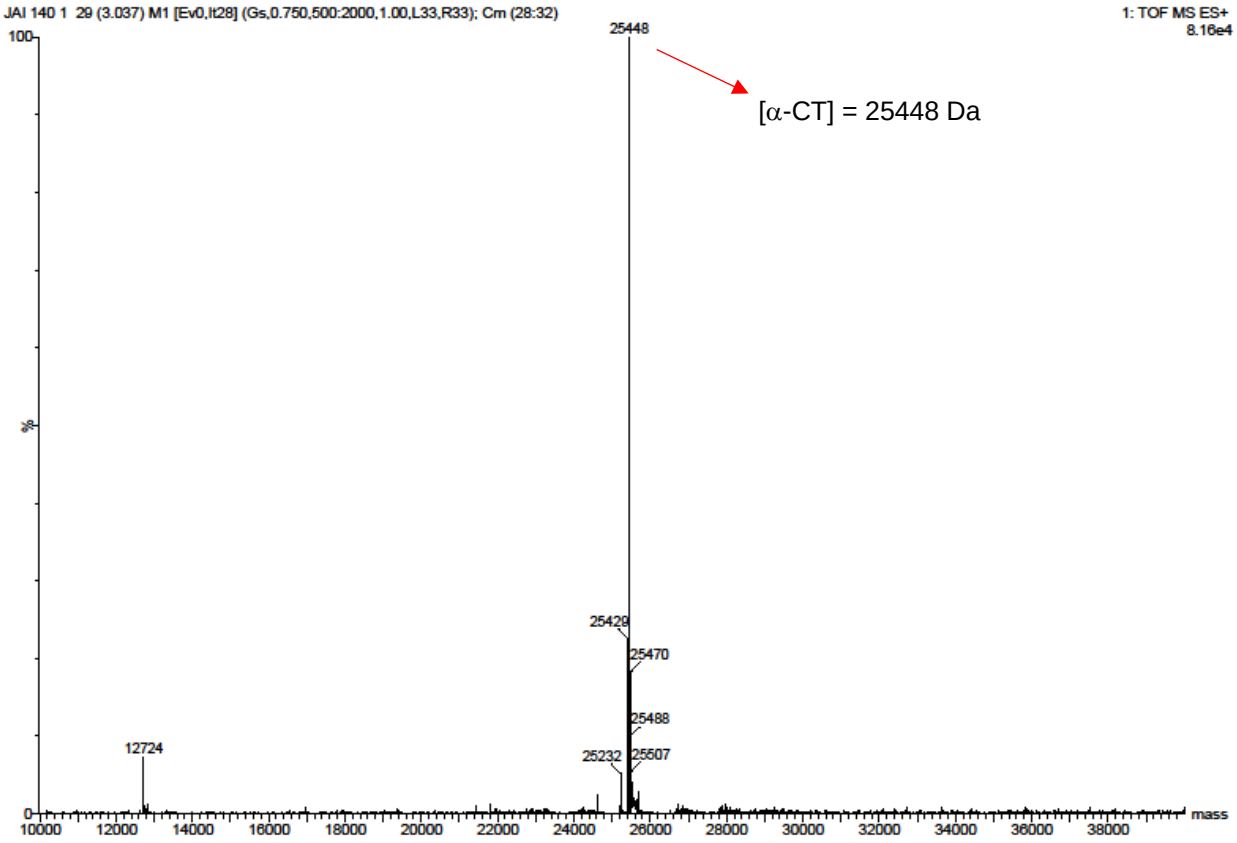

C.

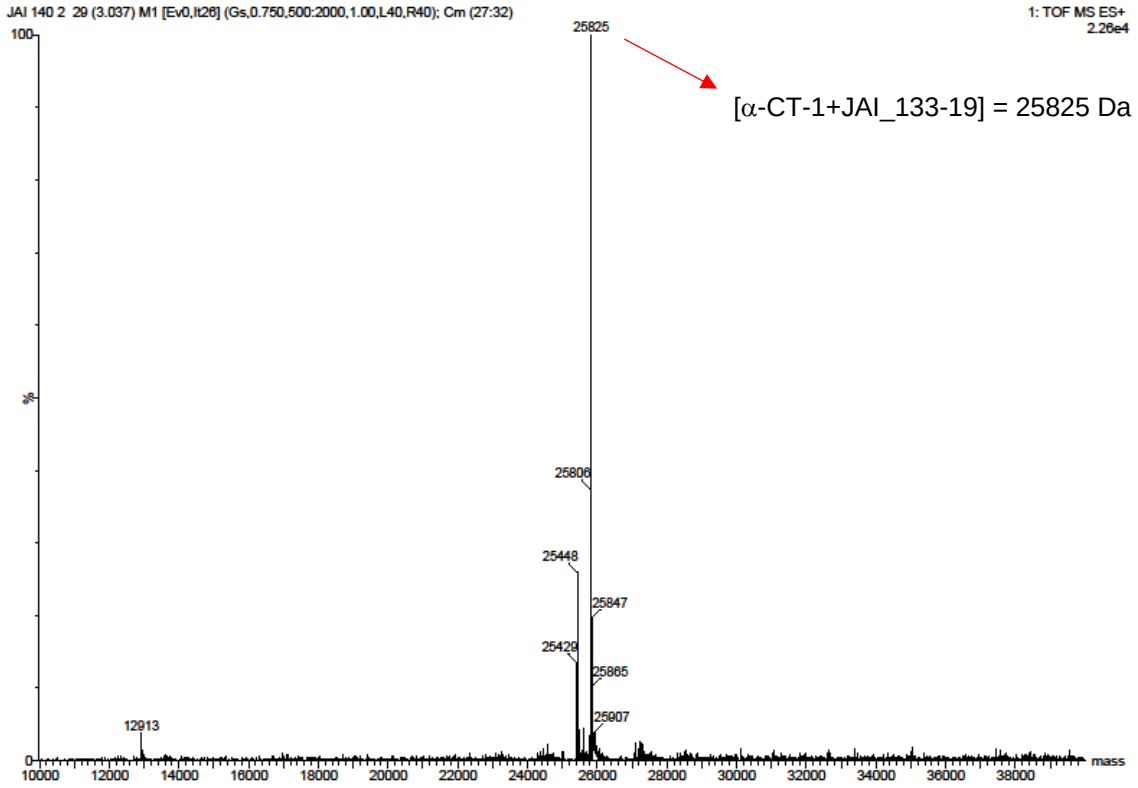

Figure 3.9. A) Structure of probe **81**. **B)** TOF MS ES$^+$ spectra of α-CT (1 mg/mL) (40 μM) in H_2O shows the peak of 25448 Da which corresponds to the untreated α-CT. **C) 81** (40 μM in DMSO) was incubated at rt for 1 h in α-CT (1 mg/mL) in H_2O and analysed by TOF MS ES$^+$. Two peaks are observed: the major of 25825 Da for the [α-CT-ABP] complex and the residual untreated α-CT.

Whilst the previous experiment confirmed that the aryl FP could engage with a serine protease, this did not necessarily indicate selectivity of binding. Consequently, to validate that aryl-FP probe interacts only with active serine residues, a key aspect for an activity-based probe, the previous experiment was repeated using the same conditions but increasing the enzyme-ABP ratios to 1:3 (40:120 μM) and 1:10 (40:400 μM) respectively and the samples were then analysed by LCMS. As observed in Figure 3.10, only mono binding was observed despite the increase in probe concentration demonstrating indirectly that the 22 non-active serine or other

nucleophilic residues present in α-CT are not sufficiently nucleophilic to covalently bind with the aryl fluorophosphonate probe.

A.

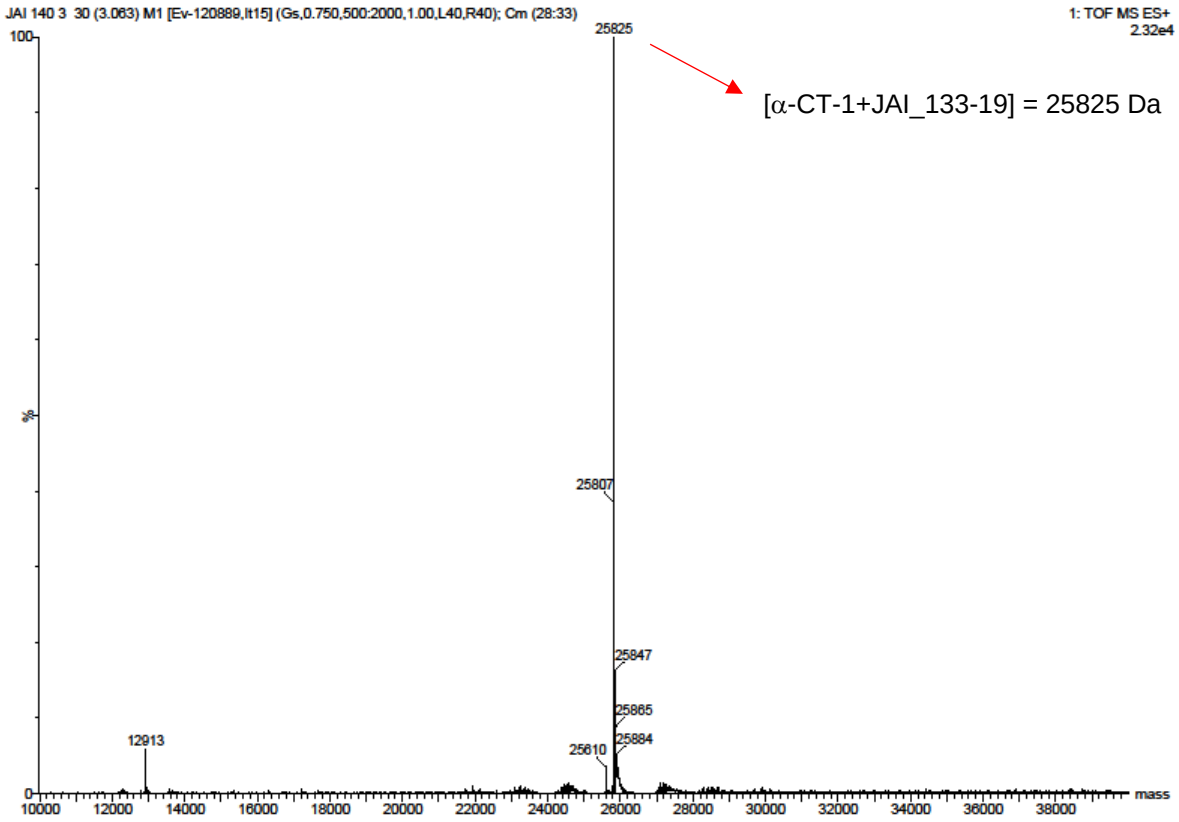

B.

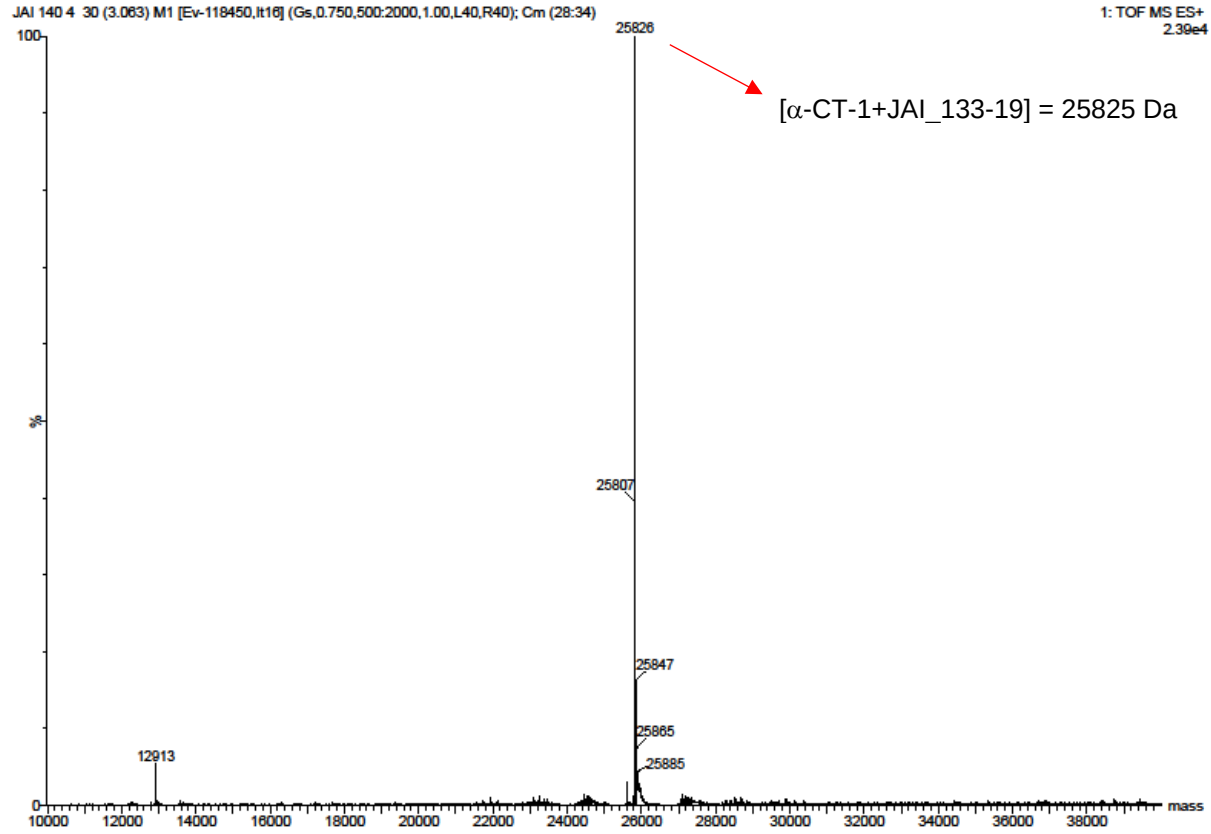

Figure 3.10. α-CT (1 mg/mL) (40 μM) in H_2O was incubated with **81** in **A)** 1:3 enzyme:ABP ratio (40:120 μM) and **B)** 1:10 enzyme:ABP ratio (40:400 μM) and analysed by TOF MS ES^+. Only mono-binding is observed in both cases.

To further explore the selectivity of probe-protein engagement additional experiments were then undertaken varying the probe and the model enzyme. When **77** (60 μM) (Figure 3.11 A) was incubated with α-CT (1 mg/mL), the presence of enzyme-ABP complex was observed in MS spectra reinforcing aryl FPs as activity-based probes (Figure. 3.11 B). In contrast, when **81** and **77** were tested using serine protease proteinase K under the same conditions, no mass corresponding to the complex enzyme-ABP was observed. Both proteases possess similar substrate affinity, where α-CT cleaves the carboxyl groups of big hydrophobic residues such as Tyr, Phe,

Trp,[139] whilst proteinase K is a broad-spectrum serine protease with affinity for aromatic and hydrophobic residues.[140] Therefore, these results suggest that aryl fluorophosphonates present different affinities for different serine proteases. Nevertheless, to confirm this hypothesis the experiment should be repeated.

A.

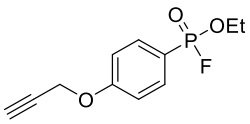

77

Molecular Weight: 242 Da

B.

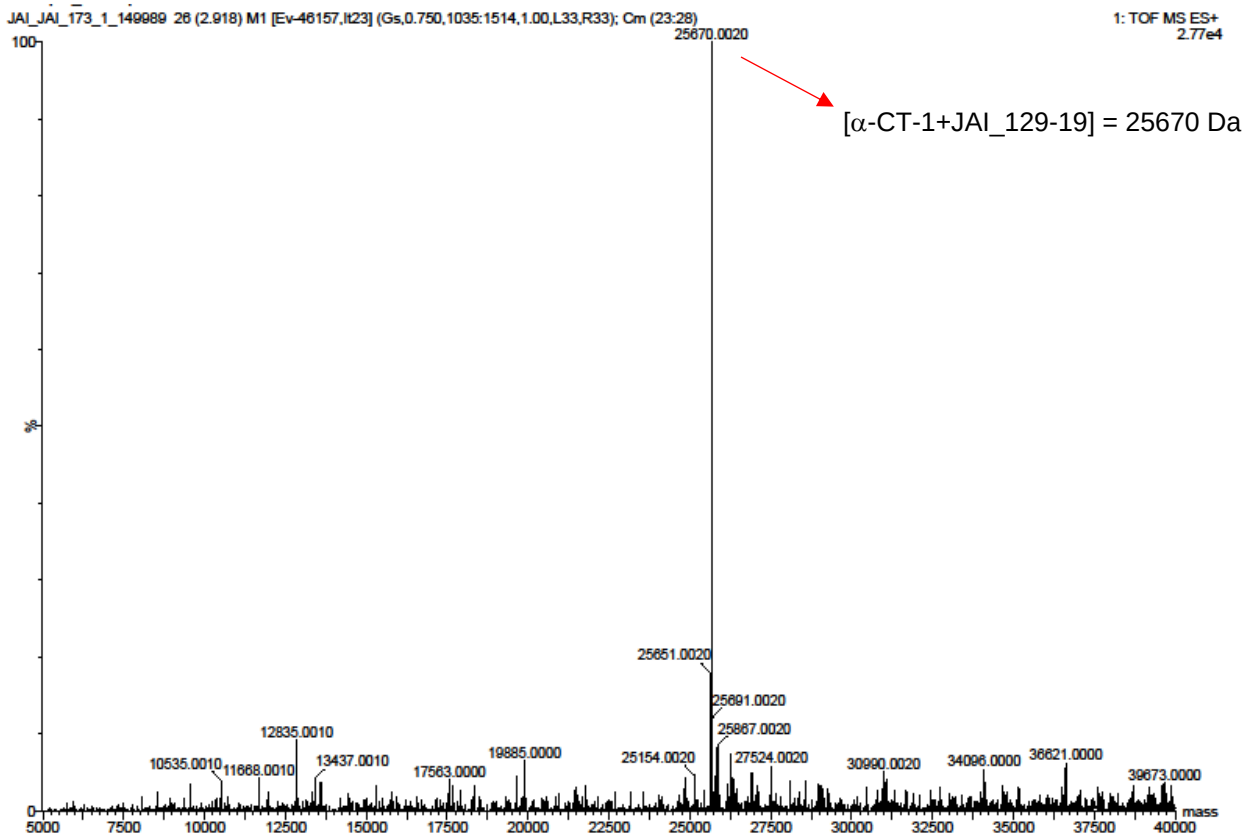

Figure 3.11 A) Structure of probe **77**. **B) 77** (60 μM in DMSO) was incubated at rt for 1 h in α-CT (1 mg/mL) in H_2O and analysed by TOF MS ES^+. The peak of 25670 Da confirms the presence of [α-CT-ABP] complex.

3.3.1.2 Aryl fluorophosphonate reactivity

Once the specificity of the probe against active serine residues was confirmed, the next step was to verify the mode of reactivity. To achieve this α-CT was incubated with the non-fluorinated phosphonate ester **59** (Figure 3.12 A) as before and analysed by LCMS. As expected, the non-activated aryl phosphonate failed to covalently bind to α-CT, validating the fluorophosphonate reactivity (Figure 3.12).

A.

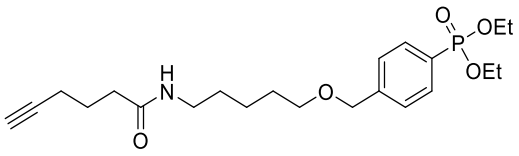

59

Molecular Weight: 423 Da

B.

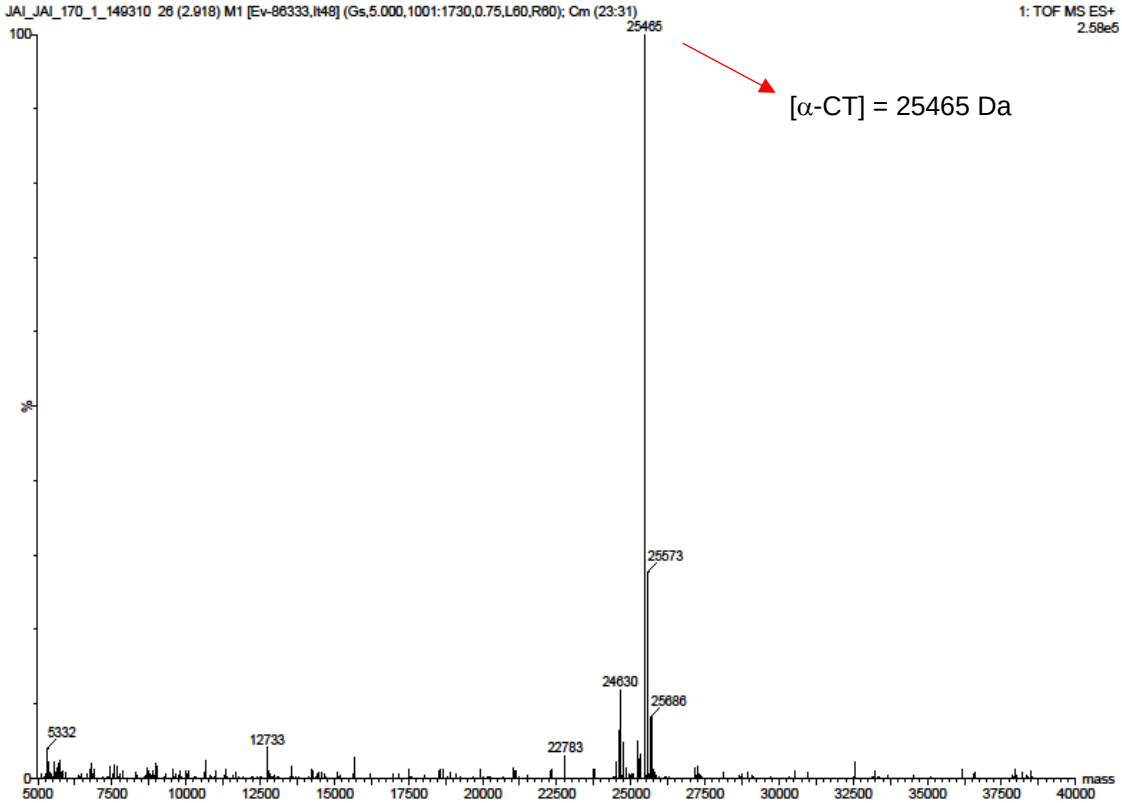

C.

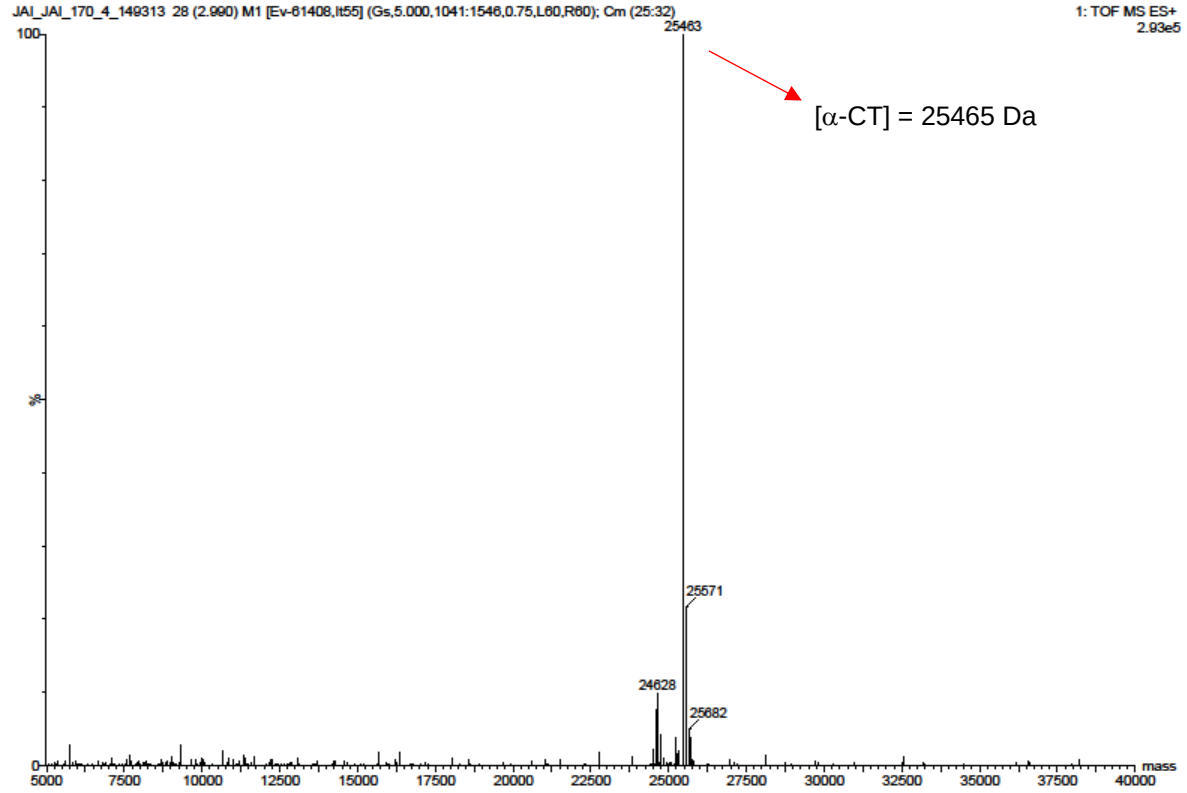

Figure 3.12. Samples **A)** α-CT (1 mg/mL) in H_2O and **B)** α-CT (1 mg/mL) in H_2O incubated with **59** (60 μM) at rt for 1h were analysed by TOF MS ES^+. In both cases, a peak of 25465 Da corresponding to α-CT is observed but no probe-protein engagement is present after incubation with probe.

3.3.1.3 Bioorthogonal Copper (I)-catalysed azide-alkyne cycloaddition (CuAAC) validation

Having validated enzyme-ABP engagement it was then necessary to validate the ABP-TAG complex formation. As described in section **3.1**, the Cu catalysed biorthogonal 1,3 dipolar cycloaddition reaction (click chemistry) was chosen to form the probe-TAG complex. For the initial experiment, non-activated probe **59** (1 eq) and the fluorinated azide **110** (1.2 eq) were selected and incubated for 1 h at rt with $CuSO_4.5H_2O$ (0.5 eq), THPTA (1 eq) and NaAsc (0.5 eq) in H_2O for 2h at rt (Scheme 3.38).

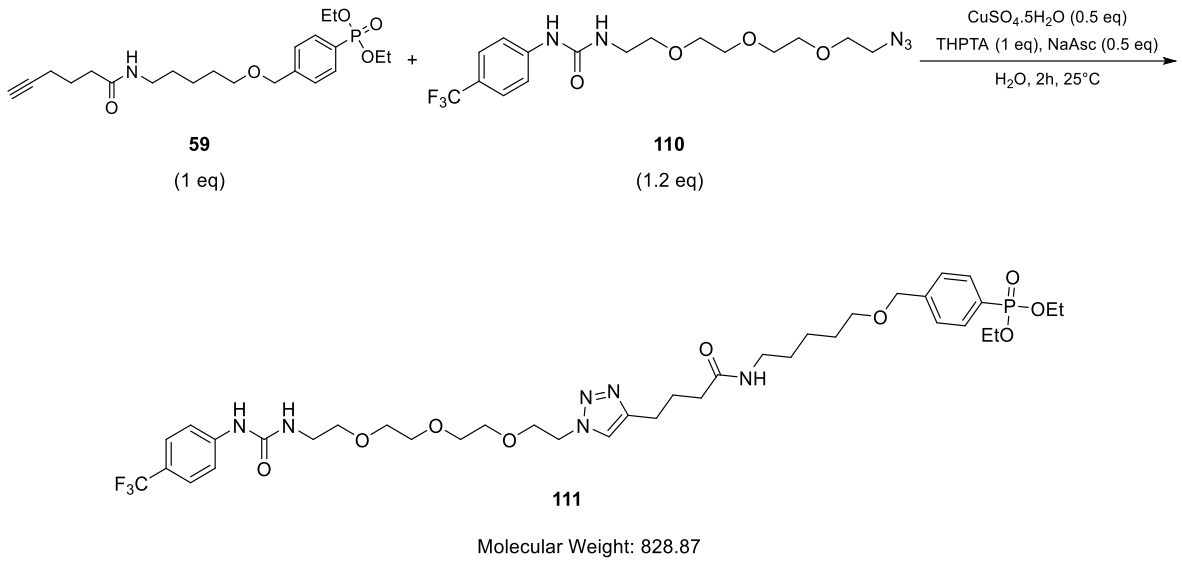

Scheme 3.38. ABP-TAG click conditions tested.

Click confirmation was obtained by analysis of ^{19}F NMR of the of the crude click reaction mixture where signals at -61.9 and -62 ppm, which correspond to the product and starting material respectively were present in an approximately 1:0.24 relation (Figure 3.13 A). This is consistent with the excess of azide **110** added initially and to verify it, **110** was added to the NMR tube and the mixture was analysed again. As expected, an increase in the signal at 62.0 ppm was observed (Figure 3.13 B). Furthermore, LCMS analysis of the crude click reaction mixture supported the NMR findings as a peak at m/z 830.7 $[M+H]^+$ was present (Figure 3.13 C).

A.

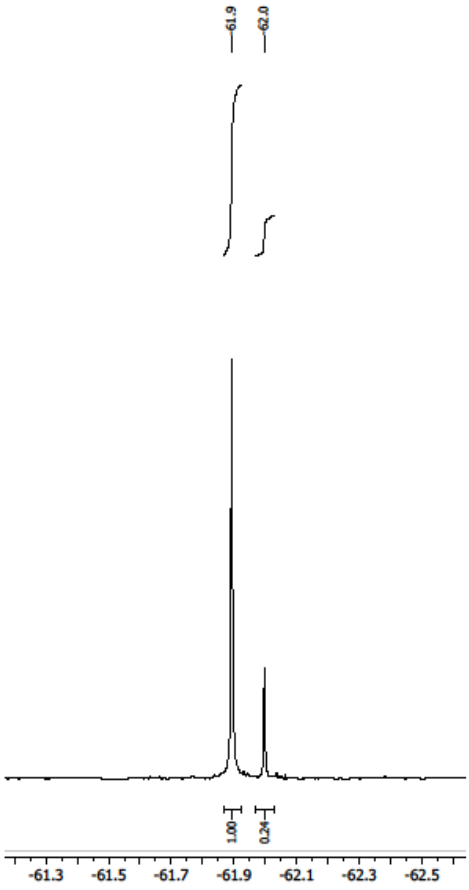

$\delta(^{19}F)$/ppm

B.

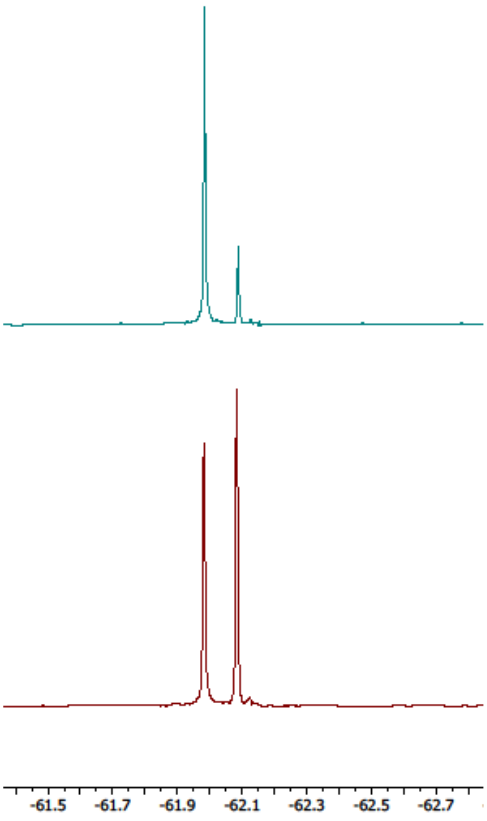

$\delta(^{19}F)$/ppm

C.

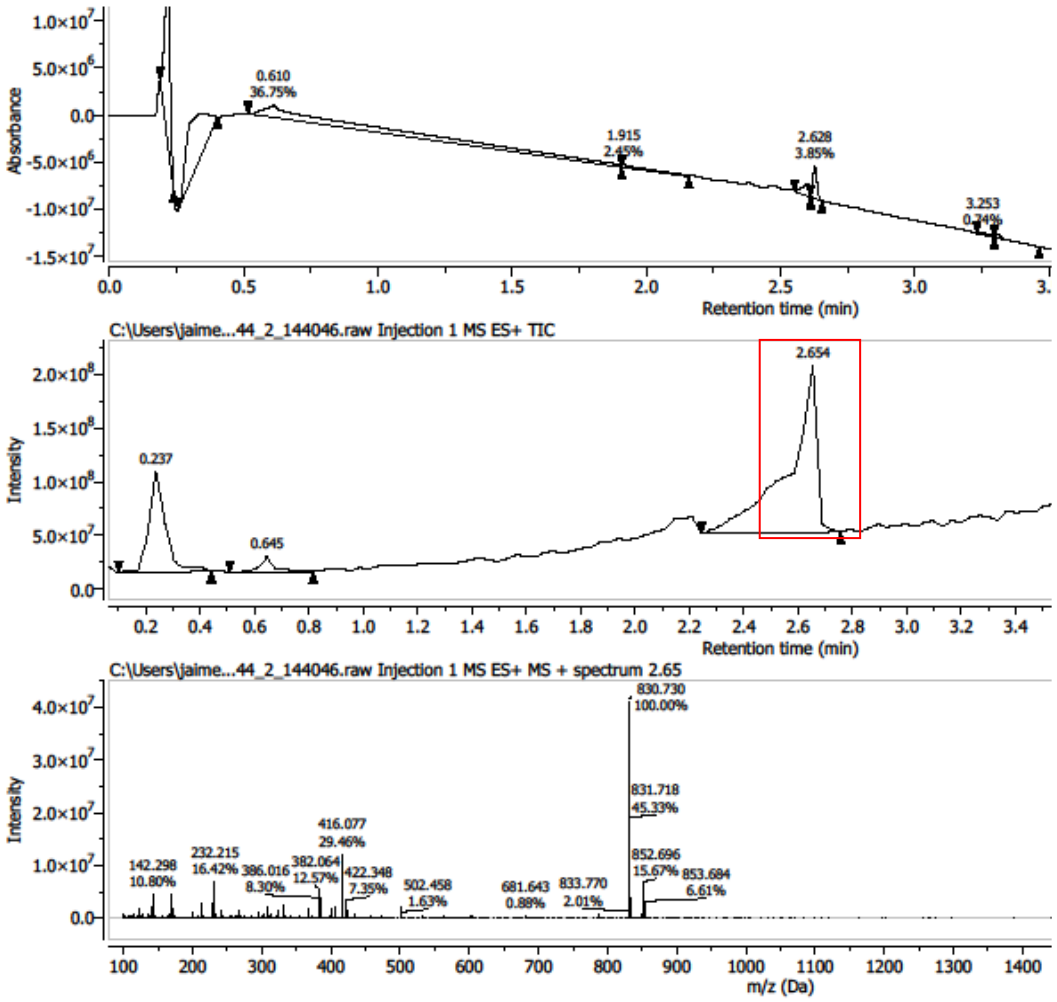

Figure 3.13 A) ^{19}F NMR spectrum showing signals corresponding to product (–61.9 ppm) and starting material (–62.0 ppm) in 4:1 ratio. **B)** ^{19}F NMR spectrum after addition of azide**110** to confirm that the signal corresponds to starting material and **C)** LCMS spectra of **111**.

Subsequently, the reaction was repeated under the conditions used in biological assays. Here, probe **81** (60 μM) and TAG Rh-N3 (**112**) (60 μM) were incubated with $CuSO_4$ (0.6 mM), TBTA (0.6 mM) and NaAsc (0.6 mM) in IP-EDTA lysis buffer (EDTA free) for 1h at rt and analysed by LCMS (Scheme 3.39).

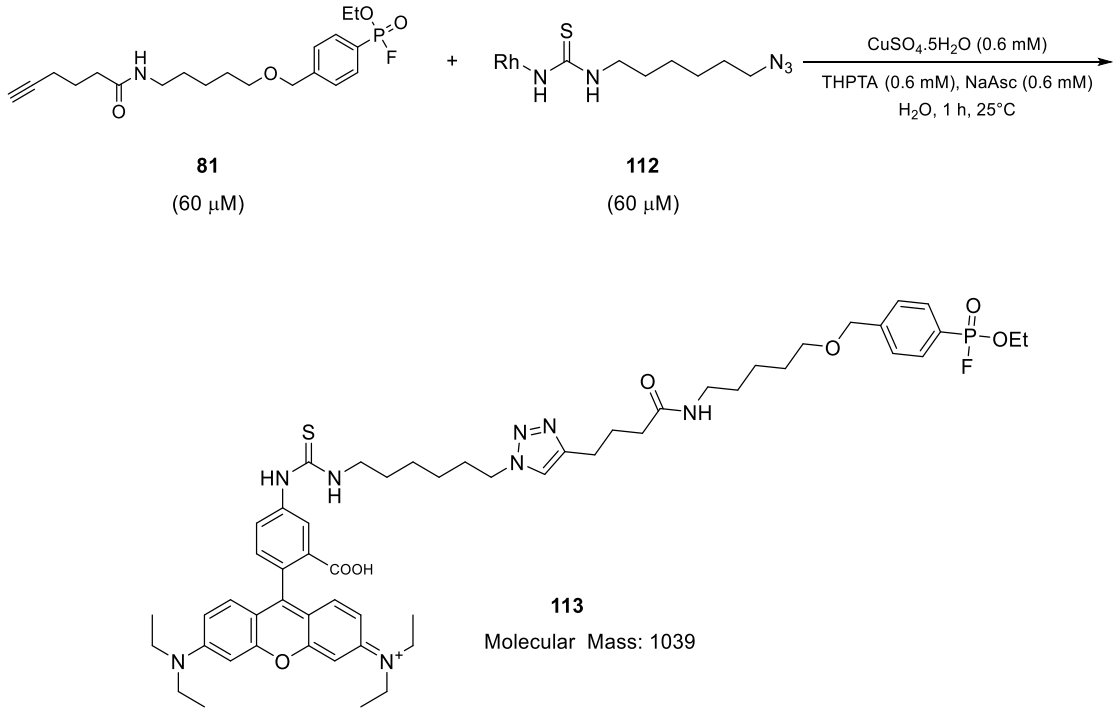

Scheme 3.39. Synthesis of **113** and click validation in biological conditions.

Once again, a peak at m/z 519 $[M/2]^+$ corresponding to the ABP-tag triazole was present whilst the signal characteristic of **81** was not, confirming full conversion and validating the click reaction for further assays (Figure 3.14).

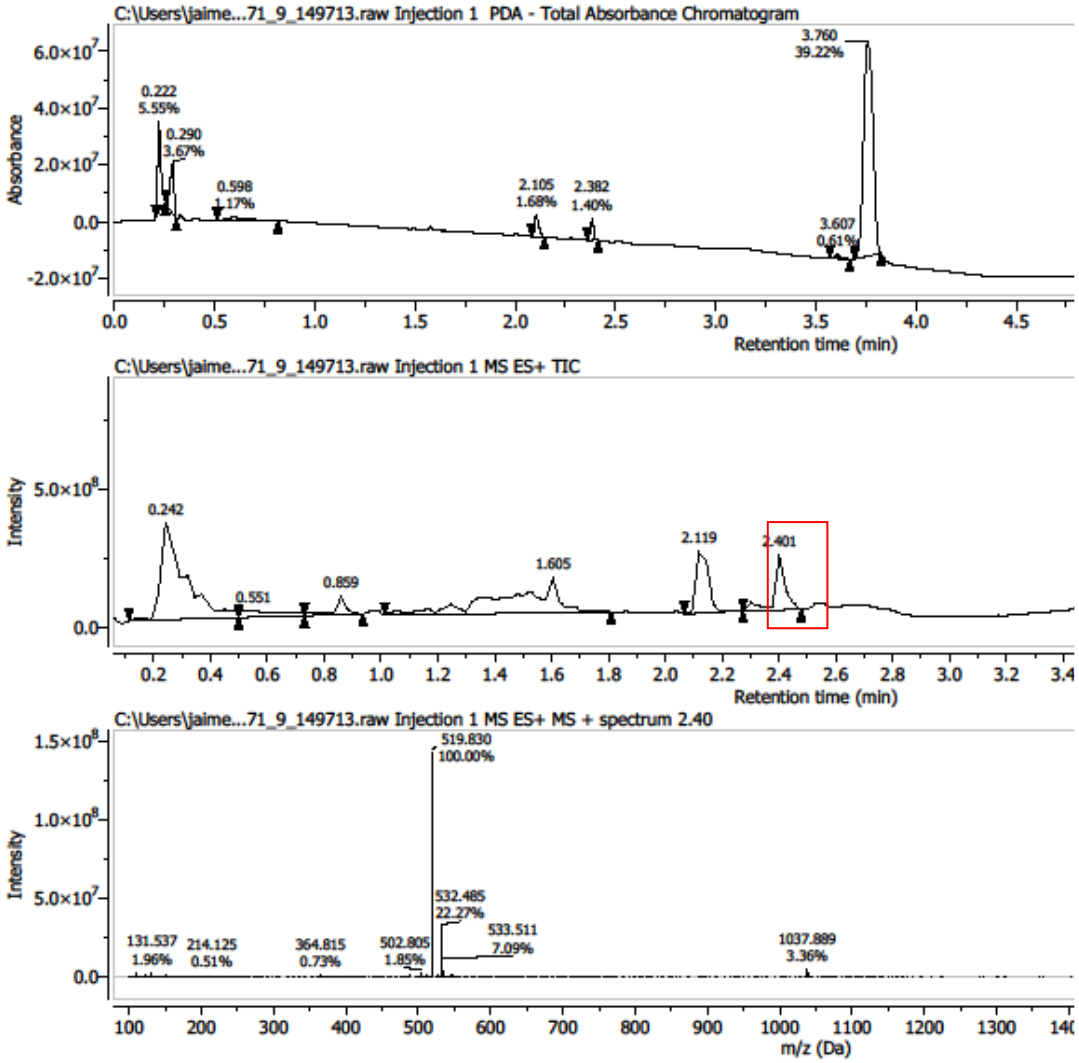

Figure 3.14. LCMS (ES^+) spectra of **114**.

3.3.1.4 Enzyme-ABP-TAG complex validation

The final validation step consisted of obtaining evidence of the complex enzyme-ABP-TAG. Such validation was achieved using in-gel fluorescence methods. To do so, α-CT (0.01 mg/mL) was incubated with different probes (**77**, **81**, Figure 3.15 A) (2 mM) for 1 h at rt, followed by the addition of different TAGs (TetraTAG (**109**), Rh-N_3 (**112**)) (2 mM) and click reagents NaAsc (1 mM), TBTA (1 mM) and $CuSO_4.5H_2O$ (1 mM) and incubated for a further hour and finally run by SDS-PAGE. As can be observed in Figure 3.15, evidence of enzyme-ABP-TAG was confirmed using both probes and

reporters (lanes 4 to 6). Moreover, no off-target interactions were observed when using either probe with the tetraTAG (lanes 1-2). Interestingly, a notable difference in fluorescence intensity was observed when using the different probes. Possible explanations are that probe **77** has lower affinity than **81** towards α-CT due to the decreased electrophilicity of its warhead or, the linker in **81** is longer than in **77**, leaving the alkyne handle more available for the click reaction.

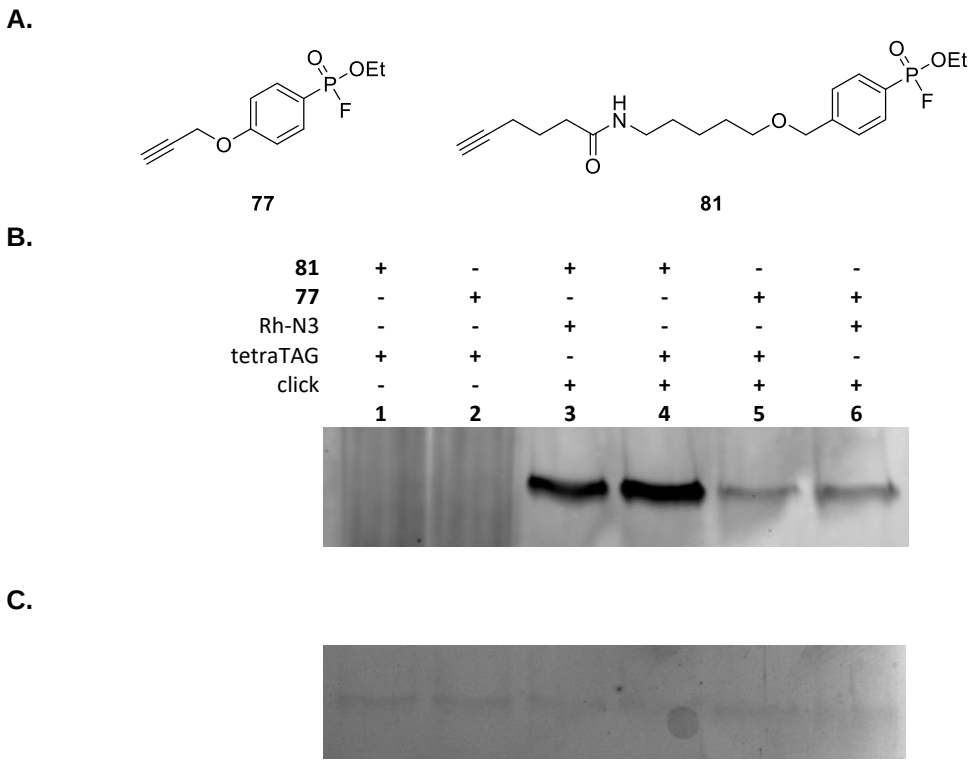

Figure 3.15. A) Structures of probes **77** and **81**. **B)** α-CT (0.01 mg/mL) was incubated with different probes (**77**, **81**) (2 mM) for 1h at rt. It was then added Rh-N_3 or TetraTAG (2 mM), $CuSO_4$ (1 mM), TBTA (1 mM), NaAsc (1mM) and incubated for a further hour. Subsequently, they were run on SDS-PAGE and analysed with fluorescent imaging. **C)** Coomassie blue protein stain.

With the results obtained so far in this section, we were able to validate the specificity and reactivity of aryl FPs towards SHs and therefore, they can be used as activity-based probes to target SHs. Moreover, the ABPP labelling workflow was also successfully tested so the focus then turned to optimization assays.

3.3.2 In-gel labelling optimization

3.3.2.1 *In vitro* optimal ABP concentration

Having established the validity of the aryl-FP probes towards the analysis of active serine residues, the next goal was to determine the optimal working concentration of probe to use on *Leishmania spp* lysates. Here, *L. amazonensis* promastigote lysates were incubated with decreasing concentrations of probe **81** (100 to 25 μM) for 15 min at rt. Subsequently, tag **109** (100 to 25 μM), NaAsc (1 mM), TBTA (0.1 mM) and $CuSO_4.5H_2O$ (1 mM) were added and incubated for a further 1 h at room temperature. Finally, the samples were run on SDS-PAGE and analysed by fluorescence. As seen on Figure 3.16, a probe concentration of 25-50 μM could be selected as optimal as above this concentration, background noise starts to become more important and also, no additional bands are observed. Below this concentration (25 mM), loss of bands was observed (figure not shown).

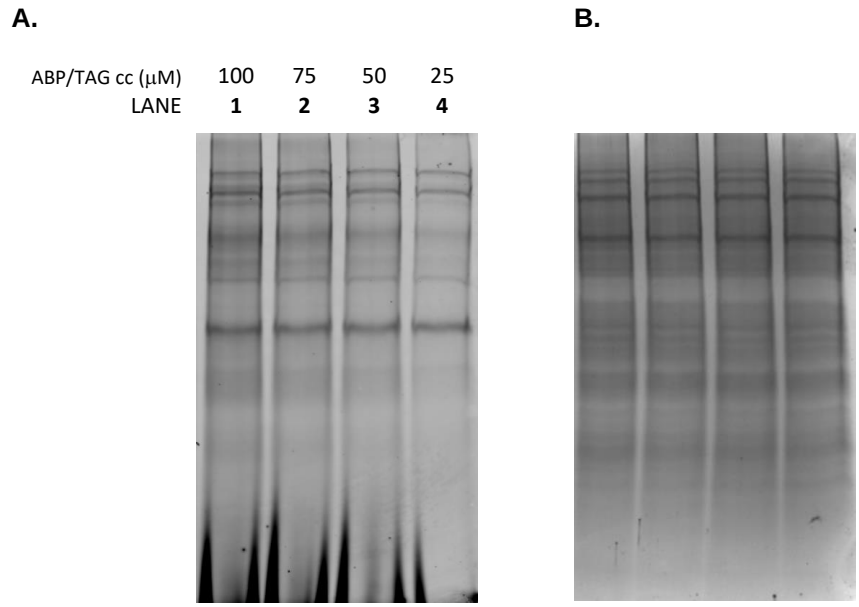

Figure 3.16. A) Determination of optimal probe and TAG concentration. *L. amazonensis* lysates (1 mg/mL) were incubated with **81** and TetraTAG **109** in decreasing concentrations (100, 75, 50 and 25 μM). The lysates were incubated with the ABP at rt for 1 h followed by addition of TetraTAG, $CuSO_4$ (1 mM), TBTA (0.1 mM), NaAsc (1 mM) respectively, and incubated for a further 1 h. Subsequently, they were run on SDS-PAGE and analysed with **A)** fluorescent imaging and **B)** Coomassie blue protein stain.

3.3.2.2 *In vivo* optimal ABP concentration

Once the optimal *in vitro* concentration was determined, similar experiments were carried on for *in vivo* labelling. Here, the parasite cultures were incubated with probe **81** (50 μM) for 70 min at 26 °C. Past this time, they were lysed and subsequent tag addition of **112** via bioorthogonal click chemistry was carried out. Finally, the samples were run on SDS-PAGE and analysed by fluorescent imaging (general procedure 5.2.1.10). As observed in figure 3.17 A, below 50 μM (lane 6), loss of bands is observed in the low molecular weight region (lanes 2-5) whilst above it (lane 7), the

background noise becomes significant. Consequently, 50 μM was chosen as working concentration.

A.

81 (μM)	-	1	5	10	25	50	100	25	-
Rh-N_3 **112** (μM)	-	10	50	100	250	500	500	250	-
FP-TAMRA	-	-	-	-	-	-	-	-	+
In vivo	-	+	+	+	+	+	+	-	-
In vitro	-	-	-	-	-	-	-	+	+
	1	2	3	4	5	6	7	8	9

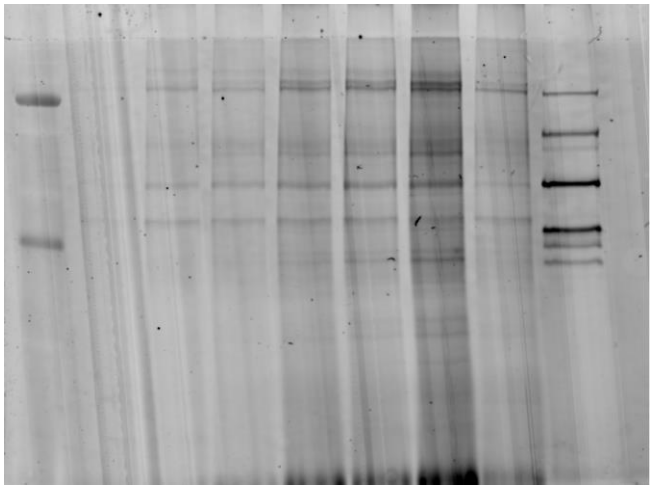

B.

81 (μM)	-	1	5	10	25	50	100	25	-
Rh-N_3 **112** (μM)	-	10	50	100	250	500	500	250	-
FP-TAMRA	-	-	-	-	-	-	-	-	+
In vivo	-	+	+	+	+	+	+	-	-
In vitro	-	-	-	-	-	-	-	+	+
	1	2	3	4	5	6	7	8	9

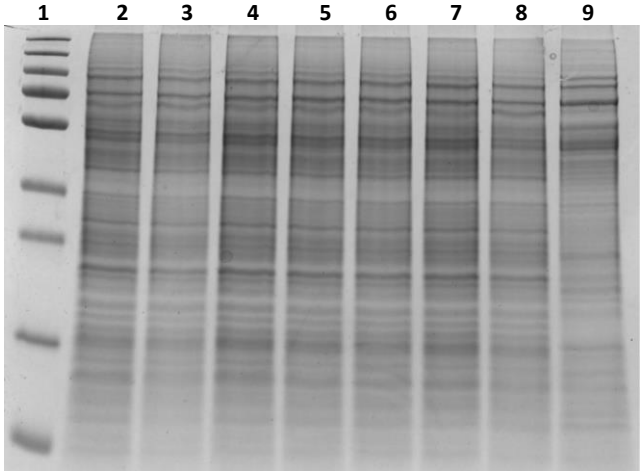

Figure 3.17. A) *L. mexicana* cultures were incubated for 70 min at 26°C with **81**. Subsequently, they were lysed (2 mg/mL) and incubated for a further 60 min at rt with Rh-N_3, $CuSO_4$ (1 mM), TBTA (0.1 mM), NaAsc (1mM). Finally, they were run on SDS-PAGE and analysed with fluorescent imaging and **B)** Coomassie blue protein stain.

3.3.2.3 Determination of optimal *in vivo* incubation time

Having established the optimal working concentration, probe **81** (50 μM) was incubated in a *L. mexicana* parasite promastigote culture for different times and analysed using earlier described methods. It can be observed that the best resolution and number of bands were obtained with a 120 min incubation time. Under this time, the resolution is good but fewer and less intesnse bands are observed, suggesting that different enzymes possess different specificity for the probe used. (Figure 3.18).

A.

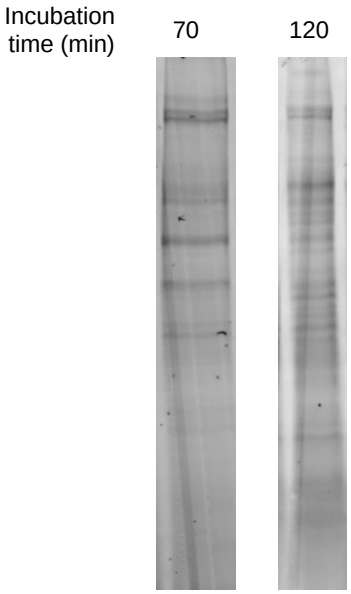

Figure 3.18. A) *L. mexicana* cultures were incubated for the stated times at 26°C with **81** (50 μM). Subsequently, they were lysed (2 mg/mL) and incubated for a further hour at rt with Rh-N_3 (0.5 mM), NaAsc (1mM), TBTA (0.1 mM) and $CuSO_4$ (1 mM) respectively. Finally, they were run on SDS-PAGE and analysed with fluorescent imaging and **B)** Coomassie blue protein stain.

3.3.2.4 Biotin-Streptavidin enrichment

In section 3.2.4.1 we discussed the advantadges of using a cleavable biotinylated tetrafunctional tag for capture, visualization and enrichment of probe-labelled enzymes since normal enrichment procedures involve harsh and time-consuming conditions necessary for the elution of the enriched proteins. In this section, we evaluate the pulldown eficiency using streptavidin magnetic spheres (Promega Streptavidin MagneSphere Paramagnetic Particles, SA-PMPs) which potentially offer advantages such as more rapid and milder conditions over the traditional methods. Probe **81**, tetratag **109** and α-CT were chosen as model probe and enzyme.

Here, after incubation of the probe with α-CT and subsequent attachment of the tag, the proteome was enriched following the manufacturer's procedure and initial experiments using dithiothreitol (DTT) as reducing agent for disulfide bond cleavage were attempted and despite following the conditions described both in the literature and from a commercial probe manufacturer, they proved unsuccessful (Table 3.2). Moreover, in all cases the solution turned black, and aggregation/precipitation was observed, suggesting that the streptavidin beads degraded during the cleavage. Consequently, other reducing agents such as TCEP[141] (Thermo Scientific Instructions CAS #51805-45-9) and 2-mercaptoethanol (BME)[141] were also tested, but similar results were observed. After a further literature search, it was found that the pH plays a key role in the reducing capacity of these compounds as protonated sulphur atoms have lowered nucleophilicities meaning that they become less potent as the pH lowers.[142]

Entry	Reducing agent	Reducing agent cc (M)	pH	Yield (%)
1	DTT	0.5	4-5	< 10*
2	DTT	0.25	4-5	< 10*
3	DTT	0.5	7.4	≈19*
4	DTT	0.25	8	≈ 65*
5	TCEP	0.5	7.4	< 10
6	BME	0.5	4-5	< 10
7	BME	0.5	4-5	< 10
8	BME+Et_3N	0.5	7.4	< 10
9	BME	0.5	7.4-8	69

(*) Degradation and aggregation observed.

Table 3.2. Disulfide bond cleavage conditions.

Consequently, to increase the concentration of thiolate anions, the cleavage was tested using a pH closer to BME pK_a (9.61) and after the pulldown, α-CT was obtained with an efficiency of 69% (Figure 3.19). In addition, it can be observed in lane 3 that the fluorescence intensity is very low, indicating very good streptavidin-biotin interaction.

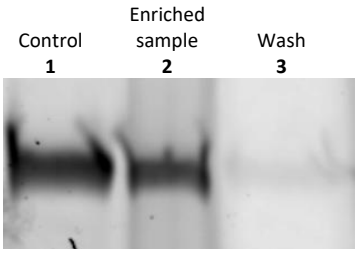

Figure 3.19. α-CT (0.01 mg/mL) was incubated with **81** (5 μM) for 1h at rt. Subsequently, TetraTAG (5 μM), $CuSO_4$ (1 mM), TBTA (1 mM), NaAsc (1 mM) were added and left for 1 h. The mixture was then incubated for 30 min with SA-PMPs. After this time, the enriched sample was washed with PBS (3 × 300 μL). Finally, it was cleaved with 2-BME (0.5 mM) (pH=8) during 1 h at rt, run on SDS-PAGE and analysed with fluorescent imaging. Lanes: 1) Control 2) Pulldown 3) Wash before cleavage.

The good results obtained after pulldown and cleavage optimization confirmed that this methodology can be used instead of normal elution methods for pulldown experiments. Moreover, when the efficiency was compared with the results obtained using traditional columns with fixed streptavidin beads by Yang and Verhelst *et al.,*[133] comparable results were obtained, demonstating this to be a good enrichment procedure for future experiments.

3.3.3 Comparison of ABP labelling profiles

After successfully validating the aryl fluorophosphonate probe and obtaining optimal working conditions, the reactivities of the 3 set of probes (Figure 3.20 A) were assesed and compared on *L. mexicana* promastigote parasites, using both *in vitro* and *in vivo* labelling (Figure 3.17 B and C) following previously described procedures.

A. ABPs

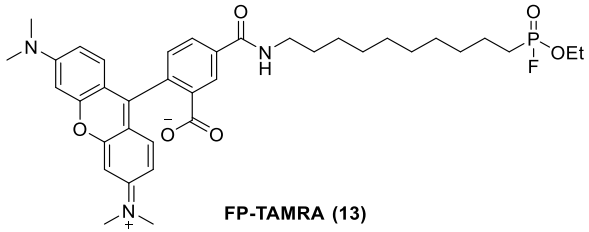

FP-TAMRA (13)

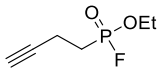

85

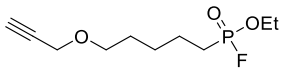

114

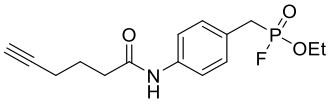

94

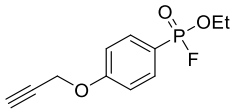

77

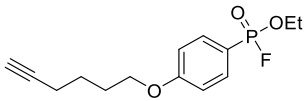

78

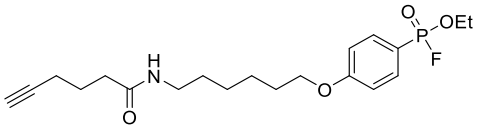

79

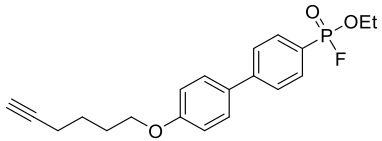

80

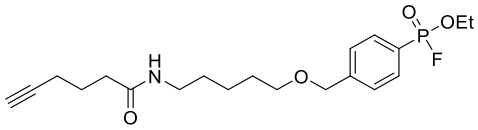

81

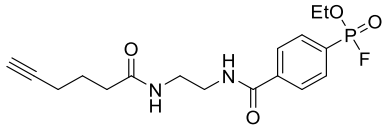

82

Gel Lanes:

1) Ladder

2) TAMRA-FP (**13**)

3) Alkyl-FP C4 (**85**)

4) Alkyl-FP C9 (**114**)

5) Benzyl-FP (**94**)

6) Aryl-FP eD-C4 (**77**)

7) Aryl-FP eD-C7 (**78**)

8) Aryl-FP eD-C14 (**79**)

9) Aryl-FP eD-BiPh (**80**)

10) Aryl-FP eN (**81**)

11) Aryl-FP eW (**82**)

B. *In vitro* ABP labelling

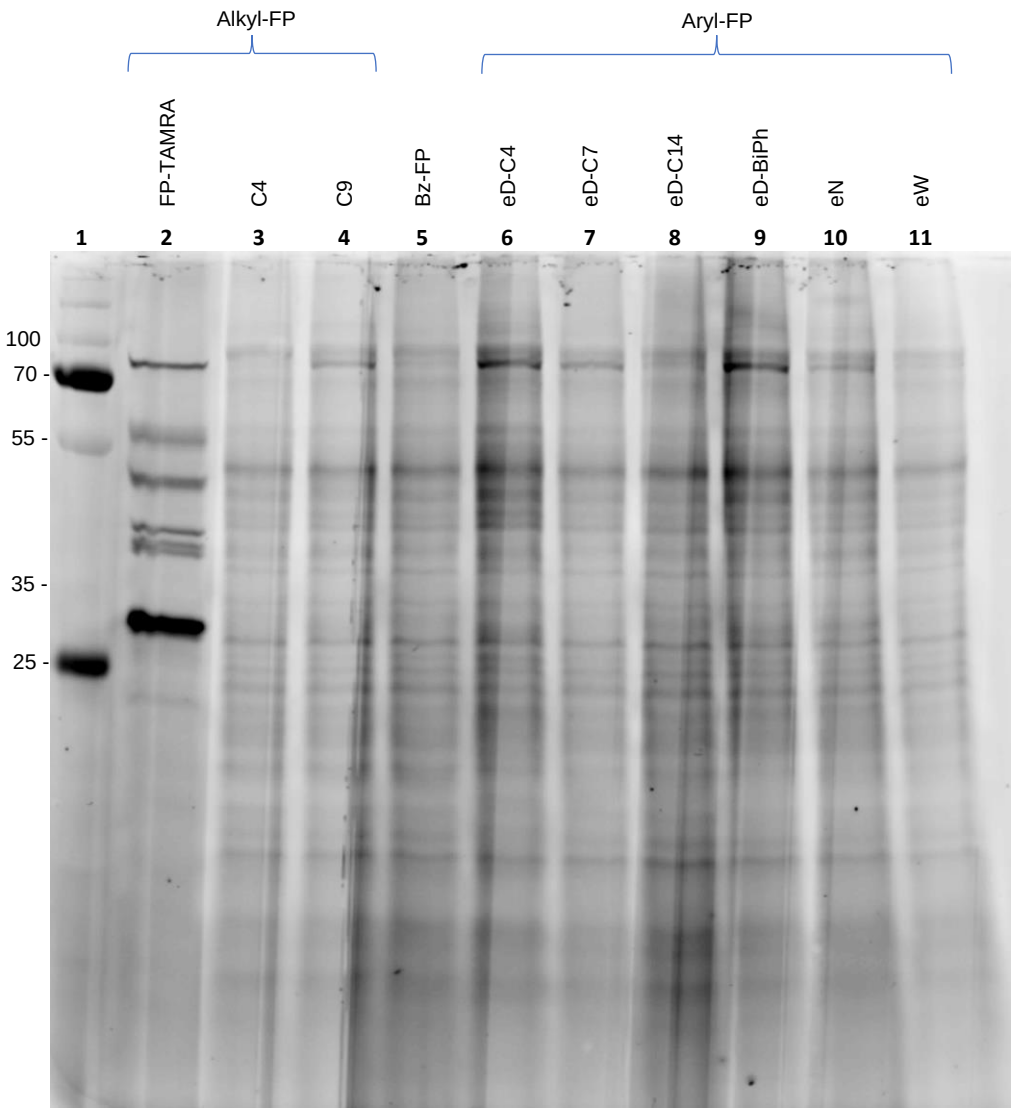

C. *In vivo* ABP labelling

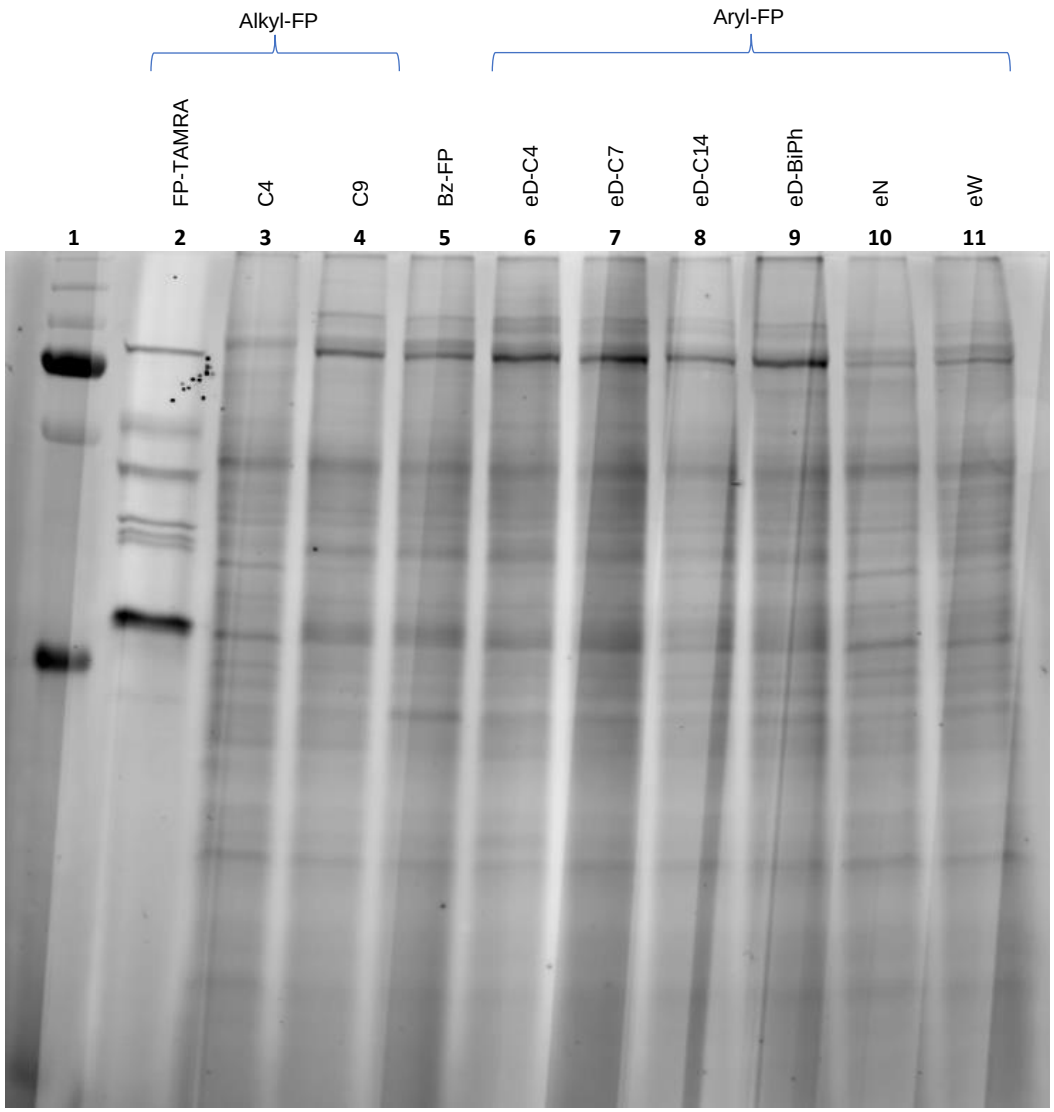

D. Coomassie blue protein stains

In vitro ABP labelling

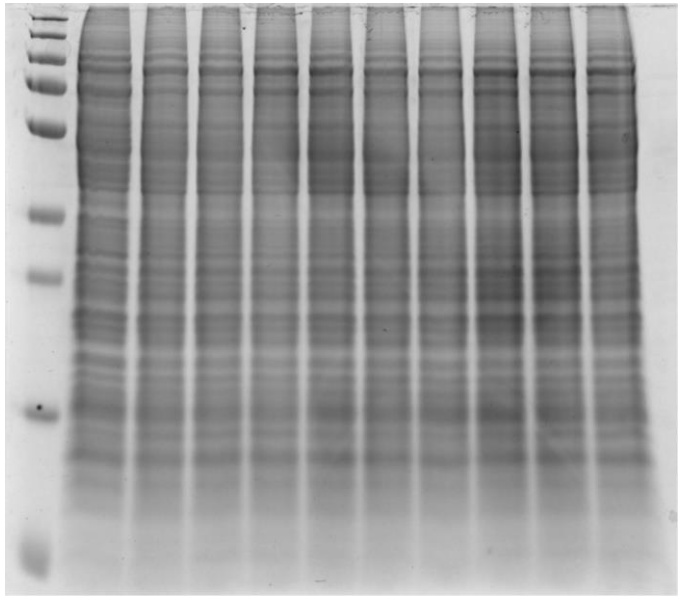

In vivo ABP labelling

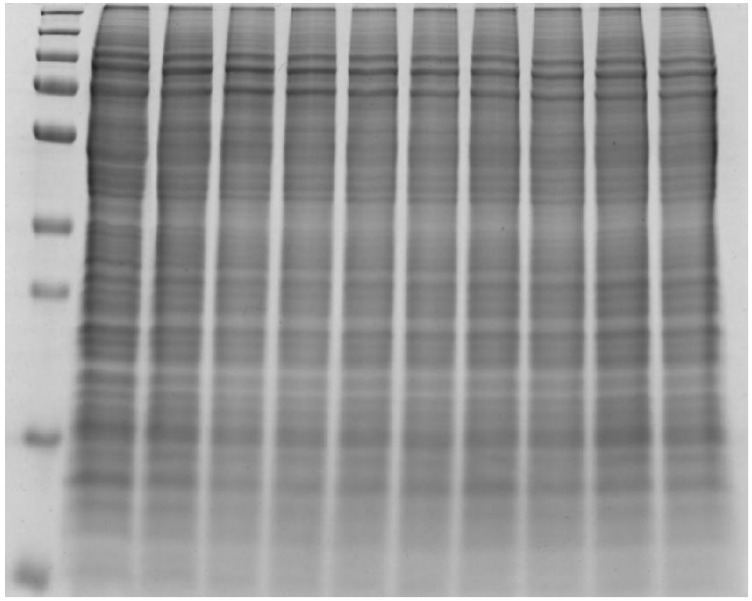

Figure 3.17. A) Probes used in *in vitro* and *in vivo* ABP labelling. **B)** *L. mexicana* lysates (2 mg/mL) were incubated with the stated FP-alkynes (50 μM) and FP-TAMRA (1 μM) at rt for 60 min. After this period, Rh-N_3 (0.5 mM), NaAsc (1 mM), TBTA (1 mM) and $CuSO_4$ (1 mM) were added, and the mixture was incubated for a further hour with periodic mixing. Finally, the samples were run on SDS-PAGE and analysed with fluorescent imaging. C) *L. mexicana* cultures were incubated with the stated FP-alkynes (50 μM) at rt for 120 min. After this period, Rh-N_3 (0.5 mM), NaAsc (1 mM), TBTA (1 mM) and $CuSO_4$ (1 mM) were added, and the mixture was incubated for a further hour with periodic mixing. Subsequently, they were lysed (2 mg/mL) and incubated for a further hour at rt with Rh-N_3 (0.5 mM), NaAsc (1 mM), TBTA (0.1 mM) and $CuSO_4$ (1 mM) respectively. Finally, they were run on SDS-PAGE and analysed with fluorescent imaging. **D)** Coomassie blue protein-stained gels of *in vitro* and *in vivo* labelling.

Labelling with FP-TAMRA vs synthesized probes

Comparison of the fingerprints obtained with TAMRA-FP (*in vitro* labelling, Figure 3.17 B, lane 2) and the synthesized probes shows that TAMRA-FP affinity is different and fewer bands are observed. This suggests that the fluorophore TAMRA could be playing an important part in modulating the affinity of the probe. This is mainly supported when it is specifically compared with alkyl-FP C9 probe **114** (*in vitro* labelling, lane 4) since they both possess the same warhead and similar linker lengths. These findings confirm the initial hypothesis of the advantages of using cell permeable probes with an alkyne handle instead of tagged-probes. To further validate this hypothesis and assess the effect of the tag, additional experiments such as switching the fluorophore from TAMRA-FP and attaching the tag to probe **114** prior to the incubation with the lysates.

In vitro vs *in vivo* labelling

When *in vitro* and *in vivo* gels are analysed and the fingerprints compared, it can be observed that the labelling of identified POP (80 kDa) is inconsistent using *in vitro* conditions. In contrast, this band was observed with consistency using *in vivo* labelling, suggesting that the lysis procedure could affect the enzyme activity. Moreover, fewer bands are observed in the low MW region of the *in vivo* gel probably due to the action of the protease inhibitors present in the lysis buffer used for *in vivo* labelling resuting in less degradation of enzymes by the action of proteases. In general, the labelling patterns using *in vitro* conditions produced similar fingerprints regardless of the probe used if compared with *in vivo* fingerprints. As the protein stains are similar both in band quantities and relative intensities, this suggests that the enzymes are present but not

active rather than degraded as they are not in their native state. Overall, theses results confirm and reinforce the advantages and need to use *in vivo* ABP labelling conditions for target discovery.

Labelling comparison between the synthesized probes

When the labelling patterns were compared using *in vivo* labelling, a number of observations were noted. For example, the fingerprint of alkyl-FP C4 probe **85** (lane 3) is different from the other probes mainly in the high MW region between 70 and 100 kDa. Additionally, it is the only probe that failed to label the previously identified POP, carboxypeptidase and lysophospholipase. Moreover, when alkyl-FP probes **85** (C4) and **114** (C9) fingerprints are compared, they present significant differences. As the reactivity of the warhead is the same, this can only be explained by their size difference, where the longer aliphatic chain could be modulating the affinity of the probe.

On the other hand, the benzyl-FP probe **94** (lane 4) labelling pattern resembles the aryl fluorophosphonates. As this warhead has a similar, but less rigid bulky group, this suggests the importance of the warhead sterics and size in relation to the capacity to modulate the affinity of an activity-based probe.

It can be observed that the difference in linker length in aryl-FP eD probes **77**, **78** and **79** do not affect their affinity as similar labelling patterns are observed (lanes 6 to 8) suggesting that the alkyne handle is similarly available for click reaction with the tag. In addition, the biphenyl eD probe **80** also showed similar labelling despite its bigger size. In contrast, clear labelling differences are observed mainly between the eD probes and the eN/eW probes **81** and **82** suggesting the importance of the

electrophilicity of the phosphorus atom for the interaction with the active serine residues.

In summary, the overal differences in labelling observed across probes confirms the importance and influence that each block of the probe; warhead, linker and tag has for its affinity. Nevertheless, as this experiment was not conducted with biological replicates, it should be repeated. Subsequent identification of the bands labelled using MS proteomics is also needed to validate the probes as ABPs capable of targeting SHs. Moreover, the identification of new SHs will help expand the *Leishmania* SH universe, and allow further exploration for drug targets within this enzyme family.

4 General Conclusions and future work

4.1 Conclusions

Leishmania is a flagellate protozoan whose life cycle requires a vector and a host for its dispersion and biological performance. During transmission from the vector to the host, the parasite undergoes a series of adaptive events required for the development of both the promastigote and amastigote forms, and serine hydrolases play a crucial role in the precise performance of this biochemical network, as they are key in processes such as degradation of exogenous proteins, parasite infectivity and parasite-host cell interactions.[84] In the present work, we have applied an ABBP approach to profile for the first time the targetable SHs present in different *Leishmania spp* through their different life stages.

Commercially available organofluorophosphonate probes such as TAMRA-FP and FP-Biotin, which have been experimentally proven in ABPP assays in animal, plant, and archaea model systems,[91,92,96,143] were used on *L. major*, *L. amazonensis*, *and L. mexicana,* representing the diversity between *Leishmania* proteomes (Old-World vs New-World species). The clear fingerprint patterns observed between New-World and Old-World species illustrates differences in the geographic separation of these species, as previously reported, where despite an overall similarity in the protein distribution, clear differences between the *L. major* and *L amazonensis* promastigote proteomes were observed, suggesting that in spite of the genome similarities between these species, their transcriptomes or post-translational modifications might be affetected.[144] Furthermore, mapping at different stages of their life cycles (non-infective early log promastigotes, infective stationary phase promastigotes, and axenic amastigotes) revealed significant changes in protein expression; particularly between the promastigote and axenic amastigote forms, where more and different enzymes

were labelled in the latter. This is no surprise since reported comparative transcriptomic analysis of gene expression between these forms of *L. mexicana*, revealed more than 3800 differentially expressed RNA sequences from the over 9000 protein coding genes. During this transition, flagellum motility proteins are downregulated, whereas cell surface proteins, transporters and peptidases are upregulated.[145] In a SH context, these findings correlate since most serine hydrolases are proteases, potentially acting as virulence factors[146] and/or participating in the parasite-macrophage interaction.[147]

Since in-gel fluorescence ABPP does not assign any identity to the probe-labelled target proteins, gel-free enrichment experiments, followed by target discovery via MS isobaric labelling iTRAQ, were used to identify two serine proteases: Carboxypeptidase LmxM.18.0450 and prolyl oligopeptidase (POP) LmxM.36.6750 and lipase lysophospholipase LmxM.24.1840. Despite these promising results, a comparison between the results obtained using in-gel and gel-free ABPP approaches, suggests that probably more enzymes should have been identified using a MS approach. This hypothesis is supported by the in-silico studies carried-out in our lab, where 28 serine proteases were predicted, and the fact that competition between FP-biotin and TAMRA-FP demonstrated that both probes interact with the observed bands. At this point, human error during experiments cannot be discarded and the gel free MS assays should be repeated.

Using a competitive ABPP approach, two small molecule inhibitors, chymostatin and ZPP were identified to interact with the labelled enzymes. Chymostatin compromised *L. mexicana* parasite survival with high potency (EC_{50} = 26 ± 5 nM in promastigotes, EC_{50} = 23 nM ± 5 in axenic amastigotes), values surprisingly lower than those reported from currently available drugs such as miltefosine on *L. amazonensis* promastigotes

(47.0 ± 3.9 μM)[115] or with antimonials on *L. major* ([Sb(III)] EC_{50} 4.3 ± 0.3 μM, [Sb(V)] EC_{50} 44 ± 6 μM).[116] Since not all its targets were identified using TAMRA-FP, these results represent only a partial picture, suggesting that the serinome data obtained using TAMRA-FP may not be complete, and that the target responsible for compromising parasite survival remains unidentified. Unfortunately, chymostatin is not a good hit candidate due to its low solubility and peptic nature, which could compromise its metabolic stability. Nevertheless, it could be considered a hit scaffold fit for the search for lead drugs. Moreover, chymostatin-based ABPs could help to understand its mode of action. In contrast, ZPP showed very high affinity (IC_{50} = 10 pM) for POP, a protease that has been related to the parasite host infectivity process, but with little effect on parasite survival. However, it has been proven that ZPP reduced the infectivity of murine macrophages by *L. infantum*, positioning POP as an attractive drug target. Collectively, these findings confirm the advantages of using competitive ABPP for target discovery and validation. A transcriptomic analysis of these proteases revealed that the levels of the carboxypeptidase decreased when moving from the promastigote to amastigote form whilst POP expression increased. This could be related to an adaptation mechanism to the host-cell environment. This is consistent with other reports on the *T. cruzi* ortholog POP Tc80 and its *L. infantum* homolog, where it was proposed that POP would have an important role in the degradation process of the extracellular matrix that allows host-cell invasion.[107,108,148]

Most ABPP workflows are carried out using tissue homogenates, where proteins are removed from their native cellular environments. As the function of an enzyme is often tied to the presence of inhibitors/activators as well as protein-protein interactions, the perturbations produced during cell lysis could lead to inactivation of enzymes and loss of binding affinity between the probes and the target enzymes. In consequence, *in*

vitro proteomic preparations can only approximate the functional state of proteins in a living cell or organism. As the commercial probes used are not fit for *in vivo* labelling due to the lack of cell permeability, sets of electronic- and sterically different alkyl-, benzyl- and aryl- fluorophosphonate probes were successfully synthesized and tested against *L. mexicana* promastigotes using both *in vitro* and *in vivo* conditions. Clear differences in the gel landscapes using *in vivo* conditions have been observed. In addition, more bands were observed in comparison with TAMRA-FP supporting the hypothesis that the presence of the tags might be interfering with the enzyme-probe interaction. Even though different fingerprint patterns were observed, which suggests that fine tuning of the warheads is possible, these present more similarities than differences. The differences observed are more related to the binding affinity in terms of expression levels, rather than the number of labelled enzymes, meaning that the binding groups introduced in the probes, were able to modulate their affinity, but failed in tuning their specificity towards different subfamilies within the SHs. A possible explanation is that since the enzyme-probe affinity starts with the positioning and interaction of the probe with the P and P_1 recognition sites of an enzyme, the probes' warheads were not structurally different enough, suggesting that more structural diversity should be incorporated in the binding groups to tune and narrow or direct the affinity of an ABP. Another possibility is that the high reactivity of the fluorophosphonate increases the promiscuity within the SH, reducing the capacity to interact with specific subsets of enzymes. All things considered, since the available FP probes have been shown to target 80-90% of metabolic SHs in complex proteomes,[64] introducing significant structural variations to address the remaining enzymes represents a challenge. Collectively, the comprehensive knowledge generated from this work would be helpful to expand the current understanding of SHs

in *Leishmania* spp and paves the way for a better drug discovery program for leishmaniasis. Additionally, the present work is one of the few which focusses on developing new cell-permeable fluorophosphonate probes, and these could represent good assets for broader spectrum SH probes used in ABPP, that could be exploited to profile this enzyme family in multiple organisms.

4.2 Future work

This project attempted to map and explore therapeutic targets within SHs present in the *Leishmania* proteome using an activity-based protein profiling (ABPP) strategy in the quest to find new protein drug targets for drug discovery as well as developing a "toolkit" of different probes capable of targeting the complete serinome. So far, this was partially done using commercially available FP probes, but these proved to be somewhat inadequate for *in vivo* conditions. In addition, new cell-permeable FP probes were developed to improve the serinome coverage. Initial in-gel labelling experiments were conducted, showing more and new bands when compared with the commercial TAMRA-FP. To confirm that the synthesized probes are specific for serine hydrolases, and thus validate them as specific SH ABPs, gel-free MS assays using isobaric labelling tags such as iTRAQ or TMT should be conducted to identify the labelled enzymes. Moreover, the comparative information obtained could provide insights for better understanding the reactivity and affinity of the different warheads used, which can help designing additional and more efficient probes.

From a chemical point of view, as previously mentioned, focus should be made in an attempt to generate a SH probes' toolkit capable of labelling the whole spectrum of the predicted SH in *Leishmania*. Therefore, the use of additional warheads should be

explored. That being said, diphenylphosphonates (DPPs) (Figure 4.1) have been commonly used to target serine proteases and pose an attractive option since the majority of the SH family present proteolytic activite. Additionally, these probes affinities can be modulated to target different protease subclasses by addition of specific amino acids in position alpha to the warhead.[89]

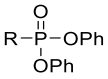

Diphenylphosphonate

Figure 4.1. General structure of diphenylphosphonate warhead.

On the other hand, 4-chloroisocoumarins (CIC) (Figure 4.2 A) have also shown to be specific for serine hydrolases. As they are not limited only to proteases, they could be a good addition to try to cover the rest of the enzyme family. Their specificity success is due to its two-hit mechanism of inhibition. Here, the active serine attacks the isocoumarin carbonyl group. Consequently, the heterocycle opens, creating an acyl intermediate. Then, the reactive intermediate isoquinonimide methide formed, product of the elimination of the 4-chloro group elimination, is attacked by the catalytic histidine present in serine hydrolases (Figure 4.2 B).[89]

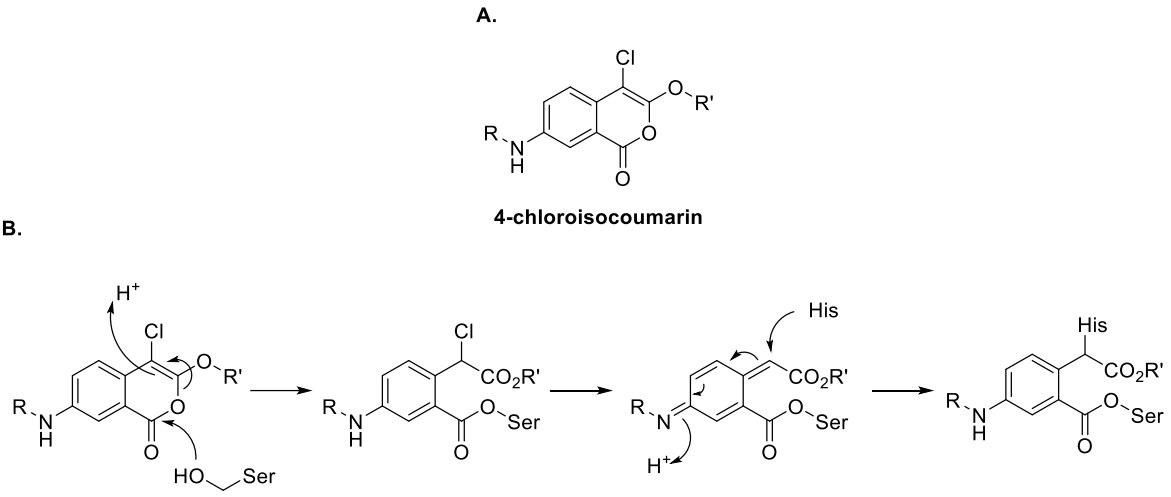

Figure 4.2. A) Structure of 4-chloroisocoumarin warhead. **B)** Warhead two-hit mechanism.[89]

These two warheads are attractive since they have been reported to possess high affinity with SH. Moreover, they offer the capacity for further modulation of affinity by attachment of different moieties in the R groups.

From a biological point of view, the final step of the project involves the evaluation of the identified enzymes as potential drug targets. To do so, a set of different experiments can be conducted, which include the identification of specific inhibitors, their capacity to compromise parasite survival and/or their infectivity capacity, and additional assays to validate modes of action.

The search for specific inhibitors, using competitive ABPP proved to be a straightforward and powerful technique that allowed screening commercially available inhibitors against carboxypeptidase and POP. In addition, to identify the target of chymostatin responsible for the low EC_{50} value observed, which represents a promising drug target, competitive ABPP assays between chymostatin and the synthesized probes needs to be conducted. Finally, to further characterise the identified lysophospholipase, and determine its essentiality for parasite survival and

infectivity, it is necessary to conduct competition assays using known and commercially available lipase inhibitors. It has been reported that inhibition of lysophospholipase (LYPLA1) blocks the replication *in vitro* of *P. falciparum,*[151] making this enzyme a promising target. For this, the broad-spectrum inhibitor orlistat could be considered. In addition, compounds ML211, ML348 and ML348 identified and used by Adibekian *et al.*[149] as specific reversible inhibitors of lysophospholipase (LYPLA) 1 and 2 in humans (Figure 4.3) could also be tested against lysophospholypase LmxM.24.1840.

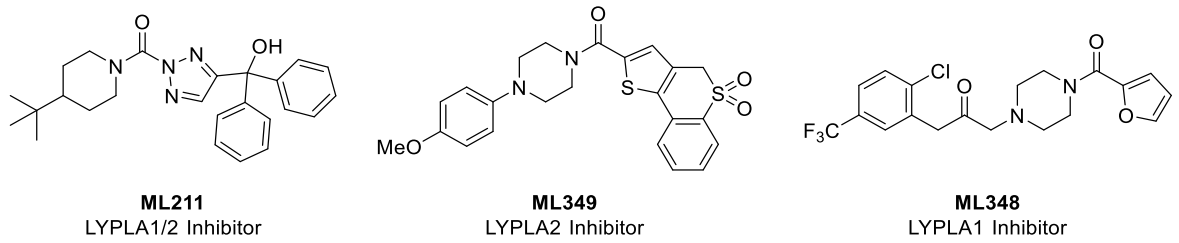

Figure 4.3. LYPLA inhibitors used by Adibekian *et al.*[149]

Subsequently, cytotoxicity of the identified inhibitors such as ZPP and chymostatin, as well as any other promising inhibitors needs to be determined to confirm that they exhibit low potency and cytotoxicity in human cell lines. To do so, macrophage cell cultures should be prepared following reported procedures, and tested against the inhibitors. Additionally, infectivity assays of in macrophages by *L. mexicana* parasites should be conducted in presence of the inhibitors to test their capacity to compromise their virulence.

A key characteristic of a good drug target is its essentiality for the organism. Gene knockouts of these enzymes can provide more information about their essentiality as

well as their involvement in the infection process. Moreover, they can help to identify the presence of enzymes with redundant function. Since the identified POP has been associated with the infectivity process of the parasite and that it can be inhibited with high specificity with ZPP, a gene knockout could be produced to analyse and verify our findings. Additionally, little is known about the other enzymes found (carboxypeptidase and lysophospholipase) and generating knockouts of these would help understanding their role and importance in the parasite. These knockouts can be produced using CRISPr-Cas9 technique already reported for kynetoplastids.[150]

As Leishmaniasis is a trypanosomatid disease closely related to Chagas disease and African sleeping sickness. All of these are considered neglected tropical diseases and require new and more efficient chemotherapeutic options. Applying an ABPP approach to profile their serinomes not only could help finding new drug targets but it would also validate the viability of the new tools developed in this project in different biological environments.

5 Experimental

5.1 Chemical synthesis

5.1.1 General Conditions and Methods

All solvents and reagents were purchased from commercial suppliers. NMR spectra were recorded on the following instruments: Bruker Neo 700 MHz spectrometer with operating frequencies of 699.73 MHz for ^{1}H, 175.95 MHz for ^{13}C, 658.41 MHz for ^{19}F, and 283.25 MHz for ^{31}P; Varian VNMRS-600 spectrometer with operating frequencies of 599.42 MHz for ^{1}H, 150.72 MHz for ^{13}C, 564.02 MHz for ^{19}F, 242.65 MHz for ^{31}P; Bruker Neo-400 spectrometer with operating frequencies of 400.20 MHz for ^{1}H, 100.63 MHz for ^{13}C, 376.57 MHz for ^{19}F, 162.00 MHz for ^{31}P; Bruker Avance III-HD-400 spectrometer with operating frequencies of 399.95 MHz for ^{1}H, 100.57 MHz for ^{13}C, 376.33 MHz for ^{19}F, 161.90 MHz for ^{31}P; Bruker Avance III-HD-400 spectrometer with operating frequencies of 400.07 MHz for ^{1}H, 100.60 MHz for ^{13}C, 376.45 MHz for ^{19}F, 161.95 MHz for ^{31}P. Spectra were referenced relative to $CDCl_3$ (δ_H 7.26 ppm, δ_C 77.16 ppm), DMSO-d6 (δ_H 2.50 ppm, δ_C 39.52 ppm) or CD_3OD (δ_H 4.87 ppm, δ_C 49.00 ppm), D_2O (δ_H 4.79 ppm) Chemical shifts are reported in parts per million (ppm), coupling constants (J) in hertz (Hz) and multiplicity as singlet (s), doublet (d), triplet (t), quartet (q), multiplet (m) or a combination thereof. All ^{1}H NMR and ^{13}C NMR spectral assignments were made with the aid of ^{1}H-^{1}H COSY, ^{1}H-^{13}C HSQC and ^{1}H-^{13}C HMBC NMR experiments. Infra-red spectra were recorded on a PerkinElmer Frontier FTIR spectrometer equipped with a Specac Quest ATR accessory with extended range diamond puck. IR assignments are reported in wavenumbers (cm^{-1}). Thin layer chromatography was performed using Merck F254 silica gel 60 aluminium sheets pre-coated with silica gel. High resolution mass spectrometry (HRMS) and liquid chromatography mass spectrometry (LCMS) were recorded on a

Waters TQD mass spectrometer ESI-LC water (0.1 % formic acid): MeCN, flow rate 0.6 mL min-1 with a UPLC BEH C18 1.7 µm (2.1 mm × 50 mm) column.

5.1.2 General Methods

5.1.2.1 General procedure A – Michaelis-Arbuzov reaction

The stated aryl/alkyl halide (1 eq) was added to triethylphosphite (10-20 eq) in a round bottom flask at room temperature. The reaction mixture was heated at 140-160 °C overnight under an Ar atmosphere. Subsequently, it was diluted with EtOAc and washed with H_2O and brine. The organic layer was dried ($MgSO_4$), and the volatiles were removed under high vacuum (24-72 h) to afford the desired phosphonate.

5.1.2.2 General procedure B - Aryl phosphonate synthesis (Hirao cross coupling reaction)

A round bottom flask charged with dry EtOH (volume adjusted to achieve 0.2 M limiting reactant), $Pd(OAc)_2$ (0.03 eq) and PPh_3 (0.09 eq) was degassed and stirred at 90 °C for 30 min. under N_2. Subsequently, aryl halide (1 eq), *N,N*-dicyclohexylmethylamine (1.5 eq) and diethyl phosphite (1.2 eq) were added via syringe, and the reaction mixture was stirred at 90 °C overnight. Upon completion, the volatiles were removed, and the remaining residue was taken in EtOAc. The remaining residue was then washed with 1 M HCl, H_2O, and brine, dried ($MgSO_4$) and purified by flash chromatography to afford the desired phosphonate.

5.1.2.3 General procedure C – Williamson etherification

Anhydrous K_2CO_3 (2.0 eq) was added to a solution of the stated hydroxy aryl phosphonate (1.0 eq) in dry acetone (5 mL) and the resulting mixture was stirred for 0.5 h. Subsequently the tosylated alkyne (1.2 eq) and TBAI (10 mol %) were added to the solution and stirred for an additional 12-36 h at reflux temperature under N_2. The residue obtained after removing the volatiles was extracted with EtOAc and washed with water and brine. The organic layer was then dried ($MgSO_4$) and purified by flash chromatography with the stated solvent system to afford the desired ether.

5.1.2.4 General procedure D – Fluorophosphonate synthesis

NaOH (2-3 eq) was added to a solution of phosphonate intermediate (1 eq) in either H_2O or H_2O:EtOH (1:1) (0.05 – 0.2 M) and the mixture was stirred at 80-85 °C until no starting material was observed by TLC (2-72 h). It was then concentrated to remove the EtOH, diluted with water, acidified with 1N HCl and extracted with EtOAc. The combined organic extracts were concentrated, and the resultant crude product was dissolved in DCM (0.05 – 0.2 M), cooled to −78 °C and DAST (2.5 eq) was added dropwise. The mixture was allowed to warm to rt over 2 h and stirred at this temperature for a further 1 h. It was then diluted with EtOAc and washed with H_2O and brine. The organic extract was then dried ($MgSO_4$) and concentrated. Purification with flash chromatography with the solvent system (Hex:EtOAc / DCM:MeOH gradients), stated in each individual reaction, afforded the desired fluorophosphonate.

5.1.2.5 General procedure E -Acyl chloride synthesis

To a stirred solution of carboxylic acid (1.0 eq) in DCM (0.2M) and 2 drops of DMF, $(COCl)_2$ (1.3 eq) was added dropwise. The mixture was then stirred at rt for 2 h under N_2 after which it was concentrated to carry on with the next synthetic step without further purification.

5.1.2.6 General procedure F - *N*-Boc deprotection

The *N*-Boc carbamate (1.0 eq) was treated with a solution of HCl 4M in dioxane (8.4 mL) under N_2 at rt for 1 h. Subsequently, the mixture was concentrated in vacuo to afford the deprotected amine hydrochloride salt. The product was used directly with no further purification

5.1.2.7 General procedure G – Amide coupling

A round bottom flask charged with dry DCM (0.2 M), carboxylic acid (1.2 eq), EDC (1.5 eq) and DMAP (2.0 eq) was degassed and stirred at 50 °C for 30 min under N_2. Subsequently, the amine (1.0 eq) was added, and the reaction was heated under reflux temperature for a further 19 h. The crude reaction mixture was then washed with 1N HCl and brine; dried (Mg_2SO_4) and the volatiles were removed under high vacuum to afford the desired phosphonate. When stated, purification with flash chromatography in the stated solvent system afforded the desired amide.

General procedure Gb – Amide coupling

A solution of acyl chloride (1.0 eq) in DCM (0.1-0.2 M) was added dropwise to a round bottom flask charged with the coupling amine (1.2 eq) and Et_3N (1.1 eq) in dry DCM (0.1-0.2 M) under N_2. The mixture was left to react at rt overnight. Upon completion, it was washed with H_2O and sat. aq. $NaHCO_3$, dried ($MgSO_4$) and the volatiles removed under high vacuum to afford the desired amide**.** When stated, purification with flash chromatography in the stated solvent system afforded the desired amide.

5.1.3 Experimental Procedures

Diethyl Tolylphosphonate (**26**)

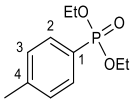

26

General procedure B was applied to 4-bromotoluene (**25**). Column eluent 75% EtOAc in hexanes. **26** (216 mg, 59%) was obtained as a colourless oil. ν_{max} (ATR) 1249 (P=O stretch) cm^{-1}. δ_H (400 MHz, $CDCl_3$) 7.71 (2H, dd, $^3J_{C\text{-}P}$ 13.1, *J* 7.8, 2-***H***), 7.32 – 7.26 (2H, m, 3-***H***), 4.20 – 4.01 (4H, m, -O-C***H***$_2$-CH_3), 2.41 (3H, s, Ar-C***H***$_3$), 1.32 (6H, m, -CH_2-C***H***$_3$). δ_C (101 MHz, $CDCl_3$) 142.9 (d, $^4J_{C\text{-}P}$ 3.1, ***C***-4), 131.8 (d, $^3J_{C\text{-}P}$ 10.3, ***C***-3), 129.2 (d, $^2J_{C\text{-}P}$ 15.3, ***C***-2), 125.0 (d, $^1J_{C\text{-}P}$ 189.9, ***C***-1), 62.0 (d, $^2J_{C\text{-}P}$ 5.3, -O-***C***H_2-CH_3),

21.7 (d, $^{5}J_{C\text{-}P}$ 1.4, Ar-C***H***$_3$), 16.3 (d, $^{3}J_{C\text{-}P}$ 6.6, -CH$_2$-***C***H$_3$). δ_P (162 MHz, CDCl$_3$) 19.6. *m/z* (LCMS ES$^+$) 229.0 [M+H]$^+$. All the data are in accordance with the literature.[152]

Diethyl 4-bromobenzylphosphonate (28)

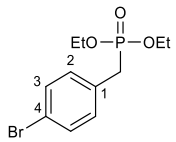

28

General procedure A was applied to 4-bromobenzyl bromide (**27**). After the volatiles were removed 28 (72 mg, 72%) was obtained as a yellow oil. ν_{max} (ATR) 1249 (P=O stretch) cm^{-1}. δ_H (599 MHz, CDCl$_3$) 7.43-7.39 (2H, m, 2-***H***), 7.18 – 7.13 (2H, m, 3-***H***), 4.05 – 3.95 (4H, m, -O-C***H***$_2$-CH$_3$), 3.07 (2H, d, $^{2}J_{H\text{-}P}$ 21.7, Ar-C***H***$_2$-P(O)(OEt)$_2$), 1.26 – 1.20 (6H, m, -CH$_2$-C***H***$_3$). δ_C (151 MHz, CDCl$_3$) 131.6 (d, $^{3}J_{C\text{-}P}$ 3.1, ***C***-2), 131.4 (d, $^{4}J_{C\text{-}P}$ 6.6, ***C***-3), 130.7 (d, $^{5}J_{C\text{-}P}$ 9.2, ***C***-4), 120.9 (d, $^{2}J_{C\text{-}P}$ 4.6, ***C***-1), 62.2 (d, $^{2}J_{C\text{-}P}$ 6.8, -O-***C***H$_2$-CH$_3$), 33.2 (d, $^{1}J_{C\text{-}P}$ 138.6, Ar-***C***H$_2$-P(O)(OEt)$_2$), 16.3 (d, $^{3}J_{C\text{-}P}$ *5*.9, -CH$_2$-***C***H$_3$). δ_P (162 MHz, CDCl$_3$) 25.5. *m/z* (LCMS ES$^+$) 307.1 [M(^{79}Br)+H]$^+$ 309.1 [M(^{81}Br)+H]$^+$. All the data are in accordance with the literature.[153]

Diethyl(4-hydroxyphenyl)phosphonate (33)

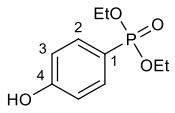

33

General procedure B was applied to p-bromophenol (**32**). Column eluent 0-5% MeOH in DCM. **33** (3572 mg, 90%) was obtained as a colourless oil. ν_{max} (ATR) 3122 (br, -OH), 1208 (P=O stretch), cm^{-1}. δ_H (400 MHz, $CDCl_3$) 10.00 (1H, s, -O***H***), 7.65 (2H, dd, $^3J_{H-P}$ 12.9, 8.6, 2-***H***), 7.03 (2H, dd, *J* 8.6, $^4J_{H-P}$ 3.7, 3-***H***), 4.22 – 3.97 (4H, m, -O-C***H***$_2$-CH_3), 1.32 (6H , t, *J* 7.1, -CH_2-C***H***$_3$). δ_C (101 MHz, $CDCl_3$) 161.9 (d, $^4J_{C-P}$ 3.4, ***C***-4), 133.8 (d, $^2J_{C-P}$ 11.7, ***C***-2), 116.1 (d, $^1J_{C-P}$ 197.0, ***C***-1), 116.0 (d, $^3J_{C-P}$ 16.4, ***C***-3), 62.3 (d, $^2J_{C-P}$ 5.4, -O-***C***H_2-CH_3), 16.2 (d, $^3J_{C-P}$ 6.6, -CH_2-***C***H_3). δ_P (162 MHz, $CDCl_3$) 21.1. *m/z* (LCMS ES^+) 231.1 $[M+H]^+$, 461.2 $[2M+H]^+$. All the data are in accordance with the literature.[154]

4-(diethoxyphosphoryl)phenyltrifluoromethanesulfonate (34)

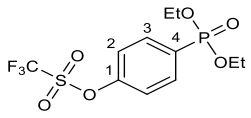

34

Trifluoromethanesulfonic anhydride (0.125 mL, 0.74 mmol, 1.2 eq) was added dropwise to a solution of pyridine (0.100 mL, 1.24 mmol, 2.0 eq) and diethyl (4-hydroxyphenyl)phosphonate (150 mg, 0.62 mmol, 1.0 eq) in anhydrous DCM (4.0 mL) at 0 °C under Ar. After complete addition, the mixture was warmed to room temperature and allowed to react for 5 minutes. The mixture was then diluted with DCM and quenched with ice cold saturated $NaHCO_3$. The aqueous phase was extracted with DCM and washed with H_2O and brine. The organic layer was then dried ($MgSO_4$) and concentrated. The residue obtained (197 mg) was purified by flash chromatography (Hexane:EtOAc, 0-100% gradient) to afford the titled triflate phosphonate **26,** (107 mg, 48%) as a colourless liquid.ν_{max} (ATR) 1433 (S=O stretching), 1254 (P=O stretching) cm^{-1}. δ_H (700 MHz, $CDCl_3$) 7.90 (2H, dd, $^3J_{H-P}$ 12.8, *J* 8.7, 3-***H***), 7.36 (2H, dd, *J* 8.7, $^4J_{H-P}$ 3.0, 2-***H***), 4.20 – 4.06 (4H, m, -C***H₂***-CH_3), 1.32 (6H, t, *J* 7.1, -CH_2-C***H₃***). δ_C (176 MHz, $CDCl_3$) 152.1 (d, $^4J_{C-P}$ 4.1, ***C***-1), 134.1 (d, $^2J_{C-P}$ 11.0, ***C***-3), 129.6 (d, $^1J_{C-P}$ 190.7, ***C***-4), 121.5 (d, $^3J_{C-P}$ 15.8, ***C***-2), 118.7 (q, $^1J_{C-F}$ 320.8, ***C***-F_3), 62.5 (d, $^2J_{C-P}$ 5.6, -***C***H_2-CH_3), 16.3 (d, $^3J_{C-P}$ 6.3, -CH_2-***C***H_3). δ_F (376 MHz, $CDCl_3$) -72.8. δ_P (162 MHz, $CDCl_3$) 16.0. m/z LCMS (ES^+) 363.2 $[M+H]^+$, 404.9 $[M+H+CH_3CN]^+$, 725.3 $[2M+H]^+$. HRMS (ES^+) found $[M+H]^+$ 363.0283; $C_{11}H_{15}F_3O_6PS$ requires *M* 363.0279.

Diethyl 4-hydroxy-[1,1'-biphenyl]-4'-ylphosphonate (36)

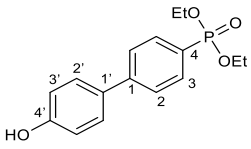

36

Procedure A: A round bottom flask was charged with THF/H_2O (4:1, 4 mL), $Pd(OAc)_2$ (1.2 mg, 0.005 mmol, 0.02 eq) and SPhos (2.6 mg, 0.006 mmol, 0.024 eq). After the reaction vessel was degassed, the reaction mixture was stirred for 0.5 h under Ar. Subsequently, KF (51 mg, 0.9 mmol, 3.3 eq), 4-(diethoxyphosphoryl) phenyl trifluoromethanesulfonate (97 mg, 0.27 mmol, 1.0 eq) and 4-hydroxyphenilboronic acid (50 mg, 0.35 mmol, 1.3 eq) were added. The reaction mixture was stirred at 40 °C for 16 h. The resulting solution was concentrated, filtered through celite, and purified in flash chromatography (Hex:EtOAc, 0-100 % gradient) to afford the titled biphenyl phosphonate **36**, (37 mg, 45%) as a yellow oil. **Procedure B**: General procedure B was applied to 4-bromo-4'-hydroxybiphenyl (**37**). **36** (54 mg, 31%) was obtained as a yellow oil. Column eluent 0-100% EtOAc in Hexanes. ν_{max} (ATR) 3179 (br, -OH stretching), 1218 (P=O stretching) cm^{-1}. δ_H (700 MHz, $CDCl_3$) 8.13 (1H, s, -O***H***), 7.80 (2H, dd, $^3J_{H-P}$ 13.2, *J* 7.9, 3-***H***), 7.62-7.52 (2H, m, 2-***H***), 7.48-7.36 (2H, m, 2'-***H***), 6.97 (2H, d, *J* 8.4, 2'-***H***), 4.22 – 4.08 (4H, m, -O-C***H***$_2$-CH_3), 1.33 (6H, t, *J* 7.1, -CH_2-C***H***$_3$). δ_C (176 MHz, $CDCl_3$) 157.4 (***C***-4'), 145.4 (***C***-1'), 132.2 (d, $^2J_{C-P}$ 10.5, ***C***-3), 131.1 (***C***-1), 128.3 (***C***-2'), 126.6 (d, $^3J_{C-P}$ 15.6, ***C***-2), 124.8 (d, $^1J_{C-P}$ 205.0, ***C***-4), 116.13 (***C***-3'), 62.55 (m, -O-***C***H_2-CH_3), 16.25 (d, $^3J_{C-P}$ 6.6, O-CH_2-***C***H_3). δ_P (162 MHz, $CDCl_3$)

19.4. m/z (LCMS ES^+) 307.3 $[M+H]^+$, 613.4 $[2M+H]^+$. HRMS (ES^+) found $[M+H]^+$ 307.1096; $C_{16}H_{20}O_4P$ requires *M* 307.1099. All the data are in accordance with the literature.[155]

Hex-5-yn-1-yl 4-methylbenzene-1'-sulfonate (38)

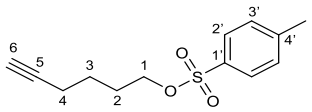

38

p-toluensulfonyl chloride (3.27 g, 17.0 mmol, 1.7 eq) was added to a solution of 5-hexyn-1-ol (1.1 mL, 10 mmol, 1.0 eq) and pyridine (20 mL). The reaction mixture was stirred at 0 °C for 12 h, followed by another 12 h at rt under Ar. The resulting solution was washed with saturated $NaHCO_3$ solution (20 mL) and extracted with Et_2O (3 x 20 mL). Subsequently the organic layers were washed with 2M HCl (3 x 20 mL) and water (20 mL). The combined organic layers were dried ($MgSO_4$) and concentrated. The residue was purified by flash chromatography (Hexane:EtOAc, 3:1) to afford the titled tosylate **38** (1.33 g, 53%) as a colourless oil. ν_{max} (ATR) 3298 (C-H stretching alkyne), 2123 (C≡C stretching), 1358 (S=O stretching) cm^{-1}. δ_H (599 MHz, $CDCl_3$) 7.77 (2H, d, *J* 8.1, 2'-***H***), 7.33 (2H, d, *J* 8.1, 3'-***H***), 4.05 (2H, t, *J* 6.3, 1-$\boldsymbol{H_2}$), 2.43 (3H, s, 4'-C$\boldsymbol{H_3}$), 2.14 (2H, td, *J* 6.9, 2.6, 4-$\boldsymbol{H_2}$), 1.90 (1H, t, *J* 2.6, 6-***H***), 1.79 – 1.72 (2H, m, 2-$\boldsymbol{H_2}$), 1.63 – 1.53 (2H, m, 3-$\boldsymbol{H_2}$). δ_C (151 MHz, $CDCl_3$) 144.8 (***C***-4'), 133.1 (***C***-1'), 129.8 (***C***-3'), 127.9 (***C***-2'), 83.4 (***C***-5), 69.9 (***C***-1), 68.9 (***C***-6), 27.8 (***C***-2), 24.2 (***C***-3), 21.7 (-***C***H_3),

17.7 (***C***-4). *m/z* (LCMS ES$^+$) $[M+H]^+$ 253.3, $[2M+Na]^+$ 527.3. All the data are in accordance with the literature.[124]

6-Bromohex-1-yne (39)

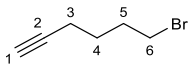

39

PBr_3 (0.968 mL, 10.0 mmol, 0.5 eq) was added dropwise to a solution of 5-hexyn-1-ol (**38**) (2.3 mL, 20 mmol, 1.0 eq) and dry Et_2O (60 mL) at 0 °C. The reaction was stirred for 4 h and then warmed to room temperature. Subsequently, it was quenched by pouring onto ice-cold saturated $NaHCO_3$ solution. The organic phase was washed with $NaHCO_3$ (1 x 20 mL), brine (1 x 20 mL), dried ($MgSO_4$) and concentrated. Finally, it was purified by flash chromatography (Hexane 100%) to afford the titled brominated alkyne **39** (178 mg, 6%) as a colourless liquid. ν_{max} (ATR) 3305 (C-H stretching alkyne), 2121 (C≡C stretching), 632 (C-Br stretching) cm^{-1}. δ_H (400 MHz, $CDCl_3$) 3.37 (2H, t, *J* 6.7, 6-***H***$_2$), 2.18 (2H, td, *J* 7.1, 2.7, 3-***H***$_2$), 1.98 – 1.89 (3H, m, 1-***H*** and 5-***H***), 1.66 – 1.57 (2H, q, *J* 7.1, 4-***H***$_2$). δ_C (101 MHz, $CDCl_3$) 83.6 (***C***-2), 69.0 (***C***-1), 33.1 (***C***-6), 32.0 (***C***-5), 26.8 (***C***-4), 17.6 (***C***-3). All the data are in accordance with the literature.[156]

Diethyl [4-(prop-2'-yn-1'-yloxy)phenyl]phosphonate (42)

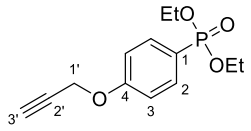

42

General procedure C was applied to diethyl(4-hydroxyphenyl)phosphonate (**33**). After the volatiles were removed, 42 (176 mg, 79%) was obtained as a brown oil. ν_{max} (ATR) 3297 (C-H stretching alkyne), 2118 (C≡C stretching), 1228 (P=O stretching) cm^{-1}. δ_H (599 MHz, $CDCl_3$) 7.74 (2H, dd, $^3J_{H-P}$ 12.8, *J* 8.8, 2-***H***), 7.02 (2H, dd, *J 8.8,* $^4J_{H-P}$ 3.3, 3-***H***), 4.71 (2H, d, *J* 2.4, 1'-$\boldsymbol{H_2}$), 4.14 – 3.99 (4H, m, O-C$\boldsymbol{H_2}$-CH_3), 2.53 (1H, t, *J* 2.4, 3'-***H***), 1.29 (6H, t, *J* 7.1, -C$\boldsymbol{H_3}$). δ_C (151 MHz, $CDCl_3$) 160.7 (d, $^4J_{C-P}$ 3.4, ***C***-4), 133.7 (d, $^2J_{C-P}$ 11.3, ***C***-2), 120.7 (d, $^1J_{C-P}$ 194.4, ***C***-1), 114.8 (d, $^3J_{C-P}$ 16.0, ***C***-3), 77.8 (***C***-2'), 76.1 (***C***-3'), 61.9 (d, $^2J_{C-P}$ 5.3, (CH_3-***C***H_2-O-), 55.7 (***C***-1'), 16.3 (d, $^3J_{C-P}$ 6.5, -***C***H_3). δ_P (162 MHz, $CDCl_3$), 19.2. m/z (LCMS ES^+) 269.2 $[M+H]^+$. HRMS (ES^+) found $[M+H]^+$ 269.0951; $C_{13}H_{18}O_4P$ requires *M* 269.0943.

Diethyl 4'-(hex-5-yn-1-yloxy)phenylphosphonate (43)

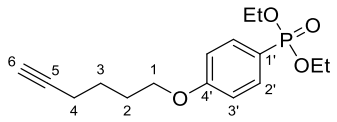

43

General procedure C was applied to diethyl-(4-hydroxyphenyl)phosphonate (**33**). Column eluent 0-100% EtOAc in hexanes. **43** (334 mg, 99%) was obtained as a colourless oil. ν_{max} (ATR) 3301 (C-H stretching alkyne), 2116 (C≡C stretching), 1603, 1242 (P=O stretching) cm^{-1}. δ_H (700 MHz, $CDCl_3$) 7.69 (2H, dd, $^3J_{H-P}$ 12.7, 8.7, 2'-***H***), 6.91 (2H, dd, *J* 8.7, $^4J_{H-P}$ 3.4, 3'-***H***), 4.11 – 3.96 (6H, m, -O-C***H***$_2$-CH_3, 1-***H***$_2$), 2.24 (2H, td, *J* 7.0, 2.7, 4-***H***$_2$), 1.94 (1H, t, *J* 2.7, 6-***H***), 1.92 – 1.87 (2H, m, 2-***H***$_2$), 1.71 – 1.65 (2H, m, 3-***H***$_2$), 1.27 (6H, t, *J* 7.1, -O-CH_2-C***H***$_3$). δ_C (176 MHz, $CDCl_3$) 162.2 (d, $^4J_{C-P}$ 3.4, ***C***-4'), 133.7 (d, $^3J_{C-P}$ 11.3, ***C***-3'), 119.4 (d, $^1J_{C-P}$ 194.8, ***C***-1'), 114.4 (d, $^2J_{C-P}$ 15.9, ***C***-2'), 83.8 (***C***-5), 68.7 (***C***-6), 67.3 (***C***-1), 61.8 (d, $^2J_{C-P}$ 5.3, -O-***C***H_2-CH_3), 28.0 (***C***-2), 24.9 (***C***-3), 18.1 (***C***-4), 16.3 (d, $^3J_{C-P}$ 6.5, -CH_2-***C***H_3). δ_P (162 MHz, $CDCl_3$) 19.8. m/z (LCMS ES^+) 311.3 $[M+H]^+$, 621.5 $[2M+H]^+$. HRMS (ES^+) found 311.1405 $[M+H]^+$; $C_{16}H_{24}O_4P$ requires *M* 311.1412.

Diethyl [4'-(hex-5''-yn-1''-yloxy)-[1,1'-biphenyl]-4-yl]phosphonate (44)

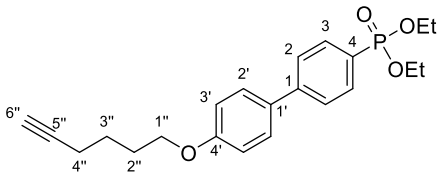

44

General procedure C was applied on diethyl 4'-hydroxy-[1,1'-biphenyl]-4-ylphosphonate (**36**). Column eluent 0-100% EtOAc in hexanes. **44** (182 mg, 85%) was obtained as a colourless oil. ν_{max} (ATR) 3301 (H-C≡C stretching), 2121 (C≡C stretching), 1249 (P=O stretching) cm^{-1}. δ_H (700 MHz, $CDCl_3$) 7.83 (2H, dd, $^3J_{H-P}$ 13.0, 8.3, 3-***H***), 7.63 (2H, dd, *J* 8.3, $^4J_{H-P}$ 3.8, 2-***H***), 7.54 – 7.51 (2H, m, 2'-***H***), 6.98 – 6.95 (2H, m, 3'-***H***), 4.18 – 4.05 (4H, m, -O-C***H***$_2$-CH_3), 4.02 (2H, t, *J* 6.3, 1´´-***H***$_2$), 2.28 (2H, td, *J* 7.1, 2.6, 4´´-***H***$_2$), 1.96 (1H, t, *J* 2.6, 6´´-***H***), 1.95 – 1.90 (2H, m, 2´´-***H***$_2$), 1.76 – 1.70 (2H, m, 3´´-***H***$_2$), 1.32 (6H, t, *J* 7.1, -O-CH_2-C***H***$_3$). δ_C (176 MHz, $CDCl_3$) 159.2 (***C***-4'), 144.7 (d, $^4J_{C-P}$ 3.1, ***C***-1), 132.3 (d, $^2J_{C-P}$ 10.2, ***C***-3), 132.2 (d, $^5J_{C-P}$ 9.9, ***C***-1'), 128.3 (***C***-2'), 126.6 (d, $^3J_{C-P}$ 15.3, ***C***-2), 126.0 (d, $^1J_{C-P}$ 190.9, ***C***-4), 114.9 (***C***-3'), 84.0 (***C***-5''), 68.7 (***C***-6''), 67.4 (***C***-1''), 62.0 (d, $^3J_{C-P}$ 5.2, -O-***C***H_2-CH_3), 28.2 (***C***-2''), 25.0 (***C***-3''), 18.1 (***C***-4''),16.3 (d, $^3J_{C-P}$ 6.6, -CH_2-***C***H_3). δ_P (162 MHz, $CDCl_3$) 19.2. m/z (LCMS ES^+) 387.4 $[M+H]^+$, 774,6 $[2M+H]^+$. HRMS (ES^+) found $[M+H]^+$ 387.1734; $C_{22}H_{28}O_4P$ requires *M* 387.1725.

6-(Boc-amino)-1-hexanol (46)

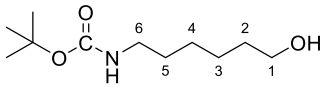

46

6-Amino-1-pentanol (**45**) (2.0 g, 17 mmol, 1 eq) was dissolved in dry DCM (43 mL) in a round bottom flask equipped with a magnetic stirrer and a pressure equalising addition funnel. Subsequently, a solution of Boc_2O (3.8 g, 17 mmol, 1 eq) in dry DCM (43 mL) was added dropwise over 30 min. After stirring for 12 h under N_2, the reaction mixture was washed with saturated $NaHCO_3$ (2 x 25 mL) and H_2O (1 x 25 mL), dried, and concentrated to afford the protected amino alcohol (3.4 g, 91%) as a light-yellow solid. ν_{max} (ATR) 3352 (OH), 1695 (C=O) cm^{-1}. δ_H NMR (599 MHz, $CDCl_3$) 4.48 (1H, s, -O***H***), 3.62 (2H, t, *J* 6.6, 1-***H₂***), 3.10 (2H, t, *J* 7.1, 6-***H₂***), 1.59 – 1.53 (2H, m, 2-***H₂***), 1.51 – 1.45 (2H, m, 5-***H₂***), 1.43 (9H, s, -C(C***H₃***)$_3$), 1.41 – 1.30 (4H, m, 3-***H₂*** ,4-***H₂***). δ_C NMR (151 MHz, $CDCl_3$) 156.1 (C=O), 82.1 (-***C***$(CH_3)_3$), 62.7 (***C***-1), 40.4 (***C***-6), 32.6 (***C***-2), 30.1 (***C***-5), 28.4 (-C(***C***$H_3)_3$), 26.4 (***C***-4), 25.2(***C***-3). m/z LCMS (ES^+) 240.4 $[M+Na]^+$; 118.2 $[M-Boc]^+$. All the data are in accordance with the literature.[157]

Tert-butyl N-{6-[(4'-methylbenzenesulfonyl)oxy]hexyl}carbamate (47)

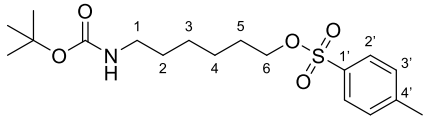

47

6-(Boc-amino)1-hexanol **46** (1.0 g, 5 mmol, 1 eq) was dissolved in dry DCM (23 mL). Triethylamine (1.2 mL, 9 mmol, 2 eq), p-toluenesulfonyl chloride (1.5 g, 7.8 mmol, 1.7 eq) and a catalytic amount of DMAP (0.06 g, 0.5 mmol, 0.1 eq) were added. The solution was stirred at room temperature overnight. After this time, the volatiles were removed, and the residue was partitioned between ethyl acetate (150 ml) and 0.1 M HCl (150 ml). The organic layer was separated, and the aqueous phase was extracted with EtOAc (2 x 150 ml); the combined organic layers were washed with H_2O (2 x 150 ml), dried, filtered and concentrated under reduced pressure to afford the tosylated amino alcohol **47** (1.3 g, 78%) as a colourless oil. The product was used directly with no further purification. δ_H NMR (400 MHz, $CDCl_3$) 7.78 (2H, d, *J* 8.0, Ar-***H***), 7.34 (2H, d, *J* 8.0, Ar-***H***), 4.01 (2H, t, *J* 6.4, 6-***H₂***), 3.05 (2H, t, *J* 7.1, 1-***H₂***), 2.45 (3H, s, Ph-C***H₃***), 1.63 (2H, m, 5-***H₂***), 1.43 (11H, s, -C***H₂***-, C(C***H₃***)$_3$), 1.28 (4H, m, 2 x -C***H₂***-). δ_C NMR (101 MHz, $CDCl_3$) 156.0 (C=O), 144.7 (***C***-1'), 133.1 (***C*** -4'), 129.8 (Ar-***C***), 127.9 (Ar- ***C***), 79.3 (***C***$(CH_3)_3$), 70.5 (-O***C***H_2-), 40.4 (-N***C***H_2-), 29.9 (***C***H_2), 28.7 (***C***H_2), 28.4 (C(***C***$H_3)_3$), 26.1 (***C***H_2), 25.1 (***C***H_2), 21.7 (Ph-***C***H_3). m/z LCMS (ES^+) 316.3 $[M-101+46]^+$ (McLafferty rearrangement + H_2CO_2). All the data are in accordance with literature.

Tert-butyl N-{6-[4'-(diethoxyphosphoryl)phenoxy]hexyl}carbamate (48)

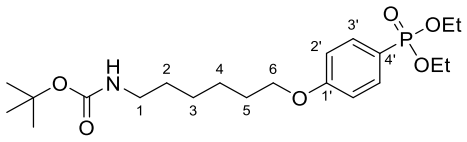

48

Phosphonate **33** and **47** were treated following the general procedure C. Column eluent 0-20% EtOH in DCM. **48** (400 mg, 72%) was obtained as a light-yellow oil. ν_{max} (ATR) 1703 (C=O), 1245 (P=O) cm^{-1}. δ_H NMR (599 MHz, $CDCl_3$) 7.71 (2H, dd, $^3J_{H-P}$ 12.7, *J* 8.5, 3'-***H*₂**), 6.93 (2H, dd, *J* 8.5, $^4J_{H-P}$ 3.3, 2'-***H*₂**), 4.51 (1H, s br, -N***H***), 4.11-4.03 (m, 4H, O-C***H*₂**-CH_3), 3.98 (2H, t, *J* 6.5, 6-***H*₂**), 3.11 (2H, t br, *J* 7.1, 1-***H*₂**), 1.78 (2H, p, *J* 6.5, 5-***H*₂**), 1.54 – 1.34 (13H, m, 4-***H*₂**, 3-***H*₂**, C(C***H*₃**)$_3$, 2-***H*₂**), 1.30 (6H, t, *J* 7.0, -CH_2-C***H*₃**). δ_C NMR (151 MHz, $CDCl_3$) 162.5 (d, $^4J_{C-P}$ 3.4, ***C***-1'), 156.1 (C=O), 133.9 (d, $^2J_{C-P}$ 11.3, ***C***-3'), 119.4 (d, $^1J_{C-P}$ 194.7, ***C***-4'), 114.6 (d, $^3J_{C-P}$ 16.0, ***C***-2'), 68.0 (***C***-6), 62.0 (d, $^2J_{C-P}$ 5.3, O-***C***H_2-CH_3), 60.5 (***C***$(CH_3)_3$), 40.6 (***C***-1), 30.2 (***C***-4), 29.1 (***C***-5), 28.5 (C(***C***$H_3)_3$), 26.6 (***C***-3), 25.8 (***C***-2), 16.4 (d, $^3J_{C-P}$ 6.5). δ_P NMR (162 MHz, $CDCl_3$) 19.82. HRMS (ES^+) found $[M+H]^+$ 430.2348, $C_{21}H_{37}NO_6P$ requires *M* 430.2059.

Diethyl (4-{[6'-(hex-5''-ynamido)hexyl]oxy}phenyl)phosphonate (49)

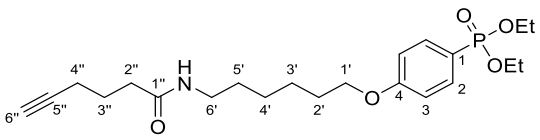

49

Boc protection was removed from **48** following general procedure **F** (m/z LCMS (ES+) 330.4[M+H]$^+$). Subsequent amide coupling with 5-hexynoic acid following general procedure **G** afforded **49** (155 mg, 31%) as a yellow oil. Column eluent 0-30% EtOH in DCM. ν_{max} (ATR) 3312 (C≡C-H), 2247 (C≡C), 1653 (C=O), 1237 (P=O) cm^{-1}. δ_H NMR (599 MHz, $CDCl_3$) 7.72 (2H, dd, $^3J_{H-P}$ 12.7, *J* 8.7, 2-***H***), 6.94 (2H, dd, *J* 8.7, $^4J_{H-P}$ 3.4, 3-***H***), 5.60 (1H, s, -N***H***-), 4.15 – 4.00 (4H, m, -O-C***H₂***-CH_3), 3.99 (2H, t, *J* 6.4, 1'-***H₂***), 3.26 (2H, td, *J* 7.2, 5.7, 6'-***H₂***), 2.31 (2H, t, *J* 7.1, 2''-***H₂***), 2.25 (2H, td, *J* 7.1, 2.7, 4''-***H₂***), 1.97 (1H, t, *J* 2.7, ***6''-H***), 1.86 (2H, p, *J* 7.1, 3''-***H₂***), 1.82 – 1.76 (2H, m, 2'-***H₂***), 1.57 – 1.45 (4H, m, 5'-***H₂***, 3'-***H₂***), 1.43 – 1.36 (2H, m, 4'-***H₂***), 1.31 (t, *J* 7.0, -O-CH_2-***C***H_3). δ_C NMR (151 MHz, $CDCl_3$) 172.3 (C=O), 162.5 (d, $^4J_{C-P}$ 3.4, ***C***-4), 133.9 (d, $^2J_{C-P}$ 11.3, ***C***-2), 119.4 (d, $^1J_{C-P}$ 194.8, ***C***-1), 114.6 (d, $^3J_{C-P}$ 16.0, ***C***-3), 83.7 (***C***-5''), 69.3 (***C***-6''), 68.0 (***C***-1'), 62.0 (d, $^2J_{C-P}$ 5.3, -O-***C***H_2-CH_3), 39.6 (***C***-6'), 35.2 (***C***-2''), 29.7 (***C***-5'), 29.1 (***C***-2'), 26.7 (***C***-4'), 25.8 (***C***-3'), 24.3 (***C***-3''), 17.9 (***C***-4''), 16.5 (d, $^3J_{C-P}$ 6.6, -O-CH_2-***C***H_3). δ_P NMR (162 MHz, $CDCl_3$) 19.8. HRMS (ES$^+$) found [M+H]$^+$ 424.2256; $C_{22}H_{35}NO_5P$ requires *M* 424.2253.

Diethyl(4-bromomethylphenyl)phosphonate (50)

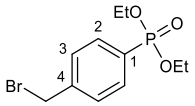

50

2,2'-Azobis(2-methylpropionitrile) (0.216 mL, 0.92 mmol, 1.0 eq) (AIBN) was added dropwise to a refluxing suspension of diethyl *p*-tolylphosphonate (0.216 mL, 0.92 mmol, 1.0 eq) (**25**) and *N*-bromosuccinimide (182 mg, 1.01 mmol, 1.1 eq) (NBS) in anhydrous CCl_4 under Ar. The mixture was stirred at reflux for 4 h. After that period, it was cooled to 10 °C and filtered to remove the succinimide present. The filtrate was washed with water (1 x 20 mL) and brine (1 × 20 mL). The organic layer was then dried ($MgSO_4$) and concentrated. The residue was then purified by flash chromatography (Hex:EtOAc 0-100% gradient) to afford the titled phosphonate **50**, (37 mg, 15%), as a colourless oil. ν_{max} (ATR) 1249 (P=O stretching) cm^{-1}. δ_H (700 MHz, $CDCl_3$) 7.76 (2H, dd, $^3J_{H-P}$ 13.1, *J* 8.1, 2-***H***), 7.46 (2H, dd, *J* 8.1, $^4J_{H-P}$ 3.8, 3-***H***), 4.46 (2H, s, Br-C***H***$_2$-Ar), 4.16 – 4.01 (4H, m, -O-C***H***$_2$-CH_3), 1.31 – 1.28 (6H, m, -CH_2-C***H***$_3$). δ_C (176 MHz, $CDCl_3$) 142.0 (d, $^4J_{C-P}$ 3.3, ***C***-4), 132.2 (d, $^2J_{C-P}$ 10.2, ***C***-2), 129.0 (d, $^3J_{C-P}$ 15.4, ***C***-3), 128.6 (d, $^1J_{C-P}$ 198.7, ***C***-1), 62.2 (d, $^2J_{C-P}$ 5.5, -O-***C***H_2-CH_3), 32.1 (d, $^5J_{C-P}$ 1.4, Br-***C***H_2-Ar), 16.3 (d, $^3J_{C-P}$ 6.5, -CH_2-***C***H_3). δ_P (162 MHz, $CDCl_3$) 18.0. *m/z* (LCMS ES$^+$) [M(^{79}Br)+H]$^+$ 307.2, [M(^{81}Br)+H]$^+$ 309.2. All the data are in accordance with the literature.[121]

1-bromo-4-[(hexyloxy)methyl]benzene (51)

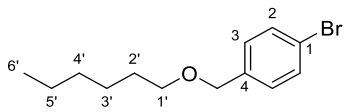

51

To a stirred solution of NaH (31 mg, 0.8 mmol, 1.3 eq) in dry THF (3 mL), 1-hexanol (89 µL, 0.70 mmol, 1.2 eq) was added and the mixture was left to react at rt for 30 min under N_2. Subsequently, 4-bromobenzyl bromide (150 mg, 0.59 mmol, 1.0 eq) and TBAI (22 mg, 0.06 mmol, 0.1 eq) were added, and the reaction mixture was stirred at rt for 45 minutes. Afterwards, the residue was concentrated, redissolved with EtOAc (10 mL), and washed with H_2O (3 mL) and brine (3 mL); dried ($MgSO_4$), and concentrated to afford **51** (137 mg; 86%) as a colourless liquid. ν_{max} (ATR) 1098 (C-O) cm^{-1}. δ_H (700 MHz, $CDCl_3$) 7.48 – 7.42 (2H, m, 2-***H***), 7.22 – 7.17 (2H, m, 3-***H***), 4.43 (2H, s, -O-C***H₂***-Ar), 3.44 (2H, t, *J* 6.7, 1´-***H₂***), 1.59 (2H, dt, *J* 6.7, 2´-***H₂***), 1.38 – 1.23 (6H, m, 3´-***H₂***, 4´-***H₂***, 5´-***H₂***), 0.88 (3H, t, *J* 7.0, 6´-***H₃***). δ_C (176 MHz, $CDCl_3$) 137.8 (***C***-4), 131.4 (***C***-2), 129.2 (***C***-3), 121.2 (***C***-1), 72.0 (-O-***C***H_2-Ar), 70.7 (-O-***C***H_2-CH_2-), 31.6 (-***C***H_2-CH_3), 29.7 (-O-CH_2-***C***H_2-), 25.8 (-O-CH_2-CH_2-***C***H_2-, 22.6 (-***C***H_2-CH_2-CH_3), 14.0 (-***C***H_3).

5-(Boc-amino)-1-pentanol (55)

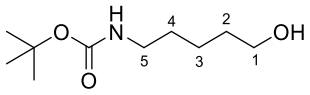

55

5-amino-1-pentanol (2.0 g, 18 mmol, 1.0 eq) was dissolved in dry DCM (45 mL) in a round bottom flask equipped with a magnetic stirrer and a pressure equalising addition funnel. A solution of di-tert-butyl dicarbonate (4.0 g, 18 mmol, 1.0 eq) in dry DCM (45 mL) was added dropwise over 30 min. After stirring for 12 h under N_2, the reaction mixture was washed with saturated $NaHCO_3$ and brine, dried ($MgSO_4$) and concentrated to afford the protected amino alcohol **55** (3.8 g, 99%) as a light-yellow oil. ν_{max} (ATR) 3345 (-OH), 1685 (C=O), 1166 (C-O) cm^{-1}. δ_H (700 MHz, $CDCl_3$) 4.58 (1H, s, -N***H***-), 3.64 – 3.55 (2H, m,1-***H₂***), 3.13-3.07 (2H, m, 5-***H₂***), 1.59 – 1.53 (2H, m, 2-***H₂***), 1.51 – 1.45 (2H, m, 4-***H₂***), 1.41 (9H, s, -C***H₃***), 1.39-1.34 (2H, 3-***H₂***). δ_C (176 MHz, $CDCl_3$) 156.0 (***C***=O), 79.1 (-***C***-$(CH_3)_3$), 62.6 (***C***-1), 40.4 (***C***-5), 32.2 (***C***-2), 29.8 (***C***-4), 28.4 (-***C***H_3), 22.9 (***C***-3). m/z LCMS (ES^-) 248.2 $[M-H+46]^-$.

Tert-butyl N-{5-[(4'-bromophenyl)methoxy]pentyl}carbamate (56)

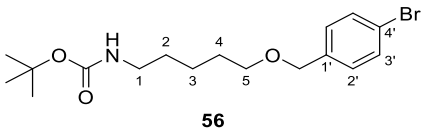

56

To a stirred solution of NaH (122 mg, 3.0 mmol, 1.3 eq) in dry THF (12 mL) under N_2, 5-(Boc-amino)-1-pentanol (**55**) (523 µL, 2.47 mmol, 1.05 eq) was added. After stirring at rt for 30 min, 4-bromobenzyl bromide (**27**) (600 mg, 2.35 mmol, 1.0

eq) and TBAI (87 mg, 0.23 mmol, 0.1 eq) were added and the reaction was left until no starting material was observed by TLC. It was then concentrated, redissolved in EtOAc (20 mL), washed with water (2 x 10 mL), dried ($MgSO_4$) and purified by flash chromatography (Hex:EtOAc 0-100% gradient) to afford the titled carbamate **56** (600 mg, 69%) as a colourless oil. ν_{max} (ATR) 1695 (C=O), 1170 (C-O) cm^{-1}. δ_H (700 MHz, $CDCl_3$) 7.45 (2H, d, *J* 8.3, 3'-***H***), 7.19 (2H, d, *J* 8.3, 2'-***H***), 4.50 (1H, s, -N***H***-), 4.42 (2H, s, -O-C***H₂***-Ar), 3.44 (2H, t, *J* 6.5, 5-***H₂***), 3.10 (2H, d, *J* 9.0, 1-***H₂***), 1.63 – 1.58 (2H, m, 4-***H₂***), 1.48 (2H, p, *J* 7.0, 2-***H₂***), 1.42 (9H, s, -C***H₃***), 1.41 – 1.35 (2H, m, 3-***H₂***). δ_C (176 MHz, $CDCl_3$) 155.9 (C=O), 137.6 (***C***-1'), 131.4 (***C***-3'), 129.2 (***C***-2'), 121.3 (***C***-4'), 79.0 -***C***$(CH_3)_3$, 72.1 (-O-***C***H_2-Ar), 70.3 (***C***-5), 40.5 (***C***-1), 29.9 (***C***-2), 29.3 (***C***-4), 28.4 (-***C***H_3), 23.5 (***C***-3). m/z (ES^-) [M (^{79}Br)-H+46]$^-$ 416.1; [(^{81}Br)-H+46]$^-$ 418.1. HRMS (ES^+) found $[M+H]^+$ 372.1181; $C_{17}H_{27}NO_3{}^{79}Br$ requires *M* 372.1174.

Tert-butyl N-(5-{[4'-(diethoxyphosphoryl)phenyl]methoxy}pentyl)carbamate (57)

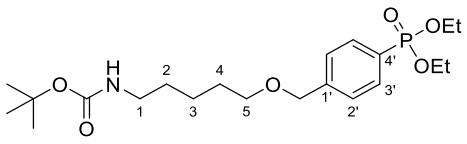

57

General procedure B was applied to **56**. Column eluent 0-100% H_2O in MeCN, using a C18 reverse phase column. **57** (992 mg, 61%) was obtained as a colourless oil. (ATR) 3318 (N-H), 1708 (C=O), 1243 (P=O), 1019 (C-O) cm^{-1}. δ_H (599 MHz, $CDCl_3$) 7.77 (2H, dd, $^3J_{H-P}$ 13.1, *J* 7.8, 3'-***H***), 7.41 (2H, dd, *J* 7.8, $^4J_{H-P}$ 3.9, 2'-***H***), 4.55 (1H, s, -N***H***-), 4.51 (2H, s, -O-C***H₂***-Ar), 4.16 – 3.99 (4H, m, -O-C***H₂***-CH_3), 3.47 (2H, t, *J* 6.6, 5-***H₂***), 3.13-3.07 (2H, m, 1-***H₂***), 1.62 (2H, dt, *J* 14.4, 6.6, 4-***H₂***), 1.48 (2H, p, *J* 7.2,

2-***H₂***), 1.44 – 1.35 (11H, m, -C(C***H₃***)₃, 3-***H₂***), 1.30 (6H, t, *J* 7.1, -O-CH₂-C***H₃***). δ_C (151 MHz, $CDCl_3$) 155.9 (C=O), 143.4 (d, $^4J_{C\text{-}P}$ 3.1, ***C***-1'), 131.9 (d, $^2J_{C\text{-}P}$ 10.3, ***C***-3'), 127.3 (d, $^1J_{C\text{-}P}$ 188.5, ***C***-4'), 127.2 (d, $^3J_{C\text{-}P}$ 15.2, ***C***-2'), 79.0 (-***C***$(CH_3)_3$), 72.2 (-O-***C***H_2-Ar), 70.6 (***C***-5), 62.0 (d, $^2J_{C\text{-}P}$ 5.3, -O-***C***H_2-CH_3), 40.5 (***C***-1), 29.9 (***C***-2), 29.3 (***C***-4), 28.4 (-C(***C***$H_3)_3$), 23.4 (***C***-3), 16.3 (d, $^3J_{C\text{-}P}$ 6.5, -O-CH_2-***C***H_3). δ_P (162 MHz, $CDCl_3$) 18.9. HRMS (ES^+) found $[M+H]^+$ 430.2368; $C_{21}H_{37}NO_6P$ requires *M* 430.2359.

Diethyl (4-{[(5'-aminopentyl)oxy]methyl}phenyl)phosphonate (58)

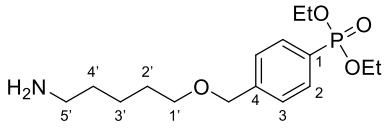

58

General procedure F was applied to **57**. After the volatiles were removed, the titled amine **58** was obtained as a yellow oil. The product was used directly with no further purification. ν_{max} (ATR) 3417 (N-H) 1225 (P=O), 1022 (C-O) cm^{-1}. δ_H (599 MHz, MeOD) 7.75 (2H, dd, $^3J_{H\text{-}P}$ 13.2, 7.7 2-***H***), 7.51 (2H, dd, *J* 7.7, $^4J_{H\text{-}P}$ 3.9, 3-***H***), 4.57 (2H, s, -O-C***H₂***-Ar), 4.16 – 4.04 (4H, m, -O-C***H₂***-CH_3), 3.55 (2H, t, *J* 6.1, 1'-***H₂***), 2.92 (2H, t, *J* 7.5, 5'-***H₂***), 1.72 - 1.64 (4H, m, 2'-***H₂***, 4'-***H₂***), 1.54-1.46 (2H, m, 3-***H₂***), 1.31 (6H, t, *J* 7.0, -O-CH_2-C***H₃***). δ_C (599 MHz, MeOD) 144.1 (d, $^4J_{C\text{-}P}$ 3.1, ***C***-4), 131.4 (d, $^2J_{C\text{-}P}$ 10.4, ***C***-2), 127.2 (d, $^3J_{C\text{-}P}$ 15.4, ***C***-3), 126.4 (d, $^1J_{C\text{-}P}$ 191.0, ***C***-1), 71.7 (-O-***C***H_2-Ar), 70.0 (***C***1'), 62.4 (d, $^2J_{C\text{-}P}$ 5.8, -O-***C***H_2-CH_3), 39.3 (***C***-5'), 28.8 (***C***-2'), 27.0 (***C***-4'), 22.9 (***C***-3'), 15.2 (d, $^3J_{C\text{-}P}$ 6.3, -O-CH_2-***C***H_3). δ_P (162 MHz, MeOD) 19.3. HRMS (ES^+) found $[M+H]^+$ 330.1834; $C_{16}H_{28}NO_4P$ requires *M* 330.1834.

Diethyl [4-({[5´-(hex-5´´-ynamido)pentyl]oxy}methyl) phenyl] phosphonate (59)

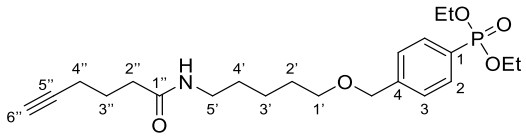

59

General procedure G was applied to **58**. After workup, **59** (402 mg, 65%) was obtained as a white solid. The product was used directly with no further purification. ν_{max} (ATR) 3468 (N-H), 3299 (C≡C-H), 1646 (C=O), 1236 (P=O), 1022 (C-O) cm^{-1}. δ_H (599 MHz, $CDCl_3$) 7.71 (2H, dd, $^3J_{H-P}$ 13.1, 8.1, 2-***H***), 7.42 (2H, dd, *J* 8.1, $^4J_{H-P}$ 3.9, 3-***H***), 5.56 (1H, m, -N***H***-), 4.52 (2H, s, -O-C***H₂***-Ar), 4.17 – 4.00 (4H, m, -O-C***H₂***-CH_3), 3.48 (2H, t, *J* 6.4, 1'-***H₂***), 3.24 (2H, td, *J* 7.2, 5.8, 5'-***H₂***), 2.28 (2H, t, *J* 7.1, 2''-***H₂***), 2.24 (2H, td, *J* 7.1, 2.6, 4''-***H₂***), 1.96 (1H, t, *J* 2.6, 6''-***H***), 1.84 (2H, p, *J* 7.1, 3''-***H₂***), 1.64 (2H, dt, *J* 14.9, 6.4, 2'-***H₂***), 1.52 (2H, p, *J* 7.2, 4'-***H₂***), 1.44 – 1.38 (2H, m, 3'-***H₂***), 1.31 (2H, t, *J* 7.0, -CH_2-C***H₃***). δ_C (599 MHz, $CDCl_3$) 172,1 (C=O), 143.3 (d, $^4J_{C-P}$ 3.1, ***C***-4), 131.9 (d, $^2J_{C-P}$ 10.2, ***C***-2), 127.4 (d, $^1J_{C-P}$ 189.2, ***C***-1), 127.2 (d, $^3J_{C-P}$ 15.3, ***C***-3), 83.5 (***C***-5''), 72.3 (-O-***C***H_2-Ar), 70.6 (***C***-1'), 69.1 (***C***-6''), 62.0 (d, $^2J_{C-P}$ 5.4, -O-***C***H_2-CH_3), 39.4 (***C***-5'), 35.1 (***C***-2''), 29.5 (***C***-4'), 29.3 (***C***-2'), 24.2 (***C***-3''), 23.6 (***C***-3'), 17.8 (***C***-4''), 16.3 (d, $^3J_{C-P}$ 6.4, -O-CH_2-***C***H_3). δ_P (162 MHz, $CDCl_3$) 18.8. HRMS (ES^+) found $[M+H]^+$ 424.2256; $C_{22}H_{34}NO_4P$ requires *M* 424.2253.

Methyl 4-(diethoxyphosphoryl)benzoate (61)

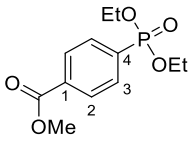

61

General procedure B was applied to methyl 4-iodobenzoate (**60**). **61** (497 mg, 82%) was obtained as a colourless oil. Column eluent 0-100% EtOAc in hexanes. ν_{max} (ATR) 1728 (C=O), 1250 (P=O), 1017 (C-O) cm^{-1}. δ_H (400 MHz, $CDCl_3$) 8.16 – 8.09 (2H, dd, *J* 8.0, $^4J_{H-P}$ 3.8, 2-***H***), 7.94 – 7.85 (2H, dd, $^3J_{H-P}$ 13.0, *J* 8.0, 3-***H***), 4.24 – 4.04 (4H, m, -O-C***H₂***-CH_3), 3.98 – 3.91 (3H, m, -O-C***H₃***), 1.33 (6H, *J* 7.0, -O-CH_2-C***H₃***). δ_C (101 MHz, $CDCl_3$) 166.2 (***C***=O), 133.5 (d, $^4J_{C-P}$ 3.2, ***C***-1), 133.3 (d, $^1J_{C-P}$ 186.5, ***C***-4), 131.8 (d, $^2J_{C-P}$ 10.1, ***C***-3), 129.4 (d, $^3J_{C-P}$ 15.0, ***C***-2), 62.4 (d, $^2J_{C-P}$ 5.5, -O-***C***H_2-CH_3), 52.5, 16.3 (d, $^3J_{C-P}$ 6.3, -O-CH_2-***C***H_3). δ_P (162 MHz, $CDCl_3$) 17.0. m/z LCMS (ES^+) 273.3 $[M+H]^+$; 545.3 $[2M+H]^+$.

Diethyl {4-[(2´-aminoethyl)carbamoyl]phenyl}phosphonate (64)

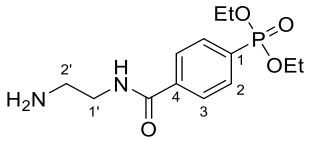

64

General procedure F was applied to **69**. After the volatiles were removed, **64** (478 mg, 94%) was obtained as a yellow oil. ν_{max} (ATR) 3406 (N-H), 3277 (N-H), 1652 (C=O),

1228 (P=O) cm^{-1}.δ_H (700 MHz, $CDCl_3$) 8.82 (1H, s, -N***H***-C(O)-), 8.40 – 8.20 (2H, m, -N***H₂***), 8.00 (2H, dd, *J* 8.2, $^4J_{H-P}$ 3.7, 3-***H***), 7.71 (2H, dd, $^3J_{H-P}$ 13.0, *J* 8.2, 2-***H***), 4.07 – 3.93 (4H, m, -O-C***H₂***-CH_3), 3.75 – 3.65 (2H, m, 1´-***H₂***), 3.27 – 3.15 (2H, m, 2´-***H₂***), 1.22 (6H, t, *J* 7.1, -O-CH_2-C***H₃***). δ_C (176 MHz, $CDCl_3$) 167.4 (C=O), 137.2 (d, $^4J_{C-P}$ 2.85, ***C***-4), 131.5 (d, $^2J_{C-P}$ 10.3, ***C***-2), 130.6 (d, $^1J_{C-P}$ 187.6, ***C***-1), 127.9 (d, $^3J_{C-P}$ 14.8, ***C***-3), 62.6 (d, $^2J_{C-P}$ 5.8, -O-***C***H_2-CH_3), 39.9 (***C***-1´), 37.7 (***C***-2´), 16.2 (d, $^3J_{C-P}$ 6.4, -O-CH_2-***C***H_3). δ_P (162 MHz, $CDCl_3$) 11.79. HRMS (ES^+) found $[M+H]^+$ 301.1327; $C_{13}H_{22}N_2O_4P$ requires *M* 301.1317.

4-(diethoxyphosphoryl)benzoic acid (66)

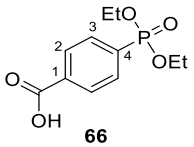

66

General procedure B was applied to 4-iodobenzoic acid (**65**). After workup, **66** (960 mg*,* 94%) was obtained as a dark brown oil. ν_{max} (ATR) 3414 (-OH), 1718 (C=O), 1211 (P=O), 1014 (C-O). cm^{-1}. δ_H (400 MHz, $CDCl_3$) 10.62 (1H, s, -O***H***), 8.22 (2H, dd, *J* 8.3, $^4J_{H-P}$ 3.8, 2-***H***), 7.96 (2H, dd, $^3J_{H-P}$ 13.1, *J* 8.3, 3-***H***), 4.30 – 4.09 (4H, m, -O-C***H₂***-CH_3), 1.36 (6H, t, *J* 7.1, -O-CH_2-C***H₃***). δ_C (101 MHz, $CDCl_3$) 169.5 (***C***=O), 133.5 (d, $^4J_{C-P}$ 3.0, ***C***-1), 133.2 (d, $^1J_{C-P}$ 186.5, ***C***-4), 131.9 (d, $^2J_{C-P}$ 10.2, ***C***-2), 130,0 (d, $^3J_{C-P}$ 15.1, ***C***-2), 62.8 (d, $^2J_{C-P}$ 5.6, -O-***C***H_2-CH_3), 16.3 (d, $^3J_{C-P}$ 6.5, -O-CH_2-***C***H_3). δ_P (162 MHz, $CDCl_3$) 17.1. m/z LCMS (ES^+) 259.1 $[M+H]^+$; 517.2 $[2M+H]^+$ and m/z LCMS (ES^-) 257.2 $[M-H]^-$; 515.3 $[2M-H]^-$.

Diethyl [4-(carbonochloridoyl)phenyl]phosphonate (67)

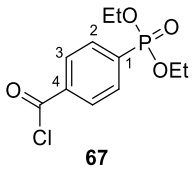

67

General procedure E was applied to **66**. After the volatiles were removed, **67** was obtained as a yellow oil. ν_{max} (ATR) 1719 (C=O), 737 (C-Cl) cm^{-1}. δ_H (400 MHz, $CDCl_3$) 8.22 (2H, dd, *J* 8.6, $^4J_{H-P}$ 3.6, 3-***H***), 8.02 – 7.94 (2H, dd, $^3J_{H-P}$ 12.9, *J* 8.6, 2-***H***), 4.29 – 4.07 (4H, m, -O-C***H₂***-CH_3), 1.36 (6H, t, *J* 7.1, -O-CH_2-C***H₃***). δ_C (101 MHz, $CDCl_3$) 132.3 (d, $^2J_{C-P}$ 10.0, ***C***-2), 131.0 (d, $^3J_{C-P}$ 14.9, ***C***-3), 62.7 (d, $^2J_{C-P}$, -O-***C***H_2-CH_3), 16.4 (d, $^3J_{C-P}$ 6.5, -O-CH_2-***C***H_3). δ_P (162 MHz, $CDCl_3$) 15.6.

Tert-butyl N-(2-{[4´-(diethoxyphosphoryl)phenyl]formamido}ethyl)carbamate (69)

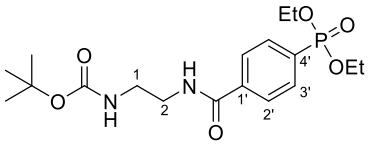

69

General procedure Gb was applied to **67** and **68**. After workup, **69** (676 mg, 87%) was obtained as a yellow oil. ν_{max} (ATR) 3328 (N-H), 1701 (C=O), 1651 (C=O), 1241 (P=O) cm^{-1}. δ_H (700 MHz, $CDCl_3$) 7.89 – 7.83 (3H, m, 2'-***H***, -N***H***-), 7.72 (2H, dd, $^3J_{H-P}$ *13*.0, *J* 8.0, 3'-***H***), 5.53 (1H, t, *J* 6.1, -N***H***-), 4.10 – 3.96 (4H, m, -C***H₂***-CH_3), 3.52 - 3.47 (2H, m,

2-***H***), 3.38 – 3.32 (2H, m, 1-***H***), 1.35 (9H, s, -C-(C***H₃***)₃), 1.25 (6H, t, *J* 7.1, -CH_2-C***H₃***). δ_C (176 MHz, $CDCl_3$) 166.9 (-NH-***C***(O)-Ar), 157.4 (-***C***(O)-NH-CH_2-), 131.8 (d, $^2J_{C-P}$ 10.2, ***C***-3'), 131,0 (d, $^1J_{C-P}$ 184.2, ***C***-4')128.7 (d, $^4J_{C-P}$ 12.3, ***C***-1'), 127.1 (d, $^3J_{C-P}$ 15.0, ***C***-2'), 79.7 (-***C***$(CH_3)_3$), 62.4 (d, $^2J_{C-P}$ 5.6, -***C***H_2-CH_3), 42.0 (***C***-2), 39.9 (***C***-1), 28.3 (-C(***C***$H_3)_3$), 16.2 (d, $^3J_{C-P}$ 6.3, -CH_2-***C***H_3). δ_P (162 MHz, $CDCl_3$) 17.4. HRMS (ES^+) found $[M+H]^+$ 401.1838; $C_{18}H_{30}N_2O_6P$ requires *M* 401.1842.

Hex-5-ynoyl-chloride (70)

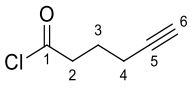

70

General procedure E was applied to 5-hexynoic acid. **70** was obtained as a red liquid. No purification was conducted. ν_{max} (ATR) 3254 (≡C-H), 1732 (C=O), 742 (C-Cl) cm^{-1}.

Diethyl (4-{[2'-(hex-5''-ynamido)ethyl]carbamoyl}phenyl)phosphonate (71)

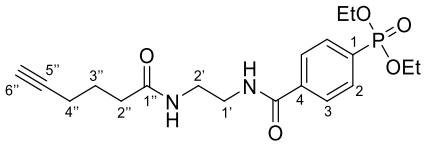

71

General procedure Ga was applied to **64**. After workup, **71** (208 mg, 54%) was obtained as a dark yellow solid. ν_{max} (ATR) 3481 (N-H), 3305 (≡C-H), 2260 (C≡C), 1650 (C=O), 1232 (P=O) cm^{-1}. δ_H (700 MHz, $CDCl_3$) 7.88 (2H, dd, *J* 8.2, $^4J_{H-P}$ 3.8, 3-

H), 7.83 (2H, dd, $^{3}J_{H\text{-}P}$ 12.9, *J* 8.2, 2-***H***), 7.68 (1H, t, *J* 4.9, -1´-N***H***), 6.47 (1H, d, *J* 6.3, -2´-N***H***), 4.17 – 4.02 (4H, m, -O-C***H₂***-CH_3), 3.59 – 3.55 (2H, m, 2'-***H₂***), 3.51 (2H, m, 1'-***H₂***), 2.34 (2H, t, *J* 7.4, 2''-***H₂***), 2.21 (2H, td, *J* 6.9, 2.7, 4''-***H₂***), 1.93 (1H, t, *J* 2.7, 6''-***H***), 1.83 (2H, p, *J* 6.9, 3''-***H₂***), 1.31 (6H, t, *J* 7.1, -O-CH_2-C***H₃***). δ_C (176 MHz, $CDCl_3$) 174.3 (-CH_2-***C***(O)-NH-), 167.1 (-NH-***C***(O)-Ar), 137.6 (d, $^{4}J_{C\text{-}P}$ 3.3, ***C***-4), 132.0 (d, $^{2}J_{C\text{-}P}$ 10.0, ***C***-2), 131.6 (d, $^{1}J_{C\text{-}P}$ 188.3, ***C***-1), 127.0 (d, $^{3}J_{C\text{-}P}$ 15.1, ***C***-3), 83.2 (***C***-5''), 69.3 (***C***-6''), 62.4 (d, $^{2}J_{C\text{-}P}$ 5.5, -O-***C***H_2-CH_3), 41.8 (***C***-2'), 39.6 (***C***-1'), 34.9 (***C***-2''), 24.1 (***C***-3''), 17.8 (***C***-4''), 16.3 (d, $^{3}J_{C\text{-}P}$ 6.4, -O-CH_2-***C***H_3). δ_P (162 MHz, $CDCl_3$) 17.2. HRMS (ES^+) found $[M+H]^+$ 395.1737; $C_{19}H_{28}N_2O_5P$ requires *M* 395.1736.

Ethyl [4-(prop-2'-yn-1'-yloxy)phenyl]phosphonofluoridate (77)

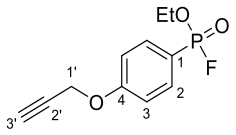

77

Phosphonate **42** was treated following the general procedure D using H_2O as solvent for the hydrolysis step and stirred during 13 h to afford the intermediate phosphinic acid. m/z LCMS (ES^+) 241.1 $[M+H]^+$, 481.1 $[2M+H]^+$. Subsequent fluorination afforded the title fluorophosphonate **77** (16 mg, 36%) as a brown oil. Column eluent 0-100% EtOAc in hexanes. ν_{max} (ATR) 3305 (H-C≡C), 2125 (C≡C), 1140 (P=O), 1036 (C-O) cm^{-1}. δ_H (599 MHz, $CDCl_3$) 7.80 (2H, dd, $^{3}J_{H\text{-}P}$ 13.8, 8.8, 2-***H***), 7.12 – 7.03 (2H, m, 3-***H***), 4.76 (2H, d, *J* 2.4, 1'-***H₂***), 4.36 – 4.26 (2H, m, O-C***H₂***-CH_3), 2.55 (1H, t, *J* 2.4, 3'-***H***), 1.41 (3H, t, *J* 7.1, -C***H₃***). δ_C (151 MHz, $CDCl_3$) 161.6 (d, $^{4}J_{C\text{-}P}$ 3.8, ***C***-4), 133.8

(d, $^{2}J_{C\text{-}P}$ 12.5, ***C***-2), 116.8 (dd, $^{1}J_{C\text{-}P}$ 209.4, $^{2}J_{C\text{-}F}$ 30.9, ***C***-1), 115.1 (d, $^{3}J_{C\text{-}P}$ 17.5, ***C***-3), 77.5 (***C***-2'), 76.4 (***C***-3'), 63.6 (d, $^{2}J_{C\text{-}P}$ 6.1, -O-***C***H_2-CH_3), 55.8 (***C***-1'), 16.3 (d, $^{3}J_{C\text{-}P}$ 6.0, -***C***H_3). δ_P (162 MHz, $CDCl_3$), 17.7 (d, $^{1}J_{P\text{-}F}$1035.1). δ_F (376 MHz, $CDCl_3$) -63.5 (d, $^{1}J_{F\text{-}P}$1035). HRMS (ES+) found $[M+H]^+$ 243.0575; $C_{11}H_{13}O_3FP$ requires *M* 243.0586.

Ethyl [4-(hex-5´-yn-1´-yloxy)phenyl]phosphonofluoridate (78)

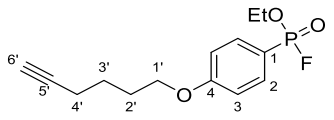

78

Phosphonate **43** was treated following the general procedure D using H_2O as solvent for the hydrolysis step and stirred for 6 h to afford the intermediate phosphinic acid. After the fluorination, **78** (62 mg, 68%) was obtained as a brown oil. Column eluent 0-100% EtOAc in hexanes. ν_{max} (ATR) 3309 (C≡C-H), 2247 (C≡C) cm^{-1}. δ_H (599 MHz, $CDCl_3$) 7.79 – 7.70 (2H, m, 2-***H***), 6.96 (2H, dd, *J* 8.3, $^{4}J_{H\text{-}P}$ 3.9, 3-***H***), 4.34 – 4.22 (2H, m, -O-C***H₂***-CH_3), 4.03 (2H, t, *J* 6.3, *1´-**H***), 2.27 (2H, td, *J* 7.0, 2.7, 4'-***H₂***), 1.96 (1H t, *J* 2.7, 6'-***H₂***), 1.95 – 1.90 (2H, m, 2'-***H₂***), 1.74 – 1.68 (2H, m, 3'-***H₂***), 1.39 (3H, t, *J* 7.1, -O-CH_2-C***H₃***). δ_C (151 MHz, $CDCl_3$) 163.2 (d, $^{4}J_{C\text{-}P}$ 3.6, ***C***-4), 133.8 (d, $^{2}J_{C\text{-}P}$ 12.9, ***C***-2), 116.3 (dd, $^{1}J_{C\text{-}F}$ 209.9, $^{1}J_{C\text{-}P}$ 30.5, ***C***-1), 114.7 (d, $^{3}J_{C\text{-}P}$ 17.5, ***C***-3), 83.8 (***C***-5'), 68.8 (***C***-6'), 67.5 (***C***-1'), 63.5 (d, $^{2}J_{C\text{-}P}$ 6.1, -O-***C***H_2-CH_3), 28.0 (***C***-2'), 24.9 (***C***-3'), 18.1 (***C***-4'), 16.3 (d, $^{2}J_{C\text{-}P}$ 6.1, -O-***C***H_2-CH_3). δ_P (162 MHz, $CDCl_3$) 18.3 (d, $^{1}J_{P\text{-}F}$ 1033.5). δ_F (376 MHz, $CDCl_3$) -63.7 (d, $^{1}J_{P\text{-}F}$ 1033.5). HRMS (ES^+) found $[M+H]^+$ 285.1068, $C_{14}H_{18}FO_3P$ requires *M* 285.1056.

Ethyl (4-{[6-(hex-5-ynamido)hexyl]oxy}phenyl)phosphonofluoridate (79)

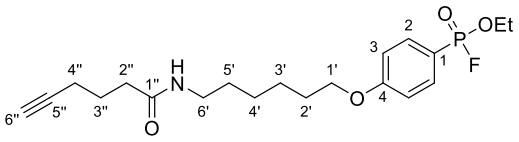

79

Phosphonate **49** was treated following the general procedure D using EtOH:H_2O (1:1) as solvent system for the hydrolysis step and stirred for 46 h. After the fluorination, **79** (42 mg, 60%) was obtained as a yellow oil. Column eluent 0-10% MeOH in DCM. ν_{max} (ATR) 3315 (C≡C-H), 1645 (C=O), 1263 (P=O) cm^{-1}. δ_H NMR (599 MHz, $CDCl_3$) 7.76 (2H, dd, $^3J_{H-P}$ 13.8, *J* 8.8, 2-***H***), 6.77 (2H, dd, *J* 8.8, $^4J_{H-P}$ 3.7, 3-***H***), 5.53 (1H, s br., -N***H***-), 4.36 – 4.25 (2H, m, -O-C***H₂***-CH_3), 4.00 (2H, t, *J* 6.4, 1'-***H₂***), 3.26 (2H, td, *J* 7.2, 5.8, 6'-***H₂***), 2.31 (2H, t, *J* 7.1, 2''-***H₂***), 2.25 (2H, td, *J* 7.1, 2.6, 4''-***H₂***), 1.97 (1H, t, *J* 2.6, 6''-***H***), 1.86 (2H, p, *J* 7.1, 3''-***H₂***), 1.83 – 1.76 (2H, m, 2'-***H₂***), 1.58 – 1.45 (4H, m, 5'-***H₂***, 3'-***H₂***), 1.43 – 1.36 (6H, m, 4'-***H₂***, -O-CH_2-***C***H_3). δ_C NMR (151 MHz, $CDCl_3$) 172.3 (C=O), 163.5 (d, $^4J_{C-P}$ 3.6, ***C***-4), 134.0 (d, $^2J_{C-P}$ 12.5, ***C***-2), 115.6 (d, $^1J_{C-P}$ 179.1, ***C***-1), 114.9 (d, $^3J_{C-P}$ 17.4, ***C***-3), 83.7 (***C***-5''), 69.3 (***C***-6''), 68.2 (***C***-1'), 63.7 (d, $^2J_{C-P}$ 6.0, -O-***C***H_2-CH_3), 39.6 (***C***-6'), 35.2 (***C***-2''), 29.8 (***C***-5'), 29.1 (***C***-2'), 26.7 (***C***-4'), 25.8 (***C***-3'), 24.3 (***C***-3''), 17.9 (***C***-4''), 16.5 (d, $^3J_{C-P}$ 6.1, -O-CH_2-***C***H_3). δ_P (162 MHz, $CDCl_3$) 18.3 (d, $^1J_{P-F}$ 1033). δ_F (376 MHz, $CDCl_3$) -63.7 (d, $^1J_{P-F}$ 1033). HRMS (ES^+) found $[M+H]^+$ 398.1880; $C_{20}H_{30}FNO_4P$ requires *M* 398.1897.

Ethyl [4'-(hex-5''-yn-1''-yloxy)-[1,1'-biphenyl]-4-yl]phosphonofluoridate (80)

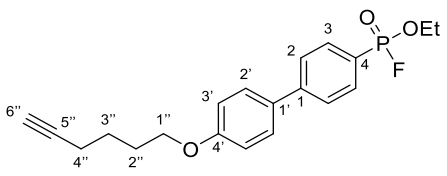

80

Phosphonate **44** was treated following the general procedure D using EtOH:H_2O (1:1) as solvent system for the hydrolysis step and stirred for 26 h. After the fluorination, **80** (11 mg, 54%) was obtained as a white oil. Column eluent 0-30% MeOH in DCM. ν_{max} (ATR) 3311 (C≡C-H stretch), 1041 (C-O) cm^{-1}. δ_H (599 MHz, $CDCl_3$) 7.88 (2H, dd, $^3J_{H-P}$ 14.1, *J* 8.4, 3-***H***), 7.71-7.65 (2H, m, 2-***H***), 7.57 – 7.52 (2H, m, 2'-***H***), 7.01 – 6.97 (2H, m, 3'-***H***), 4.42 – 4.27 (2H, m, -O-C***H***$_2$-CH_3), 4.05 (2H, t, *J* 6.3, 1´´-***H***$_2$), 2.30 (2H, td, *J* 7.2, 2.6, 4´´-***H***$_2$), 1.96 (1H, t, *J* 2.6, 6´´-***H***), 1.97 – 1.92 (2H, m, 2´´-***H***$_2$), 1.78 – 1.72 (2H, p, *J* 7.2, 3´´-***H***$_2$), 1.44 (3H, t, *J* 7.1, -O-CH_2-C***H***$_3$). δ_C (151 MHz, $CDCl_3$) 159.7 (***C***-4'), 146.2 (d, $^4J_{C-P}$ 3.4, ***C***-1), 132.4 (d, $^2J_{C-P}$ 11.3, ***C***-3), 132.0 (***C***-1'), 128.6 (***C***-2'), 127.0 (d, $^3J_{C-P}$ 16.7, ***C***-2), 122.4 (dd, $^1J_{C-P}$ 204.1 $^2J_{C-F}$ 30.3, ***C***-4), 115.2 (***C***-3'), 84.2 (***C***-5''), 68.8 (***C***-6''), 67.6 (***C***-1''), 64.0 (d, $^3J_{C-P}$ 6.2, -O-***C***H_2-CH_3), 28.4 (***C***-2''), 25.2 (***C***-3''), 18.3 (***C***-4''),16.5 (d, $^3J_{C-P}$ 6.0, -CH_2-***C***H_3). δ_P (162 MHz, $CDCl_3$) 17.6 (d, $^1J_{P-F}$ 1039.5). δ_F (376 MHz, CDCl3) -63.8 (d, $^1J_{F-P}$ 1039.5). HRMS (ES^+) found $[M+H]^+$ 361.1349; $C_{20}H_{23}FO_3P$ requires *M* 361.1369.

Ethyl [4-({[5´-(hex-5´´-ynamido)pentyl]oxy}methyl)phenyl] phosphonofluoridate (81)

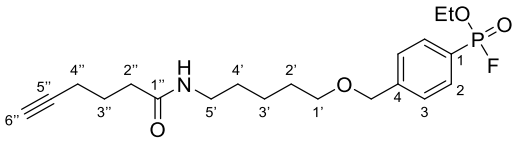

81

Phosphonate **59** was treated following the general procedure D using H_2O as solvent for the hydrolysis step and stirred for 6.5 h. After fluorination, **81** (51 mg, 64%) was obtained as a brown oil. Column eluent 0-100% EtOAc in hexanes. ν_{max} (ATR) 3513 (N-H), 3310 (C≡C-H), 1652 (C=O), 1279 (P=O) 1039 (C-O) cm^{-1}. δ_H (700 MHz, $CDCl_3$) 7.81 (2H, dd, $^3J_{H-P}$ 14.1, 8.0, 2-***H***), 7.46 (2H, dd, *J* 8.0, $^4J_{H-P}$ 4.6, 3-***H***), 5.52 (1H, s, -N***H***-), 4.55 (2H, s, -O-C***H₂***-Ar), 4.37 – 4.27 (2H, m, -O-C***H₂***-CH_3), 3.49 (2H, t, *J* 6.5, 1'-***H₂***), 3.25 (2H, dt, *J* 7.2, 6.7, 5'-***H₂***), 2.29 (2H, t, *J* 7.2, 2''-***H₂***), 2.24 (2H, td, *J* 7.2, 2.7, 4''-***H₂***), 1.96 (1H, t, *J* 2.7, 6''-***H***), 1.84 (2H, p, *J* 7.2, 3''-***H₂***), 1.64 (2H, dt, *J* 14.8, 6.5, 2'-***H₂***), 1.52 (2H, p, *J* 7.3, 4'-***H₂***), 1.41 (5H, m, 3'-***H₂***, -O-CH_2-C***H₃***). δ_C (176 MHz, $CDCl_3$) 172,1 (C=O), 144.9 (d, $^4J_{C-P}$ 3.4, ***C***-4), 131.8 (d, $^2J_{C-P}$ 11.3, ***C***-2), 127.3 (d, $^3J_{C-P}$ 16.6, ***C***-3), 123.6 (d, $^1J_{C-P}$ 202.9, $^1J_{C-P}$ 30.4, ***C***-1), 83.5 (***C***-5''), 72.1 (-O-***C***H_2-Ar), 70.6 (***C***-1'), 69.1 (***C***-6''), 63.8 (d, $^2J_{C-P}$ 6.1, -O-***C***H_2-CH_3), 39.4 (***C***-5'), 35.1 (***C***-2''), 29.5 (***C***-4'), 29.3 (***C***-2'), 24.2 (***C***-3''), 23.6 (***C***-3'), 17.8 (***C***-4''), 16.3 (d, $^3J_{C-P}$ 6.0, -O-CH_2-***C***H_3). δ_P (162 MHz, $CDCl_3$) 17.2 (d, $^1J_{P-F}$ 1041). δ_F (376 MHz, $CDCl_3$) -63.9 (d, $^1J_{P-F}$ 1041). m/z LCMS (ES^+) 398.4 $[M+H]^+$. HRMS (ES^+) found $[M+H]^+$ 398.1878, $C_{20}H_{30}FNO_4P$ requires *M* 398.1897. Phosphinic acid intermediate m/z LCMS (ES^+) 396.4 $[M+H]^+$.

Ethyl (4-{[2'-(hex-5''-ynamido)ethyl]carbamoyl}phenyl)phosphonofluoridate (82)

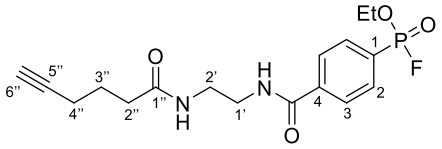

82

Phosphonate **71** was treated following the general procedure D using H_2O as solvent for the hydrolysis step and stirred for 3 h. After the fluorination, **82** (10 mg, 45%) was obtained as a brown oil. Column eluent 0-30% MeOH in DCM. ν_{max} (ATR) 3319 (C≡C-H), 1656 (C=O), 1554 (C=O), 1275 (P=O), 1042 (C-O) cm^{-1}. δ_H (599 MHz, $CDCl_3$) 7.99-7.86 (4H, m, 3-***H***, 2-***H***), 7.67 (1H, s, 1'-N***H***), 6.24 (1H, d, 2'-N***H***) 4.42 – 4.28 (2H, m, -O-C***H₂***-CH_3), 3.62 – 3.58 (2H, m, 1'-***H₂***), 3.58-3.51 (2H, m, 2'-***H₂***), 2.37 (2H, t, *J* 7.1, 2''-***H₂***), 2.23 (2H, td, *J* 7.1, 2.7, 4''-***H₂***), 1.96 (1H, t, *J* 2.7, 6''-***H***), 1.83 (2H, p, *J* 7.1, 3''-***H₂***), 1.43 (3H, t, *J* 7.0, -O-CH_2-C***H₃***). δ_C (151 MHz, $CDCl_3$) 174.9 (***C''***-1), 166.6 (-NH-***C***(O)-Ar), 138.8 (d, $^4J_{C\text{-}P}$ 3.3, ***C***-4), 132.2 (d, $^2J_{C\text{-}P}$ 11.2, ***C***-2), 127.8 (dd, $^1J_{C\text{-}P}$ 200.7 $^1J_{C\text{-}F}$ 32.1, ***C***-1), 127.4 (d, $^3J_{C\text{-}P}$ 16.6, ***C***-3), 83.3 (***C***-5''), 69.9 (***C***-6''), 64.4 (d, $^2J_{C\text{-}P}$ 6.3, -O-***C***H_2-CH_3), 42.4 (***C***-1'), 39.7 (***C***-2'), 35.0 (***C***-2''), 24.2 (***C***-3''), 17.9 (***C***-4''), 16.5 (d, $^3J_{C\text{-}P}$ 5.9, -O-CH_2-***C***H_3). δ_P (162 MHz, $CDCl_3$) 15.6 (d, $^1J_{P\text{-}F}$ 1045). δ_F (376 MHz, CDCl3) -58.8 (d, $^1J_{P\text{-}F}$ 1045). HRMS (ES^+) found $[M+H]^+$ 369.1367; $C_{17}H_{23}N_2O_4PF$ requires *M* 369.1379.

Diethyl (but-3-yn-1-yl)phosphonate (84)

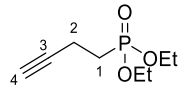

84

A mixture of $P(OEt_3)$ (1.0 mL, 0.006 mol, 1 eq) and 4-bromo-1-butyne (1.2 mL, 0.01 mol, 2.1 eq) was heated for 2.5 h at 150 °C. The reaction mixture was then cooled to rt and after the volatiles were removed, **84** (412 mg, 38%) was obtained as a yellow oil. ν_{max} (ATR) 3311 (C-H alkyne), 2244 (C≡C), 1242 (P=O) cm^{-1}. δ_H NMR (400 MHz, $CDCl_3$) 4.19 – 4.01 (4H, m, -OC***H₂***CH_3), 2.47 (2H, m, 1-***H₂***), 2.05 – 1.93 (3H, m, 4-***H***, 2-***H₂***), 1.32 (6H, t, *J* 7.0, -OCH_2C***H₃***). δ_C NMR (101 MHz, $CDCl_3$) 82.8 (d, $^3J_{C\text{-}P}$ 20.6, ***C***-3), 69.2 (d, $^4J_{C\text{-}P}$ 1.8, ***C***-4), 61.9 (d, $^2J_{C\text{-}P}$ 6.5, -O***C***H_2CH_3), 25.34 (d, $^1J_{C\text{-}P}$ 142.0, ***C***-1), 16.6 (d, $^3J_{C\text{-}P}$ 6.0, -OCH_2***C***H_3), 12.7 (d, $^2J_{C\text{-}P}$ 3.6, ***C***-2). δ_P NMR (162 MHz, $CDCl_3$) 28.9. m/z LCMS (ES^+) 191.2 $[M+H]^+$. All the data are in accordance with the literature.[158]

Synthesis of ethyl (but-3-yn-1-yl)phosphonofluoridate (85)

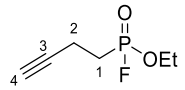

NaOH (64 mg, 1.6 mmol, 3 eq) was added to a solution of **84** (100 mg, 0.53 mmol, 1 eq) in 1:1 H_2O:EtOH (4.0 mL), and the mixture was left to react at 85 °C for 8 h. Subsequently, it was concentrated to remove the EtOH, diluted with water (1 mL), acidified with 1N HCl (1 mL), extracted with EtOAc (3 × 25 mL). The combined organic

extracts were then washed with brine (1 × 5 mL) and concentrated. The resulting crude product was dissolved in dry DCM (4.0 mL), cooled to −78 °C and DAST (0.146 mL, 1.05 mmol, 2 eq) added dropwise. The mixture was then left to stir for 3 h at −78°C. After completion, it was quenched with water, the volatiles were removed under vacuum and it was extracted with EtOAc (25.0 mL), washed with water (1 × 5 mL) and brine (1 × 5 mL), dried and purified by flash chromatography (Hex:EtOAc 0-100% gradient) to afford the titled alkyl fluorophosphonate **85** (60 mg, 69%) as a yellow liquid. ν_{max} (ATR) 3305 (C-H alkyne), 2248 (C≡C), 1677 (C=O), 1272 (P=O), 1043 (C-O) cm^{-1}. δ_H NMR (599 MHz, $CDCl_3$) 4.35 – 4.23 (2H, m, -OC***H₂***CH_3), 2.60 – 2.51 (2H, m, 2-***H₂***), 2.22 – 2.12 (2H, m, 1-***H₂***), 2.05 (1H, t, *J* 2.7, 4-***H***), 1.39 (3H, t, *J* 7.1, -OCH_2C***H₃***). δ_C NMR (151 MHz, $CDCl_3$) 81.4 (d, $^3J_{C\text{-}P}$ 20.1, ***C***-3), 70.0 (d, $^4J_{C\text{-}P}$ 1.8, ***C***-4), 63.8 (d, $^2J_{C\text{-}P}$ 7.1, -O***C***H_2CH_3), 24.2 (dd, $^1J_{C\text{-}P}$ 145.8, $^1J_{C\text{-}F}$ 24.0, ***C***-1), 16.5 (d, $^3J_{C\text{-}P}$ 5.6, -OCH_2***C***H_3), 12.1 (d, $^2J_{C\text{-}P}$ 3.5, ***C***-2). δ_P NMR (162 MHz, $CDCl_3$) 28.1 (d, $^1J_{P\text{-}F}$ 1070). δ_F NMR (376 MHz, $CDCl_3$) -63.6 (d, $^1J_{F\text{-}P}$ 1070). HRMS (ES^+) found $[M+H]^+$ 165.0476; $C_6H_{10}FO_2P$ requires *M* 165.0481.

Diethyl [(4-nitrophenyl)methyl]phosphonate (90)

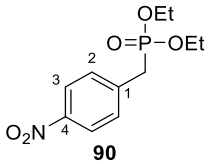

90

A solution of 4-nitrobenzyl bromide (**86**) (2.0 g, 9 mmol, 1.0 eq) in $P(OEt_3)$ (32 mL, 0.18 mol, 20 eq) was heated for 1.75 h at 150 °C. The reaction mixture was then cooled to 20 °C and quenched with a solution of saturated $NaHCO_3$ solution (100 mL),

and the extracted with AcOEt (3 × 50 mL). The combined organic layers were washed with H_2O (2 × 50 mL) and brine (50 mL). The solvent was then removed in vacuo, and the residue was purified by flash chromatography (Hexane:EtOAc 0-100% gradient) to afford the titled phosphonate **90** as a yellow oil (1.1 g, 44%). ν_{max} (ATR) 1522 (N-O stretching), 1352 (C-N stretching) cm^{-1}. δ_H (400 MHz, $CDCl_3$) 8.18 (1H, d, *J* 8.5, 3-***H***), 7.47 (1H, dd, *J* 8.5, $^{3}J_{H-P}$ 2.5, 2-***H***), 4.10 – 3.99 (4H, m, -OC***H₂***CH_3), 3.24 (2H, d, $^{2}J_{H-P}$ 22.4, Ar-C***H₂***P), 1.28 – 1.23 (6H, t, *J* 7.3, -OCH_2C***H₃***). δ_C (101 MHz, $CDCl_3$) 147.1 (d, $^{5}J_{C-P}$ 4.1, ***C***-4), 139.9 (d, $^{4}J_{C-P}$ 9.2, ***C***-1), 130.8 (d, J_{C-P} 6.4, ***C***-2), 123.8 (d, J_{C-P} 3.0, ***C***-3), 62.5 (d, $^{2}J_{C-P}$ 6.6, -O***C***H_2CH_3), 34.1 (d, $^{1}J_{C-P}$ 137.7, Ar-***C***H_2P), 16.5 (d, $^{3}J_{C-P}$ 6.0, -O**C**H_2***C***H_3). δ_P NMR (162 MHz, $CDCl_3$) 24.1. m/z LCMS (ES^+) 274.2 $[M+1]^+$, 316.4 $[M+1+MeCN]^+$. All the data are in accordance with the literature.[159]

Diethyl (4-aminophenyl)methylphosphonate (91)

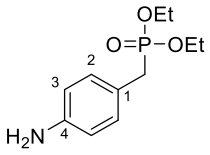

91

NH_4Cl (0.6 g, 0.01 mol, 3 eq) in water (0.2 M) and Zn (1.0 g, 16 mmol, 4 eq) were added to a solution of diethyl 4-nitrobenzyl phosphonate (1.1 g, 4 mmol, 1 eq) in ethanol (20 mL) and the resulting mixture was stirred at reflux temperature for 2 h. On completion of the reaction, it was filtered, and the filtrate was concentrated under vacuum, redissolved in water (20 mL), and extracted with EtOAc (3 × 50 mL). The organic layers were combined, dried, and concentrated under vacuum to afford the titled amine **91** (0.85 g, 86%) as a yellow oil. ν_{max} (ATR) 3349 (N-H stretching),

1628 (N-H bending) cm^{-1}. δ_H (400 MHz, $CDCl_3$) 7.13 – 7.08 (2H, m, 2-***H***), 6.68 – 6.64 (2H, m, 3-***H***), 4.07 – 3.95 (4H, *m*, -OC***H₂***CH_3), 3.64 (2H, s br, -N***H₂***), 3.05 (2H, d, $^{2}J_{H\text{-}P}$ 22.4, Ar-C***H₂***P), 1.28 – 1.18 (6H, t, *J* 7.2, -OCH_2C***H₃***). δ_C (101 MHz, $CDCl_3$) 145.2 (d, $^{5}J_{C\text{-}P}$ 4.1, ***C***-4), 130.8 (d, $J_{C\text{-}P}$ 3.1, ***C***-2), 121.2 (d, $J_{C\text{-}P}$ 6.4, ***C***-1), 115.5 (d, $^{4}J_{C\text{-}P}$ 3.0, ***C***-3), 62.3 (d, $^{2}J_{C\text{-}P}$ 6.6, -O***C***H_2CH_3), 32.8 (d, $^{1}J_{C\text{-}P}$ 137.7, Ar-***C***H_2P), 16.5 (d, $^{3}J_{C\text{-}P}$ 6.0, -O***C***H_2***C***H_3). δ_P NMR (162 MHz, $CDCl_3$) 27.3. m/z LCMS (ES^+) 244.3 $[M+H]^+$, 487. $[2M+H]^+$.

2,5-dioxopyrrolidin-1'-yl hex-5'-ynoate (92)

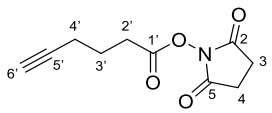

92

NHS (1.1 mg, 10 mmol, 1.1 eq) and EDC.HCl (1.9 mg, 10 mmol, 1.1 eq) were added to a solution of 5-hexynoic acid (1.0 mL, 9.2 mmol, 1.0 eq) in dry DCM (46 mL) and the reaction mixture was stirred for 8 h at room temperature. It was then washed with water (2 × 10 mL), brine (10 mL), dried, filtered, and concentrated in vacuo. The residue was purified by flash chromatography (Hex:EtOAc gradient) to afford the titled NHS-ester **92** (956 mg, 50%) as a white solid. ν_{max} (ATR) 3288 (C≡C-H), 2260 (C≡C-H), 2262 (C≡C),1820 (C=O), 1786 (C=O), 1740 (C=O) cm^{-1}. δ_H (400 MHz, $CDCl_3$) 2.87 – 2.81 (4H, m, 2-***H***, 3-***H***), 2.77 (2H, t, *J* 7.1, 2'-***H***), 2.37 (2H, td, *J* 7.1, 2.7, 4'-***H***), 2.04 (1H, t, *J* 2.7, 6'-***H***), 2.00 (2H, p, *J* 7.1, 3'-***H***). δ_C (101 MHz, $CDCl_3$) 169.1 (***C***-2, ***C***-5), 168.2 (***C***-1'), 82.4 (***C***-5'), 69.8 (***C***-6'), 29.7 (***C***-2'), 25.6 (***C***-3, ***C***-4), 23.3 (***C***-3'),

17.6 (***C***-4'). m/z LCMS (ES^+) found 210.2 $[M+1]^+$. All data are in accordance with literature.[160]

Diethyl {[4-(hex-5-ynamido)phenyl]methyl}phosphonate (93)

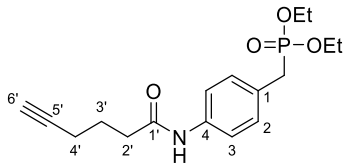

93

NHS-ester **92** (0.968 mL, 4.62 mmol, 1.25 eq) was dissolved in MeOH (37.0 mL) and stirred for 24 h at rt with 4-amino benzyl phosphonate **91** (0.900 mL, 3.70 mmol, 1 eq). Upon completion, the solvent was removed and the remaining crude was taken up in EtOAc (75 mL) and washed with brine (3 × 10 mL), dried and purified by flash chromatography (0-100% EtOAc:Hexane gradient) to afford the titled phosphonate **93** (1.6 g, 42 %) as a yellow solid. ν_{max} (ATR) 3302 (C≡C-H), 1673 (C=O), 1234 (P=O) cm^{-1}. δ_H (700 MHz, $CDCl_3$) 7.51 (1H, s br, -N***H***), 7.46 (2H, d, *J* 8.3, 3-***H***), 7.23 (2H, dd, *J* 8.3, $^3J_{H\text{-}P}$ 2.5, 2-***H***), 4.06 – 3.96 (4H, m, -OC***H₂***CH_3), 3.11 (2H, d, $^2J_{H\text{-}P}$ 21.4, Ar-C***H₂***P), 2.51 (2H, t, *J* 7.0, 2'-***H₂***), 2.33 (2H, td, *J* 7.0, 2.6, 4'-***H₂***), 2.00 (1H, t, *J* 2.6, 6'-***H***), 1.95 (2H, p, *J* 7.0 Hz, 3'-***H₂***), 1.25 (6H, t, *J* 7.1, -OCH_2C***H₃***). δ_C (176 MHz, $CDCl_3$) 170.6 (***C***-1'), 137,0 (***C***-4), 130.4 (d, $^3J_{C\text{-}P}$ 6.5, ***C***-2), 127.2 (d, $^2J_{C\text{-}P}$ 10.0, ***C***-1), 120.0 (d, $^4J_{C\text{-}P}$ 3.0 ***C***-3), 69.5 (***C***-6'), 62.3 (d, $^2J_{C\text{-}P}$ 7.0, -O***C***H_2CH_3), 36.1 (***C***-2'), 33.3 (d, $^1J_{C\text{-}P}$ 138.7, Ar-***C***H_2P), 24.1 (***C***-3'), 18.0 (***C***-4'), 16.55 (d, $^3J_{C\text{-}P}$ 5.8, -OCH_2***C***H_3). δ_P NMR (162 MHz, $CDCl_3$) 26.4. m/z LCMS (ES^+) 338.3 $[M+H]^+$, 675.5 $[2M+H]^+$.

Synthesis of ethyl {[4-(hex-5'-ynamido)phenyl]methyl}phosphonofluoridate (94)

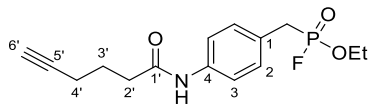

94

NaOH (11 mg, 0.3 mmol, 3 eq) was added to a solution of **93** (30 mg, 0.09 mmol, 1.0 eq) in 1:1 H_2O:EtOH (4.0 mL), and the mixture was left to react at 80 °C for 72 h. Subsequently, it was concentrated to remove the EtOH, diluted with H_2O (1 mL), acidified with 1N HCl (1 mL) and extracted with EtOAc (3 x 25 mL). The combined organic extracts were then washed with H_2O (1 × 10 mL) and concentrated. The resulting crude product was dissolved in dry DCM (4.0 mL), cooled to −78 °C and DAST (14 µL, 0.1 mmol, 1.1 eq) added dropwise. The mixture was then left to stir for 2 h at −78 °C when it was quenched by addition to water at 0 °C. The volatiles were removed and the aqueous layer extracted with EtOAc (3 × 10 mL), concentrated, dried and purified by flash chromatography (Hex: EtOAc 0-100% gradient) to afford the benzylic fluorophosphonate **94** (10 mg, 37%) as a yellow oil. ν_{max} (ATR) 3311 (C≡C-H), 2250 (C≡C), 1677 (C=O) cm^{-1}. δ_H NMR (599 MHz, $CDCl_3$) 7.49 (2H, d, *J* 8.3, 3-***H₂***), 7.40 (1H, s, -N***H***), 7.24 (2H, dd, *J* 8.3, $^3J_{H-P}$ 2.7, 2-***H₂***), 4.24 – 4.15 (2H, m, -OC***H₂***CH_3), 3.32 – 3.21 (2H, m, Ar-C***H₂***-P), 2.51 (2H, t, *J* 7.0, 2'-***H₂***), 2.33 (2H, td, *J* 7.0, 2.7, 4'-***H₂***), 2.01 (1H, t, *J* 2.7, 6'-***H₂***), 1.95 (2H, p, *J* 7.0 Hz, 3'-***H₂***), 1.30 (3H, t, *J* 7.1, -OCH_2C***H₃***). δ_C NMR (151 MHz, $CDCl_3$) 170.5 (***C***-1'), 137.4 (d, $^5J_{C-P}$ 4.1, ***C***-4), 130.2 (d, $^3J_{C-P}$ 7.1, ***C***-2), 124.9 (d, $^2J_{C-P}$ 10.0, ***C***-1), 120.1 (d, $^4J_{C-P}$ 3.2, ***C***-3), 83.4 (***C***-5'), 69.4 (***C***-6'), 64.0 (d, $^2J_{C-P}$ 7.4, -O***C***H_2CH_3), 35.9 (***C***-2'), 31.6 (dd, $^1J_{C-P}$ 142.9, $^1J_{C-F}$ 24.5), 23.8 (***C***-3'), 17.8 (***C***-4'), 16.2 (d, $^3J_{C-P}$ 5.5, -OCH_2***C***H_3). δ_P NMR (162 MHz, $CDCl_3$) 25.0

(d, $^{1}J_{P\text{-}F}$ 1079). δ_F NMR (376 MHz, $CDCl_3$) -64.5 (d, $^{1}J_{P\text{-}F}$ 1079). HRMS (ES^+) found $[M+H]^+$ 12.1160; $C_{15}H_{20}NO_3FP$ requires *M* 312.1165.

3-[(2-aminoethyl)disulfanyl]propanoic acid (97)

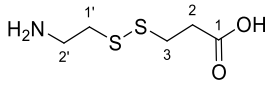

97

Cystamine dihydrochloride **95** (471 mg, 2.0 mmol, 1.0 eq) was dissolved in dry MeOH (18 mL) and cooled in an ice bath. Subsequently, a solution of mCPBA (555 mg, 2.4 mmol, 1.2 eq) in dry DCM (4 mL) was added dropwise. The resulting solution was stirred overnight at room temperature under Ar. The white residue obtained after concentration of the mixture was suspended in dry MeOH (9 mL) and 3-mercaptopropionic acid **96** (0.178 mL, 2.0 mmol, 1.0 eq) was added dropwise and the solution was stirred for 2.5 h at room temperature until concentration of the mixture afforded a solid that was purified by flash chromatography using 2-step purification ($CHCl_3$:MeOH - EtOAc:AcOH+H_2O(2:1)) to afford the titled acid **97**, (286 mg, 82%) as a white solid. ν_{max} (ATR) 3395 (br, -OH), 2907 (br), 1695 (C=O) cm^{-1}. δ_H (700 MHz, D_2O) 3.24 (2H, t, *J* 6.5, 2'-***H***$_2$), 2.87 – 2.83 (4H, m, 3-***H***$_2$, 1'-***H***$_2$), 2.69 (2H, t, *J* 6.8, 2-***H***$_2$). δ_C (176 MHz, D_2O) 176.8 (***C***-1), 37.7 (***C***-2´), 33.7 (***C***-3, ***C***-1´), 32.3 (***C***-2). m/z (LCMS ES^+) 182.2 $[M+H]^+$. HRMS (ES^+) found $[M+H]^+$ 182.0306; $C_5H_{12}NO_2S_2$ requires *M* 182.0309. All the data are in accordance with the literature.[161]

NHS-Biotin (2,5-dioxopyrrolidin-1-yl 5-[(3aS,4S,6aR)-2-oxo-hexahydro-1H-thieno[3,4-d]imidazol-4-yl]pentanoate) (100)

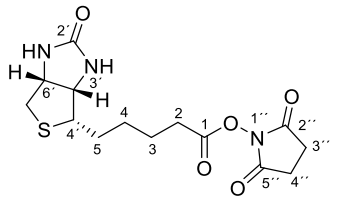

100

Biotin (200 mg, 0.82 mmol, 1.0 eq) and N-hydroxysuccinimide (207 mg, 1.76 mmol, 2.2 eq) were dissolved in hot DMF (8 mL) under Ar. *N,N′*-dicyclohexylcarbodiimide (251 mg, 1.2 mmol, 1.5 eq) was added, and the solution was stirred for 20 h at rt, during which time a white precipitate was formed. The reaction mixture was filtered, and the filtrate was evaporated. The crude precipitate obtained was redissolved in hot 2-propanol and recrystallized to afford the titled NHS-Biotin **100** (199 mg, 73%) as a white solid. ν_{max} (ATR) 3238 (N-H), 1748 (C=O), 1732 (C=O), 1699 (C=O), 1211, 1071, 658. δ_H (700 MHz, DMSO-d_6) 6.38 (1H, s, -N***H***), 6.33 (1H, s, -N***H***), 4.29 – 4.26 (1H, m, 6'-***H***), 4.14 – 4.10 (1H, m, 3'-***H***), 3.11 – 3.06 (1H, m, 4'-***H***), 2.84 – 2.53 (8H, m, -C***H***$_2$-S-, 3''-***H***$_2$, 4''-***H***$_2$, 2-***H***$_2$), 1.66 – 1.35 (6H, m, 3-***H***, 4-***H***, 5-***H***). δ_C (176 MHz, DMSO-d_6) 170.7 (***C***-2'', ***C***-5''), 169.4 4 (***C***-1), 163.1 ***C***-2', 61.4 (***C***-3'*), 59.6 (***C***-6'*), 55.7 (***C***-4'), 40.4 (***C***-2), 30.4 (-***C***H$_2$S-), 28.3 (***C***-5), 28.0 (***C***-4), 25.9 (***C***-3'', ***C***-4''), 24.7 (***C***-3) m/z (LCMS ES$^+$) 342.3 [M+H]$^+$. HRMS (ES$^+$) found [M+H]$^+$ 342.1134; $C_{14}H_{20}N_3O_5S$ requires *M* 342.1124. All the data are in accordance with the literature.[135]

3-[(2-{5-[(3aS,4S,6aR)-2-oxo-hexahydro-1H-thieno[3,4-d]imidazol-4-yl]pentanamido}ethyl)disulfanyl]propanoic acid (101)

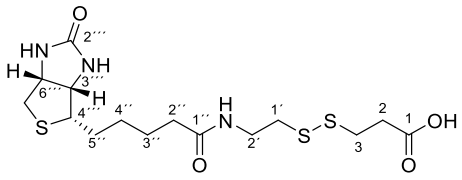

101

A solution of 3-[(2-aminoethyl)disulfanyl]propanoic acid **97**, (67 mg, 0.37 mmol, 1.4 eq) in water (0.6 mL) was added to a solution of NHS-Biotin, **100** (110 mg, 0.32 mmol, 1.0 eq) and Et_3N (0.140 mL, 1.05 mmol, 4.0 eq) in DMF (2 mL). The mixture was stirred at room temperature for 2 h under Ar. Subsequently, the solution was washed with Et_2O, and the DMF/water phase was evaporated leaving a yellow oil. The white solid obtained after addition of HCl 0.01M (5 mL), was filtrated and dried under high vacuum to afford the title biotinylated acid **101**, (65 mg, 50%) as a white solid. ν_{max} (ATR) 3295 (br, -OH), 2930 (br, NH), 1704 (C=O), 1651 (C=O), 1544 (C=O), 1247 (C-N stretching). δ_H (599 MHz, DMSO-d_6) 12.32 (1H , s, 1-***H***), 7.94 (1H ,t, *J* 5.7, C2'-N***H***), 6.38 (1H, s, C2'''-N***H***), 6.32 (1H, s, C2'''-N***H***), 4.30 – 4.25 (1H, m, 6'''-***H***), 4.10 (1H, td, *J* 5.4, 4.9, 2.2, 3'''-***H***), 3.28 (2H, m, 2'-***H***), 3.10 – 3.04 (1H, m, 4'''-***H***), 2.85 (2H, t, *J* 7.0, 3-***H***), 2.79 (1H, dd, *J* 12.4, 5.1, -C***H***$_2$-S), 2.74 (2H, t, *J* 6.8, 1'-***H***), 2.59 (2H, t, *J* 6.9, 2-***H***), 2.55 (1H, d, *J* 12.4, -C***H***$_2$-S), 2.03 (2H, t, *J* 7.4, 2''-***H***), 1.58 (1H, td, *J* 13.8, 11.6, 6.1, 5''-***H****), 1.53 – 1.38 (3H, m, 5''-***H****, 3''-***H***), 1.34 – 1.21 (2H, m, 4''-***H***). δ_C (176 MHz, DMSO-d6) 173.1 (***C***-1), 172.6 (***C***-1''), 163.1 (***C***-2'''), 61.5 (***C***-6'''), 59.6 (***C***-3'''), 55.8 (***C***-4'''), 40.5 (-***C***H_2S-), 38.3 (***C***-2'), 37.8 (***C***-1'), 35.6 (***C***-2''), 34.1 (***C***-2), 33.5 (***C***-3), 28.6 (***C***-4''), 28.5 (***C***-5''), 25.7 (***C***-3''). m/z LCMS (ES^+) 408.3, $[M+H]^+$ 815.4 $[2M+H]^+$. HRMS (ES^+) found $[M+H]^+$

408.1090; $C_{15}H_{26}N_3O_4S_3$ requires *M* 408.1085. All the data are in accordance with the literature.[136]

TetraTAG (9-[4-({[(5R)-5-{3-[(2-{5-[(3aS,4S,6aR)-2-oxo-hexahydro-1H-thieno[3,4-d]imidazol-4-yl]pentanamido}ethyl)disulfanyl]propanamido}-5-[(2-{2-[2-(2-azidoethoxy)ethoxy]ethoxy}ethyl)carbamoyl]pentyl]carbamothioyl}amino)-2-carboxyphenyl]-6-(diethylamino)-N,N-diethyl-3H-xanthen-3-iminium) (109)

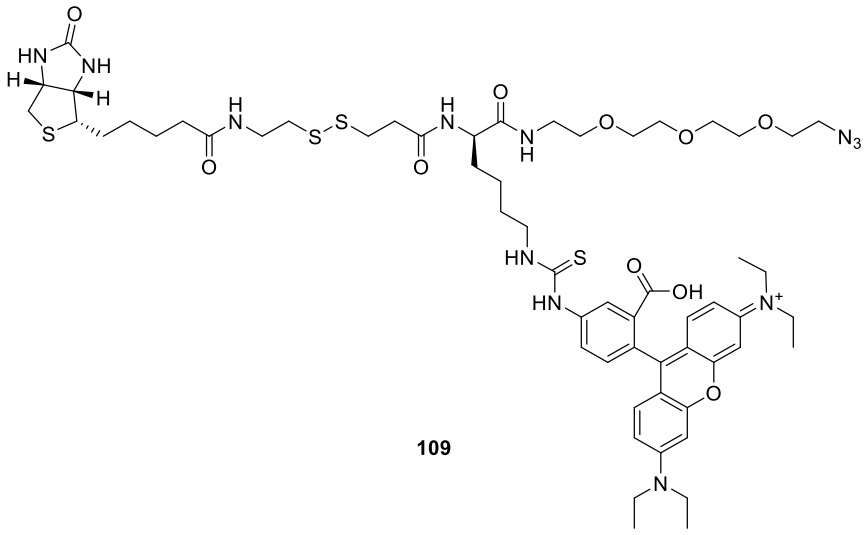

109

General procedure F was applied to Boc protected amine **108**. After the volatiles were removed, the free amine was obtained as a yellow oil) (m/z (LCMS ES^+) 369.1 $[M+H]^{2+}$, 736.7 $[M+H]^+$). Subsequently, it was added to a mixture of isomers of rhodamine B isothiocyanate (29 mg, 0.05 mmol, 1 eq), DIPEA (0.028 mL, 0.16 mmol, 3 eq) in DMF (0.270 mL) and the mixture was stirred under N_2 at rt for 24h. It was then concentrated and purified by C18 reverse phase flash chromatography (H_2O:MeCN 100-0% gradient) to afford a mixture of isomers of the titled

tetrafunctional TAG (29 mg, 43%) as a dark red/purple solid. m/z LCMS (ES^+) 618.9 $[M+H]^{2+}$; 1236.2 $[M]^+$. HRMS (ES^+) found $[M+H]^{2+}$ 618.2 and $[M]^+$ 1235.5; $C_{58}H_{82}N_{12}O_{10}S_4$ requires *M* 618.2658 and *M* 1235.5328 respectively.

Diethyl [4-({[5-(4-{1-[2-(2-{2-[2-({[4-(trifluoromethyl)phenyl]carbamoyl}amino) ethoxy]ethoxy}ethoxy)ethyl]-1H-1,2,3-triazol-4-yl}butanamido)pentyl]oxy}methyl) phenyl]phosphonate (111).

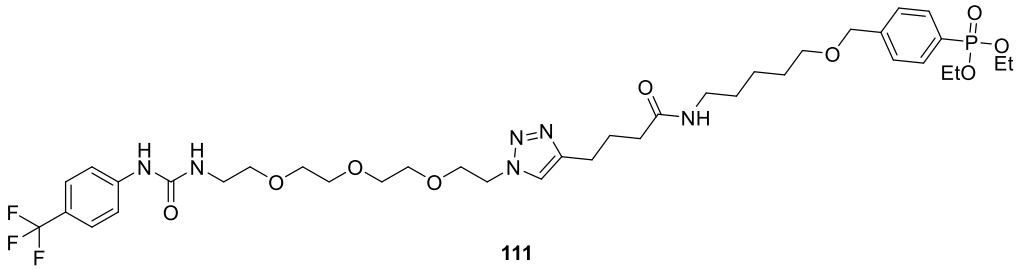

111

A mixture of $CuSO_4.5H_2O$ (2.1 mg, 8 µmol, 0.5 eq) in H_2O, THPTA (7.2 mg, 17 µmol, 1.0 eq), sodium ascorbate (1.6 mg, 8 µmol, 0.5 eq) in H_2O, and CF_3-Ph-PEG-N_3 (**110**) (8.0 mg, 0.020 mmol, 1.2 eq) was added to a solution of **59** (7.0 mg, 0.017 mmol, 1.0 eq) in H_2O:*t*-Butanol (1:1) and stirred for 2h at rt. Completion of the reaction was confirmed by analysis of LCMS and ^{19}F NMR crude spectra. δ_F (376 MHz, $CDCl_3$) -61.9. m/z LCMS (ES^+) 830.7 $[M+H]^+$.

5.2 Biological assays

5.2.1 General Conditions and Methods

5.2.1.1 Buffers, culture media and reagents used

Buffer	Stock Solution	Final Concentration
Storage Buffer	Tris HCl (1 M) Glycerol (10 mL) $MgCl_2.6H_2O$ (1 M) 1 protease inhibitor tablet	50 mM 20 % v/v 5 mM
PBS (500 mL)	NaCl (4 g) KCl (100 mg) Na_2HPO_4 (720 mg) KH_2PO_4 (120 mg)	137 mM 2.7 mM 10 mM 1.8 mM
x10 Running Buffer (1L)	Tris-base (30.2 g) Glycine (144 g) SDS (10 g)	25 mM Tris, pH 8.3 250 mM 0.1%

Table 5.1: Buffer components. Buffers were made to the desired specified pH using conc. HCl and 2 M NaOH.

Media	Stock Solution	Final Concentration
Schneider´s insect medium (1L) pH 6.8	Schneider insect media (26.2 g) FBS (50 ml) Pen-Strep (5mL) $NaHCO_3$ (0.4 g) $CaCl_2$ (0.6 g)	 10% 1% 7.1 mM 5.4 mM

Table 5.2: Media components.

5.2.1.2 Parasite stocks defrost

The frozen *Leishmania* stocks were stored in Cryovials (Starlab) and kept at -150 °C for long term storage. The frozen *Leishmania* aliquot was rapidly defrosted under the tap, using warm water before use and then the *Leishmania* promastigotes were grown

in culture flasks with 10 cm^3 supplemented Schneider's Insect Media at 26 °C.

5.2.1.3 Promastigote parasite culture

Leishmania mexicana (strain 0157), *L. major* (FV1), and *L. amazonensis* (MHOM/Br/75/JOSEFA) promastigotes were grown in Nunc EasYFlask 25 cm^2 Nunclon Delta Surface (ThermoScientific) at 26 °C. The promastigotes were grown in Schneider's insect medium (Merck, Table 6) supplemented with 15 % heat inactivated foetal bovine serum (ThermoFisher Scientific, South American origin), and 1 % Gibco™ Penicillin-Streptomycin (PenStrep, 10,000 U/mL, ThermoFisher Scientific), and filter sterilised using Sterile filter flasks (500 mL, 0.22 microns) and the filtrate stored at 4 °C.

5.2.1.4 *L. mexicana* axenic amastigote culture

L. mexicana axenic amastigotes parasite cultures were prepared following the general procedure:

Day 0. Prepare 10 ml culture using log stage parasites, in Schneiders medium, 15% FCS, pH 7.0, seeded at 5×10^5 parasites/ml. Incubate at 26 °C.

Day 3 – Parasites are procyclic (log) stage. Transfer to 10 ml of Schneiders medium, 20% FCS, pH 5.5, seeded at 5×10^5 parasites/ml. Incubate at 26 °C.

Day 9 – Parasites are metacyclic stage. Transfer to 10 ml of Schneiders medium, 20% FCS, pH 5.5, seeded at 5×10^5 parasites/ml. Transfer to 32 °C.

Day 14-16 – Parasites are in amastigote stage and ready to use.

5.2.1.5 Parasite lysate

Leishmania parasites were grown following either general procedures **5.2.1.3** or **5.2.1.4**. Subsequently, cells were harvested (1000 × *g*, 5 min, 4°C), washed three times with cold PBS. and lysed with the stated lysis buffer (Pierce IP ThermoFisher lysis buffer for click-free ABP labelling and LyBA for click ABP labelling). The resulting lysates were centrifuged (13,000 × *g*, 10 min, 4 °C) to remove insoluble material. The protein concentration in each sample was quantified using Pierce Rapid Gold BCA Protein Assay Kit (ThermoFisher) according to the manufacturers' protocol and homogenates were adjusted to the stated protein concentration (1-2 mg/mL).

Buffer	Composition
Pierce IP Lysis buffer ThermoScientific	Tris HCl (25 mM) pH 7.4, NaCl (150 mM), NP-40 (1%), EDTA (1 mM), glycerol (5%).
LyBA	Tris HCl (25 mM) pH 7.4, NaCl (150 mM), tryton X100 (1%), glycerol (5%).
RIPA Lysis and Extraction Buffer ThermoScientific	Tris HCl (25 mM) pH 7.6, NaCl (150 mM), NP-40 (1%), sodium deoxycholate (1%), SDS (0.1%).

Table 5.3: Lysis buffers used.

5.2.1.6 SDS-PAGE

Protein samples obtained following general procedure **5.2.1.5** were mixed with Laemmli 4X sample loading buffer and incubated at 95 °C for 10 min. 10-15 µL were loaded on 12% polyacrylamide-SDS gels. Samples were separated at 200 V for 1 hour in a MiniProtean system (BioRad) containing 1X running buffer. Protein prestained ladders (BioRad) were loaded onto gels as a molecular weight standard. At the end of each run, gel images were taken to detect fluorescent bands using the procedure

5.2.1.8. Subsequently, gels were stained with Quick Coomassie Brilliant Blue G-250 (Bio- Rad) to detect all protein bands.

5.2.1.7 Biorthogonal Cu catalysed click chemistry

Leishmania lysates obtained following the general procedure **5.2.1.5** were incubated with the stated FP-alkynes in the stated concentrations at rt for 1 h. After this period, TAG-N_3, NaAsc (1 mM), TBTA (0.1 mM) and $CuSO_4$ (1 mM) were added respectively, and the mixture was incubated for a further 1 h with periodic mixing. Finally, the reaction was stopped by addition of 4X LDS sample buffer.

5.2.1.8 Fluorescent Imaging

At the end of each SDS-PAGE run, fluorescent bands were detected, and images were taken using a Typhoon 9400 Variable Mode Imager. Emission filter: 580 BP 30 Cy3, TAMRA, AlexaFluor546; Laser: green (532 nm).

5.2.1.9 *In vitro* ABP labelling

Leishmania lysates obtained following the general procedure **5.2.1.5** were incubated with the stated ABPs in the stated concentrations for the stated times followed by TAG attachment (if applicable) following general procedure **5.2.1.7**. After this period, the samples were run on SDS-PAGE following the general procedure **5.2.1.6** and fluorescent bands were observed following the general procedure **5.2.1.8**.

5.2.1.10 *In vivo* ABP labelling

L. mexicana cultures were incubated at 26 °C with the stated ABPs for the stated times in the stated concentrations. Past this time, they were lysed following the general procedure **5.2.1.5**. Subsequently, the TAG was attached via bioorthogonal click chemistry following the general procedure **5.2.1.7** and the samples

5.2.1.11 Competitive ABPP

Competitive ABPP was conducted by incubating the stated inhibitors in the stated concentrations and times followed by incubation with commercial probe TAMRA-FP (1 μM, 15-30 min) on the stated *Leishmania spp* lysates. Finally, they were run on SDS-PAGE and analysed with fluorescent imaging following the general procedures **5.2.1.6** and **5.2.1.8** respectively. Fluorescence volumes were calculated using ImageQuant and bio-rad Image Lab 6.1.0.

5.2.1.12 Affinity enrichment

Unreacted Biotin-FP probe in the probe-labelled whole-cell extracts of *Leishmania mexicana* parasites was removed by passing the soluble fractions of the extracts through 7K MWCO Zeba Spin desalting columns containing 5 mL resin (Thermo Fisher Scientific) following the manufacturer's instructions. The eluates were denatured with 0.5% SDS at 95 °C for 5 minutes, allowed to cool to room temperature and diluted with PBS to yield an SDS concentration of 0.2%. NeutrAvidin-Agarose beads (50 µL per sample), freshly washed three times with 0.1% SDS buffer (0.1% SDS in PBS), were added to each of the sample and the samples were rotated on an end-over-end rotating shaker for 1.5 h at rt. The beads were then washed 3 times with

1% SDS in PBS, 2 times with PBS and once with 25 mM TEAB buffer. Each washing was performed with 10 volumes of the washing solutions with respect to the bead volume and centrifugation of the beads between washing steps were carried out at 2,000 × *g* for 1 min at rt.

5.2.1.13 On-bead reduction, alkylation, and tryptic digestion

Thoroughly washed beads from the affinity enrichment step were resuspended in 200 µl of 25 mM TEAB buffer and treated with 10 mM TCEP (200 mM stock solution in water) for 45 min at 30 °C. The beads were washed once with 25 mM TEAB buffer and resuspended in 200 µl of 25 mM TEAB buffer and treated with 15 mM chloroacetamide (CAA; 200 mM stock solution in water) in dark for 20 min at rt. The beads were again washed with 25 mM TEAB buffer and resuspended in 200 µl of fresh 50 mM TEAB buffer and treated with 5 µg of sequencing grade modified trypsin at 37 °C for 16 h. The samples were centrifuged at 5,000 × *g* for 5 min at rt to collect the supernatant. The beads were washed with 50% (v/v) acetonitrile (ACN) containing 0.1% (v/v) formic acid (FA; 50 µL for each wash) and mixed with the previous supernatant. The collected tryptic peptides were acidified to pH 3 using FA and evaporated to dryness. The peptides were then redissolved in 0.1% (v/v) FA solution in water and subjected to desalting on Pierce C-18 Spin Columns (Thermo Scientific; CN: 89873) following manufacturer's instructions. The peptides were evaporated to complete dryness under a vacuum.

5.2.1.14 iTRAQ labelling

The dried and desalted tryptic peptides were resuspended in equal volumes (30 µL) of dissolution buffer (0.5 M TEAB buffer supplied with the iTRAQ Reagents Multiplex Kit). 70 µL of absolute ethanol was added to the iTRAQ reagent vials pre-equilibrated to rt and transferred to the respective vials of peptide digests. The labelling reactions were performed for 1.5 hours at 25 °C and quenched with 100 mM Tris-base solution (1 M stock solution). The samples labelled with the different iTRAQ channels were pooled into a fresh vial and concentrated on a speed-vac. The dried peptides were reconstituted in water with 0.1% (v/v) FA and 2% (v/v) ACN and subjected to desalting on C-18 Sep-Pak Classic cartridges (Waters; WAT051910) following manufacturer's instructions. The eluted peptides were concentrated on a speed-vac and subjected to a second round of cleaning up on HILIC TopTip (PolyLC; TT200HIL) solid-phase extraction tips following manufacturer's instructions. The eluted peptides were concentrated on a speed-vac and reconstituted in aqueous 0.1% (v/v) FA.

5.2.1.15 LC-MS/MS analysis

The iTRAQ labelled peptides were resolved on an ekspert^{TM} nanoLC 425 with Low Micro Gradient Flow module (Eksigent) using a YMC-Triart C18 column (12 nm, S-3 µm, 150 x 0.3 mm ID, 1/32"; Part number: TA12S03-15H0RU). A C-18 trap column (Trap-YMC-Triart 12 nm S-5 µm, 5 x 0.5 mm ID, 1/32"; Part number: TA12S05-E5J0RU) was connected prior to the main separating column. 5 µL of peptides were separated by mobile phase A (0.1% FA in water) and mobile phase B (0.1% FA in ACN) at a flow rate of 5 µL/min. over 87 min. The gradient used was the following, 3% B to 5% B (0 to 2 min.), 5% B to 30% B (2 to 68 min.), 30% B to 35% B (68 to 73 min.),

35% B to 80% B (73 to 75 min.), at 80% (75 to 78 min.), 80% B to 3% B (78 to 79 min.), at 3% B (79 to 87 min.). The MS analyses were performed on a TripleTOF 6600 system (Sciex) in high-resolution mode. The MS acquisition time was set from gradient time 0 to 85 min. and the MS1 spectra were collected in the mass range of 400 to 1600 m/z with 250 ms accumulation time per spectrum. Further fragmentation of each MS1 spectrum occurred with a maximum of 30 precursors per cycle and 33 ms minimum accumulation time for each precursor across the range of 100 to 1500 m/z with ion selection +2 to +5, 500 cps intensity threshold, and dynamic exclusion for 15 sec. The MS/MS spectra were acquired in high sensitivity mode.

5.2.1.16 Proteomics MS data processing

For protein identification and quantification, the .wiff files from the Sciex TripleTOF 6600 system were imported into MaxQuant (version 1.6.3.4) with integrated Andromeda database search engine. The MS/MS spectra were queried against *L. mexicana* sequences from UniProt KB. Database search employed the following parameters: Reporter ion MS2 with multiplicity 4plex, trypsin digestion with maximum 2 missed cleavages, carbamidomethylation of cysteine as fixed modification, oxidation of methionine and acetylation of protein N-termini as variable modifications, maximum number of modifications per peptide set at 5, minimum peptide length of 6, and protein FDR 0.01. Appropriate correction factors for the individual iTRAQ channels for both peptide N-terminal labelling and lysine side-chain labelling as per the iTRAQ Reagent Multiplex Kit were also configured into the database search. The proteinGroups.txt file from the MaxQuant search output was processed using Perseus software version 1.6.2.3. Potential contaminants, reverse sequences, sequences only identified by site

and endogenous biotinylated proteins were filtered off. For each identified protein, ratios of the probe-treated Reporter Intensity Corrected values to the vehicle-treated Reporter Intensity Corrected values was calculated yielding the fold change (FC).

5.2.1.17 Antipromastigote dose-response assay

Leishmania promastigote and axenic amastigote parasites were quantified using a Neubauer chamber and suspended in fresh Schneider medium to a density of 1×10^6 parasites/ml. In a 96-well plate, 1×10^5 parasites were applied per well and the parasites were incubated at 26 ºC in increasing concentrations of each compound for 44 hours. Then, 10 µL of 0.1 mg/mL Resazurin solution (Fisher Scientific, Leicestershire, UK) were added per well and the plate was incubated for 4 hours at 26 ºC. Fluorescence was excited at 555 nm and read at 585 nm using a plate reader and EC_{50} values were obtained by GraphPad Prism 9, after determination of sigmoidal regression curves. At least three independent experiments were performed for each molecule with all samples in triplicates. Clemastine was used as positive control.

6 References

1. Herwaldt, B. L. Leishmaniasis. *The Lancet* **354**, 1191–1199 (1999).
2. Desjeux, P. Leishmaniasis: Public health aspects and control. *Clin Dermatol* **14**, 417–423 (1996).
3. Ashford, R. W. The leishmaniases as model zoonoses. *Annals of Tropical Medicine and Parasitology* vol. 91 693–701 Preprint at https://doi.org/10.1080/00034989760428 (1997).
4. Arenas, R., Torres-Guerrero, E., Quintanilla-Cedillo, M. R. & Ruiz-Esmenjaud, J. Leishmaniasis: A review. *F1000Research* vol. 6 Preprint at https://doi.org/10.12688/f1000research.11120.1 (2017).
5. Reithinger, R. *et al.* Cutaneous leishmaniasis. *Lancet Infect Dis* **7**, 581–596 (2007).
6. Kashif, M., Manna, P. P., Akhter, Y., Alaidarous, M. & Rub, A. Screening of Novel Inhibitors Against Leishmania donovani Calcium ion Channel to Fight Leishmaniasis. *Infect Disord Drug Targets* **17**, 120–129 (2017).
7. Díaz-Sáez, V. *et al.* High rates of Leishmania infantum and Trypanosoma nabiasi infection in wild rabbits (Oryctolagus cuniculus) in sympatric and syntrophic conditions in an endemic canine leishmaniasis area: Epidemiological consequences. *Vet Parasitol* **202**, 119–127 (2014).
8. Marcondes, M. & Day, M. J. Current status and management of canine leishmaniasis in Latin America. *Res Vet Sci* **123**, 261–272 (2019).
9. Burza, S., Croft, S. L. & Boelaert, M. Leishmaniasis. *The Lancet* **392**, 951–970 (2018).
10. Colmenares, M., Kar, S., Goldsmith-Pestana, K. & McMahon-Pratt, D. Mechanisms of pathogenesis: Differences amongst Leishmania species. *Trans R Soc Trop Med Hyg* vol. 96 S3–S7 Preprint at https://doi.org/10.1016/s0035-9203(02)90044-1 (2002).
11. Garza-Tovar, T. F., Sacriste-Hernández, M. I., Juárez-Durán, E. R. & Arenas, R. An overview of the treatment of cutaneous leishmaniasis. *Fac Rev* **9**, (2020).
12. PAHO - Pan American Health Organization.
13. Karimi, A., Alborzi, A. & Amanati, A. Visceral Leishmaniasis: An Update and Literature Review. *Arch Pediatr Infect Dis* **4**, e31612 (2016).
14. Rao Geddaid, M. *et al.* Post kala-azar dermal leishmaniasis: A threat to elimination program. **14**, e0008221 (2020).
15. Pires, M., Wright, B., Kaye, P. M., da Conceição, V. & Churchill, R. C. The impact of leishmaniasis on mental health and psychosocial well-being: A systematic review. *PLoS One* vol. 14 e0223313 Preprint at https://doi.org/10.1371/journal.pone.0223313 (2019).
16. Hay, S. I. *et al.* Global, regional, and national disability-adjusted life-years (DALYs) for 333 diseases and injuries and healthy life expectancy (HALE) for 195 countries and

territories, 1990-2016: A systematic analysis for the Global Burden of Disease Study 2016. *The Lancet* **390**, 1260–1344 (2017).

17. WHO, World Health Organization. https://www.who.int/.

18. Bravo, F. & Sanchez, M. R. New and re-emerging cutaneous infectious diseases in Latin America and other geographic areas. *Dermatologic Clinics* vol. 21 655–668 Preprint at https://doi.org/10.1016/S0733-8635(03)00090-1 (2003).

19. Oryan, A. & Akbari, M. Worldwide risk factors in leishmaniasis. *Asian Pacific Journal of Tropical Medicine* vol. 9 925–932 Preprint at https://doi.org/10.1016/j.apjtm.2016.06.021 (2016).

20. Pavli, A. & Maltezou, H. C. Leishmaniasis, an emerging infection in travelers. *Int. J. Infect. Dis.* vol. 14 e1032–e1039 Preprint at https://doi.org/10.1016/j.ijid.2010.06.019 (2010).

21. Wall, E. C., Watson, J., Armstrong, M., Chiodini, P. L. & Lockwood, D. N. Short report: Epidemiology of imported cutaneous leishmaniasis at the hospital for tropical diseases, London, United Kingdom: Use of polymerase chain reaction to identify the species. *American Journal of Tropical Medicine and Hygiene* **86**, 115–8 (2012).

22. Young, J. & Kima, P. E. *The Leishmania Parasitophorous Vacuole Membrane at the Parasite-Host Interface*. *YALE JOURNAL OF BIOLOGY AND MEDICINE* vol. 92 (2019).

23. CDC, Centre for Disease Control and Preventions. https://www.cdc.gov/.

24. Medley, G. F., Hollingsworth, T. D., Olliaro, P. L. & Adams, E. R. Health-seeking behaviour, diagnostics and transmission dynamics in the control of visceral leishmaniasis in the Indian subcontinent. *Nature* **528**, S102-8 (2015).

25. Ghorbani, M. & Farhoudi, R. Leishmaniasis in humans: drug or vaccine therapy? *Drug Des Devel Ther* **Volume 12**, 25–40 (2017).

26. Ponte-Sucre, A. *et al.* Drug resistance and treatment failure in leishmaniasis: A 21st century challenge. *PLOS Negl. Trop. Dis.* vol. 11 e0006052 Preprint at https://doi.org/10.1371/journal.pntd.0006052 (2017).

27. Croft, S. L. & Olliaro, P. Leishmaniasis chemotherapy-challenges and opportunities. *Clinical Microbiology and Infection* vol. 17 1478–1483 Preprint at https://doi.org/10.1111/j.1469-0691.2011.03630.x (2011).

28. Frézard, F., Demicheli, C. & Ribeiro, R. R. molecules Pentavalent Antimonials: New Perspectives for Old Drugs. *Molecules* **14**, 2317–2336 (2009).

29. Asilian, A., Sadeghinia, A., Faghihi, G. & Momeni, A. Comparative study of the efficacy of combined cryotherapy and intralesional meglumine antimoniate (Glucantime®) vs. cryotherapy and intralesional meglumine antimoniate (Glucantime®) alone for the treatment of cutaneous leishmaniasis. *Int. J. Dermatol.* **43**, 281–283 (2004).

30. el Darouti, M. A. & al Rubaie, S. M. Cutaneous Leishmaniasis: Treatment with Combined Cryotherapy and Intralesional Stibogluconate Injection. *Int. J. Dermatol.* **29**, 56–59 (1990).

31. Salmanpour, R., Razmavar, M. R. & Abtahi, N. Comparison of intralesional meglumine antimoniate, cryotherapy and their combination in the treatment of cutaneous leishmaniasis [5]. *Int. J. Dermatol.* vol. 45 1115–1116 Preprint at https://doi.org/10.1111/j.1365-4632.2006.02822.x (2006).

32. Minodier, P. & Parola, P. Cutaneous leishmaniasis treatment. *Travel Med Infect Dis* **5**, 150–158 (2007).

33. Kumar Saha, A., Mukherjee, T. & Bhaduri, A. Mechanism of action of amphotericin B on Leishmania donovani promastigotes. *Mol. Biochem. Parasitol.* **19**, 195–200 (1986).

34. Stone, N. R. H. *et al.* Liposomal Amphotericin B (AmBisome Ò): A Review of the Pharmacokinetics, Pharmacodynamics, Clinical Experience and Future Directions. **76**, 485–500 (2016).

35. Pinto-Martinez, A. K., Rodriguez-Durán, J., Serrano-Martin, X., Hernandez-Rodriguez, V. & Benaim, G. Mechanism of Action of Miltefosine on Leishmania donovani Involves the Impairment of Acidocalcisome Function and the Activation of the Sphingosine-Dependent Plasma Membrane Ca $^{2+}$ Channel. *Antimicrob Agents Chemother* **62**, e01614-17 (2018).

36. Sundar, S. *et al.* Efficacy of miltefosine in the treatment of visceral leishmaniasis in India after a decade of use. *Clinical Infectious Diseases* **55**, 543–550 (2012).

37. Rijal, S. *et al.* Increasing failure of miltefosine in the treatment of kala-azar in nepal and the potential role of parasite drug resistance, reinfection, or noncompliance. *Clinical Infectious Diseases* **56**, 1530–1538 (2013).

38. Wiwanitkit, V. Interest in paromomycin for the treatment of visceral leishmaniasis (kala-azar). *Ther Clin Risk Manag* **8**, 323–328 (2012).

39. Banerjee, A., De, M. & Ali, N. Combination Therapy with Paromomycin-Associated Stearylamine-Bearing Liposomes Cures Experimental Visceral Leishmaniasis through Th1-Biased Immunomodulation. *Antimicrob Agents Chemother* **55**, 1661–1670 (2011).

40. Terstappen, G. C., Schlüpen, C., Raggiaschi, R. & Gaviraghi, G. Target deconvolution strategies in drug discovery. *Nat. Rev. Drug Discov.* vol. 6 891–903 Preprint at https://doi.org/10.1038/nrd2410 (2007).

41. Kubota, K., Funabashi, M. & Ogura, Y. Target deconvolution from phenotype-based drug discovery by using chemical proteomics approaches. *Biochimica et Biophysica Acta (BBA) - Proteins and Proteomics* **1867**, 22–27 (2019).

42. Croston, G. E. The utility of target-based discovery. *Expert Opin Drug Discov* **12**, 427–429 (2017).

43. Peña, I. *et al.* New compound sets identified from high throughput phenotypic screening against three kinetoplastid parasites: An open resource. *Sci Rep* **5**, 8771 (2015).

44. Lindsay, M. A. Target discovery. *Nat. Rev. Drug Discov.* **2**, 831–838 (2003).

45. Sieber, S. A. , A.-B. P. Profiling. 2012. *Activity-Based Protein Profiling*. vol. 324 (Springer Berlin Heidelberg, 2012).

46. Hanahan, D. & Weinberg, R. A. The hallmarks of cancer. *Cell* vol. 100 57–70 Preprint at https://doi.org/10.1016/S0092-8674(00)81683-9 (2000).

47. Vogelstein, B. & Kinzler, K. W. Cancer genes and the pathways they control. *Nature Medicine* vol. 10 789–799 Preprint at https://doi.org/10.1038/nm1087 (2004).

48. Kobe, B. & Kemp, B. E. Active site-directed protein regulation. *Nature* **402**, 373–376 (1999).

49. Gygi, S. P. *et al.* Quantitative analysis of complex protein mixtures using isotope-coded affinity tags. *Nat Biotechnol.* **17**, 994–999 (1999).

50. Washburn, M. P., Wolters, D. & Yates, J. R. Large-scale analysis of the yeast proteome by multidimensional protein identification technology. *Nat Biotechnol.* **19**, 241–247 (2001).

51. Ito, T. *et al.* Roles for the two-hybrid system in exploration of the yeast protein interactome. *Mol. Cell Proteomics* vol. 1 561–566 Preprint at https://doi.org/10.1074/mcp.R200005-MCP200 (2002).

52. Macbeath, G. Protein microarrays and proteomics. *Nat. Genet.* vol. 32 526–532 Preprint at https://doi.org/10.1038/ng1037 (2002).

53. Barglow, K. T. & Cravatt, B. F. Activity-based protein profiling for the functional annotation of enzymes. *Nat Methods* **4**, 822–827 (2007).

54. Böttcher, T., Pitscheider, M. & Sieber, S. A. Natural products and their biological targets: Proteomic and metabolomic labeling strategies. *Angew Chem Int Ed Engl* vol. 49 2680–2698 Preprint at https://doi.org/10.1002/anie.200905352 (2010).

55. Cravatt, B. F., Wright, A. T. & Kozarich, J. W. Activity-based protein profiling: From enzyme chemistry to proteomic chemistry. *Annu Rev Biochem* vol. 77 383–414 Preprint at https://doi.org/10.1146/annurev.biochem.75.101304.124125 (2008).

56. Evans, M. J. & Cravatt, B. F. Mechanism-based profiling of enzyme families. *Chem. Rev* vol. 106 3279–3301 Preprint at https://doi.org/10.1021/cr050288g (2006).

57. Heal, W. P., Dang, T. H. T. & Tate, E. W. Activity-based probes: Discovering new biology and new drug targets. *Chem. Soc. Rev.* **40**, 246–257 (2011).

58. Chen, B., Ge, S. S., Zhao, Y. C., Chen, C. & Yang, S. Activity-based protein profiling: an efficient approach to study serine hydrolases and their inhibitors in mammals and microbes. *RSC Adv* vol. 6 113327–113343 Preprint at https://doi.org/10.1039/C6RA20006K (2016).

59. Dennehy, M. K., Richards, K. A. M., Wernke, G. R., Shyr, Y. & Liebler, D. C. Cytosolic and nuclear protein targets of thiol-reactive electrophiles. *Chemical Res Toxicol* **19**, 20–29 (2006).

60. Scaloni, A. *et al.* Probing the reactivity of nucleophile residues in human 2,3-diphosphoglycerate/deoxy-hemoglobin complex by aspecific chemical modifications. *FEBS Lett* **452**, 190–195 (1999).

61. Slaughter, D. E. & Hanzlik, R. P. Identification of Epoxide- and Quinone-Derived Bromobenzene Adducts to Protein Sulfur Nucleophiles. *Chem. Res. Toxicol.* **4**, 349–359 (1991).

62. Narayanan, A. & Jones, L. H. Sulfonyl fluorides as privileged warheads in chemical biology. *Chem Sci* vol. 6 2650–2659 Preprint at https://doi.org/10.1039/c5sc00408j (2015).

63. Liu, Y., Patricelli, M. P. & Cravatt, B. F. Activity-based protein profiling: The serine hydrolases. *Proc. Natl. Acad. Sci. U.S.A.* **96**, 14694–14699 (1999).

64. Kidd, D., Liu, Y. & Cravatt, B. F. Profiling serine hydrolase activities in complex proteomes. *Biochem.* **40**, 4005–4015 (2001).

65. Kolb, R., Bach, N. C. & Sieber, S. A. β-Sultams exhibit discrete binding preferences for diverse bacterial enzymes with nucleophilic residues. *Chem Commun* **50**, 427–429 (2014).

66. Fonovic, M. & Bogyo, M. Activity Based Probes for Proteases: Applications to Biomarker Discovery,Molecular Imaging and Drug Screening. *Curr Pharm Design* **13**, 253–261 (2006).

67. Meldal, M. & Tomøe, C. W. Cu-catalyzed azide - Alkyne cycloaddition. *Chem. Rev.* vol. 108 2952–3015 Preprint at https://doi.org/10.1021/cr0783479 (2008).

68. Rostovtsev, V. v., Green, L. G., Fokin, V. v. & Sharpless, K. B. A stepwise huisgen cycloaddition process: Copper(I)-catalyzed regioselective 'ligation' of azides and terminal alkynes. *Angew Chem Int Ed* **41**, 2596–2599 (2002).

69. Speers, A. E., Adam, G. C. & Cravatt, B. F. Activity-based protein profiling in vivo using a copper(I)-catalyzed azide-alkyne [3 + 2] cycloaddition. *J. Am. Chem. Soc.* **125**, 4686–4687 (2003).

70. Köhn, M. & Breinbauer, R. The Staudinger ligation - A gift to chemical biology. *Angew Chem Int Ed* vol. 43 3106–3116 Preprint at https://doi.org/10.1002/anie.200401744 (2004).

71. Saxon, E. & Bertozzi, C. R. Cell surface engineering by a modified Staudinger reaction. *Science (1979)* **287**, 2007–2010 (2000).

72. Liu, S. *et al.* Aryl vinyl sulfonates and sulfones as active site-directed and mechanism-based probes for protein tyrosine phosphatases. *J. Am. Chem. Soc.* **130**, 8251–8260 (2008).

73. Adam, G. C., Sorensen, E. J. & Cravatt, B. F. Proteomic profiling of mechanistically distinct enzyme classes using a common chemotype. *Nat Biotechnol.* **20**, 805–809 (2002).

74. Corthals, C. L., Wasinger, V. C., Hochstrasser, D. F. & Sanchez, J. C. The dynamic range of protein expression: A challenge for proteomic research. *Electrophoresis* vol. 21 1104–1115 Preprint at https://doi.org/10.1002/(SICI)1522-2683(20000401)21:6<1104::AID-ELPS1104>3.0.CO;2-C (2000).

75. Santoni, V., Molloy, M. & Rabilloud, T. Membrane proteins and proteomics: Un amour impossible? *Electrophoresis* vol. 21 1054–1070 Preprint at https://doi.org/10.1002/(SICI)1522-2683(20000401)21:6<1054::AID-ELPS1054>3.0.CO;2-8 (2000).

76. Jessani, N. *et al.* A streamlined platform for high-content functional proteomics of primary human specimens. *Nat Methods* **2**, 691–697 (2005).

77. Adam, G. C., Burbaum, J., Kozarich, J. W., Patricelli, M. P. & Cravatt, B. F. Mapping Enzyme Active Sites in Complex Proteomes. *J. Am. Chem. Soc.* **126**, 1363–1368 (2004).

78. Okerberg, E. S. *et al.* High-resolution functional proteomics by active-site peptide profiling. *Proc. Natl. Acad. Sci. U.S.A.* **102**, 4996–5001 (2005).

79. Oda, Y., Huang, K., Cross, F. R., Cowburn, D. & Chait, B. T. Accurate quantitation of protein expression and site-specific phosphorylation. *Proc. Natl. Acad. Sci. U.S.A.* **96**, 6591–6596 (1999).

80. Chen, X., Wei, S., Ji, Y., Guo, X. & Yang, F. Quantitative proteomics using SILAC: Principles, applications, and developments. *Proteomics* **15**, 3175–3192 (2015).

81. Ong, S.-E. *et al.* Stable Isotope Labeling by Amino Acids in Cell Culture, SILAC, as a Simple and Accurate Approach to Expression Proteomics. *Mol. Cell Proteomics* **1**, 376–386 (2002).

82. Unwin, R. D. Quantification of proteins by iTRAQ. *Methods mol. biol.* **658**, 205–215 (2010).

83. Wiese, S., Reidegeld, K. A., Meyer, H. E. & Warscheid, B. Protein labeling by iTRAQ: A new tool for quantitative mass spectrometry in proteome research. *Proteomics* **7**, 340–350 (2007).

84. Alves, C. R. *et al.* Understanding serine proteases implications on Leishmania spp lifecycle. *Exp. Parasitol.* vol. 184 67–81 Preprint at https://doi.org/10.1016/j.exppara.2017.11.008 (2018).

85. Powers, J. C., Asgian, J. L., Ekici, Ö. D. & James, K. E. Irreversible inhibitors of serine, cysteine, and threonine proteases. *Chem. Rev.* **102**, 4639–4750 (2002).

86. Black, R. CHAPTER 1. Development, Historical Use and Properties of Chemical Warfare Agents. in *Chemical Warfare Toxicology* vol. 1 1–28 (2016).

87. Bouma, B. N., Miles, L. A., Beretta, G. & Griffin, J. H. Human Plasma Prekallikrein. Studies of Its Activation by Activated Factor XII and of Its Inactivation by Diisopropyl Phosphofluoridate. *Biochem.* **19**, 1151–1160 (1980).

88. Mahrus, S. & Craik, C. S. Selective chemical functional probes of granzymes A and B reveal granzyme B is a major effector of natural killer cell-mediated lysis of target cells. *Chem Biol.* **12**, 567–77 (2005).

89. Faucher, F., Bennett, J. M., Bogyo, M. & Lovell, S. Strategies for Tuning the Selectivity of Chemical Probes that Target Serine Hydrolases. *Cell Chem Biol.* vol. 27 937–952 Preprint at https://doi.org/10.1016/j.chembiol.2020.07.008 (2020).

90. Simon, G. M. & Cravatt, B. F. Activity-based proteomics of enzyme superfamilies: Serine hydrolases as a case study. *J Biol Chem.* vol. 285 11051–11055 Preprint at https://doi.org/10.1074/jbc.R109.097600 (2010).

91. Dolui, A. K., Vijayakumar, A. K., Rajasekharan, R. & Vijayaraj, P. Activity-based protein profiling of rice (Oryza sativa L.) bran serine hydrolases. *Sci Rep* **10**, 15191 (2020).

92. Elahi, R. *et al.* Functional annotation of serine hydrolases in the asexual erythrocytic stage of Plasmodium falciparum. *Sci Rep.* **9**, 17532 (2019).

93. Wright, M. H. *et al.* Global Analysis of Protein N-Myristoylation and Exploration of N-Myristoyltransferase as a Drug Target in the Neglected Human Pathogen Leishmania donovani. *Chem Biol.* **22**, 342–354 (2015).

94. Damianouid, A. *et al.* Essential roles for deubiquitination in Leishmania life cycle progression. *PLoS Pathog.* **16**, e1008455 (2020).

95. Escrivani, D. O. *et al.* Chalcones identify cTXNPx as a potential antileishmanial drug target. *PLOS Negl. Trop. Dis.* **15**, e0009951 (2021).

96. Baggelaar, M. P. *et al.* Chemical Proteomics Maps Brain Region Specific Activity of Endocannabinoid Hydrolases. *ACS Chem. Biol.* **12**, 852–861 (2017).

97. Wheeler, R. J., Gluenz, E. & Gull, K. The cell cycle of Leishmania: Morphogenetic events and their implications for parasite biology. *Mol. Microbiol.* **79**, 647–662 (2011).

98. Gossage, S. M., Rogers, M. E. & Bates, P. A. Two separate growth phases during the development of Leishmania in sand flies: Implications for understanding the life cycle. *Int. J. Parasitol.* **33**, 1027–1034 (2003).

99. Bates, P. A. Complete developmental cycle of Leishmania mexicana in axenic culture. *Parasitology* **108**, 1–9 (1994).

100. Veras, P. S. T. & de Menezes, J. P. B. Using proteomics to understand how Leishmania parasites survive inside the host and establish infection. *Int. J. Mol. Sci.* vol. 17 1270 Preprint at https://doi.org/10.3390/ijms17081270 (2016).

101. Dias-Lopes, G. *et al.* Axenic amastigotes of Leishmania species as a suitable model for in vitro studies. *Acta Trop.* vol. 220 105956 Preprint at https://doi.org/10.1016/j.actatropica.2021.105956 (2021).

102. Pescher, P., Blisnick, T., Bastin, P. & Späth, G. F. Quantitative proteome profiling informs on phenotypic traits that adapt Leishmania donovani for axenic and intracellular proliferation. *Cell. Microbiol.* **13**, 978–991 (2011).

103. RIPA Lysis and Extraction Buffer. Preprint at https://www.thermofisher.com/order/catalog/product/89901.

104. Pierce™ IP Lysis Buffer Manufacturer's Instructions. Preprint at https://www.thermofisher.com/order/catalog/product/87787.

105. Polgár, L. The prolyl oligopeptidase family. *Cell. Mol. Life Sci.* vol. 59 349–362 Preprint at https://doi.org/10.1007/s00018-002-8427-5 (2002).

106. Männistö, P. T. & García-Horsman, J. A. Mechanism of action of Prolyl oligopeptidase (PREP) in degenerative brain diseases: Has peptidase activity only a modulatory role on the interactions of PREP with proteins? *Front. Aging Neurosci.* **9**, (2017).

107. Lasse, C. *et al.* Prolyl Oligopeptidase From Leishmania infantum: Biochemical Characterization and Involvement in Macrophage Infection. *Front. Microbiol.* **11**, 1060 (2020).

108. Bastos, I. M. D. *et al.* Molecular, functional and structural properties of the prolyl oligopeptidase of Trypanosoma cruzi (POP Tc80), which is required for parasite entry into mammalian cells. *Biochem. J.* **388**, 29–38 (2005).

109. Parussini, F. *et al.* Characterization of a lysosomal serine carboxypeptidase from Trypanosoma cruzi. *Mol. Biochem. Parasitol.* **131**, 11–23 (2003).

110. Monic, S. *et al.* A novel lipase with dual localisation in Trypanosoma brucei. *Sci. Rep.* **12**, 4766 (2022).

111. Wang, S. *et al.* Advanced activity-based protein profiling application strategies for drug development. *Front. pharmacol* vol. 9 353 Preprint at https://doi.org/10.3389/fphar.2018.00353 (2018).

112. Wilk, S. & Orlowski, M. Inhibition of Rabbit Brain Prolyl Endopeptidase by N-Benzyloxycarbonyl-Prolyl-Prolinal, a Transition State Aldehyde Inhibitor. *J. Neurochem.* **41**, 69–75 (1983).

113. Mina, J. G. M. *et al.* Antileishmanial Chemotherapy through Clemastine Fumarate Mediated Inhibition of the Leishmania Inositol Phosphorylceramide Synthase. *ACS Infect. Dis.* **7**, 47–63 (2021).

114. Jóźwiak, J., Komar, A., Jankowska, E. & Martirosian, G. Determination of the cytotoxic effect of Clostridium histolyticum culture supernatant on HeLa cells in the presence of protease inhibitors. *FEMS Immunol. Med. Microbiol.* **45**, 137–142 (2005).

115. Coelho, A. C., Trinconi, C. T., Costa, C. H. N. & Uliana, S. R. B. In Vitro and In Vivo Miltefosine Susceptibility of a Leishmania amazonensis Isolate from a Patient with Diffuse Cutaneous Leishmaniasis. *PLOS Negl. Trop. Dis.* **8**, e2999 (2014).

116. Mandal, G. *et al.* Species-Specific Antimonial Sensitivity in Leishmania Is Driven by Post-Transcriptional Regulation of AQP1. *PLOS Negl. Trop. Dis.* **9**, e0003500 (2015).

117. Speers, A. E. & Cravatt, B. F. Profiling enzyme activities in vivo using click chemistry methods. *Chem. Biol.* **11**, 535–546 (2004).

118. Syam Prasad, G., Manjunath, M., Kishore Kumar Reddy, K. R., Sarathi Reddy, O. V. & Suresh Reddy, C. Synthesis and antibacterial activity of new aryl / alkyl phosphonates via Michaelis-Arbuzov rearrangement. *Arkivoc* **2006**, 128–235 (2006).

119. Kalek, M. & Stawinski, J. Pd(0)-catalyzed phosphorus-carbon bond formation. Mechanistic and synthetic studies on the role of the palladium sources and anionic additives. *Organometallics* **26**, 5840–5847 (2007).

120. Gooßen, L. J. & Dezfuli, M. K. Practical protocol for the palladium-catalyzed synthesis of arylphosphonates from bromoarenes and diethyl phosphite. *Synlett* **3**, 445–448 (2005).

121. Thompson, A. L. S., Kabalka, G. W., Akula, M. R. & Huffman, J. W. The conversion of phenols to the corresponding aryl halides under mild conditions. *Synth* **4**, 547–550 (2005).

122. Ishikawa, S. & Manabe, K. Repetitive two-step method for oligoarene synthesis through rapid cross-coupling of hydroxyphenylboronic acids and anhydrides. *Chem. Lett.* **35**, 164–165 (2006).

123. Banday, A. H., Shameem, S. A., Gupta, B. D. & Kumar, H. M. S. D-ring substituted 1,2,3-triazolyl 20-keto pregnenanes as potential anticancer agents: Synthesis and biological evaluation. *Steroids* **75**, 801–804 (2010).

124. Sharma, S. & Oehlschlager, A. C. Scope and Mechanism of Stannylalumination of 1-Alkynes. *J.Org. Chem.* **54**, 5064–5073 (1989).

125. Baughman, T. W., Sworen, J. C. & Wagener, K. B. The facile preparation of alkenyl metathesis synthons. *Tetrahedron* **60**, 10943–10948 (2004).

126. Davison, E. C. *et al.* Nitrone dipolar cycloaddition routes to piperidines and indolizidines. *J. Chem. Soc., Perkin trans.* **2**, 1494–1514 (2002).

127. Cerutti, E., Damont, A., Dollé, F., Baroni, S. & Aime, S. Synthesis and characterization of an MRI Gd-based probe designed to target the translocator protein. *Magnetic Resonance in Chemistry* **51**, (2013).

128. Ha, Y. G. *et al.* Solution-deposited organic - Inorganic hybrid multilayer gate dielectrics. Design, synthesis, microstructures, and electrical properties with thin-film transistors. *J. Am. Chem. Soc.* **133**, 10239–10250 (2011).

129. Nieto, C. T., Salgado, M. M., Domínguez, S. H., Díez, D. & Garrido, N. M. Rapid access with diversity to enantiopure flexible PNA monomers following asymmetric orthogonal strategies. *Tetrahedron Asymmetry* **25**, 1046–1060 (2014).

130. Zradni, F. Z., Hamelin, J. & Derdour, A. Synthesis of amides from esters and amines under microwave irradiation. *Synth. Commun.* **32**, 3525–3531 (2002).

131. Seo, J. *et al.* Synthesis of phosphaisocoumarins through rhodium-catalyzed cyclization using alkynes and arylphosphonic acid monoesters. *Org. Lett.* **15**, 3358–3361 (2013).

132. Haggam, R., Conrad, J. & Beifuss, U. Practical and reliable synthesis of dialkyl N-arylphosphoramidates with nitroarenes as substrates. *Tetrahedron Lett.* **50**, 6227–6630 (2009).

133. Yang, Y. & Verhelst, S. H. L. Cleavable trifunctional biotin reagents for protein labelling, capture and release. *ChemComm.* **49**, 5366–5368 (2013).

134. Vurgun, N., Gõmez-Biagi, R. F. & Nitz, M. Access to Versatile β-Cyclodextrin Scaffolds through Guest-Mediated Monoacylation. *Chem. Eur. J.* **22**, 1062–1069 (2016).

135. Buller, J., Laschewsky, A., Lutz, J. F. & Wischerhoff, E. Tuning the lower critical solution temperature of thermoresponsive polymers by biospecific recognition. *Polym. Chem.* **2**, 1486–1489 (2011).

136. Marchand-Brynaert, J., Bouchet, M., Touillaux, R., Beauve, C. & Fastrez, J. Design and synthesis of a bifunctional label for selection of β-lactamase displayed on filamentous bacteriophage by catalytic activity. *Tetrahedron* **52**, 5591–5606 (1996).

137. Brauch, S. *et al.* Fast and efficient MCR-based synthesis of clickable rhodamine tags for protein profiling. *Org. Biomol. Chem.* **10**, 958–965 (2012).

138. Shamshurin, D., Krokhin, O. v., Levin, D., Sparling, R. & Wilkins, J. A. In situ activity-based protein profiling of serine hydrolases in E. coli. *EuPA Open Proteom.* **4**, 18–24 (2014).

139. Gráf, L. A., Szilágyi, L. A. & Venekei, I. A. *Chymotrypsin*. *Handbook of Proteolytic Enzymes* vol. 3 (Academic Press, 2013).

140. Saenger, W. Proteinase K. *Handbook of Proteolytic Enzymes* **3**, 3240–3242 (2013).

141. Suttapitugsakul, S., Xiao, H., Smeekens, J. & Wu, R. Evaluation and optimization of reduction and alkylation methods to maximize peptide identification with MS-based proteomics. *Mol. Biosyst.* **13**, 2443–2732 (2017).

142. Lukesh, J. C., Palte, M. J. & Raines, R. T. A potent, versatile disulfide-reducing agent from aspartic acid. *J. Am. Chem. Soc.* **134**, 4057–4059 (2012).

143. Zweerink, S. *et al.* Activity-based protein profiling as a robust method for enzyme identification and screening in extremophilic Archaea. *Nat. Commun* **8**, 15352 (2017).

144. Brobey, R. K. B., Mei, F. C., Cheng, X. & Soong, L. Comparative Two-Dimensional Gel Electrophoresis Maps for Promastigotes of Leishmania amazonensis and Leishmania major. *Braz J Infect Dis* **10**, 1–6 (2006).

145. Salloum, T., Tokajian, S. & Hirt, R. P. Advances in Understanding Leishmania Pathobiology: What Does RNA-Seq Tell Us? *Front. Cell Dev. Biol.* **9**, 702240 (2021).

146. Silva-Almeida, M., Pereira, B. A. S., Ribeiro-Guimarães, M. L. & Alves, C. R. Proteinases as virulence factors in Leishmania spp. infection in mammals. *Parasit Vectors.* **5**, 1–10 (2012).

147. Gómez, M. A. & Olivier, M. Proteases and phosphatases during Leishmania-macrophage interaction: paving the road for pathogenesis. *Virulence* **1**, 314–318 (2010).

148. Motta, F. N. *et al.* Oligopeptidase B, a missing enzyme in mammals and a potential drug target for trypanosomatid diseases. *Biochimie* **167**, 207–216 (2019).

149. Adibekian, A. *et al. Characterization of a Selective, Reversible Inhibitor of Lysophospholipase 1 (LYPLA1)*. (2010).

150. Beneke, T. *et al.* A CRISPR Cas9 high-throughput genome editing toolkit for kinetoplastids. *Royal Soc. Open Sci.* **4**, e170095 (2017).

151. Davison, D., Howell, S., Snijders, A. P. & Deu, E. Activity-based protein profiling of human and plasmodium serine hydrolases and interrogation of potential antimalarial targets. *iScience* **25**, 104996 (2022).

152. Ghasemzadeh, M. S. & Akhlaghinia, B. C-P bond construction catalyzed by Ni II immobilized on aminated Fe3O4@TiO2 yolk-shell NPs functionalized by (3-

glycidyloxypropyl)trimethoxysilane (Fe3O4@TiO2 YS-GLYMO-UNNiII) in green media. *New J. Chem.* **43**, 5341–5356 (2019).

153. Hong, M. C. *et al.* Synthesis and evaluation of stilbene derivatives as a potential imaging agent of amyloid plaques. *Bioorg. Med. Chem.* **18**, 7724–7730 (2010).

154. Kohler, M. C., Sokol, J. G. & Stockland, R. A. Development of a room temperature Hirao reaction. *Tetrahedron Lett.* **50**, 457–459 (2009).

155. Bergkamp, J. J. *et al.* Synthesis and characterization of silicon phthalocyanines bearing axial phenoxyl groups for attachment to semiconducting metal oxides. *J Porphyr Phthalocyanines* **15**, 943–950 (2011).

156. Villemin, E., Herent, M.-F. & Marchand-Brynaert, J. Functionalized Phosphonated Half-Cage Molecules as Ligands for Metal Complexes. *Eur. J. Org. Chem.* **2012**, 6165–6178 (2012).

157. Fisher, B. F. & Gellman, S. H. Impact of γ-Amino Acid Residue Preorganization on α/γ-Peptide Foldamer Helicity in Aqueous Solution. *J. Am. Chem. Soc.* **138**, 10766–10769 (2016).

158. Suzuki, I., Kiyokawa, K., Yasuda, M. & Baba, A. Indium(III) halide-catalyzed UV-irradiated radical coupling of iodomethylphosphorus compounds with various organostannanes. *Org. Lett.* **15**, 1728–1731 (2013).

159. Anthony, N. G. *et al.* Antimicrobial lexitropsins containing amide, amidine, and alkene linking groups. *J. Med. Chem.* **50**, 6116–6125 (2007).

160. Eirich, J., Orth, R. & Sieber, S. A. Unraveling the protein targets of vancomycin in living S. aureus and E. faecalis cells. *J. Am. Chem. Soc.* **133**, 12144–12153 (2011).

161. Tappertzhofen, K. *et al.* Bioreducible Poly- l -Lysine-Poly[HPMA] Block Copolymers Obtained by RAFT-Polymerization as Efficient Polyplex-Transfection Reagents. *Macromol. Biosci.* **16**, 106–120 (2016).

All the proteomics figures in this project were Created with BioRender.com

Appendix

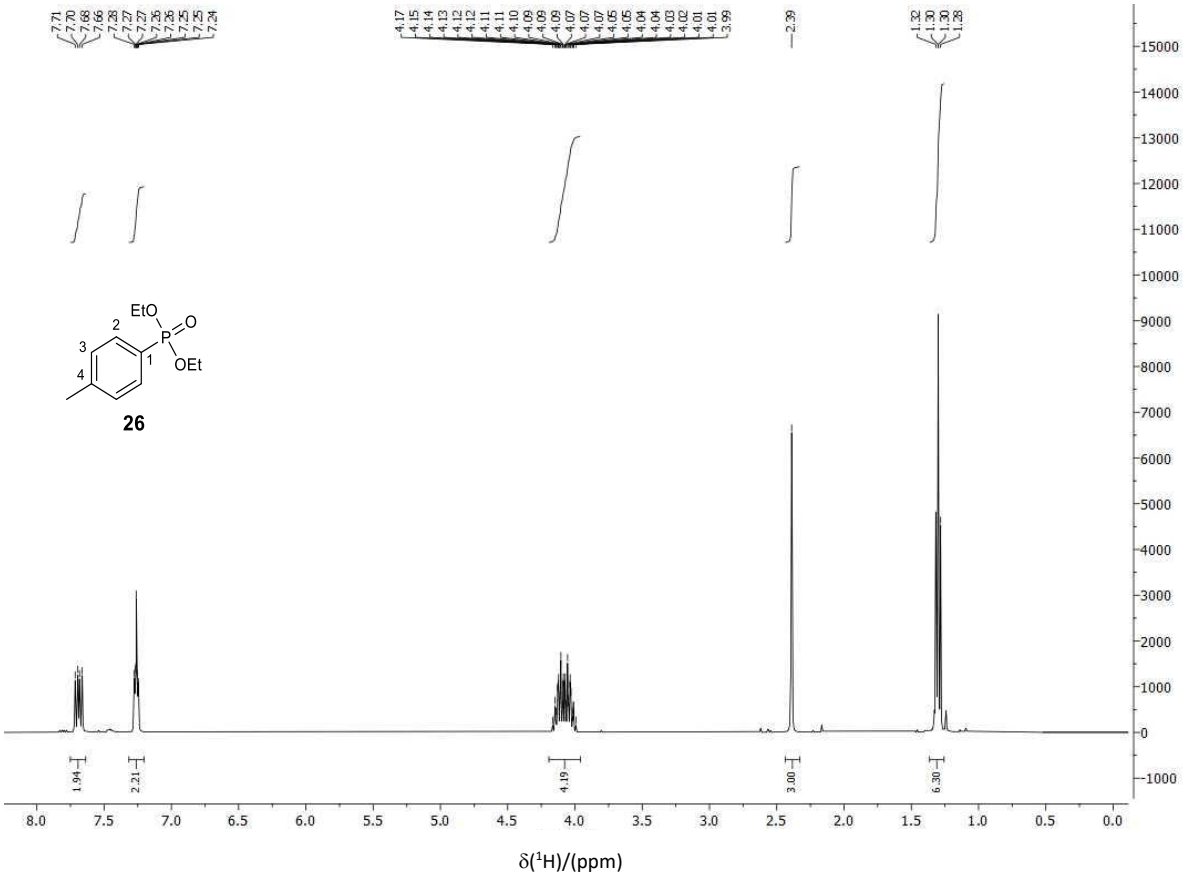
7.71
7.70
7.68
7.66
7.28
7.27
7.27
7.26
7.25
7.25
7.24
4.17
4.15
4.14
4.13
4.12
4.12
4.11
4.11
4.10
4.09
4.09
4.08
4.07
4.07
4.07
4.05
4.05
4.04
4.04
4.03
4.02
4.01
4.01
3.99
2.39
1.32
1.30
1.30
1.28
EtO
OEt
26
1.94
2.21
4.19
3.00
6.30
δ(1H)/(ppm)

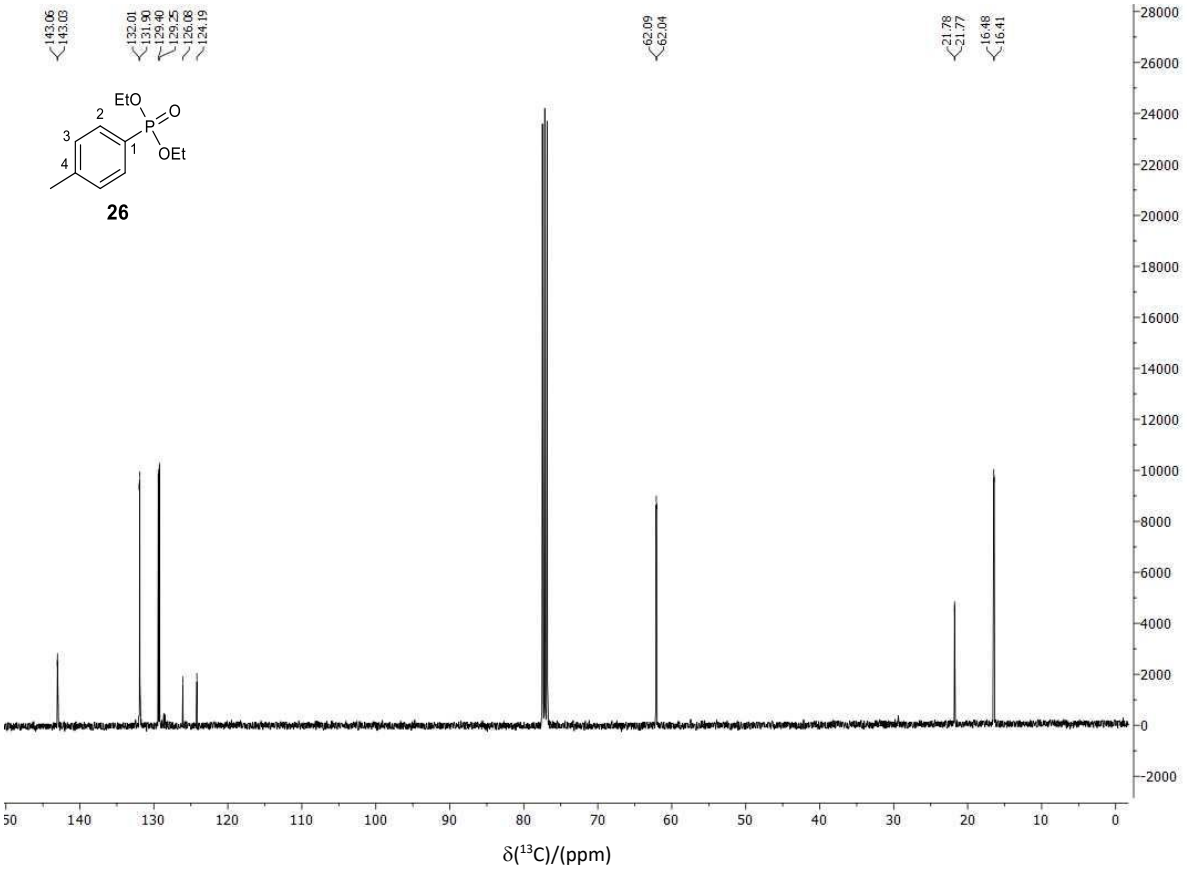
143.06
143.03
132.01
131.90
129.40
129.25
126.08
124.19
62.09
62.04
21.78
21.77
16.48
16.41
EtO
OEt
26
δ(13C)/(ppm)

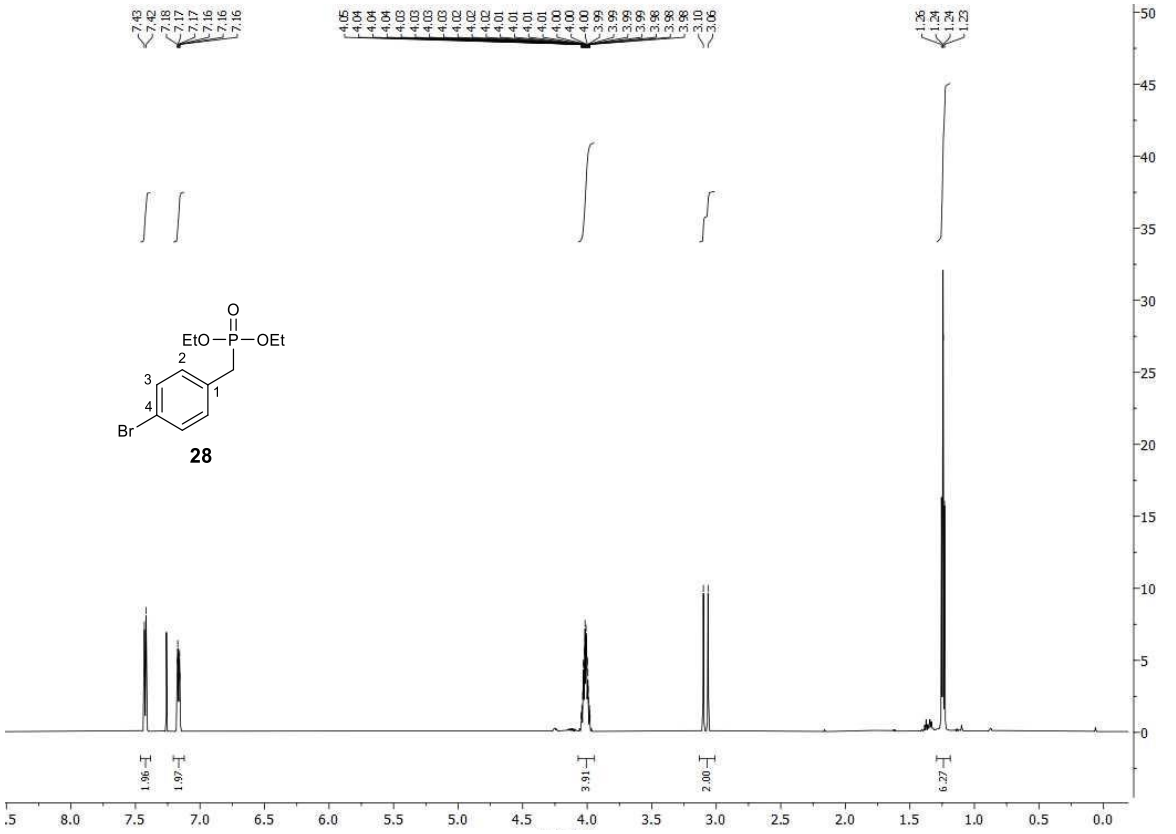
7.43
7.42
7.18
7.17
7.17
7.16
7.16
7.16
4.05
4.04
4.04
4.04
4.03
4.03
4.03
4.03
4.02
4.02
4.02
4.02
4.01
4.01
4.01
4.01
4.00
4.00
4.00
3.99
3.99
3.99
3.99
3.98
3.98
3.98
3.10
3.06
1.26
1.24
1.24
1.23
EtO
P
OEt
O
2
3
1
4
Br
28
1.96
1.97
3.91
2.00
6.27
δ(1H)/(ppm)

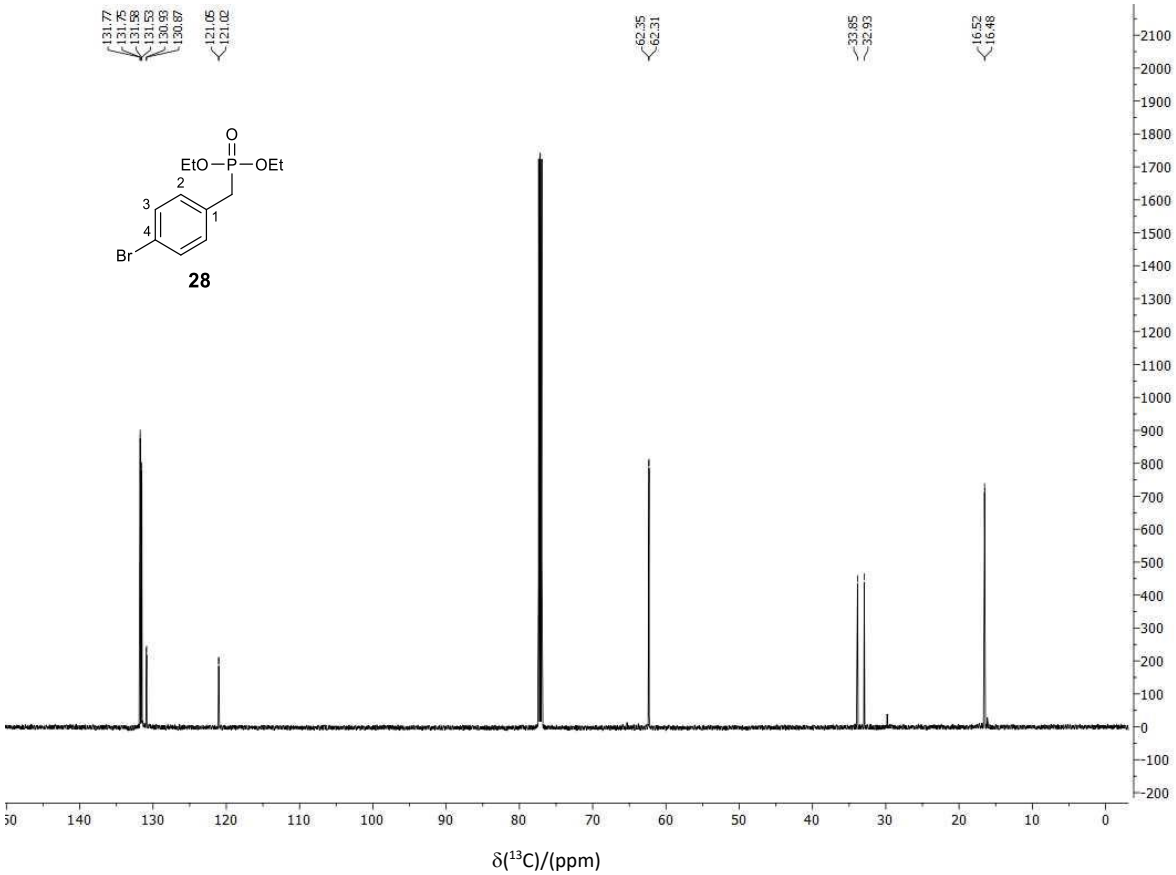
131.77
131.75
131.58
131.53
130.99
130.87
121.05
121.02
62.35
62.31
33.85
32.93
16.52
16.48
EtO
P
OEt
O
2
3
1
4
Br
28
δ(13C)/(ppm)

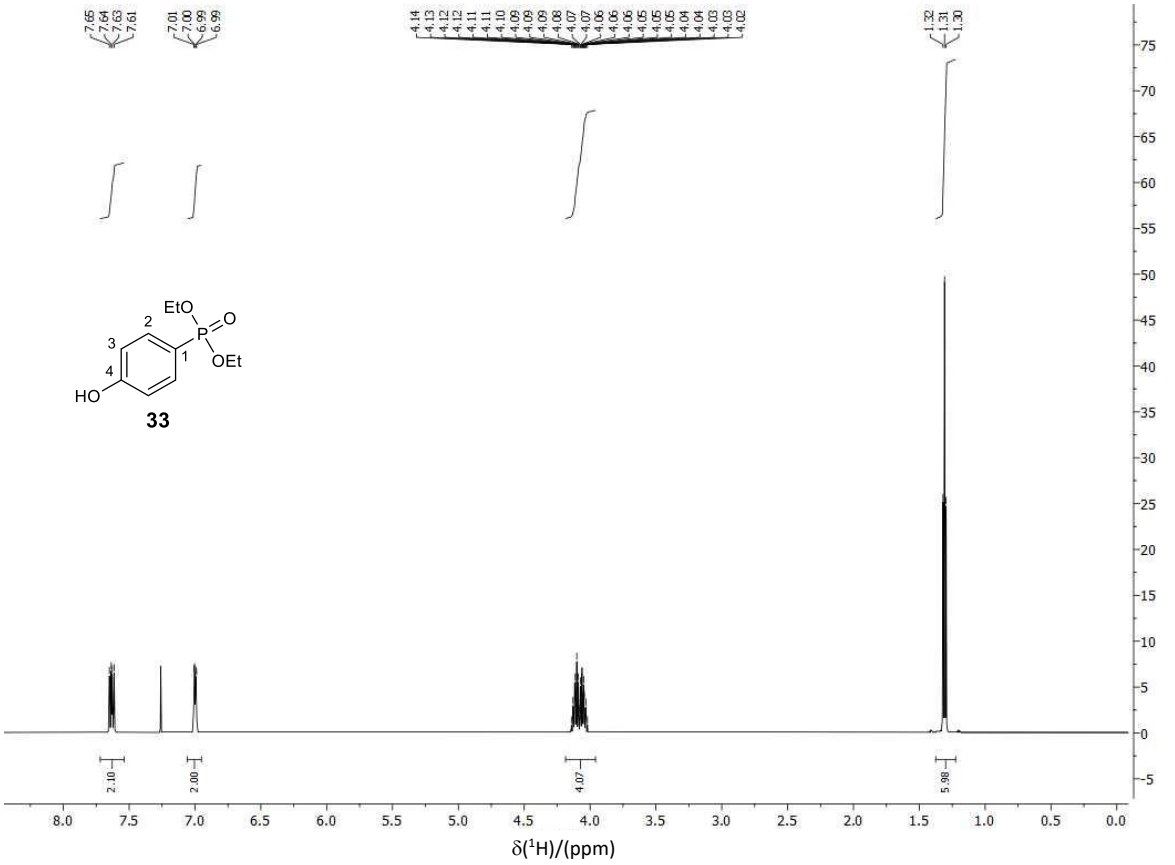
7.65
7.64
7.63
7.61
7.01
7.00
6.99
6.99
4.14
4.13
4.12
4.12
4.11
4.11
4.10
4.09
4.09
4.09
4.08
4.07
4.07
4.06
4.06
4.06
4.05
4.05
4.05
4.04
4.04
4.03
4.03
4.02
1.32
1.31
1.30
EtO
O
OEt
HO
33
2.10
2.00
4.07
5.98
δ(1H)/(ppm)

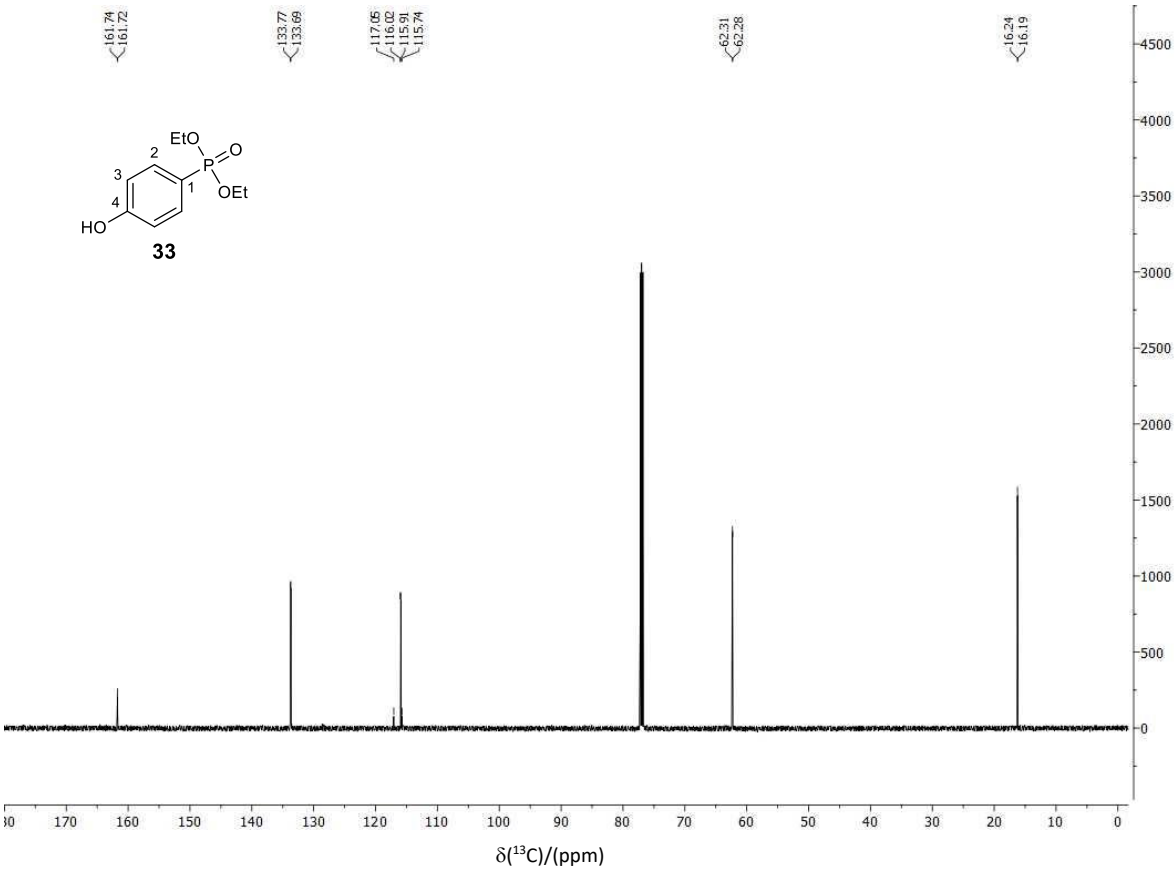
161.74
161.72
133.77
133.69
117.05
116.02
115.91
115.74
62.31
62.28
16.24
16.19
EtO
O
OEt
HO
33
δ(13C)/(ppm)

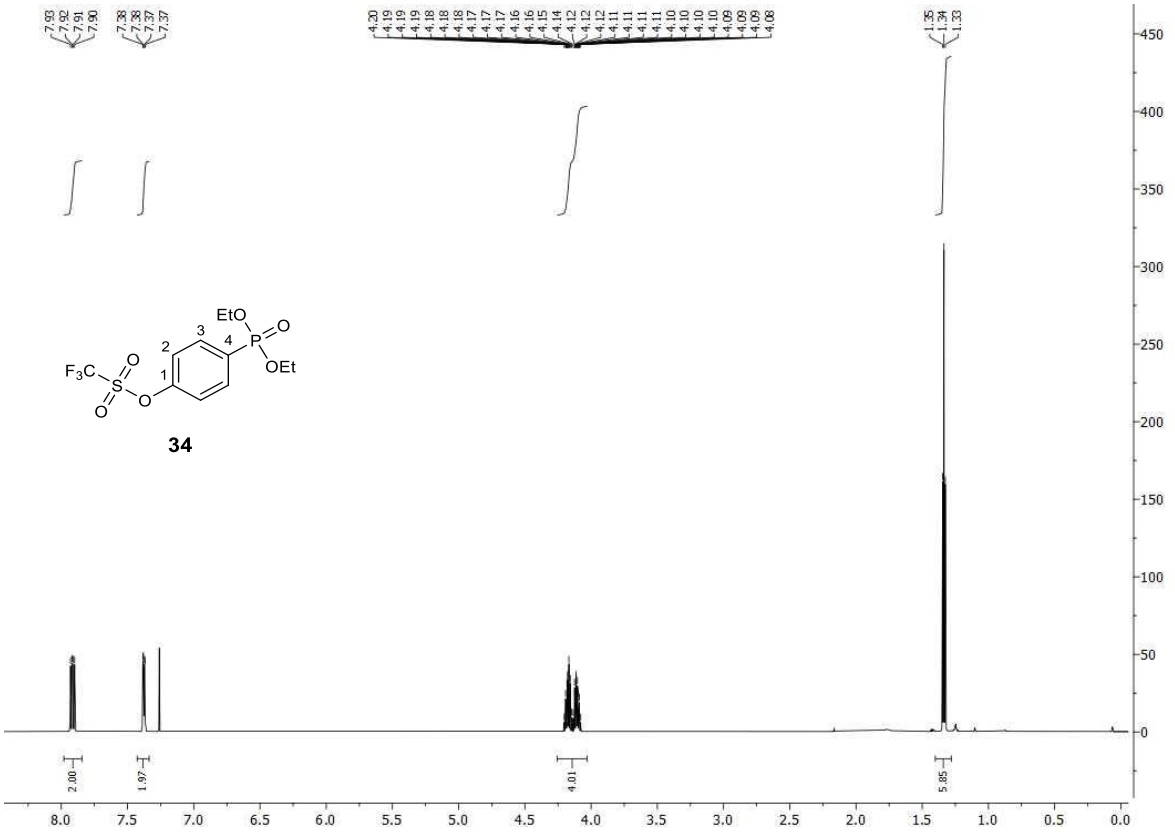
7.93
7.92
7.91
7.90
7.38
7.38
7.37
7.37
4.20
4.19
4.19
4.19
4.18
4.18
4.17
4.17
4.17
4.16
4.16
4.15
4.14
4.12
4.12
4.12
4.11
4.11
4.11
4.10
4.10
4.10
4.10
4.09
4.09
4.09
4.08
1.35
1.34
1.33
EtO
OEt
F3C
2.00
1.97
4.01
5.85
δ(1H)/(ppm)

34

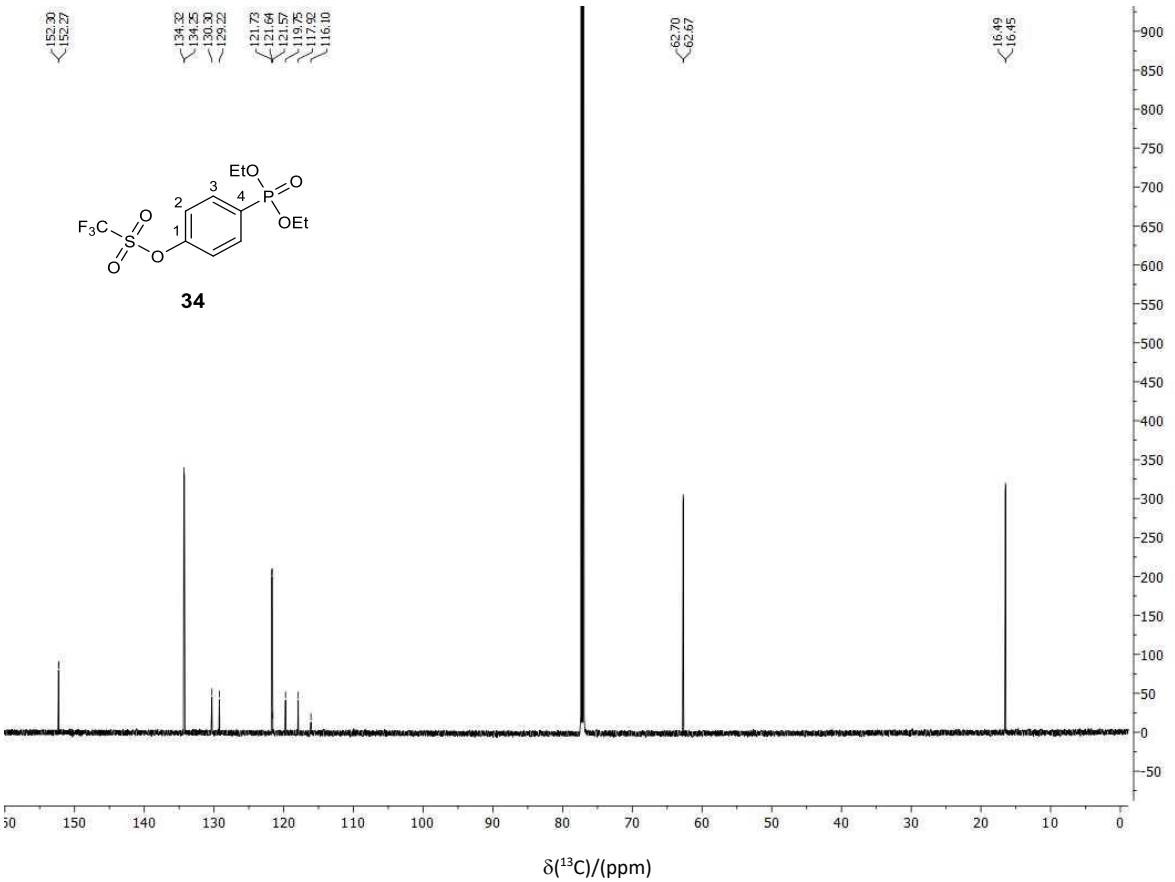
152.30
152.27
134.32
134.25
130.30
129.22
121.73
121.64
121.57
119.75
117.92
116.10
62.70
62.67
16.49
16.45
EtO
OEt
F3C
δ(13C)/(ppm)

34

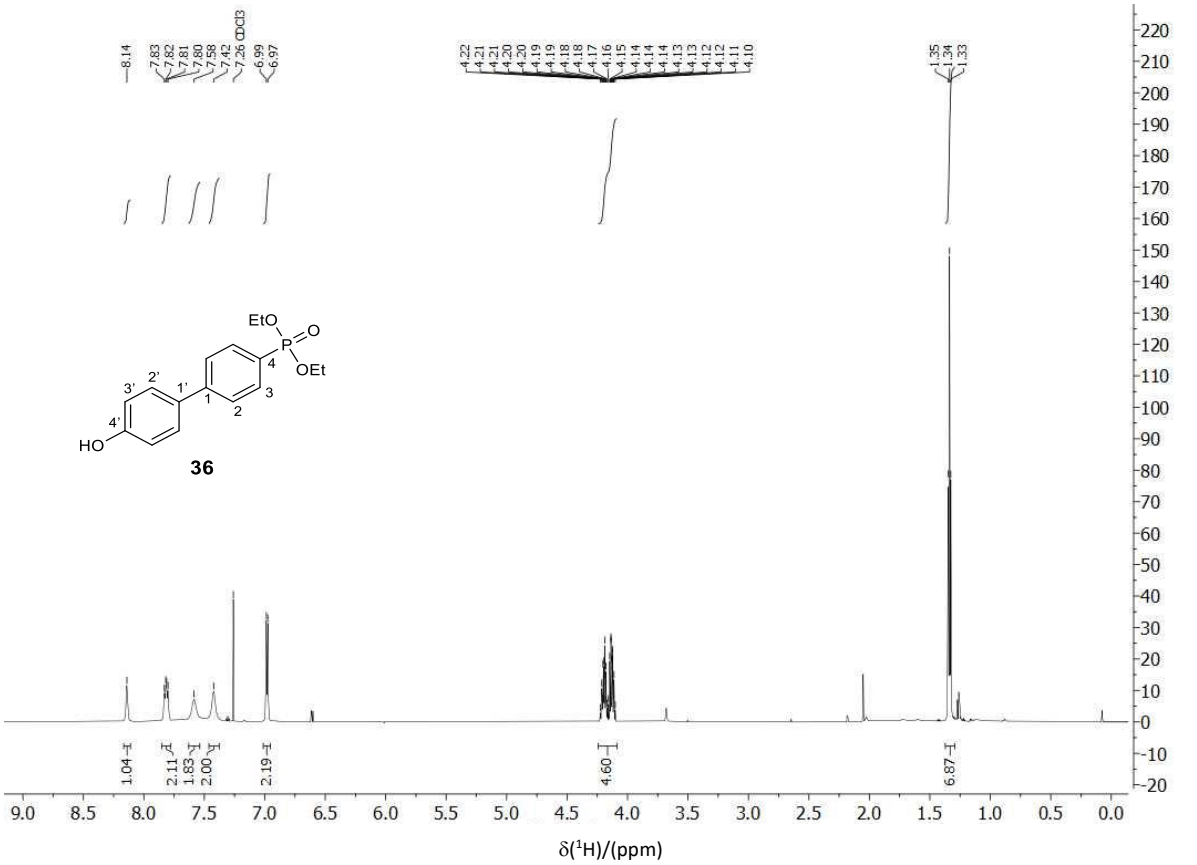
8.14
7.83
7.82
7.81
7.80
7.58
7.42
7.26 CDCl3
6.99
6.97
4.22
4.21
4.21
4.20
4.20
4.19
4.19
4.18
4.18
4.17
4.16
4.15
4.14
4.14
4.14
4.13
4.13
4.12
4.12
4.11
4.10
1.35
1.34
1.33
EtO
P
O
OEt
4
3
2
1
1'
2'
3'
4'
HO
36
1.04
2.11
1.83
2.00
2.19
4.60
6.87
δ(1H)/(ppm)

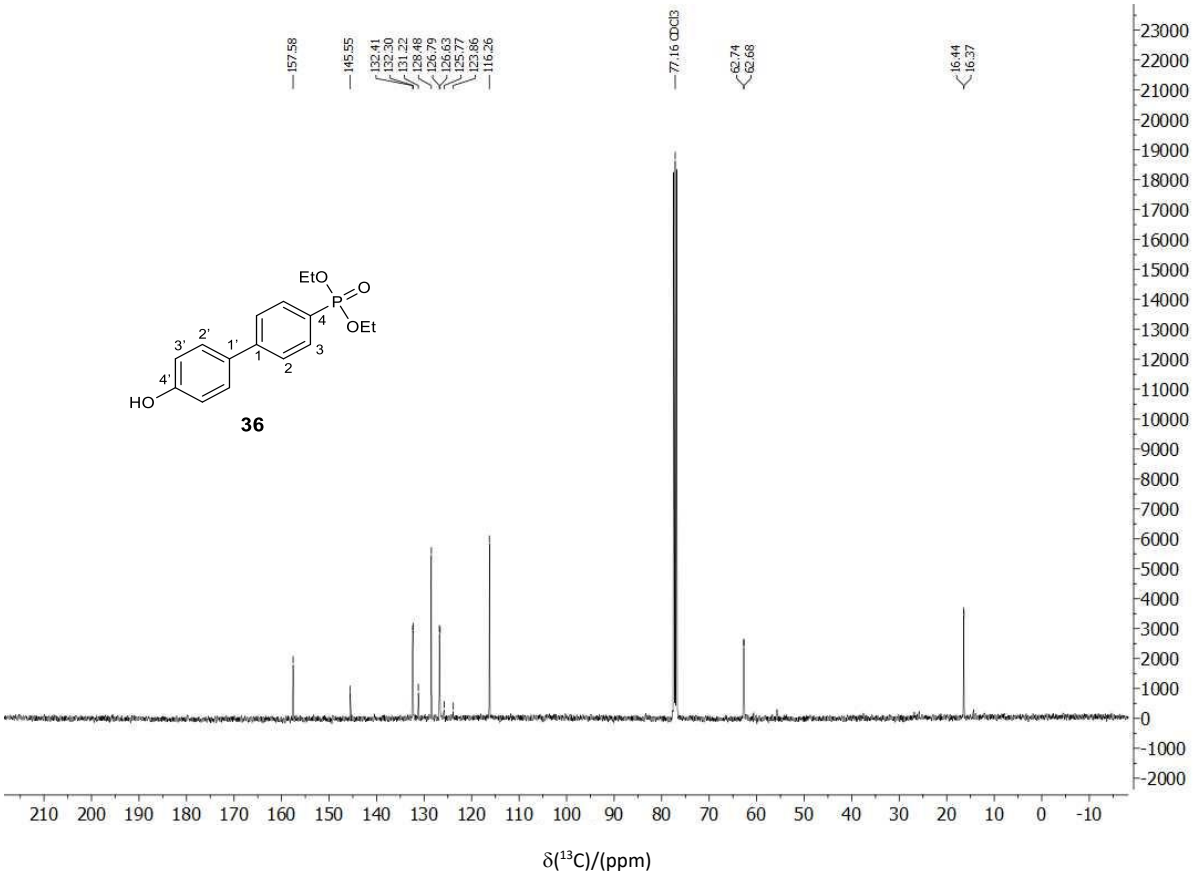
157.58
145.55
132.41
132.30
131.22
128.48
126.79
126.63
125.77
123.86
116.26
77.16 CDCl3
62.74
62.68
16.44
16.37
EtO
P
O
OEt
4
3
2
1
1'
2'
3'
4'
HO
36
δ(13C)/(ppm)

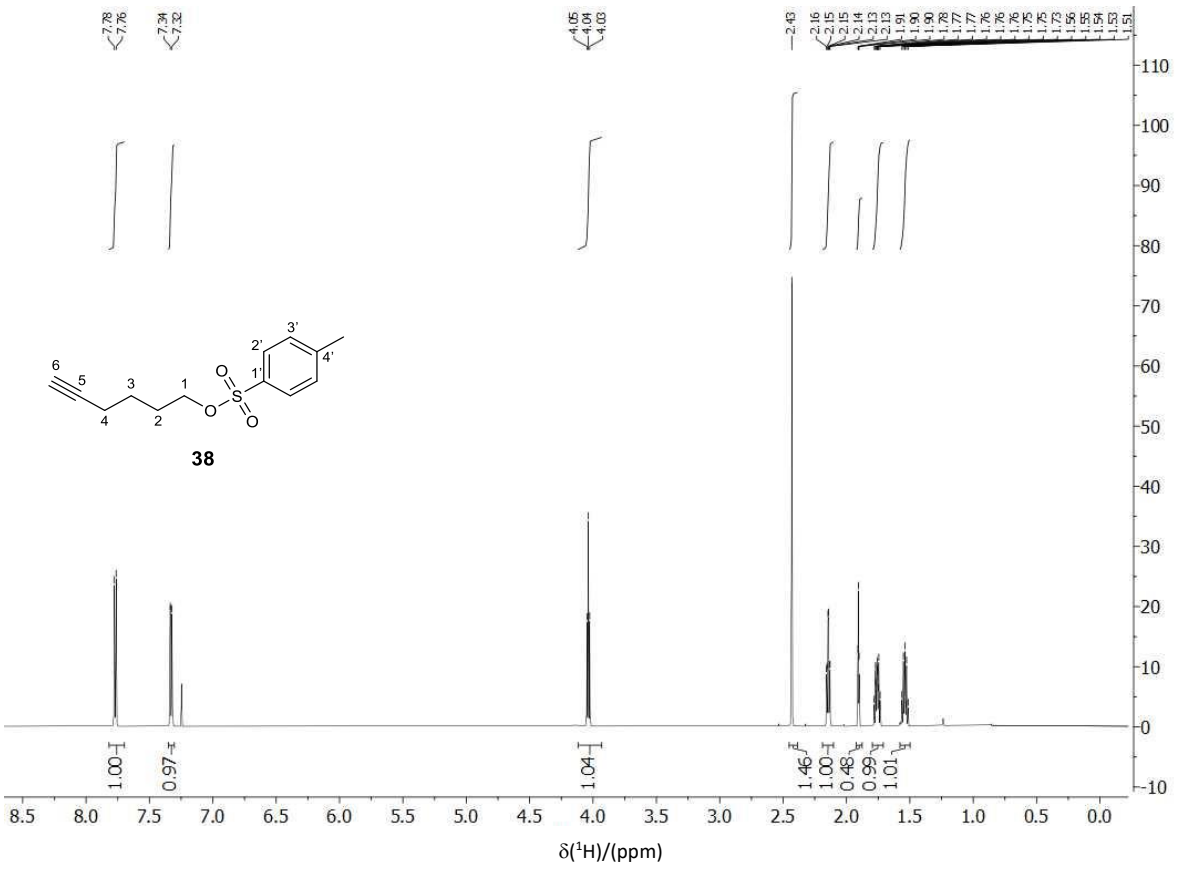
38
δ(¹H)/(ppm)

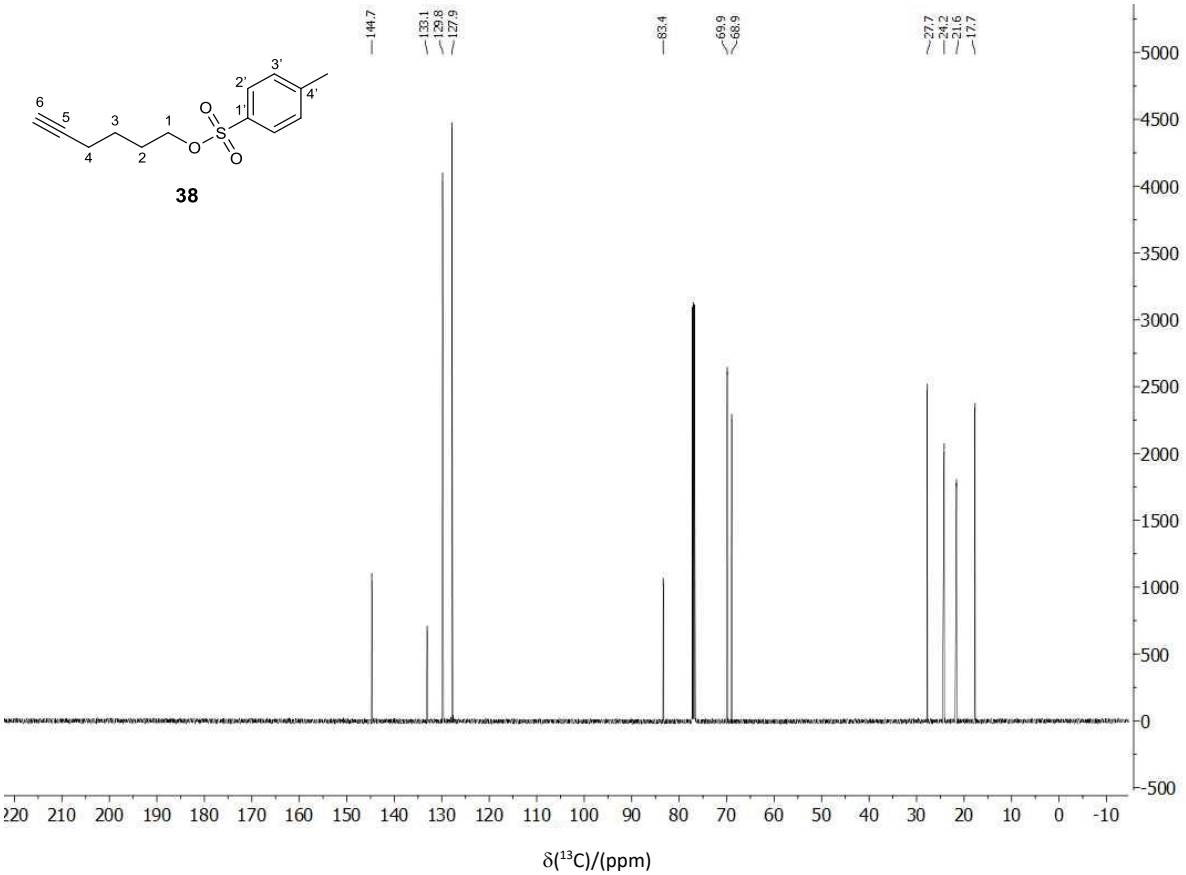
38
δ(¹³C)/(ppm)

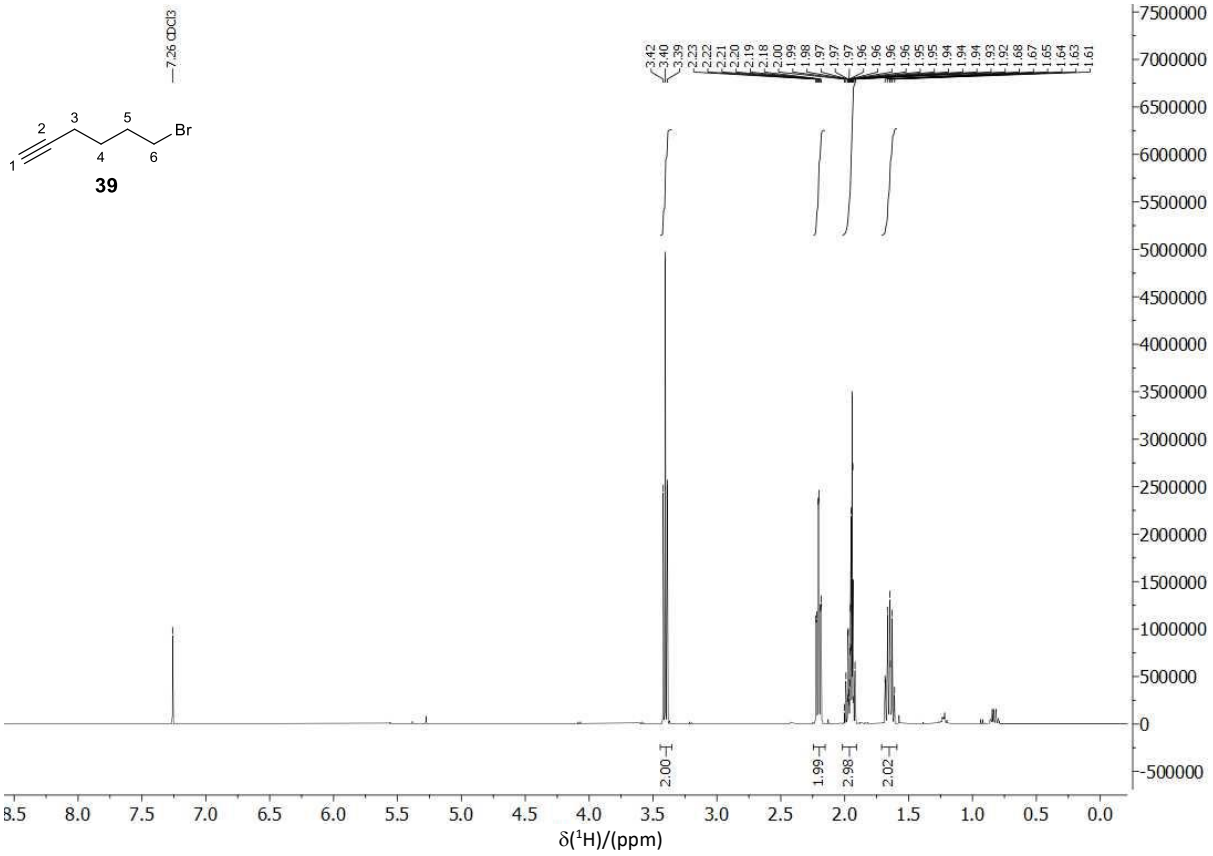
7.26 CDCl3
3.42
3.40
3.39
2.23
2.22
2.21
2.20
2.19
2.18
2.00
1.99
1.98
1.97
1.97
1.97
1.96
1.96
1.96
1.96
1.95
1.95
1.94
1.94
1.94
1.93
1.92
1.68
1.67
1.65
1.64
1.63
1.61
2.00
1.99
2.98
2.02
δ(1H)/(ppm)

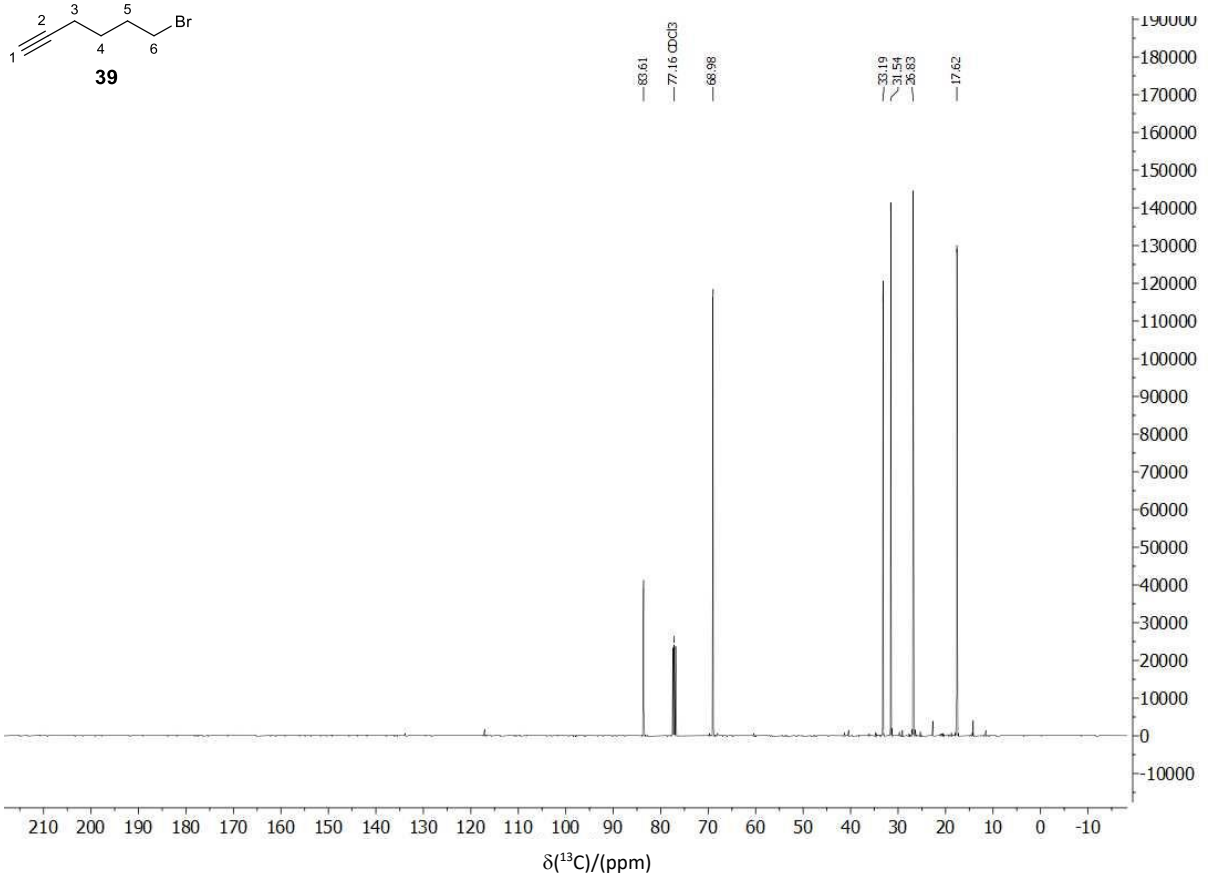
83.61
77.16 CDCl3
68.98
33.19
31.54
26.83
17.62
δ(13C)/(ppm)

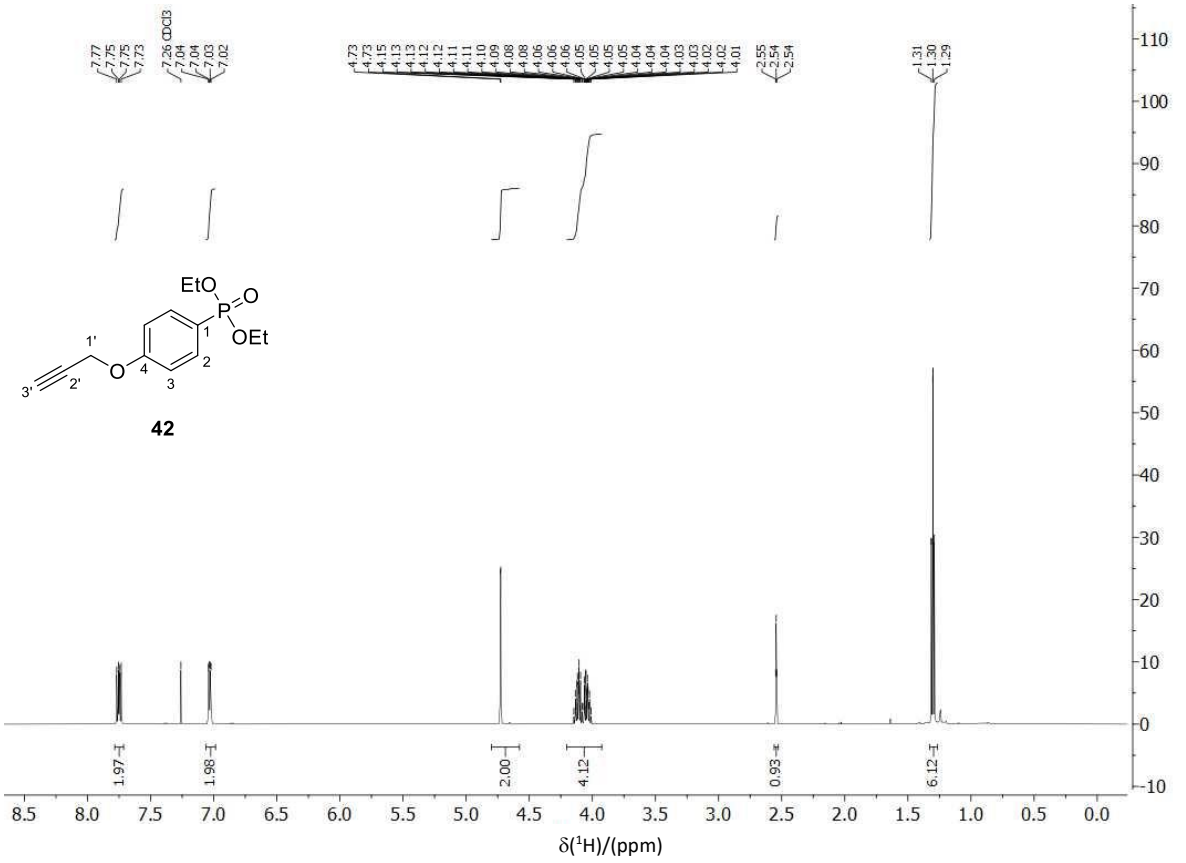
7.77
7.75
7.75
7.73
7.26 CDCl3
7.04
7.04
7.03
7.02
4.73
4.73
4.15
4.13
4.13
4.12
4.12
4.11
4.11
4.10
4.09
4.08
4.08
4.06
4.06
4.06
4.05
4.05
4.05
4.05
4.04
4.04
4.04
4.03
4.03
4.02
4.02
4.01
2.55
2.54
2.54
1.31
1.30
1.29
EtO
P
O
OEt
1'
1
2
3'
2'
O
4
3
42
1.97
1.98
2.00
4.12
0.93
6.12
δ(¹H)/(ppm)

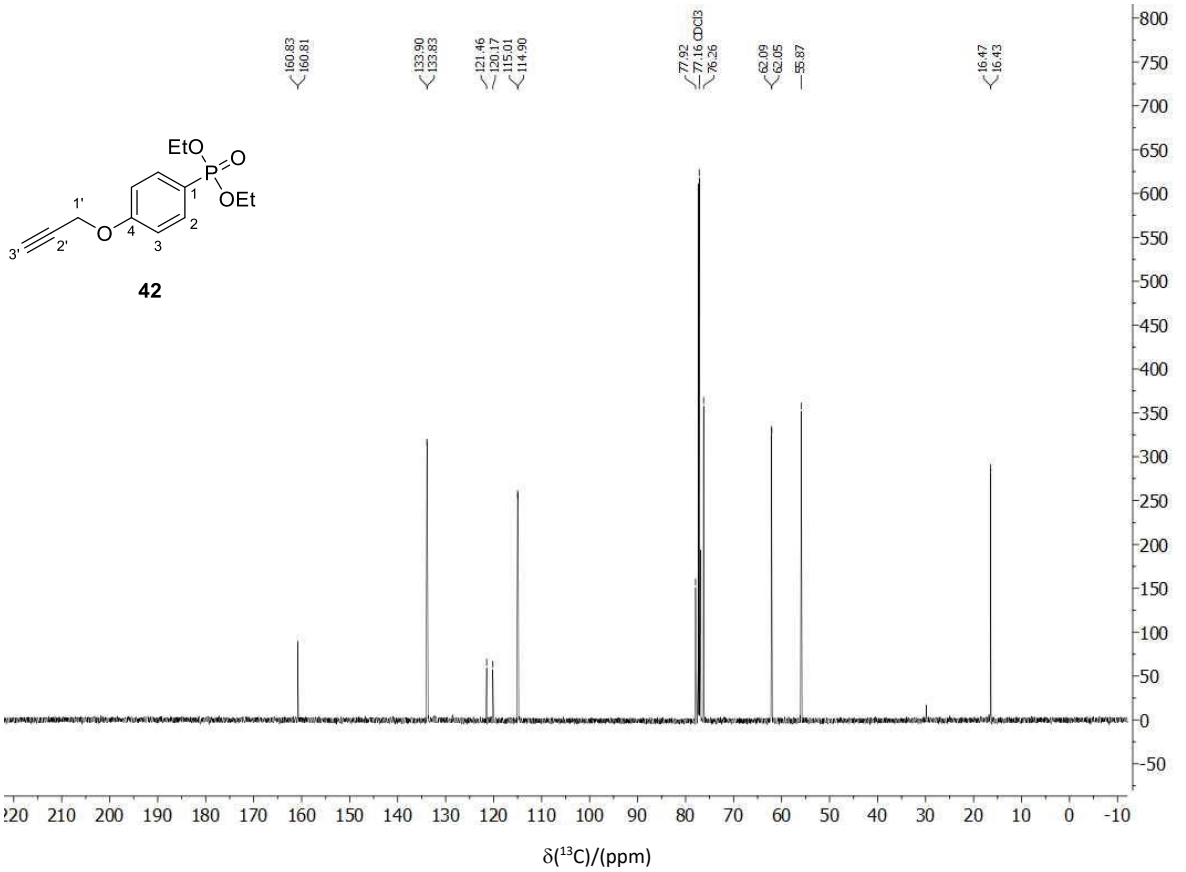
160.83
160.81
133.90
133.83
121.46
120.17
115.01
114.90
77.92
77.16 CDCl3
76.26
62.09
62.05
55.87
16.47
16.43
EtO
P
O
OEt
1'
1
2
3'
2'
O
4
3
42
δ(¹³C)/(ppm)

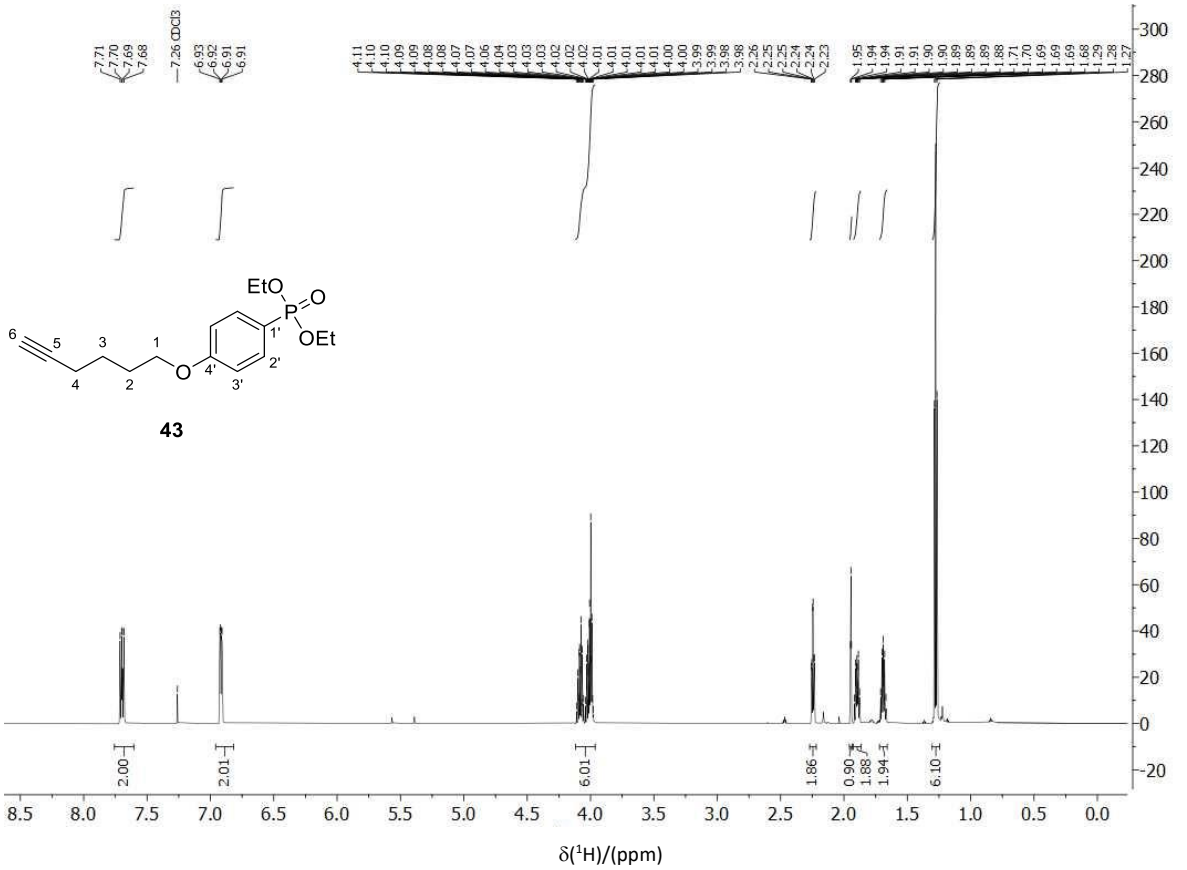
EtO
P
O
OEt
1'
2'
3'
4'
O
1
2
3
4
5
6
43
δ(¹H)/(ppm)

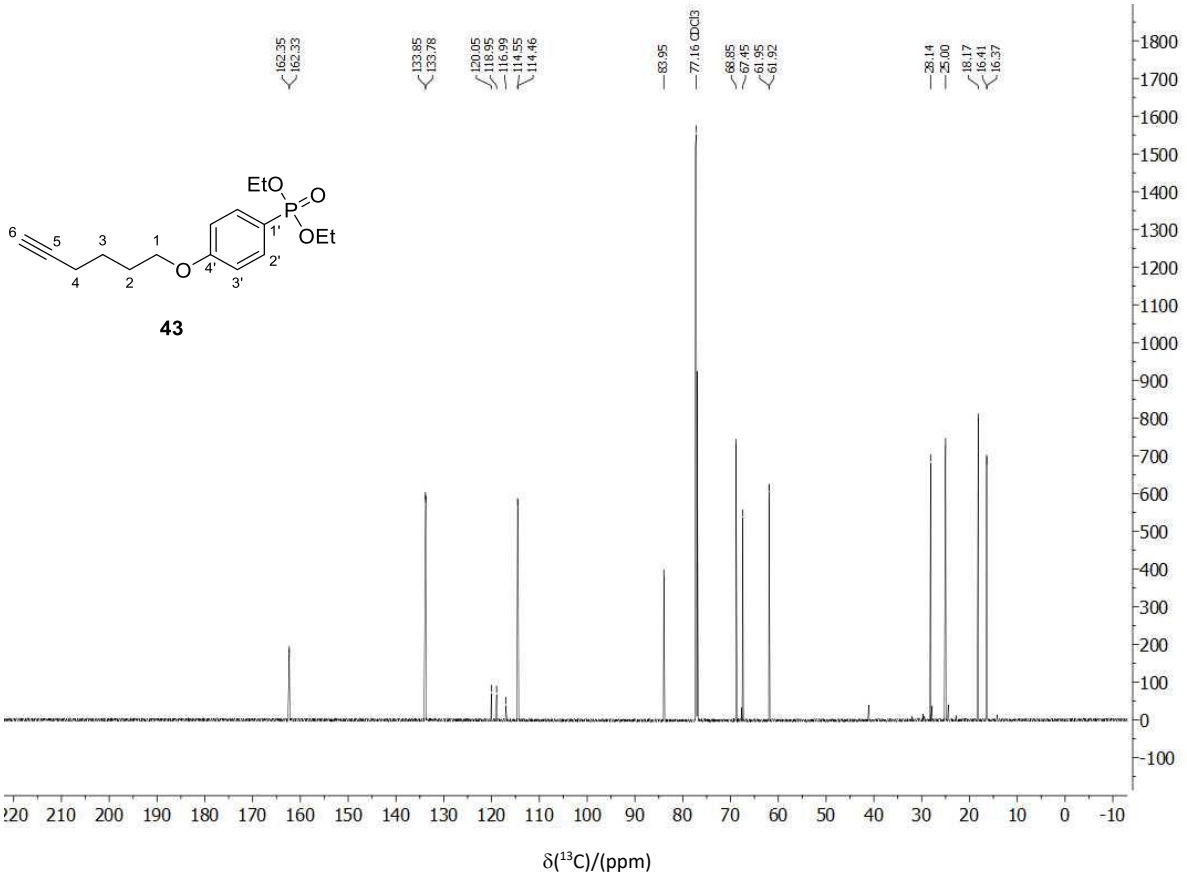
EtO
P
O
OEt
1'
2'
3'
4'
O
1
2
3
4
5
6
43
δ(¹³C)/(ppm)

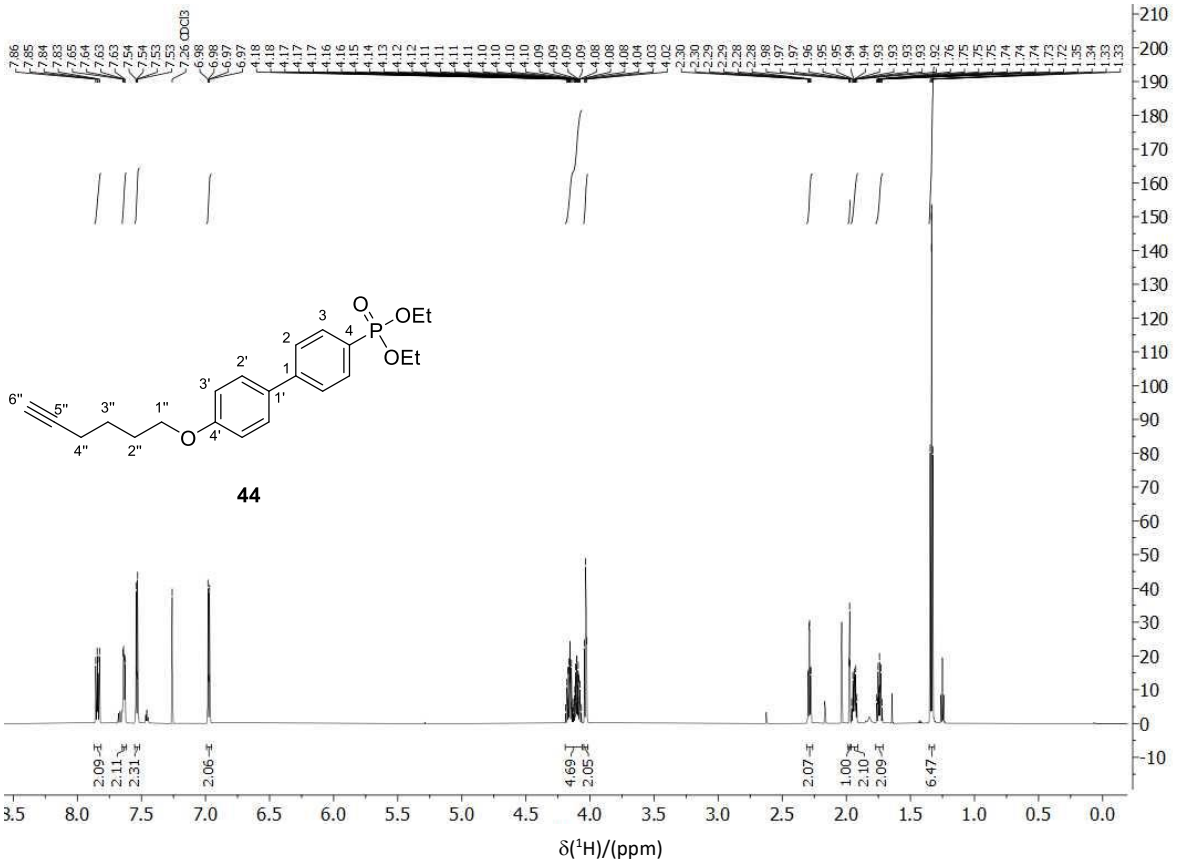
OEt
OEt
44
δ(¹H)/(ppm)

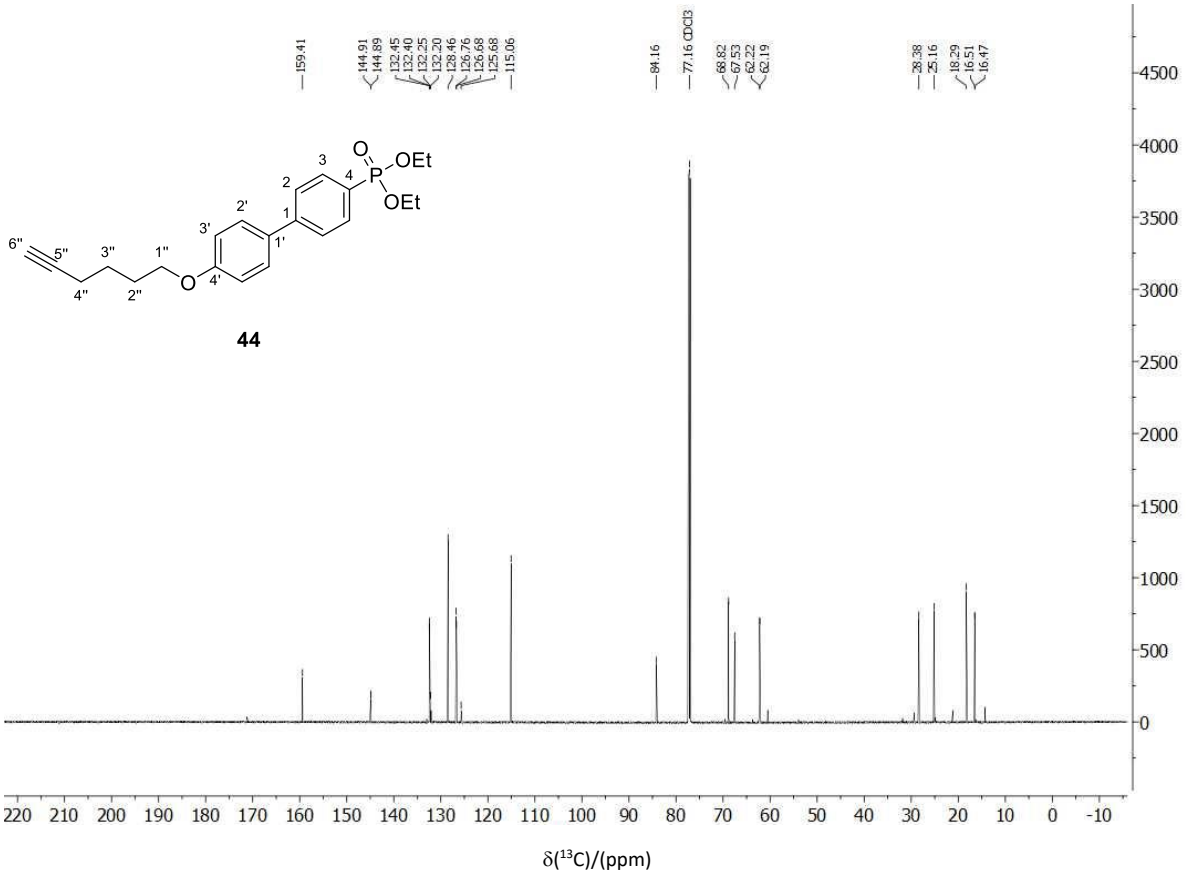
OEt
OEt
44
δ(¹³C)/(ppm)

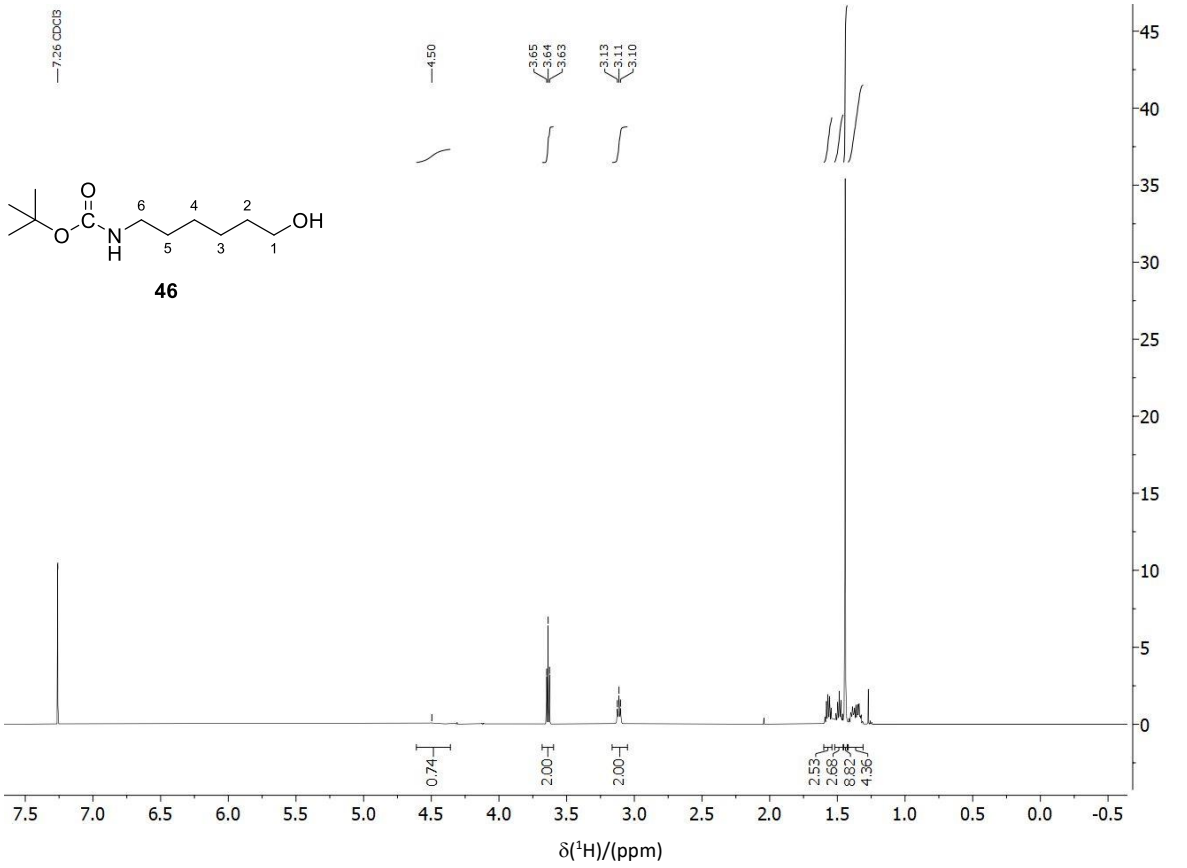
7.26 CDCl3
4.50
3.65
3.64
3.63
3.13
3.11
3.10
O
O
N
H
OH
6
5
4
3
2
1
46
0.74
2.00
2.00
2.53
2.68
8.82
4.36
δ(1H)/(ppm)

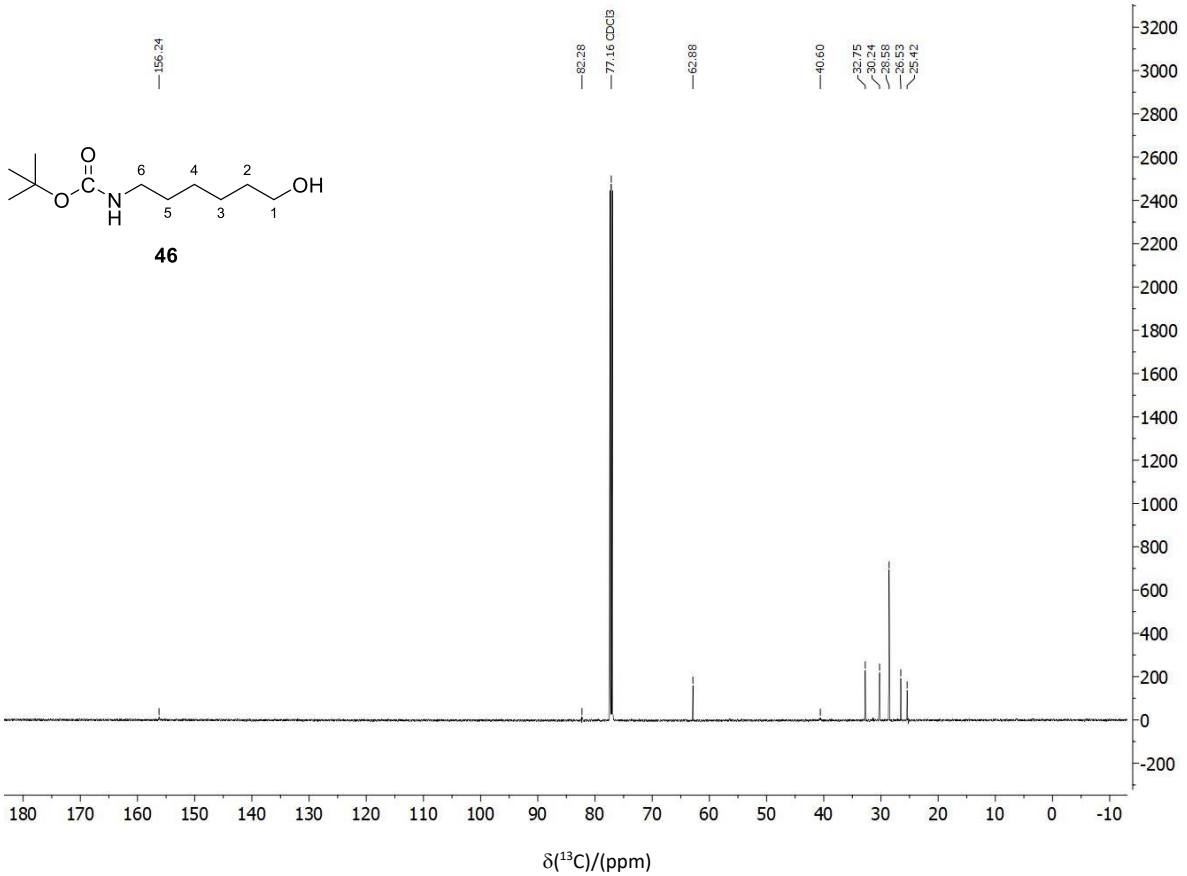
156.24
82.28
77.16 CDCl3
62.88
40.60
32.75
30.24
28.58
26.53
25.42
O
O
N
H
OH
6
5
4
3
2
1
46
δ(13C)/(ppm)

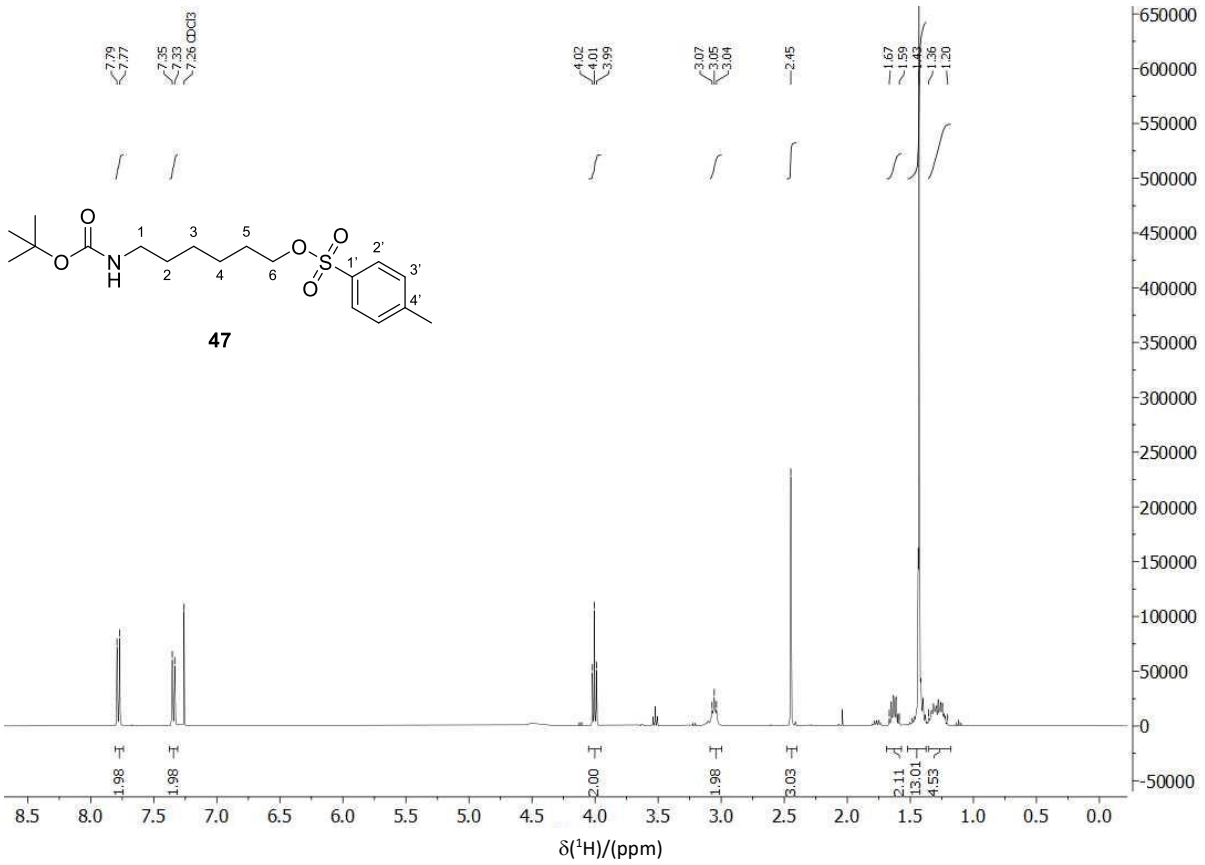
7.79
7.77
7.35
7.33
7.26 CDCl3
4.02
4.01
3.99
3.07
3.05
3.04
2.45
1.67
1.59
1.43
1.36
1.20
1.98
1.98
2.00
1.98
3.03
2.11
13.01
4.53
δ(1H)/(ppm)

47

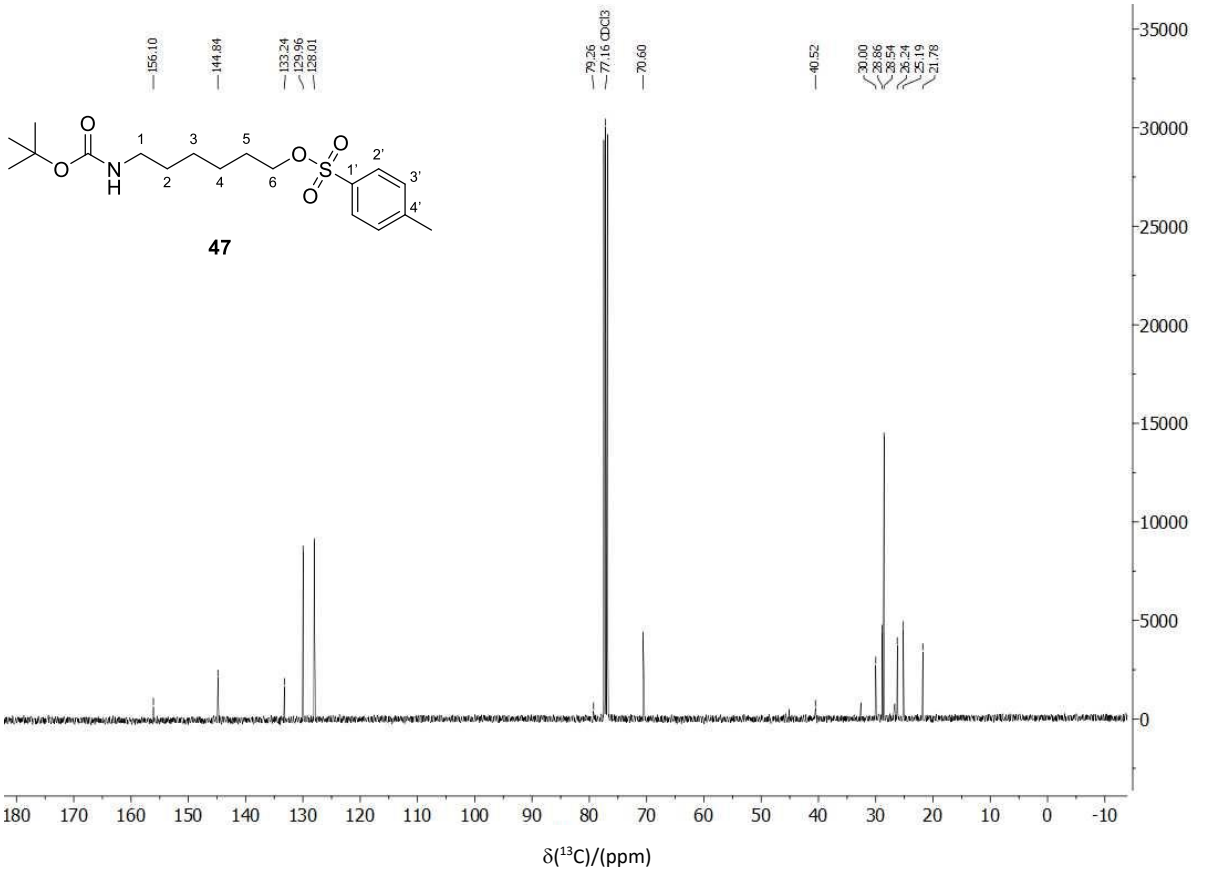
156.10
144.84
133.24
129.96
128.01
79.26
77.16 CDCl3
70.60
40.52
30.00
28.86
28.54
26.24
25.19
21.78
δ(13C)/(ppm)

47

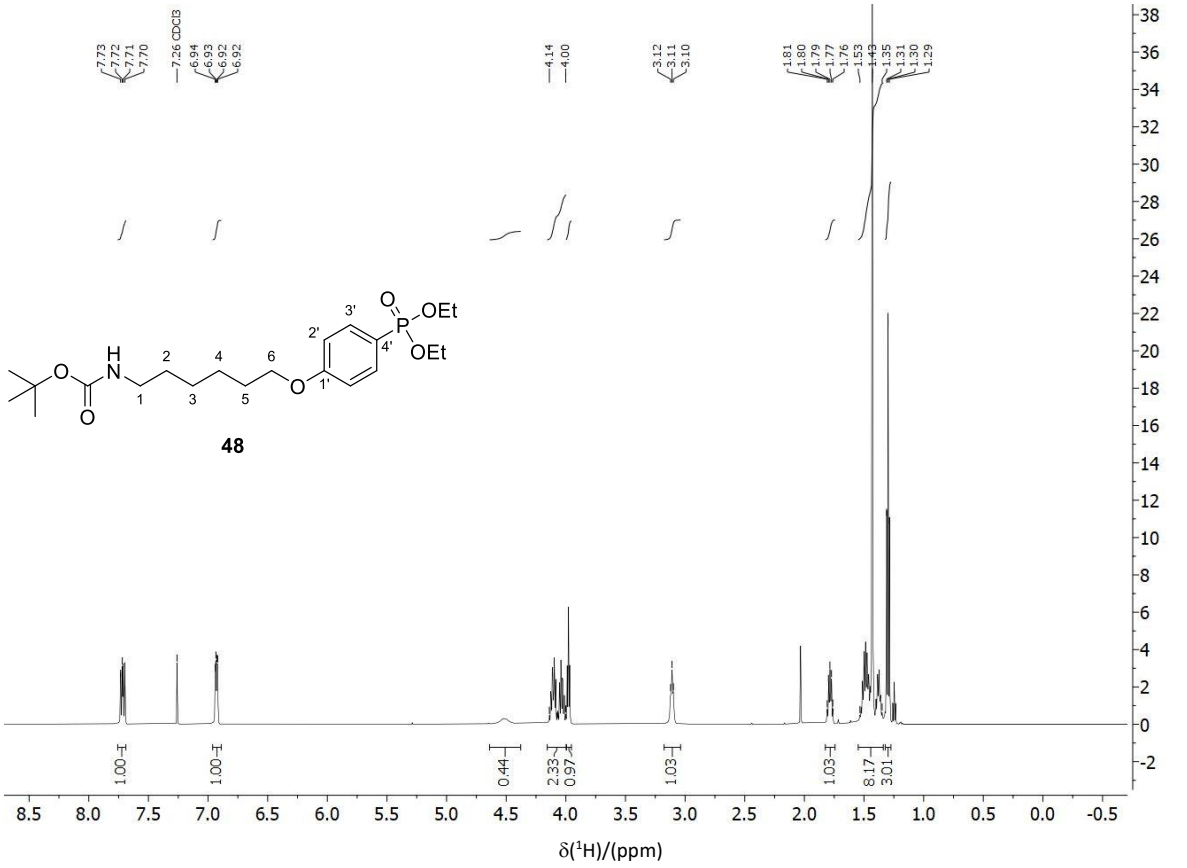
7.73
7.72
7.71
7.70
7.26 CDCl3
6.94
6.93
6.92
6.92
4.14
4.00
3.12
3.11
3.10
1.81
1.80
1.79
1.77
1.76
1.53
1.43
1.35
1.31
1.30
1.29
1.00
1.00
0.44
2.33
0.97
1.03
1.03
8.17
3.01
δ(1H)/(ppm)

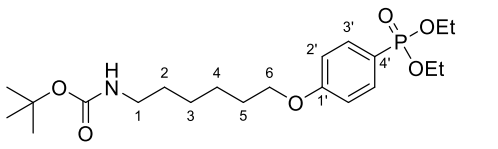
48

162.51
162.49
156.13
133.92
133.84
120.06
118.77
114.63
114.52
77.16 CDCl3
68.03
62.01
61.98
60.51
40.66
30.17
29.13
28.55
26.63
25.84
16.47
16.43
δ(13C)/(ppm)

48

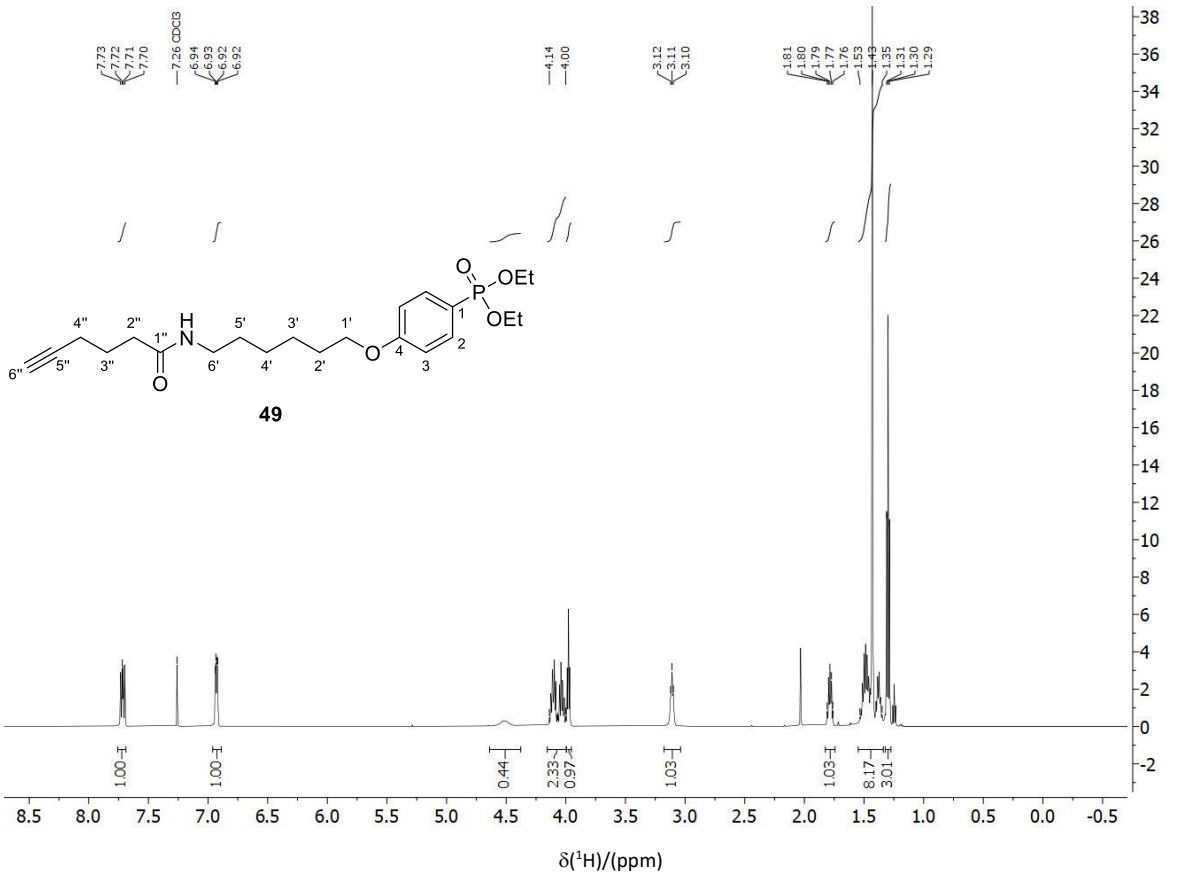
7.73
7.72
7.71
7.70
7.26 CDCl3
6.94
6.93
6.92
6.92
4.14
4.00
3.12
3.11
3.10
1.81
1.80
1.79
1.77
1.76
1.53
1.43
1.35
1.31
1.30
1.29
1.00
1.00
0.44
2.33
0.97
1.03
1.03
8.17
3.01
δ(1H)/(ppm)

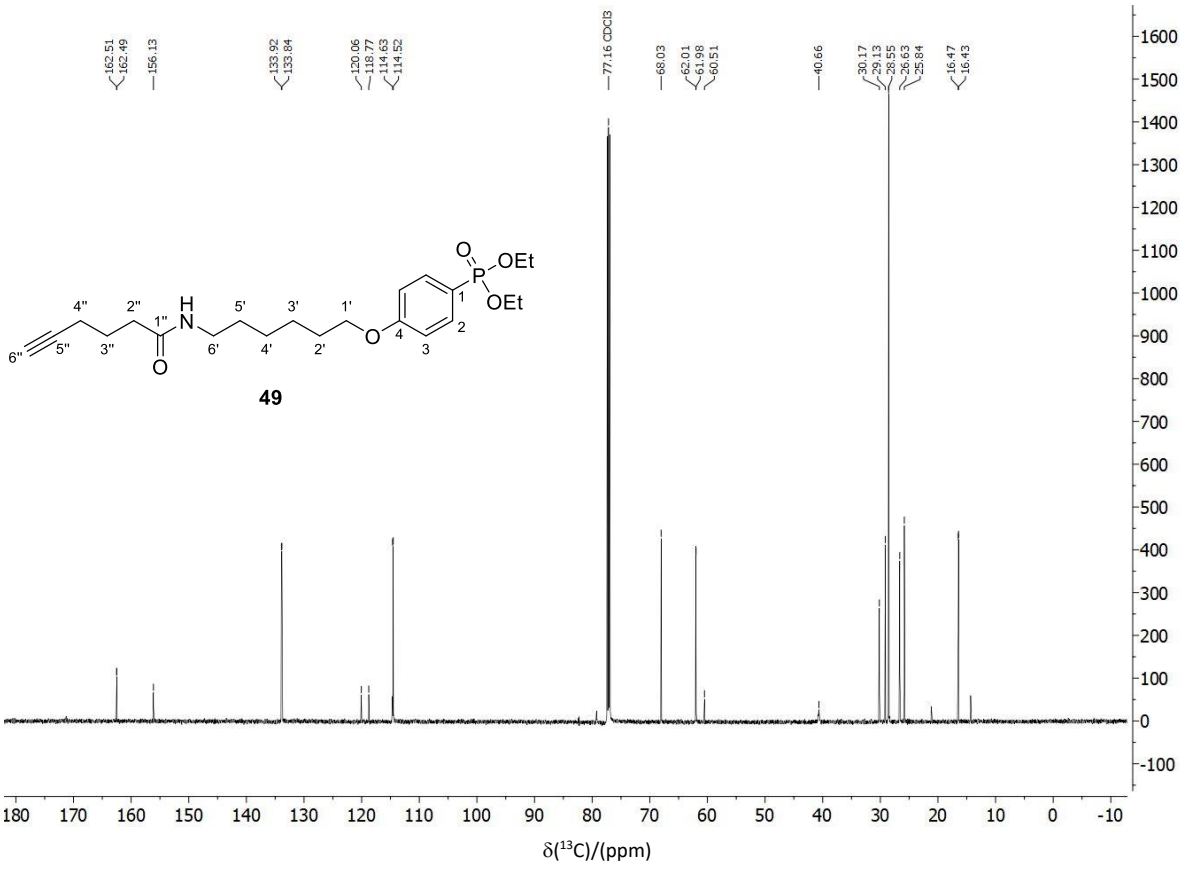
162.51
162.49
156.13
133.92
133.84
120.06
118.77
114.63
114.52
77.16 CDCl3
68.03
62.01
61.98
60.51
40.66
30.17
29.13
28.55
26.63
25.84
16.47
16.43
δ(13C)/(ppm)

49

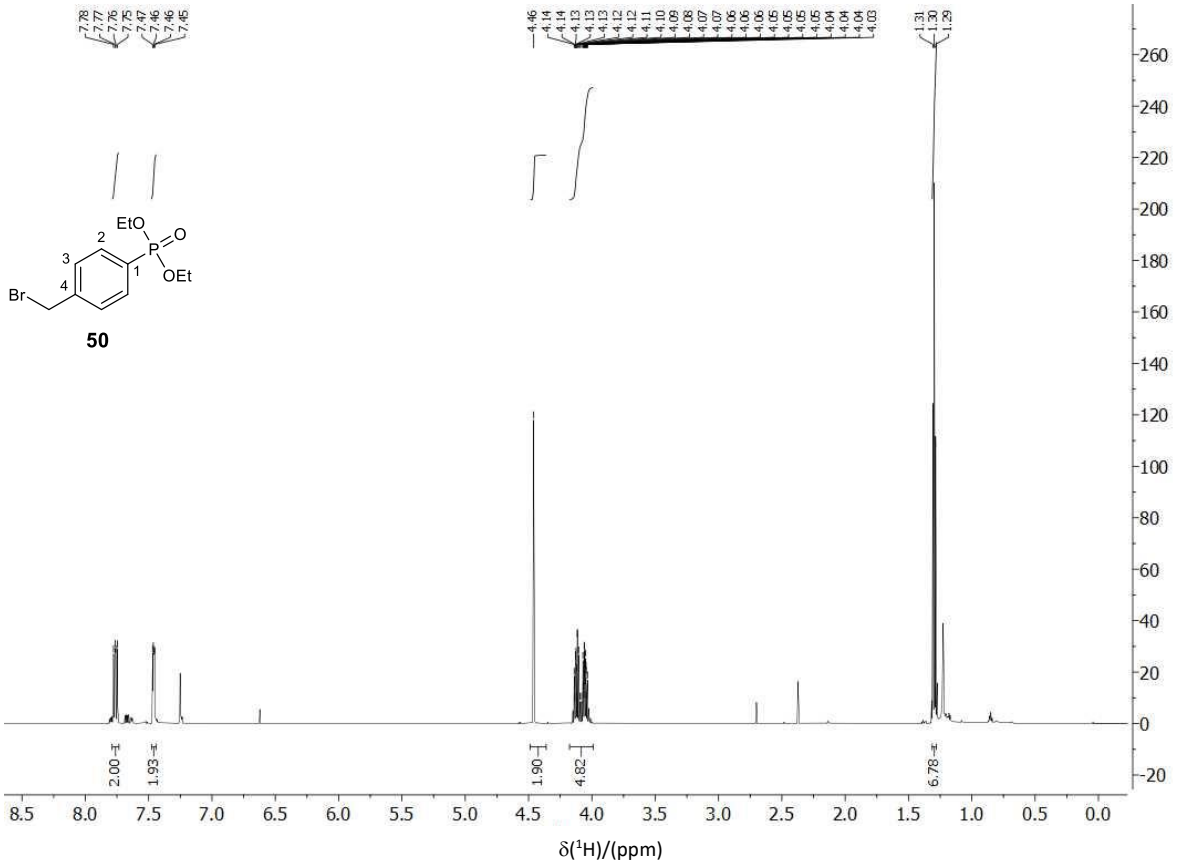
7.78
7.77
7.76
7.75
7.47
7.46
7.46
7.45
4.46
4.14
4.14
4.13
4.13
4.13
4.12
4.12
4.11
4.10
4.09
4.08
4.07
4.07
4.06
4.06
4.06
4.05
4.05
4.05
4.05
4.04
4.04
4.04
4.03
1.31
1.30
1.29
EtO
O
OEt
Br
1
2
3
4
50
2.00
1.93
1.90
4.82
6.78
δ(¹H)/(ppm)

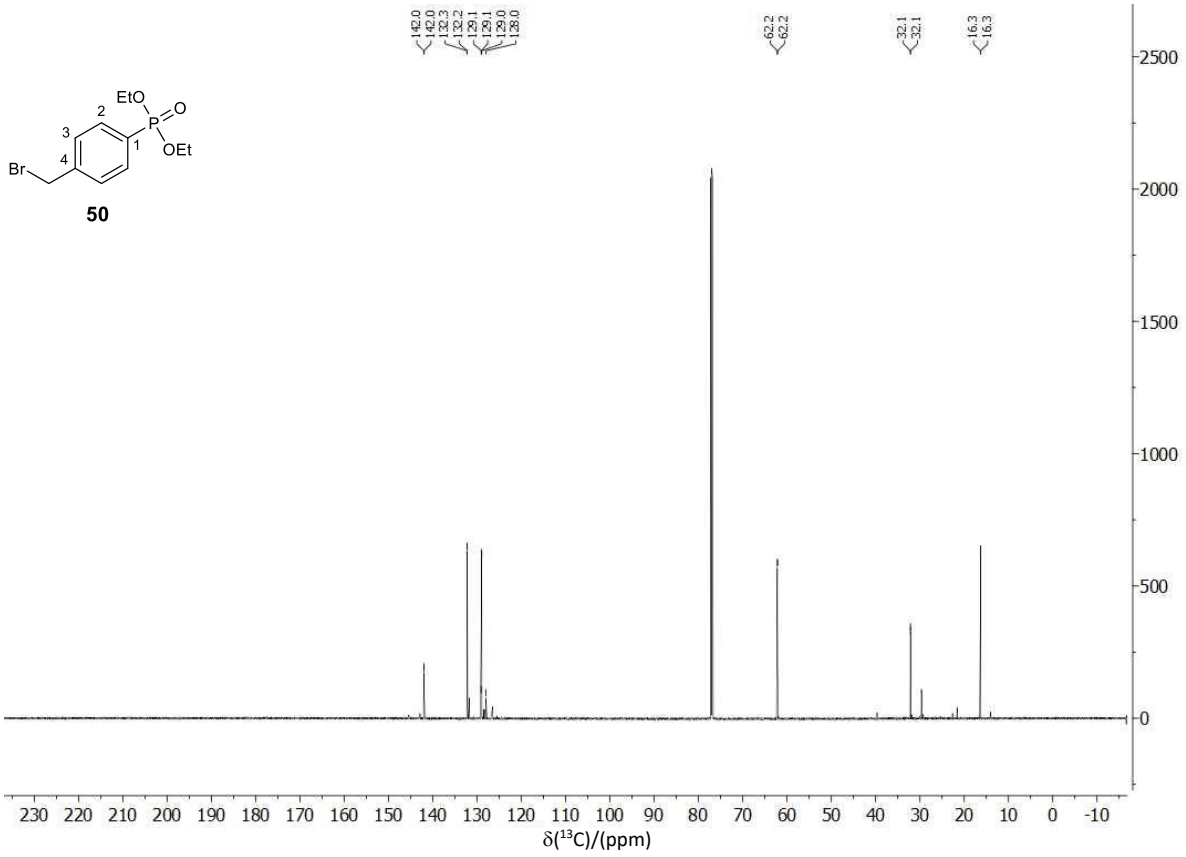
142.0
142.0
132.3
132.2
129.1
129.1
129.0
128.0
62.2
62.2
32.1
32.1
16.3
16.3
EtO
O
OEt
Br
1
2
3
4
50
δ(¹³C)/(ppm)

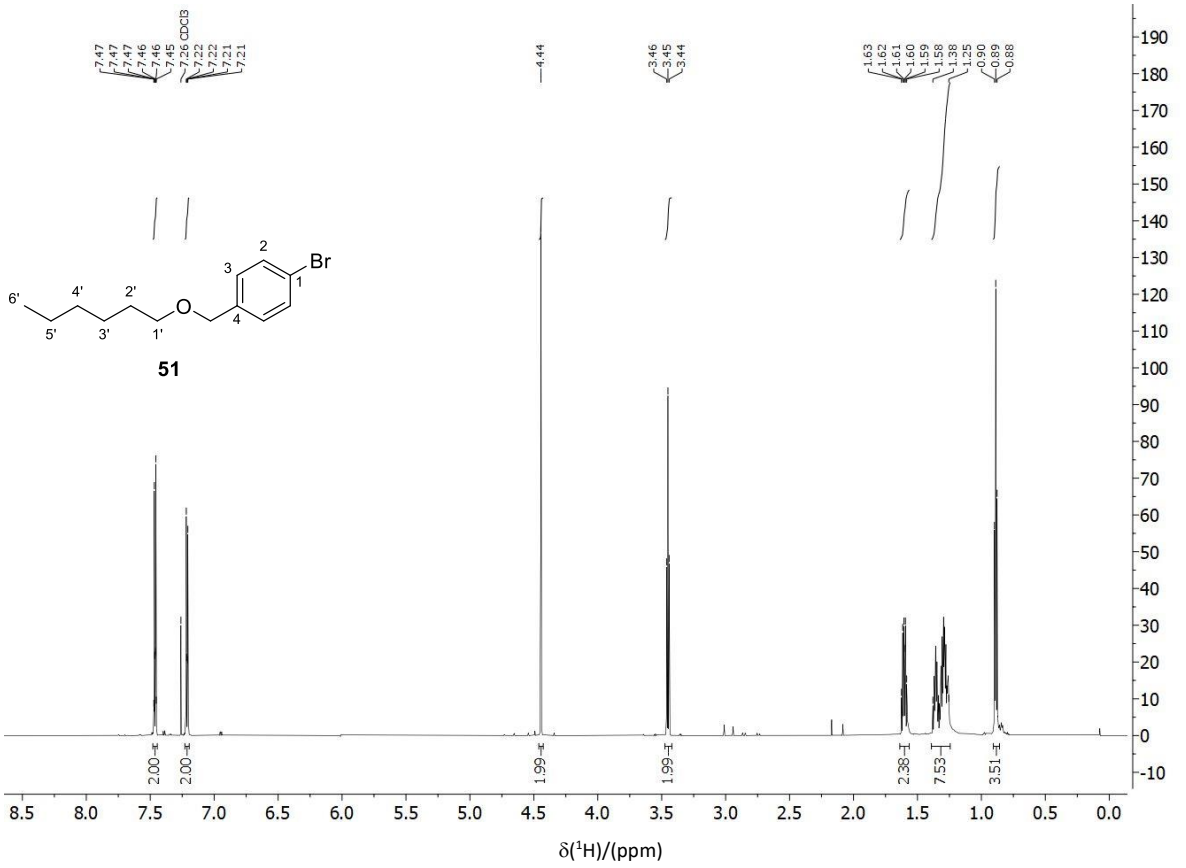
7.47
7.47
7.47
7.46
7.46
7.45
7.26 CDCl3
7.22
7.22
7.21
7.21
4.44
3.46
3.45
3.44
1.63
1.62
1.61
1.60
1.59
1.58
1.38
1.25
0.90
0.89
0.88
Br
O
2.00
2.00
1.99
1.99
2.38
7.53
3.51
δ(1H)/(ppm)

51

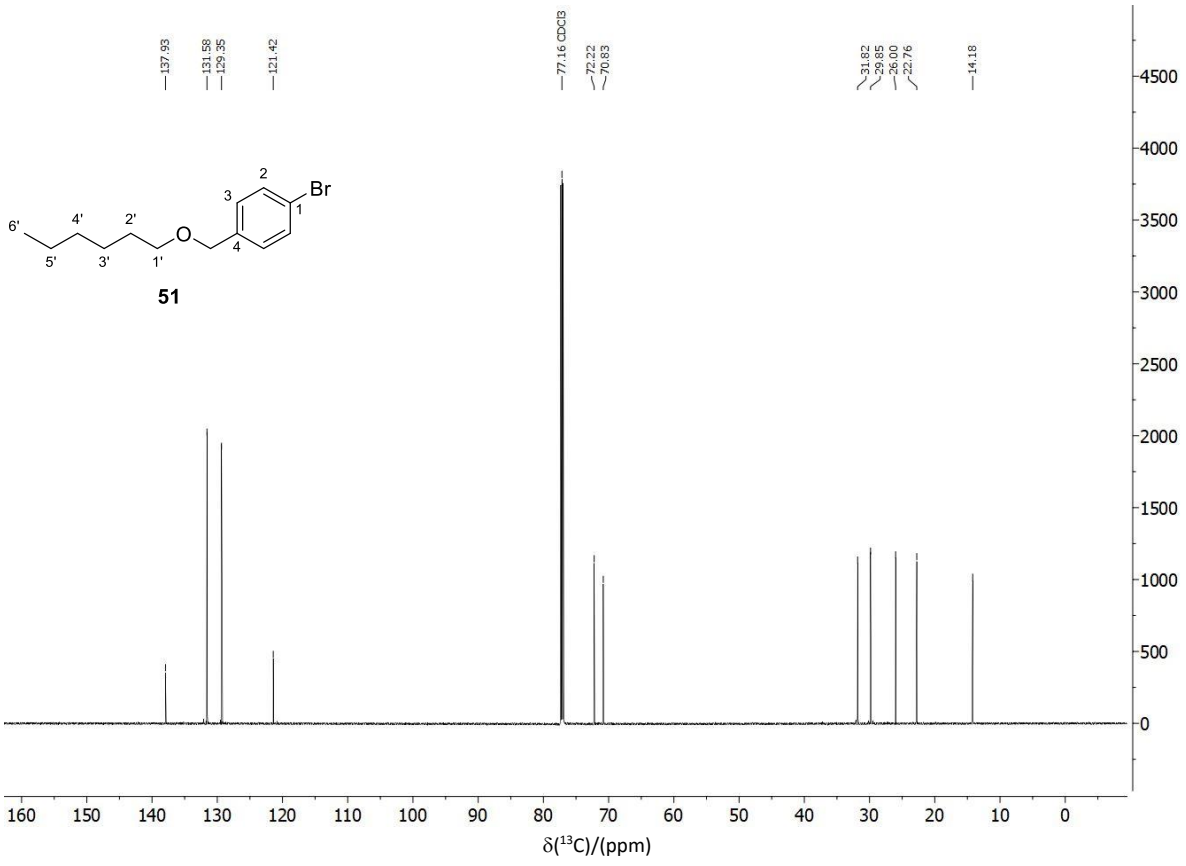
137.93
131.58
129.35
121.42
77.16 CDCl3
72.22
70.83
31.82
29.85
26.00
22.76
14.18
Br
O
δ(13C)/(ppm)

51

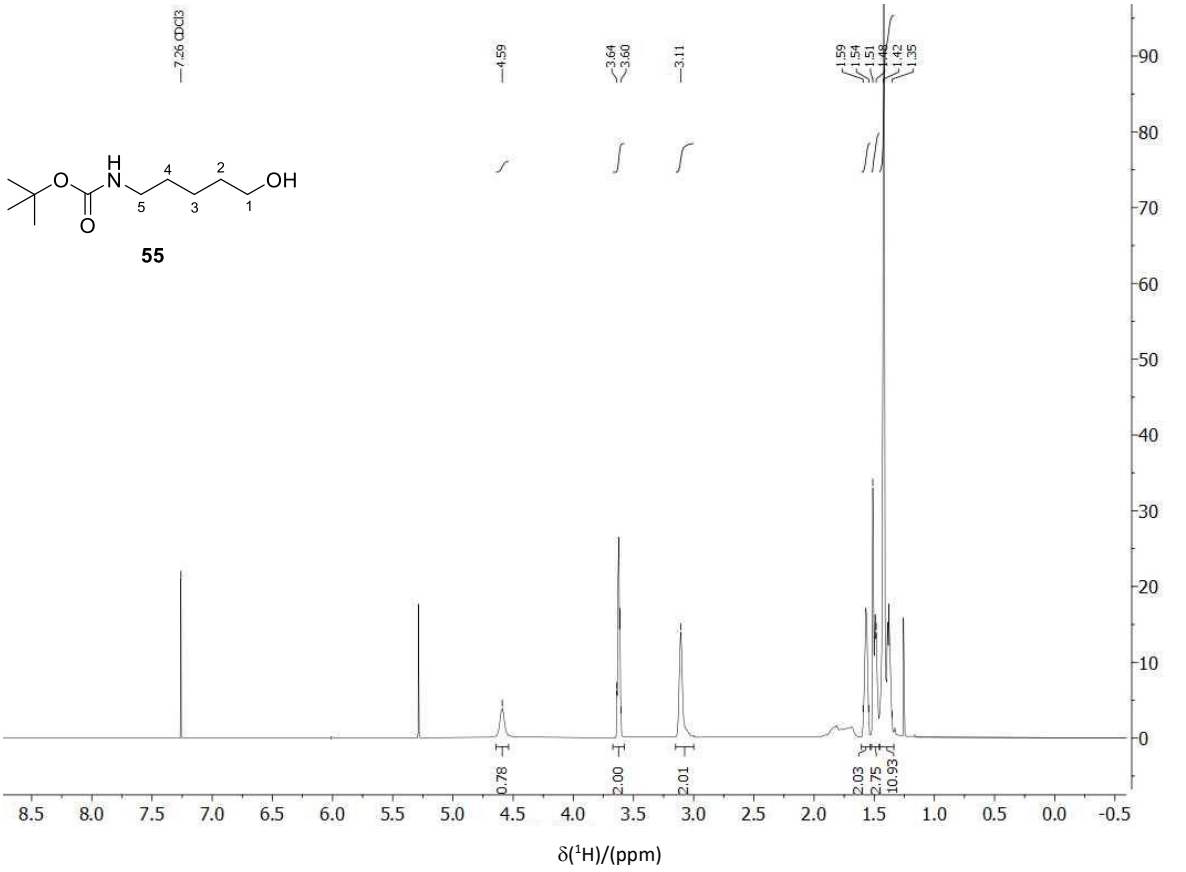
7.26 CDCl3
4.59
3.64
3.60
3.11
1.59
1.54
1.51
1.48
1.42
1.35
0.78
2.00
2.01
2.03
2.75
10.93
δ(1H)/(ppm)

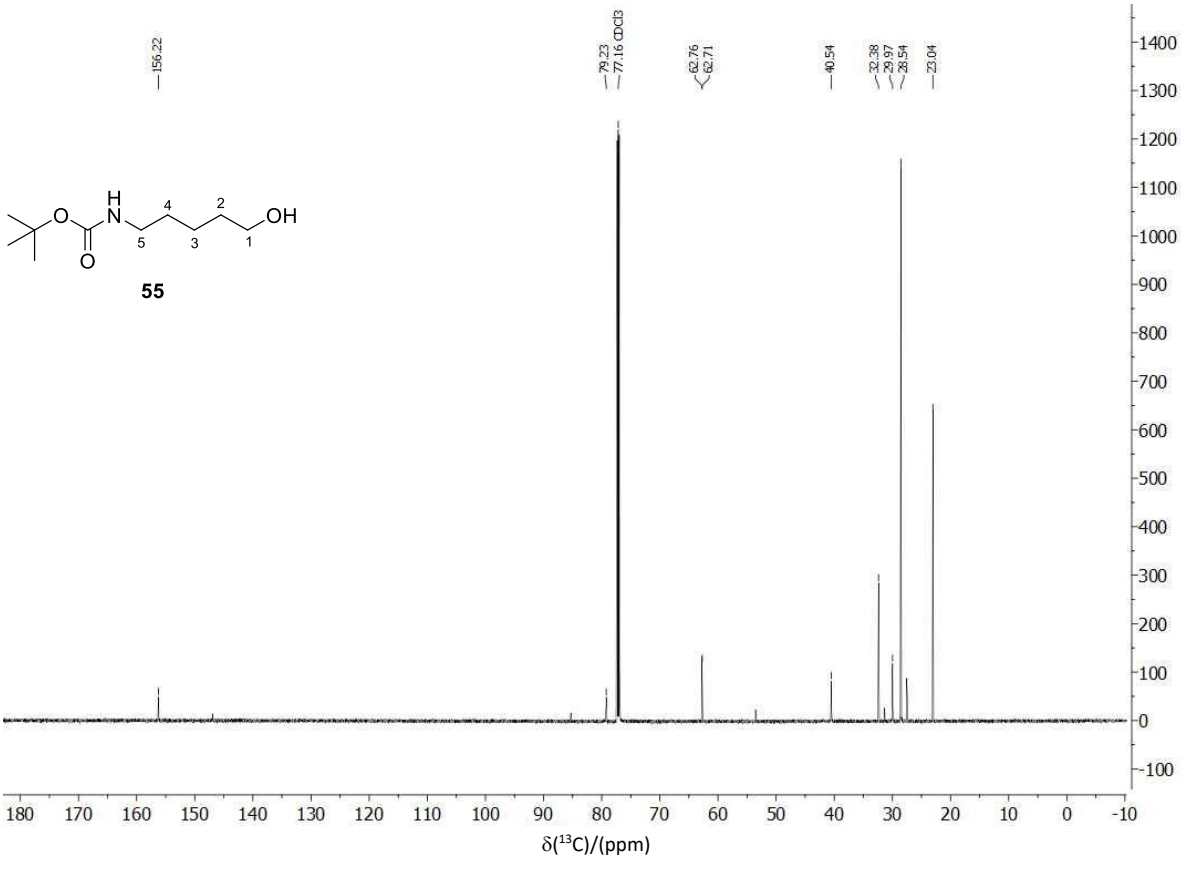
156.22
79.23
77.16 CDCl3
62.76
62.71
40.54
32.38
29.97
28.54
23.04
δ(13C)/(ppm)

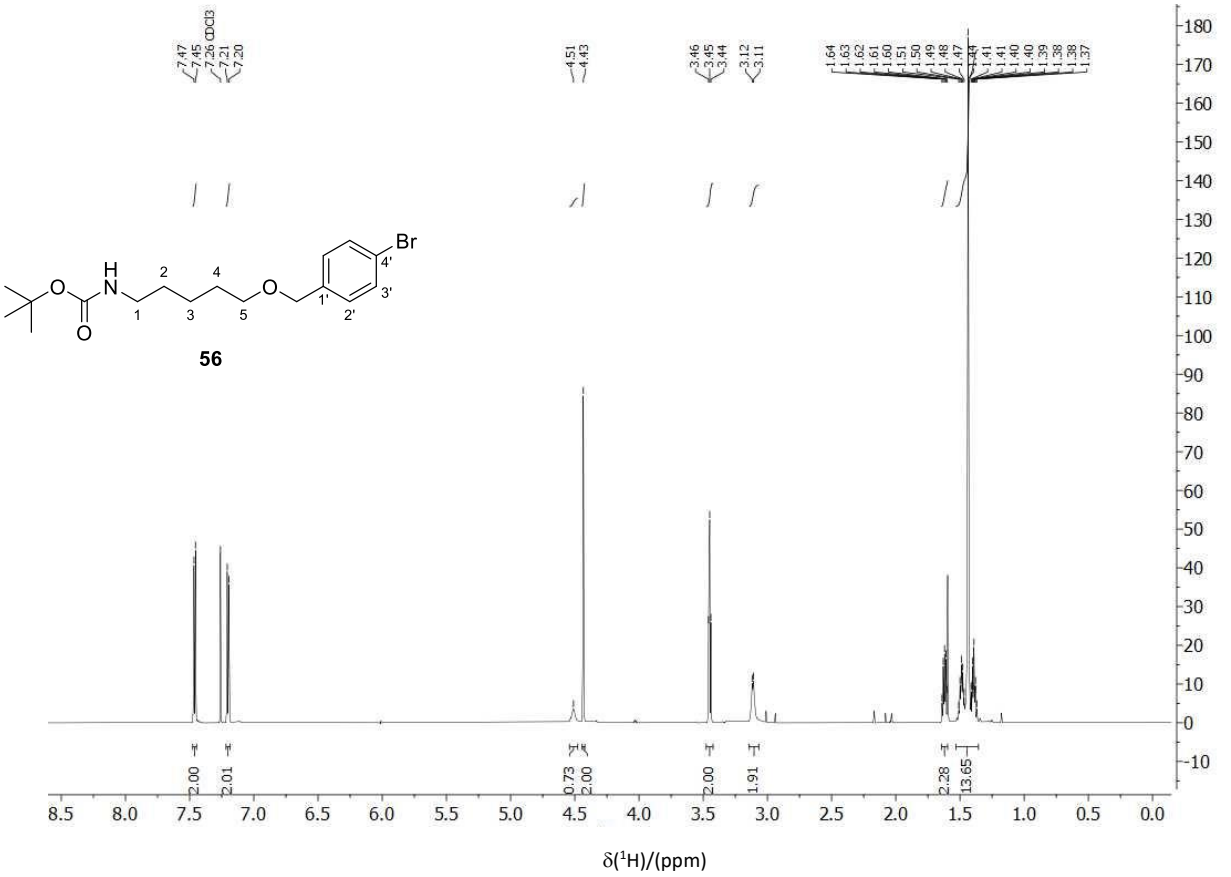
7.47
7.45
7.26 CDCl3
7.21
7.20
4.51
4.43
3.46
3.45
3.44
3.12
3.11
1.64
1.63
1.62
1.61
1.60
1.51
1.50
1.49
1.48
1.47
1.44
1.41
1.40
1.39
1.38
1.37
Br
4'
3'
H
N
O
O
O
1
2
3
4
5
1'
2'
56
2.00
2.01
0.73
2.00
2.00
1.91
2.28
13.65
δ(¹H)/(ppm)

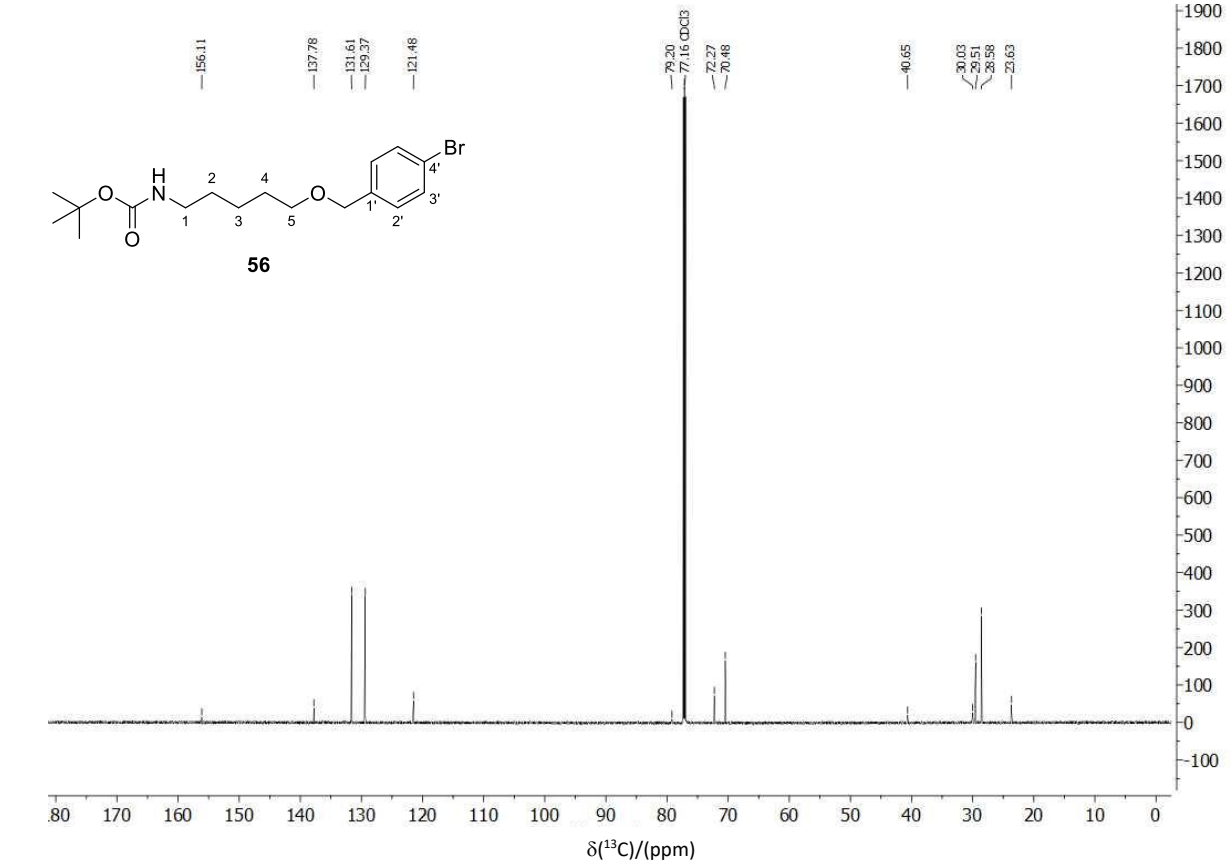
156.11
137.78
131.61
129.37
121.48
79.20
77.16 CDCl3
72.27
70.48
40.65
30.03
29.51
28.58
23.63
Br
4'
3'
H
N
O
O
O
1
2
3
4
5
1'
2'
56
δ(¹³C)/(ppm)

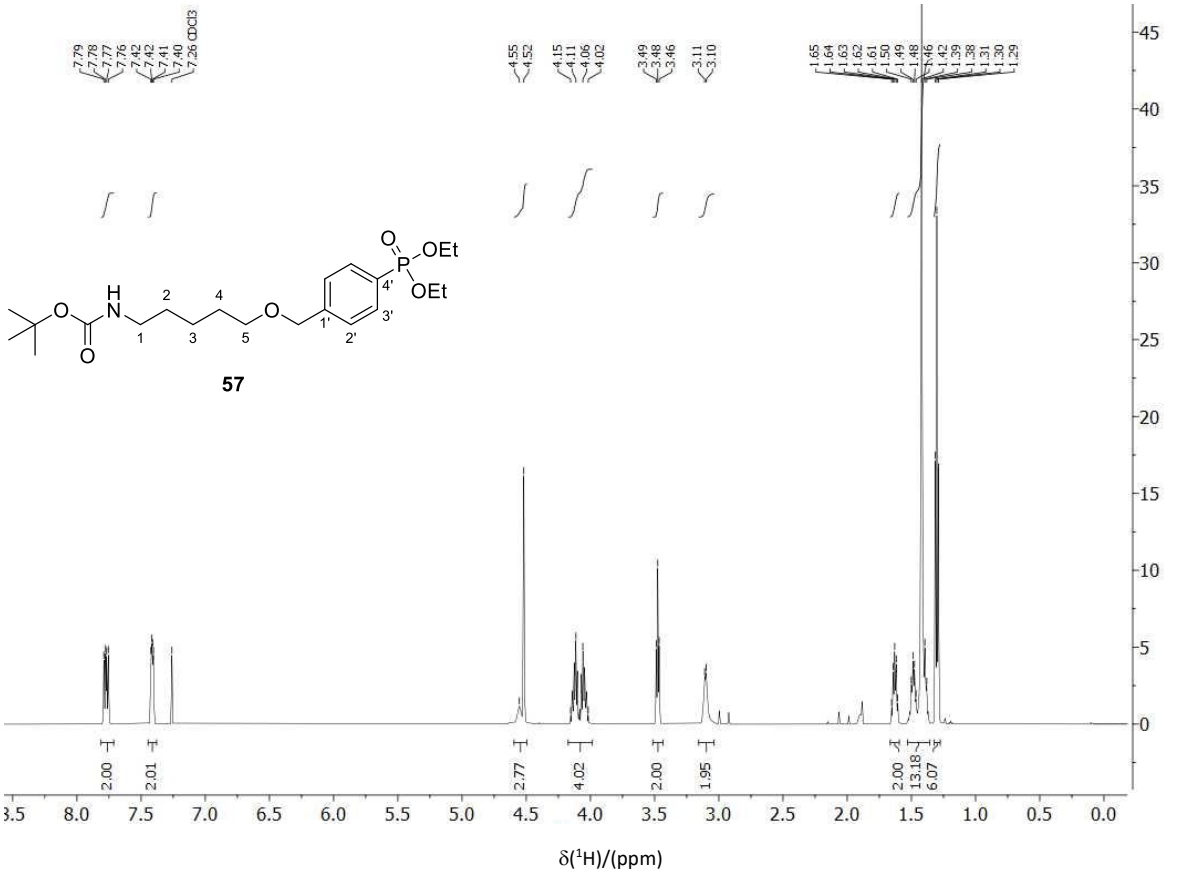
7.79
7.78
7.77
7.76
7.42
7.42
7.41
7.40
7.26 CDCl3
4.55
4.52
4.15
4.11
4.06
4.02
3.49
3.48
3.46
3.11
3.10
1.65
1.64
1.63
1.62
1.61
1.50
1.49
1.48
1.46
1.42
1.39
1.38
1.31
1.30
1.29
2.00
2.01
2.77
4.02
2.00
1.95
2.00
13.18
6.07
δ(1H)/(ppm)

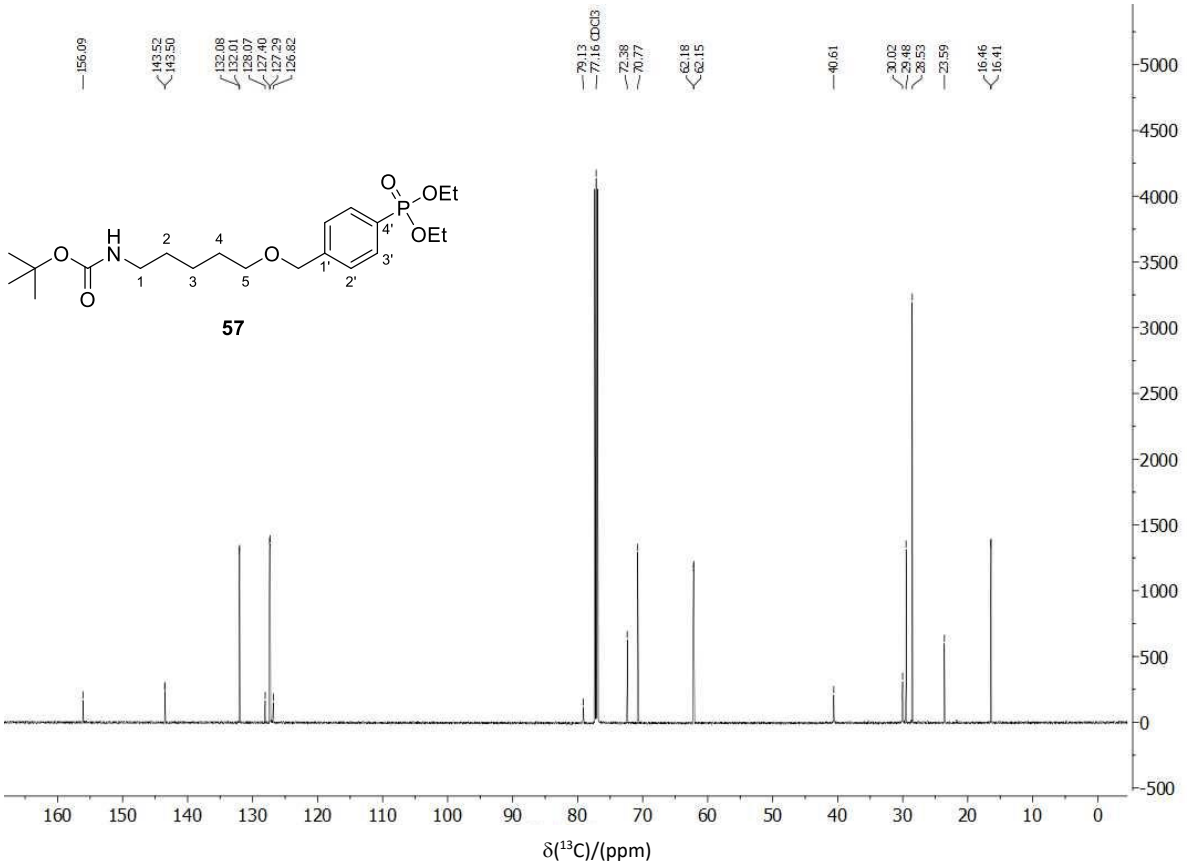
156.09
143.52
143.50
132.08
132.01
128.07
127.40
127.29
126.82
79.13
77.16 CDCl3
72.38
70.77
62.18
62.15
40.61
30.02
29.48
28.53
23.59
16.46
16.41
δ(13C)/(ppm)

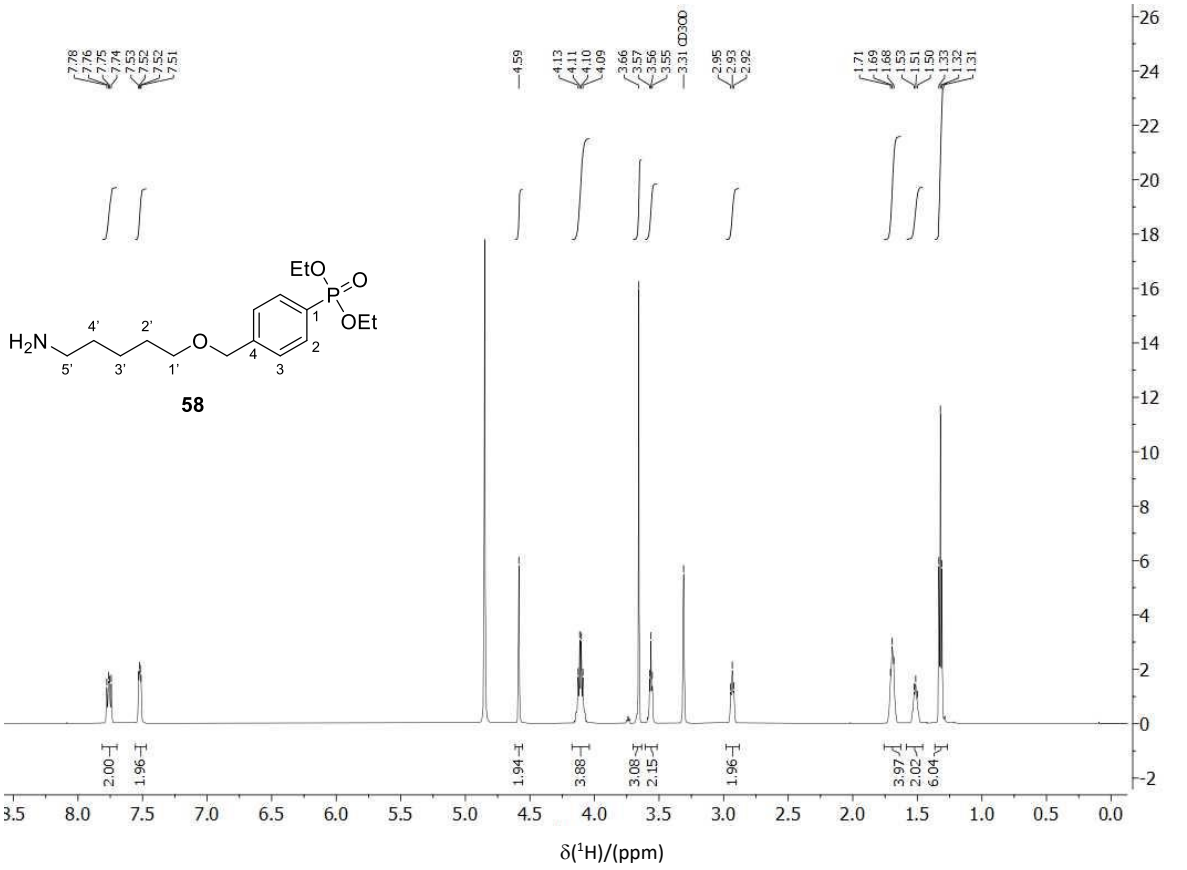
7.78
7.76
7.75
7.74
7.53
7.52
7.52
7.51
4.59
4.13
4.11
4.10
4.09
3.66
3.57
3.56
3.55
3.31
2.95
2.93
2.92
1.71
1.69
1.68
1.53
1.51
1.50
1.33
1.32
1.31
EtO
P
O
OEt
H2N
O
2.00
1.96
1.94
3.88
3.08
2.15
1.96
3.97
2.02
6.04
δ(1H)/(ppm)

58

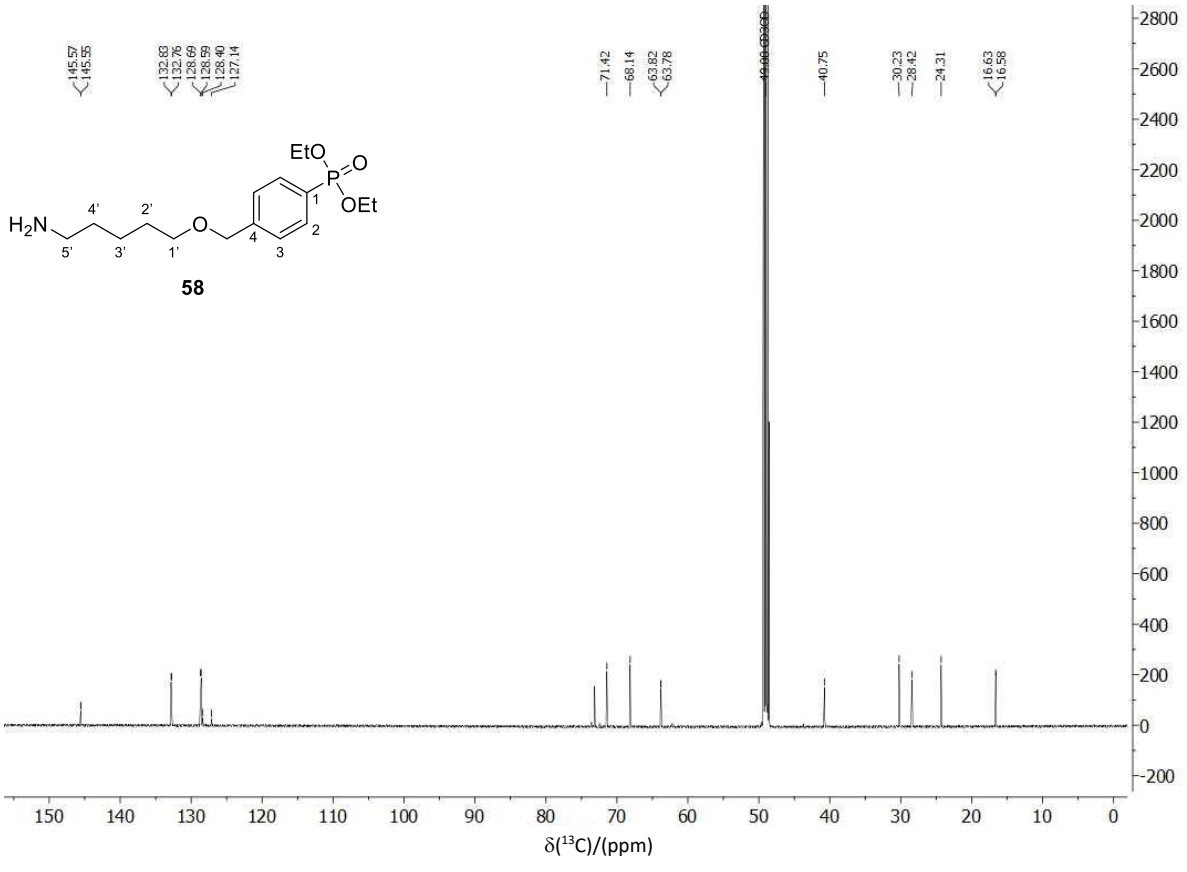
145.57
145.55
132.83
132.76
128.69
128.59
128.40
127.14
71.42
68.14
63.82
63.78
40.75
30.23
28.42
24.31
16.63
16.58
EtO
P
O
OEt
H2N
O
δ(13C)/(ppm)

58

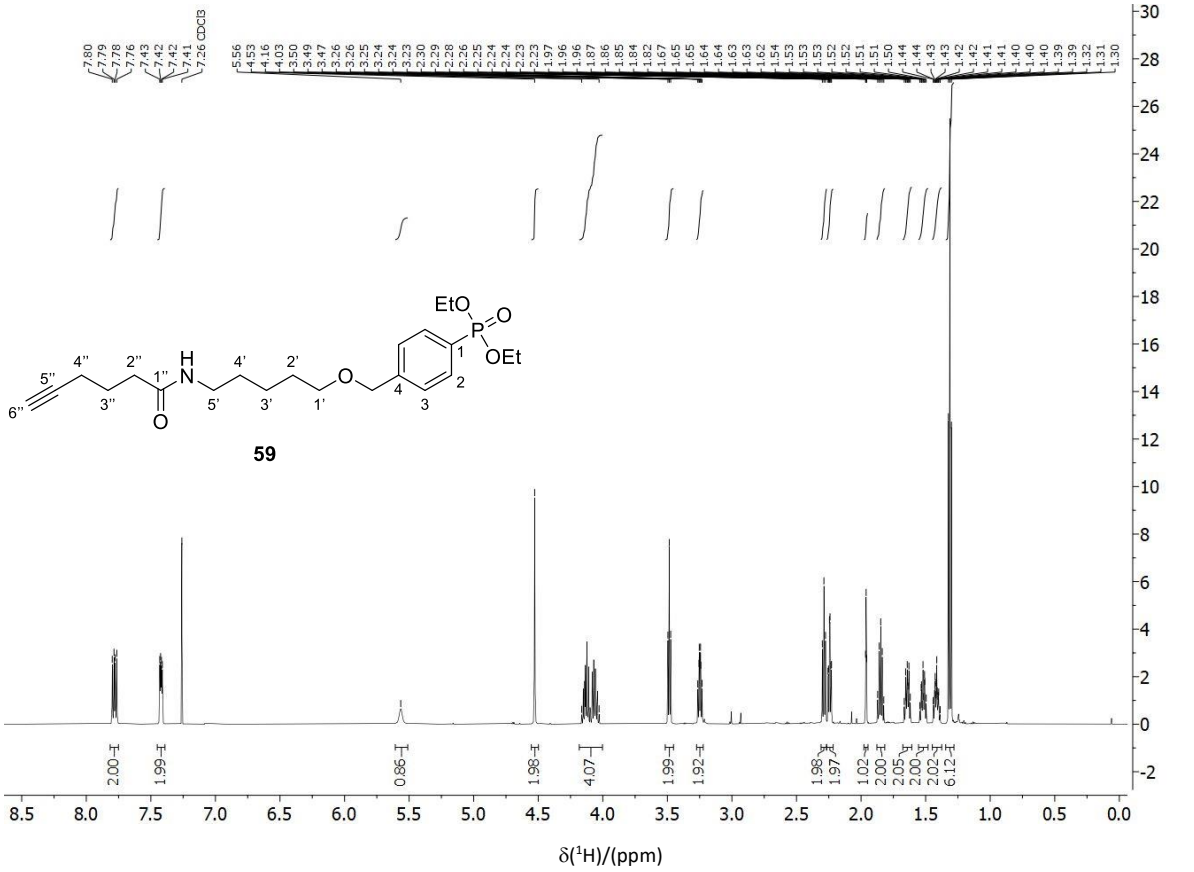
59
δ(¹H)/(ppm)

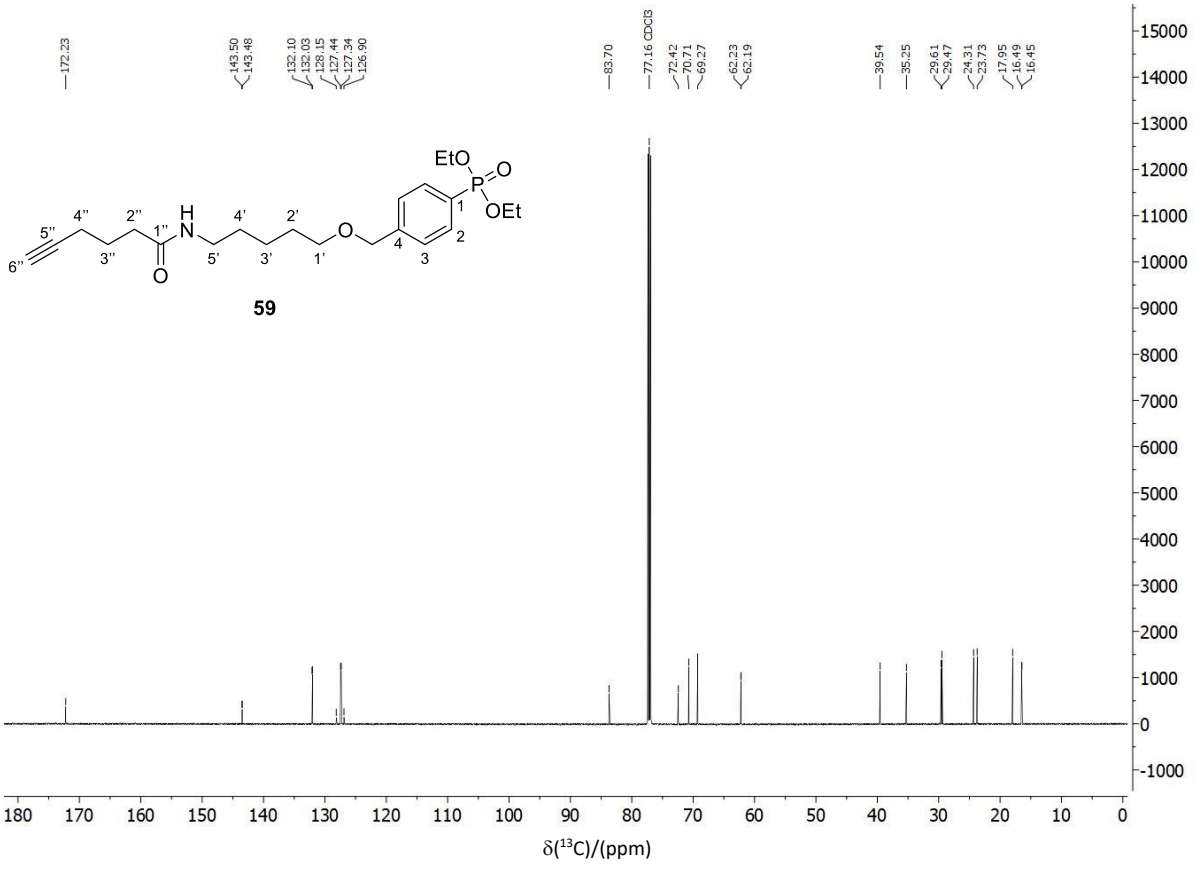
59
δ(¹³C)/(ppm)

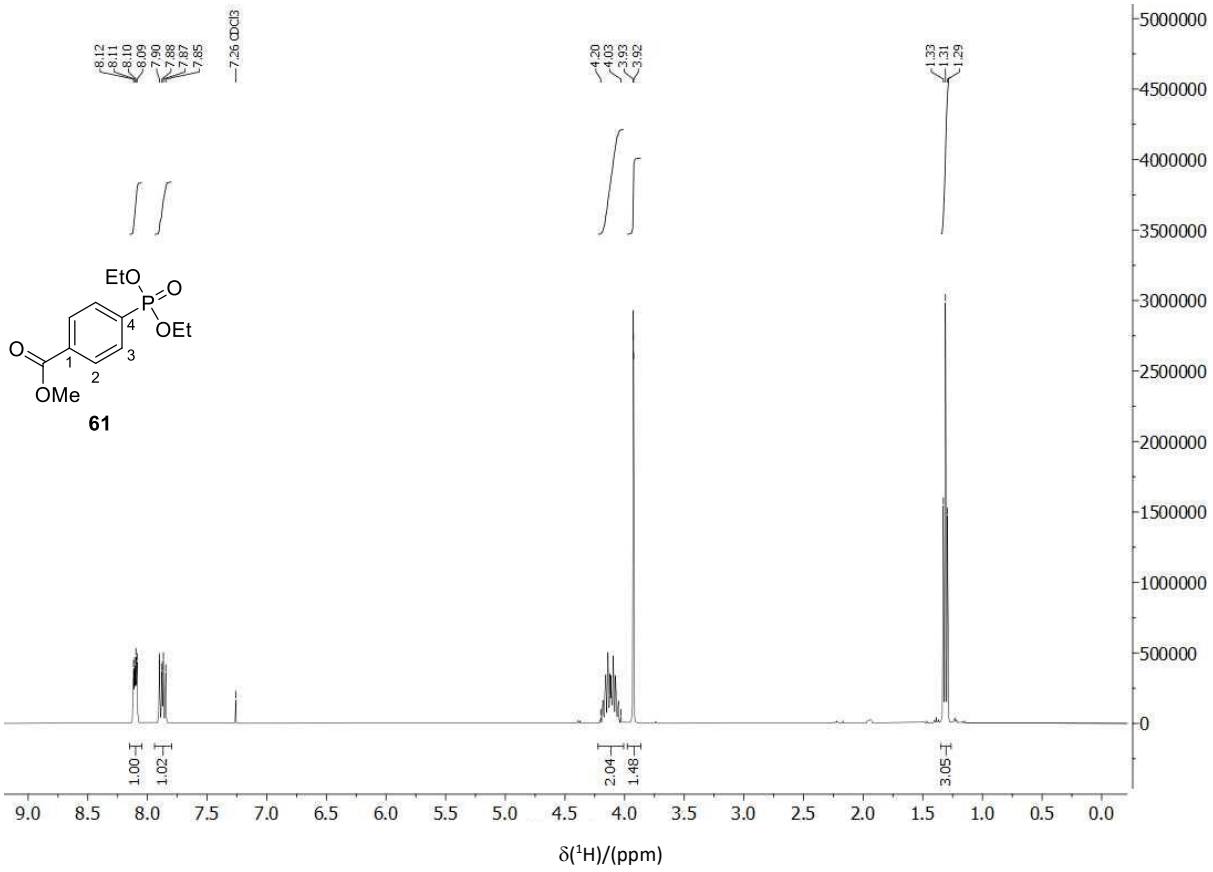
8.12
8.11
8.10
8.09
7.90
7.88
7.87
7.85
7.26 CDCl3
4.20
4.03
3.93
3.92
1.33
1.31
1.29
EtO
P
O
OEt
4
3
O
1
2
OMe
61
1.00
1.02
2.04
1.48
3.05
δ(1H)/(ppm)

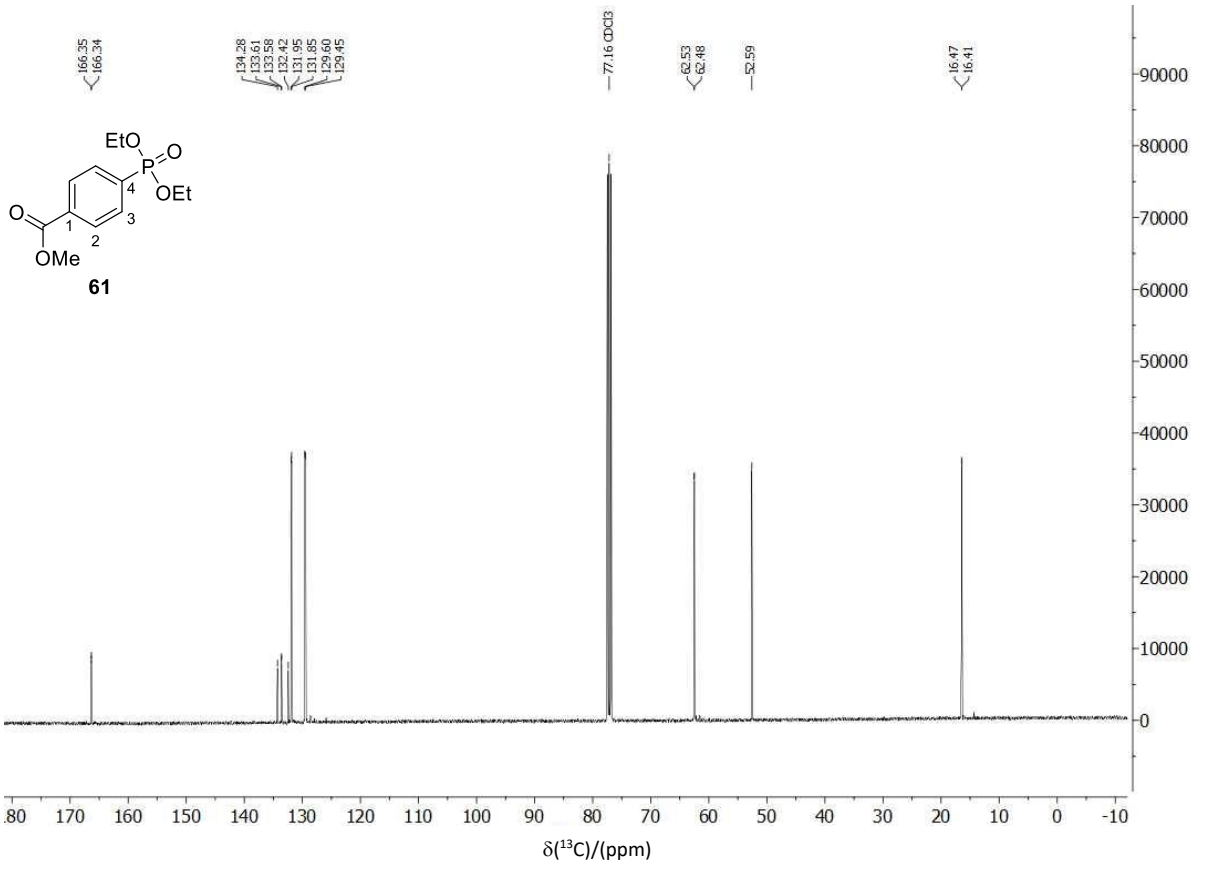
166.35
166.34
134.28
133.61
133.58
132.42
131.95
131.85
129.60
129.45
77.16 CDCl3
62.53
62.48
52.59
16.47
16.41
EtO
P
O
OEt
4
3
O
1
2
OMe
61
δ(13C)/(ppm)

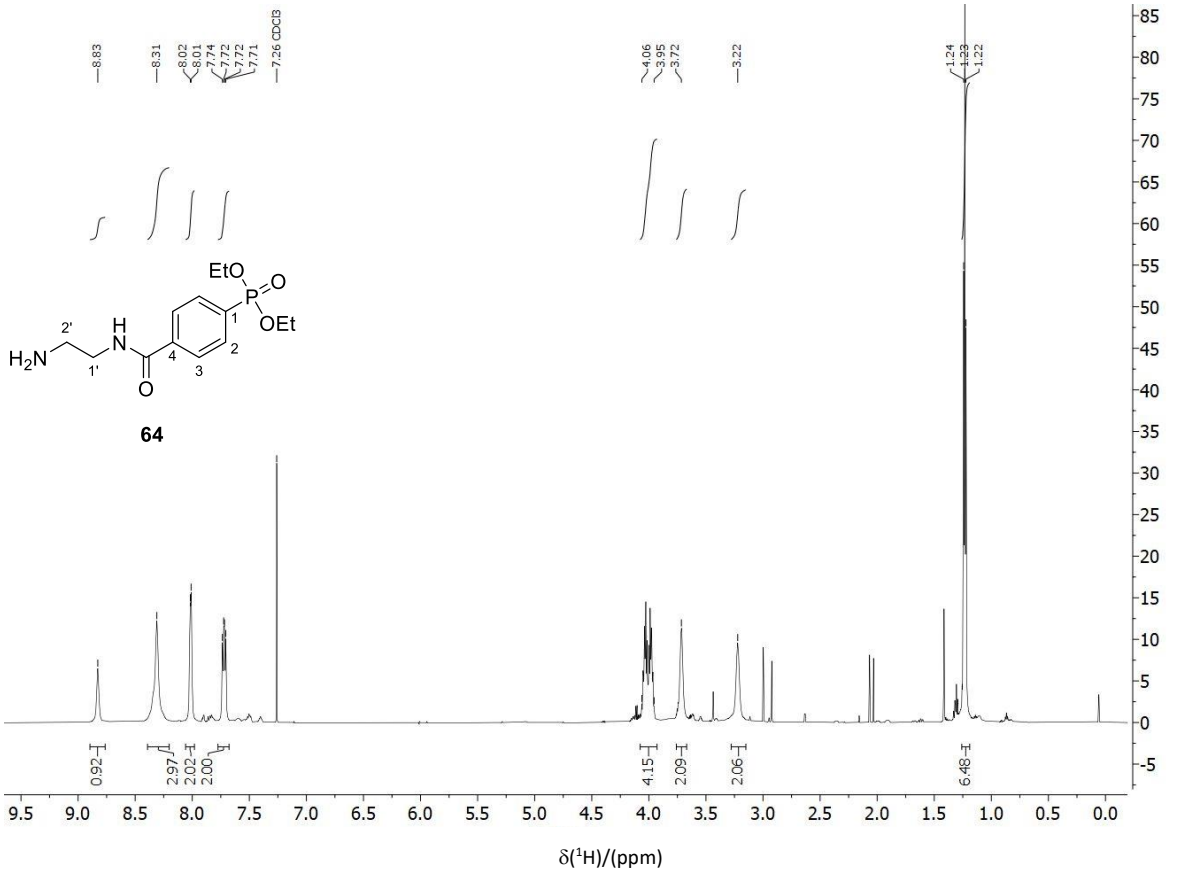
8.83
8.31
8.02
8.01
7.74
7.72
7.72
7.71
7.26 CDCl3
4.06
3.95
3.72
3.22
1.24
1.23
1.22
EtO
P
O
OEt
H
N
2'
1'
H2N
1
2
3
4
O
64
0.92
2.97
2.02
2.00
4.15
2.09
2.06
6.48
δ(1H)/(ppm)

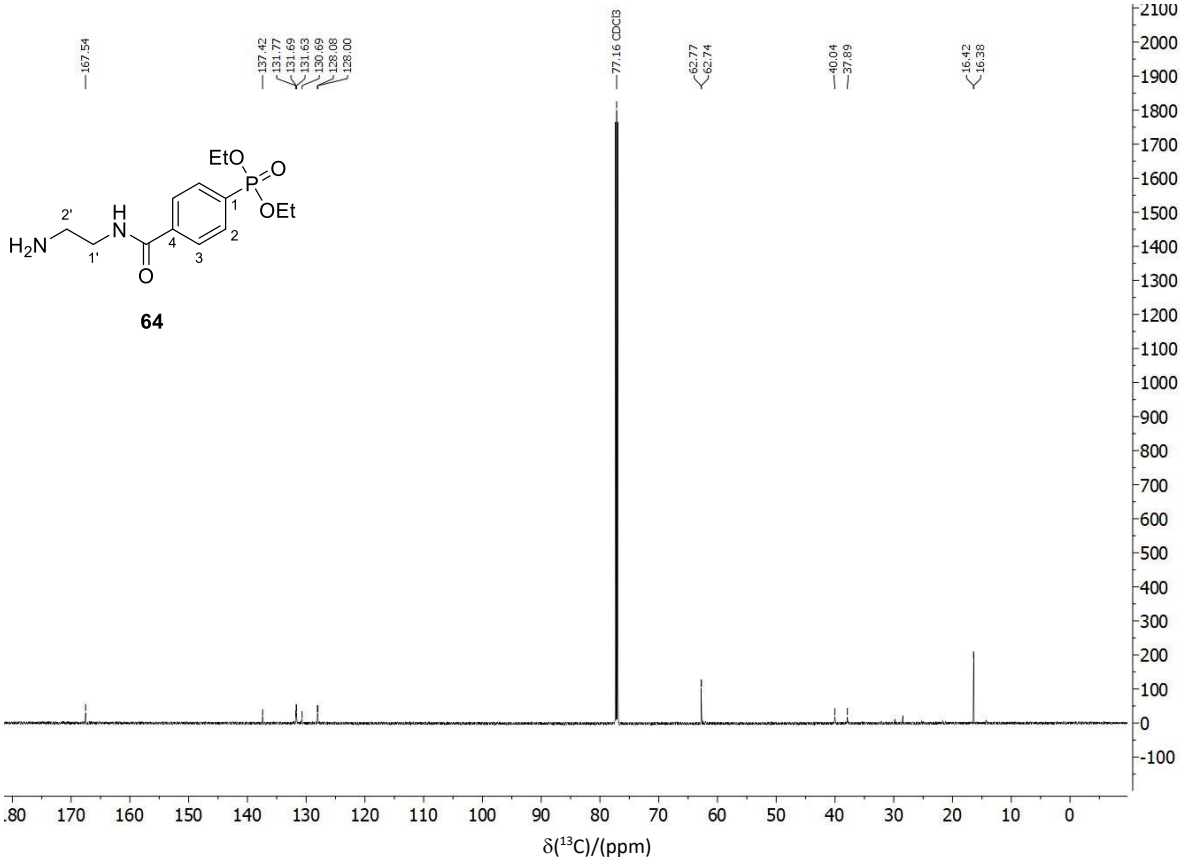
167.54
137.42
131.77
131.69
131.63
130.69
128.08
128.00
77.16 CDCl3
62.77
62.74
40.04
37.89
16.42
16.38
EtO
P
O
OEt
H
N
2'
1'
H2N
1
2
3
4
O
64
δ(13C)/(ppm)

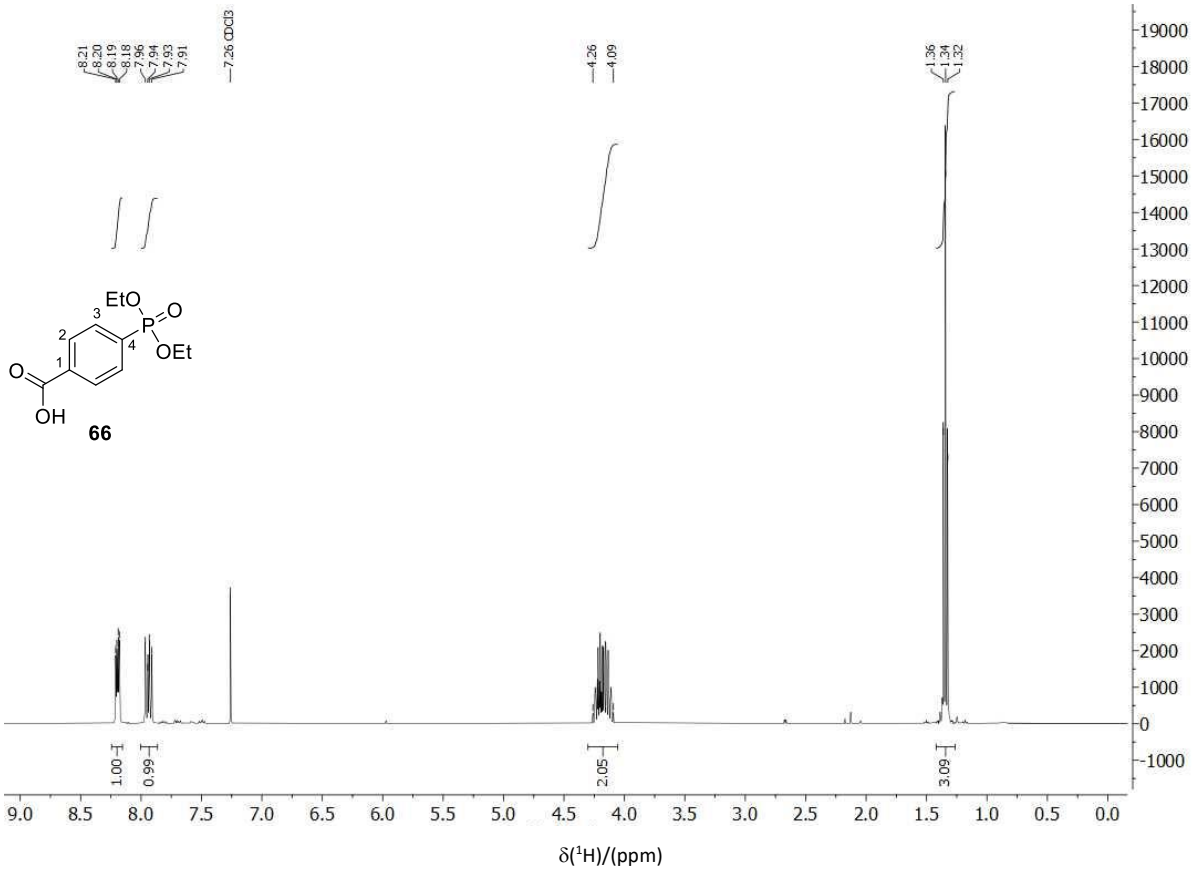
8.21
8.20
8.19
8.18
7.96
7.94
7.93
7.91
7.26 CDCl3
4.26
4.09
1.36
1.34
1.32
EtO
P
O
OEt
O
OH
1
2
3
4
66
1.00
0.99
2.05
3.09
δ(1H)/(ppm)

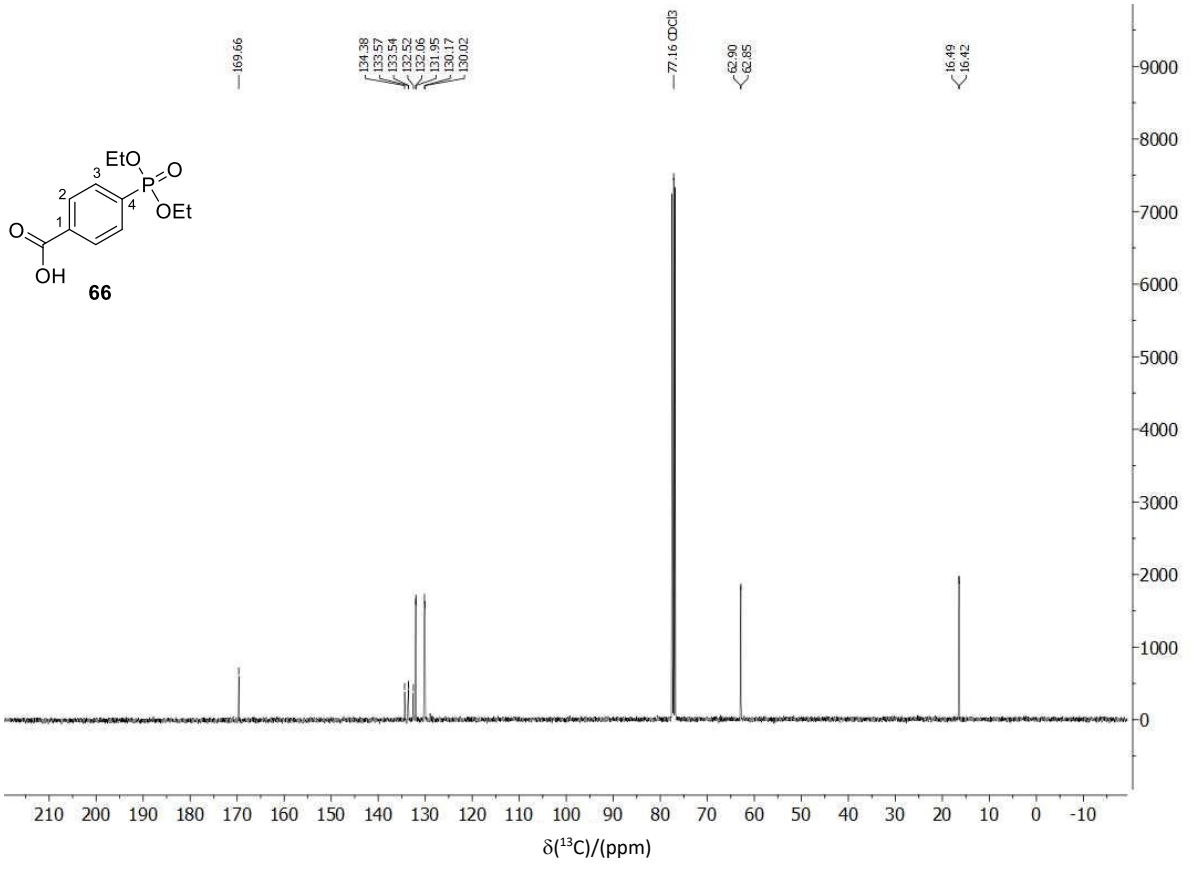
169.66
134.38
133.57
133.54
132.52
132.06
131.95
130.17
130.02
77.16 CDCl3
62.90
62.85
16.49
16.42
EtO
P
O
OEt
O
OH
1
2
3
4
66
δ(13C)/(ppm)

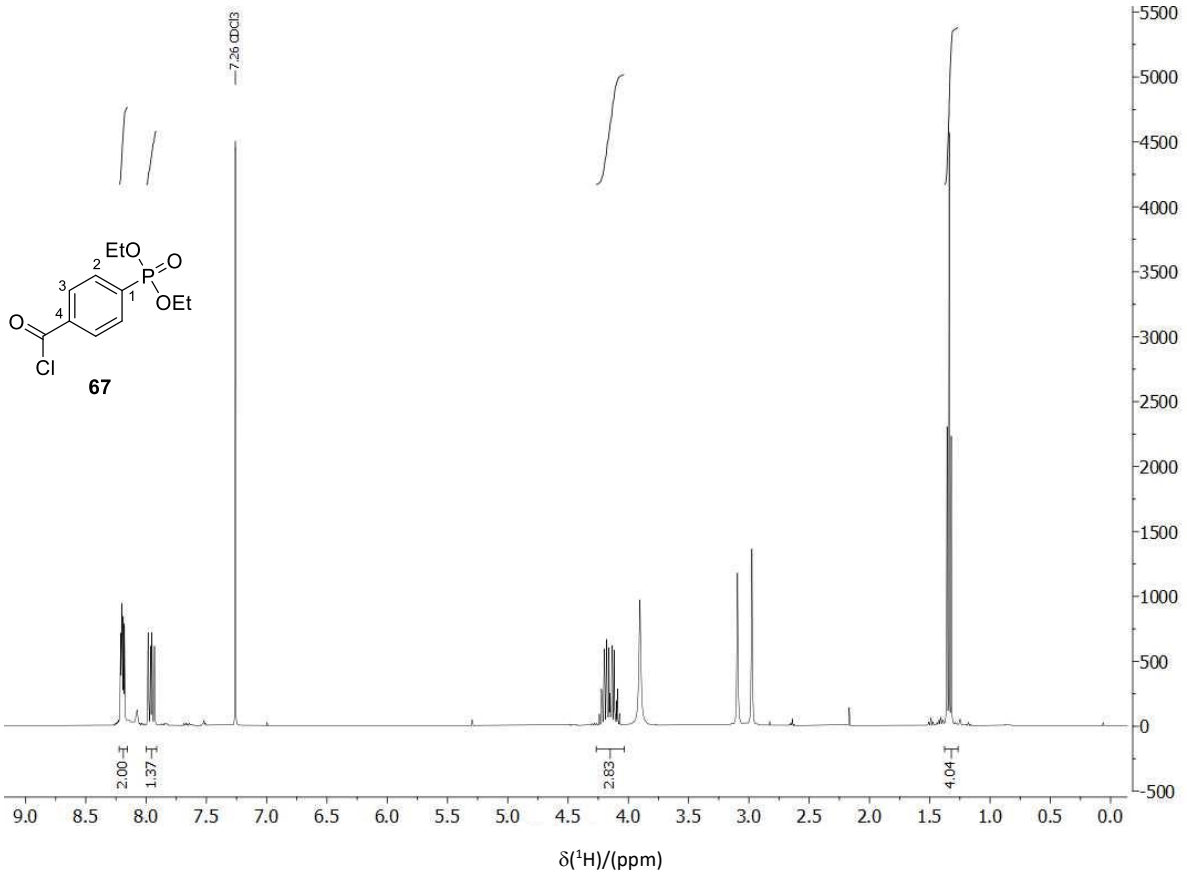
7.26 CDCl3
EtO
O
P
OEt
O
Cl
1
2
3
4
67
2.00
1.37
2.83
4.04
δ(¹H)/(ppm)

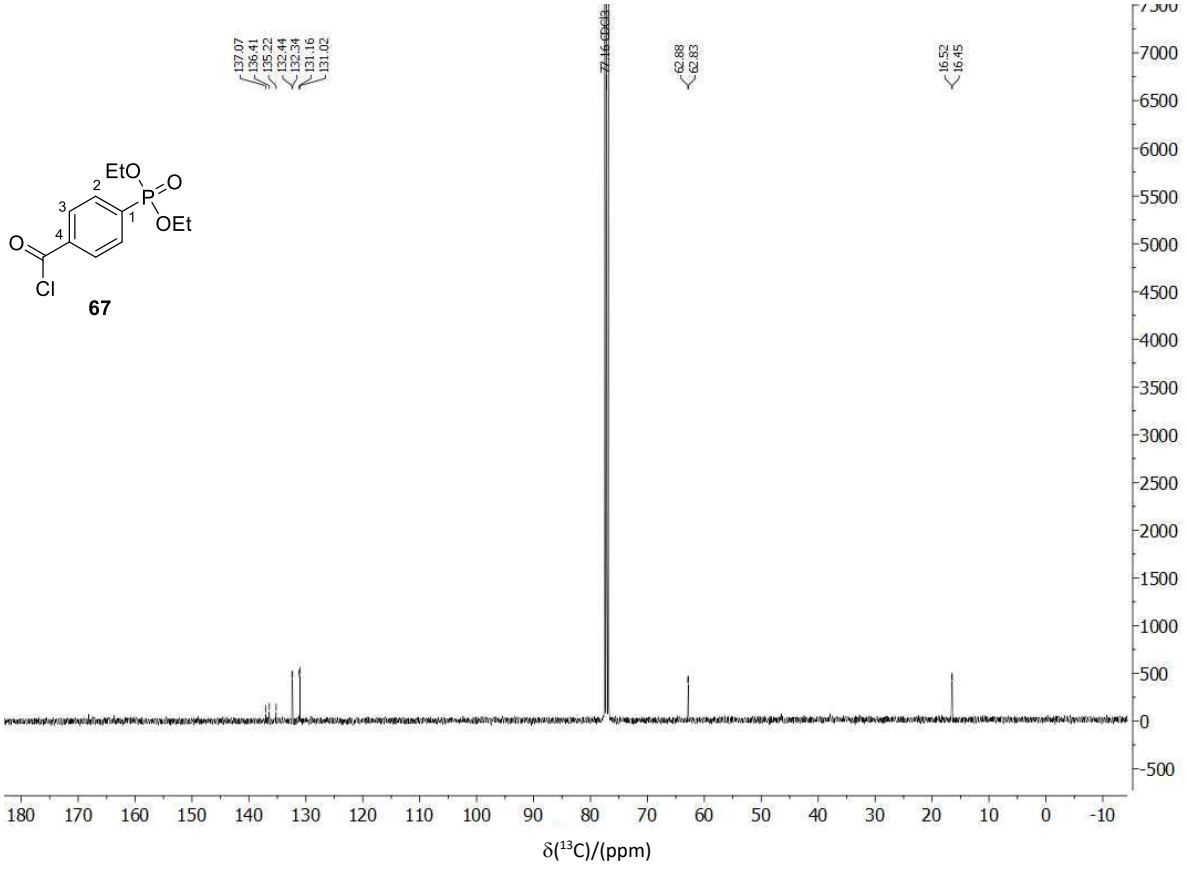
137.07
136.41
135.22
132.44
132.34
131.16
131.02
77.16 CDCl3
62.88
62.83
16.52
16.45
EtO
O
P
OEt
O
Cl
1
2
3
4
67
δ(¹³C)/(ppm)

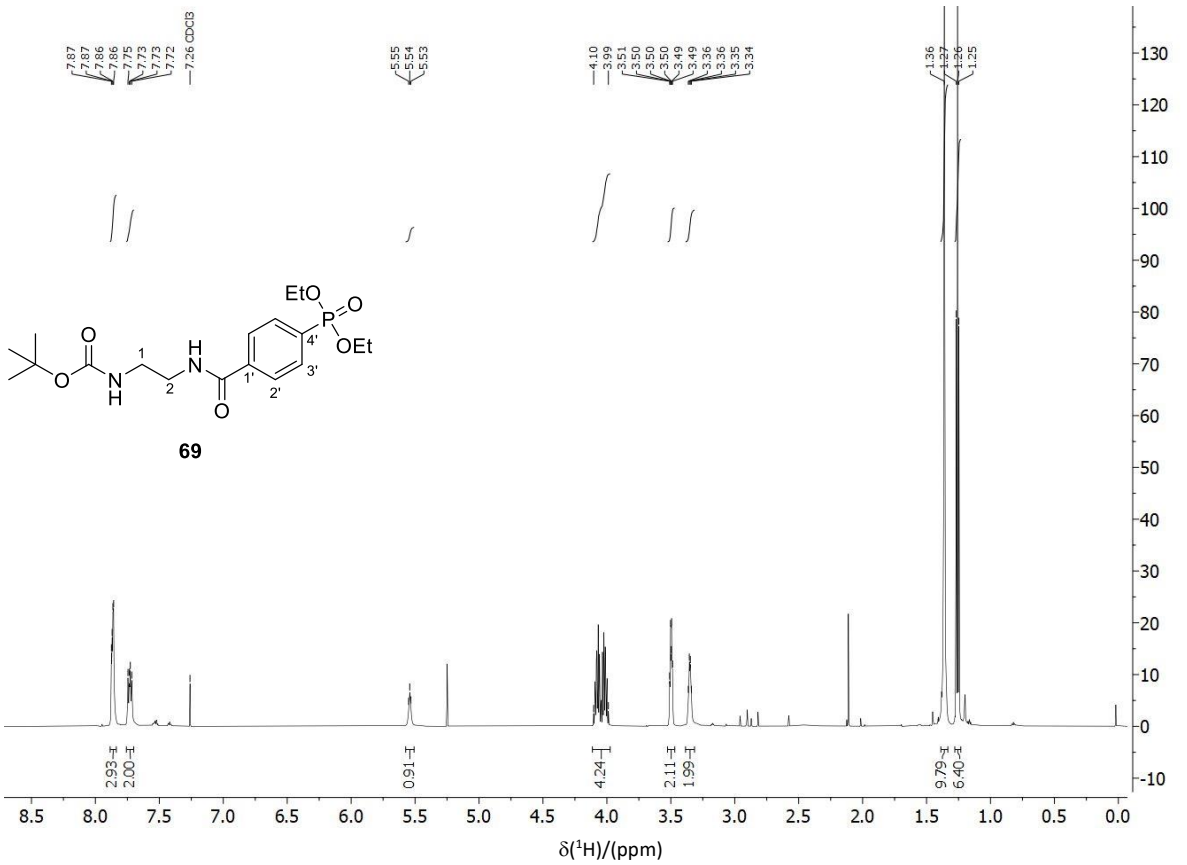
7.87
7.87
7.86
7.86
7.75
7.73
7.73
7.72
7.26 CDCl3
5.55
5.54
5.53
4.10
3.99
3.51
3.50
3.50
3.50
3.49
3.36
3.36
3.35
3.34
1.36
1.27
1.26
1.25
EtO
P
O
OEt
4'
3'
1'
2'
1
2
H
N
O
O
O
N
H
69
2.93
2.00
0.91
4.24
2.11
1.99
9.79
6.40
δ(1H)/(ppm)

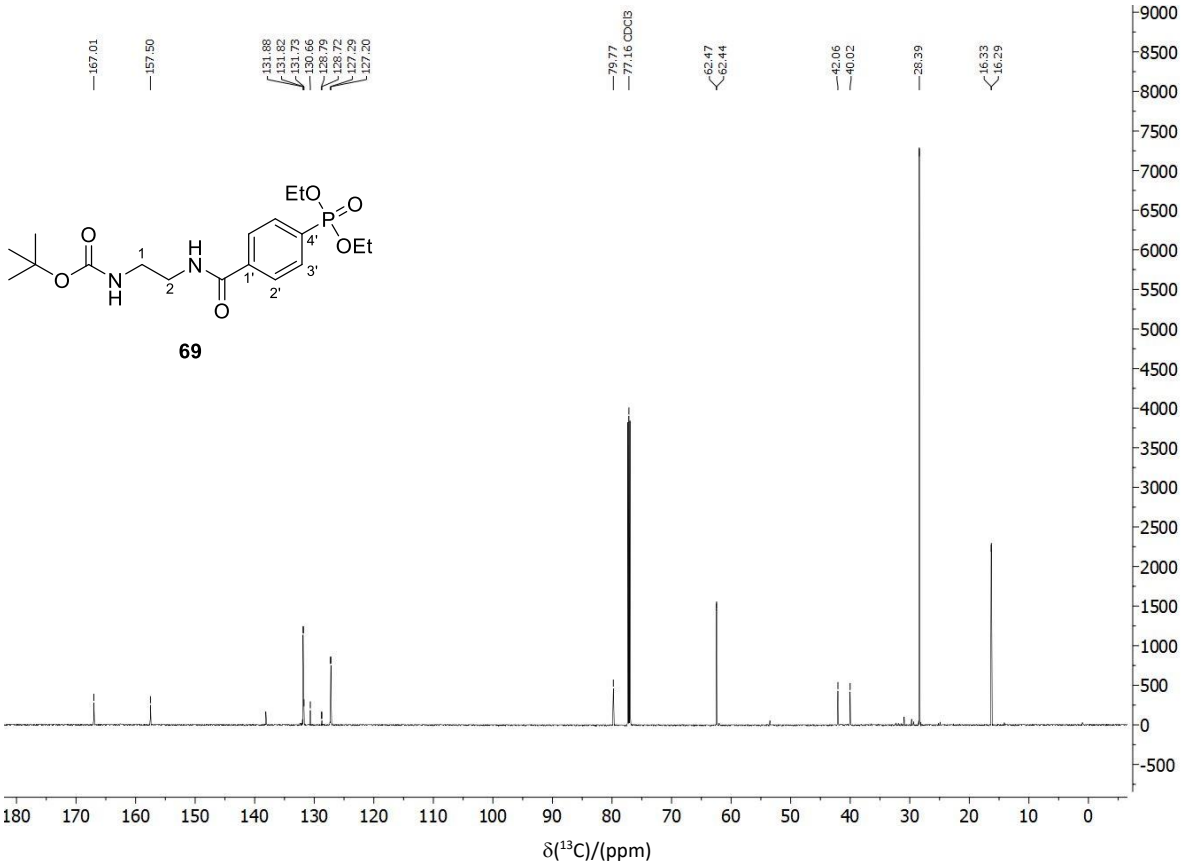
167.01
157.50
131.88
131.82
131.73
130.66
128.79
128.72
127.29
127.20
79.77
77.16 CDCl3
62.47
62.44
42.06
40.02
28.39
16.33
16.29
EtO
P
O
OEt
4'
3'
1'
2'
1
2
H
N
O
O
O
N
H
69
δ(13C)/(ppm)

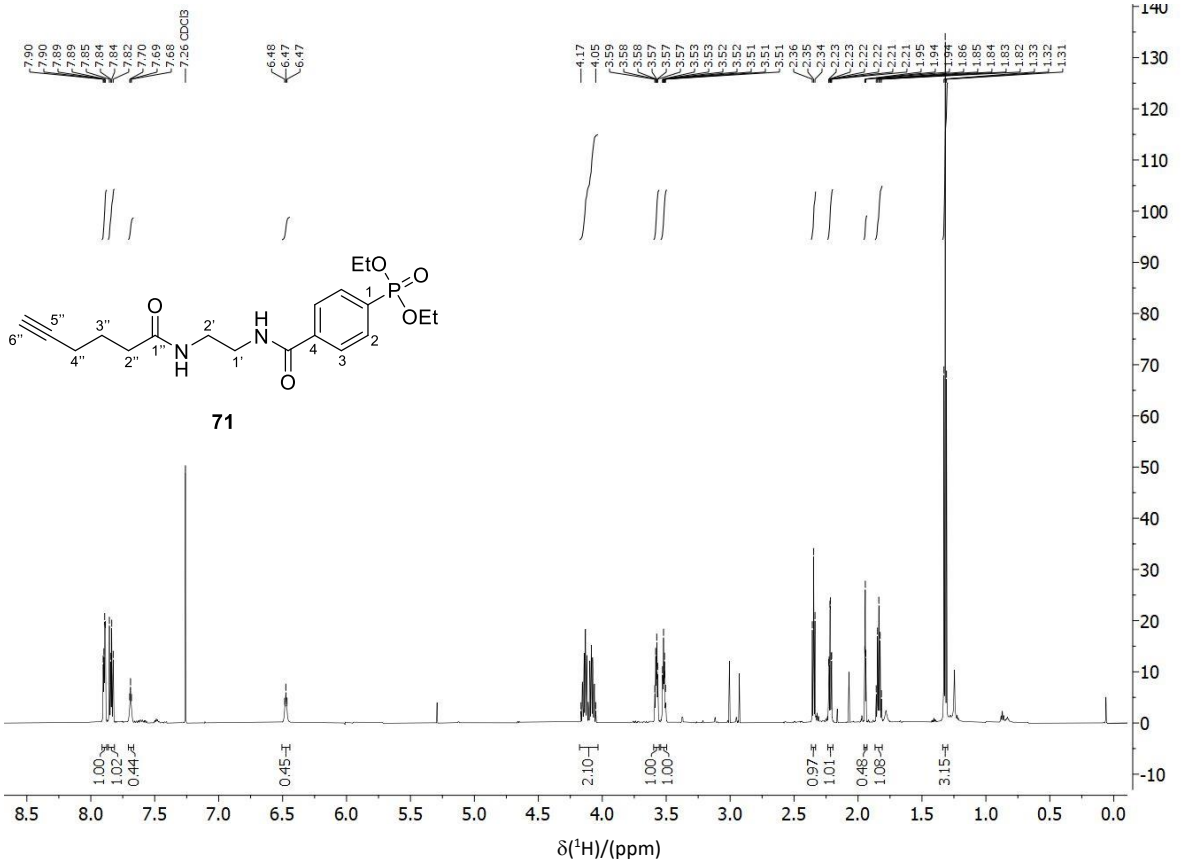
7.90
7.90
7.89
7.89
7.85
7.84
7.84
7.82
7.70
7.69
7.68
7.26 CDCl3
6.48
6.47
6.47
4.17
4.05
3.59
3.58
3.58
3.57
3.57
3.57
3.53
3.53
3.52
3.52
3.51
3.51
3.51
2.36
2.35
2.34
2.23
2.22
2.22
2.21
2.21
1.95
1.94
1.94
1.86
1.85
1.84
1.83
1.82
1.33
1.32
1.31
EtO
P
O
OEt
1
2
3
4
5''
6''
3''
4''
2''
1''
2'
1'
N
H
O
71
1.00
1.02
0.44
0.45
2.10
1.00
1.00
0.97
1.01
0.48
1.08
3.15
δ(1H)/(ppm)

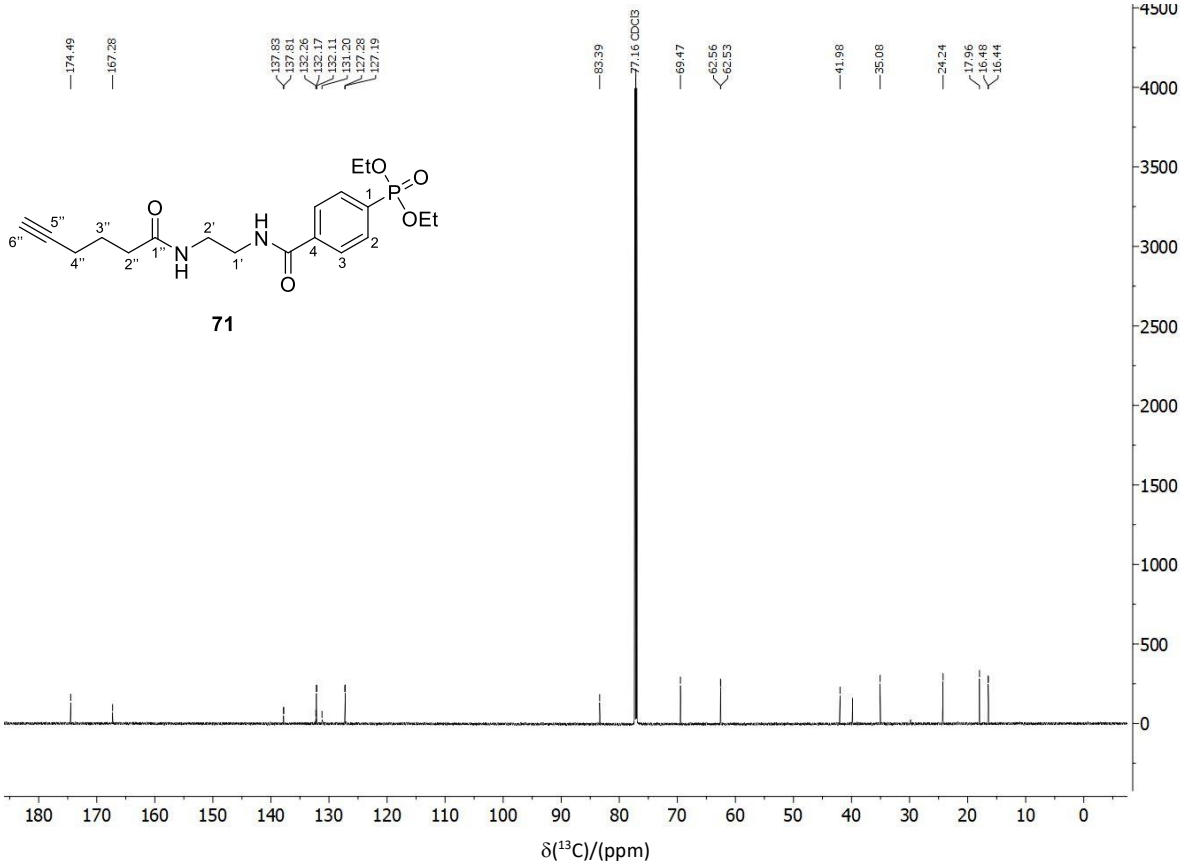
174.49
167.28
137.83
137.81
132.26
132.17
132.11
131.20
127.28
127.19
83.39
77.16 CDCl3
69.47
62.56
62.53
41.98
35.08
24.24
17.96
16.48
16.44
EtO
P
O
OEt
1
2
3
4
5''
6''
3''
4''
2''
1''
2'
1'
N
H
O
71
δ(13C)/(ppm)

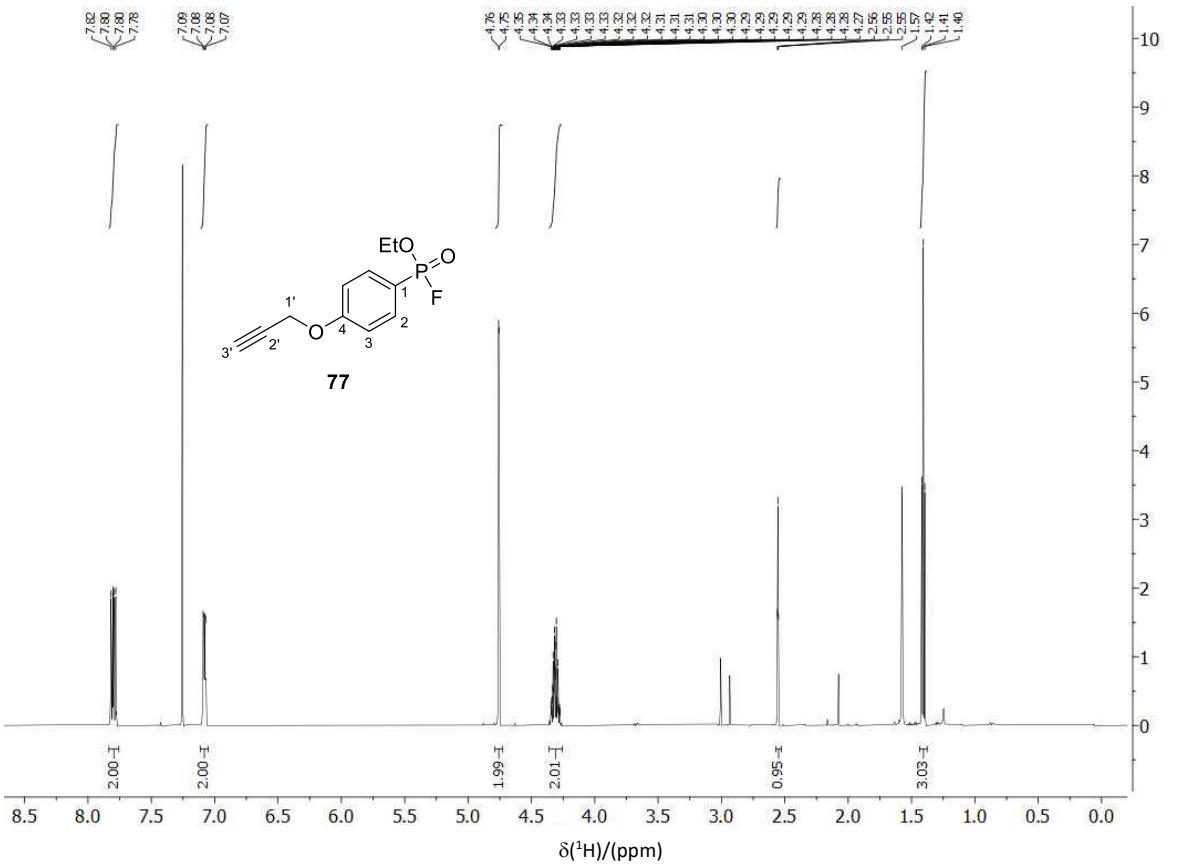
EtO
P
O
F
1
2
3
4
O
1'
2'
3'
77
δ(¹H)/(ppm)

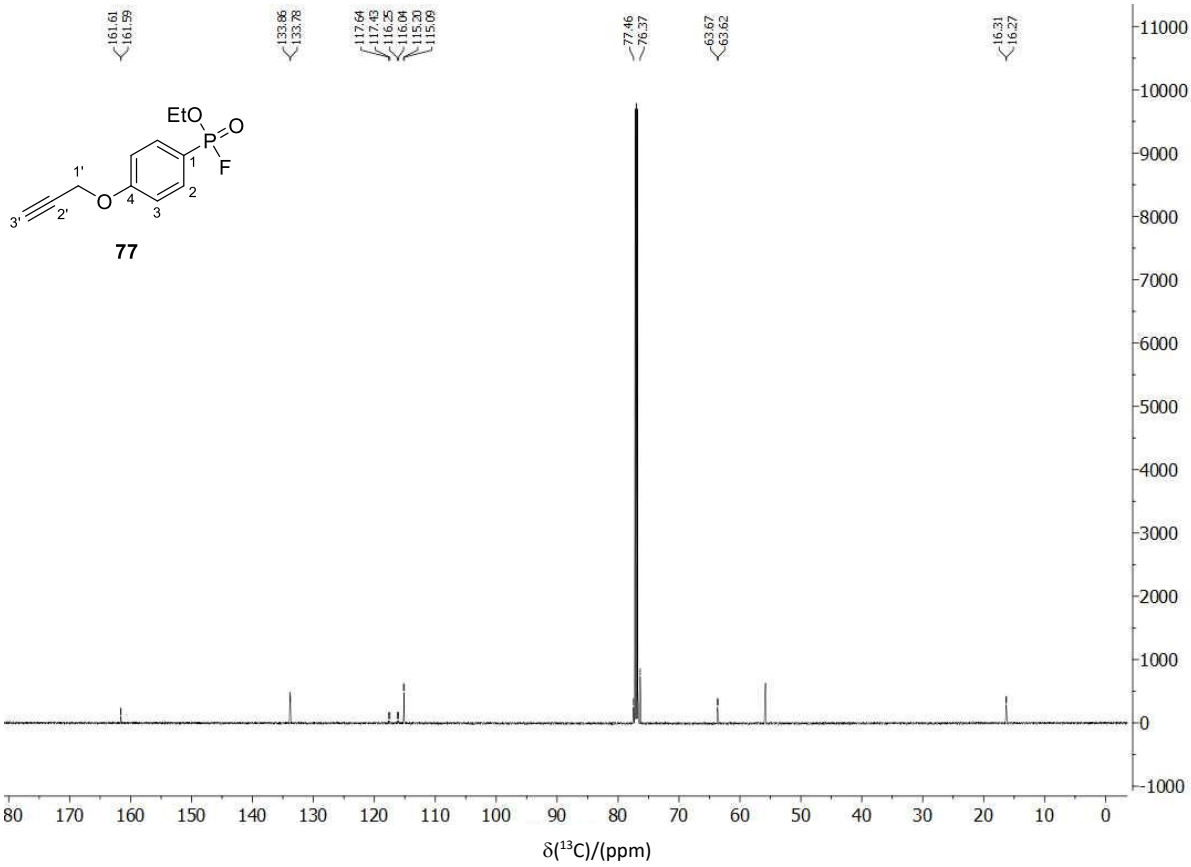
EtO
P
O
F
1
2
3
4
O
1'
2'
3'
77
δ(¹³C)/(ppm)

^{31}P NMR (162 MHz, $CDCl_3$)

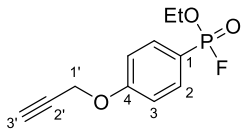

77

^{19}F NMR (376 MHz)

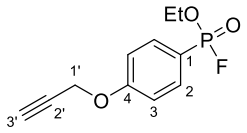

77

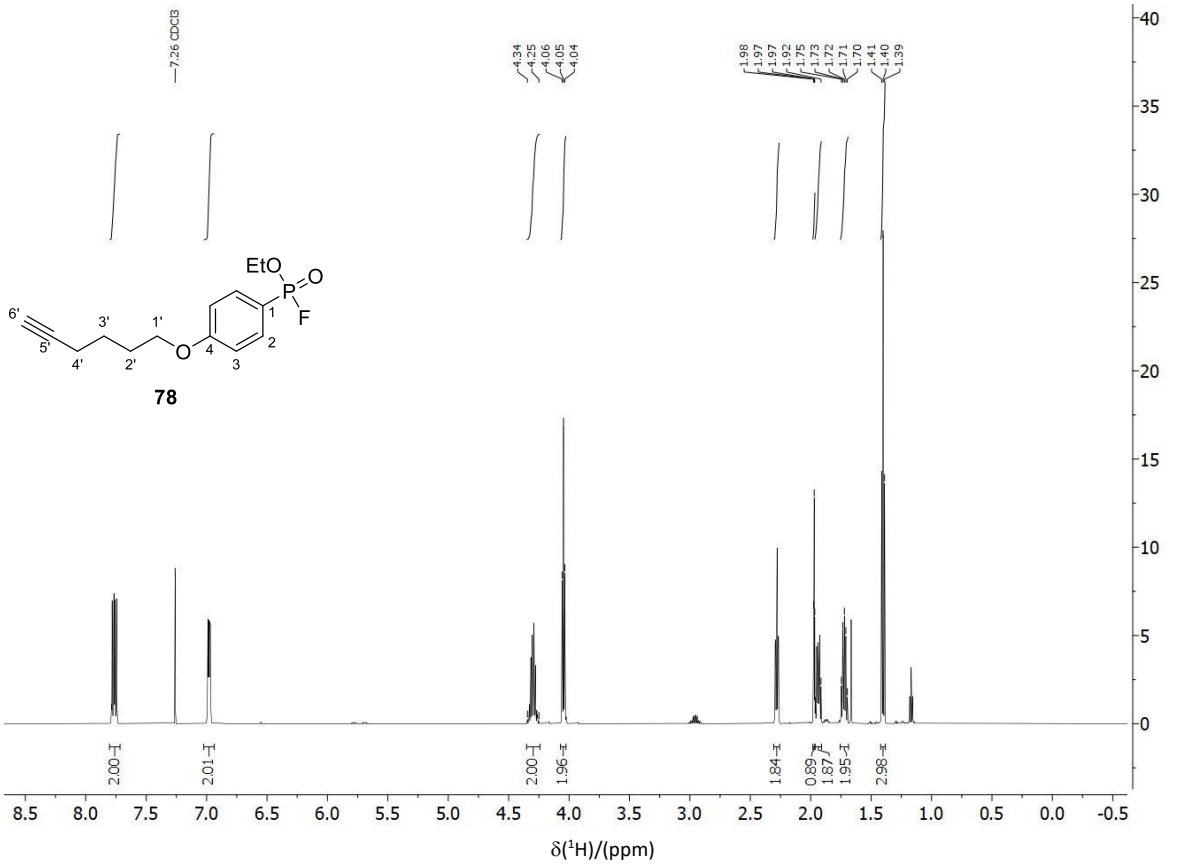
7.26 CDCl3
4.34
4.25
4.06
4.05
4.04
1.98
1.97
1.97
1.92
1.75
1.73
1.72
1.71
1.70
1.41
1.40
1.39
EtO
P
O
F
6'
5'
4'
3'
2'
1'
O
1
2
3
4
78
2.00
2.01
2.00
1.96
1.84
0.89
1.87
1.95
2.98
δ(1H)/(ppm)

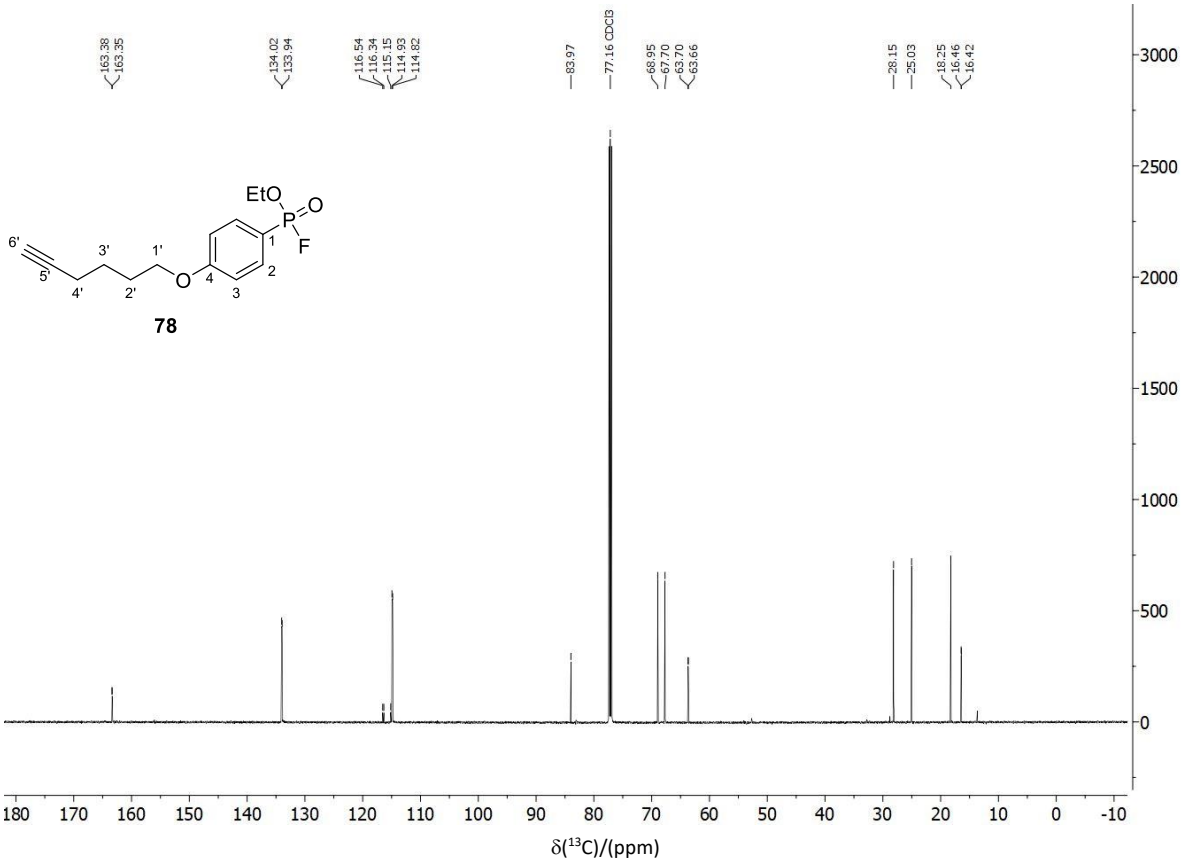
163.38
163.35
134.02
133.94
116.54
116.34
115.15
114.93
114.82
83.97
77.16 CDCl3
68.95
67.70
63.70
63.66
28.15
25.03
18.25
16.46
16.42
EtO
P
O
F
6'
5'
4'
3'
2'
1'
O
1
2
3
4
78
δ(13C)/(ppm)

^{31}P NMR (162 MHz, $CDCl_3$)

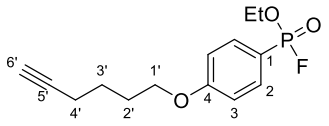

78

^{19}F NMR (376 MHz, $CDCl_3$)

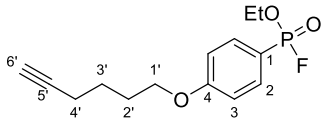

78

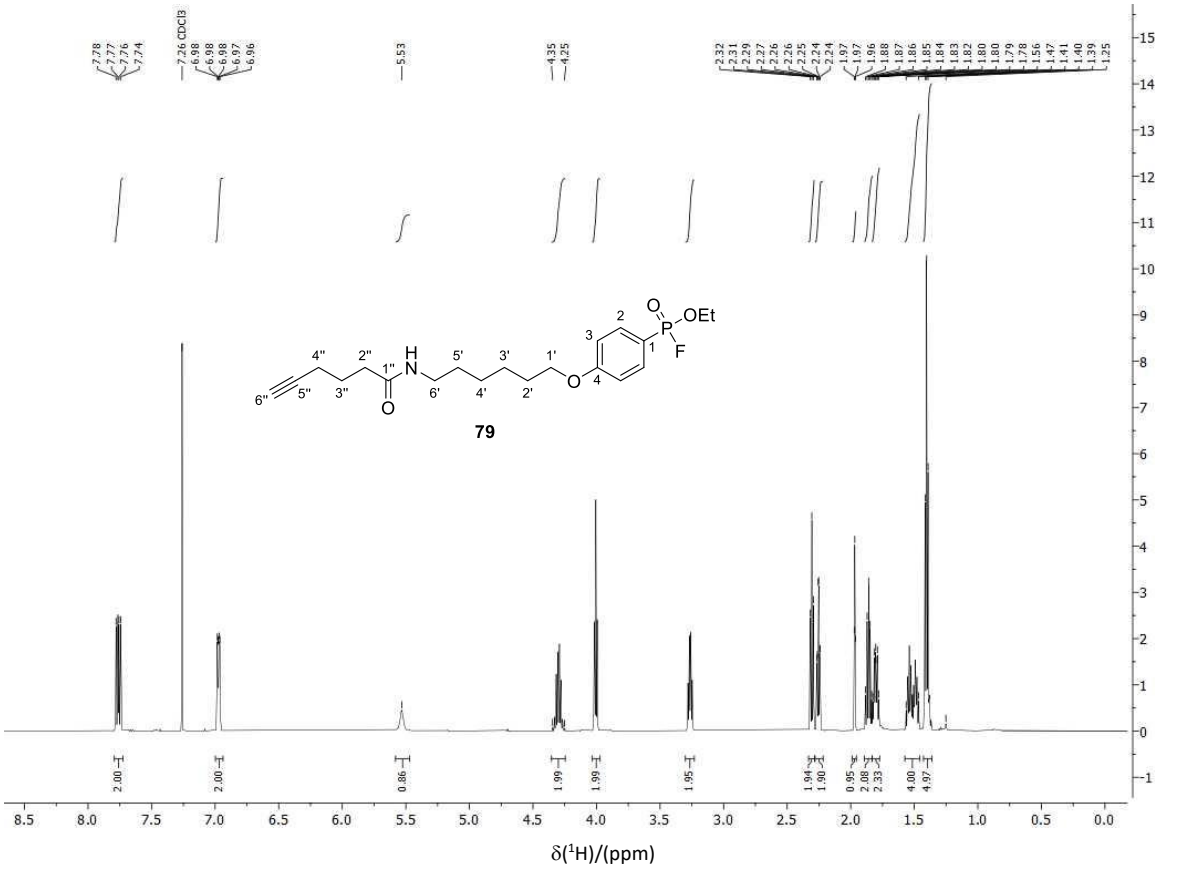
7.78
7.77
7.76
7.74
7.26 CDCl3
6.98
6.98
6.98
6.97
6.96
5.53
4.35
4.25
2.32
2.31
2.29
2.27
2.26
2.26
2.25
2.24
2.24
1.97
1.97
1.96
1.88
1.87
1.86
1.85
1.84
1.83
1.82
1.80
1.80
1.79
1.78
1.56
1.47
1.41
1.40
1.39
1.25
2.00
2.00
0.86
1.99
1.99
1.95
1.94
1.90
0.95
2.08
2.33
4.00
4.97
δ(1H)/(ppm)

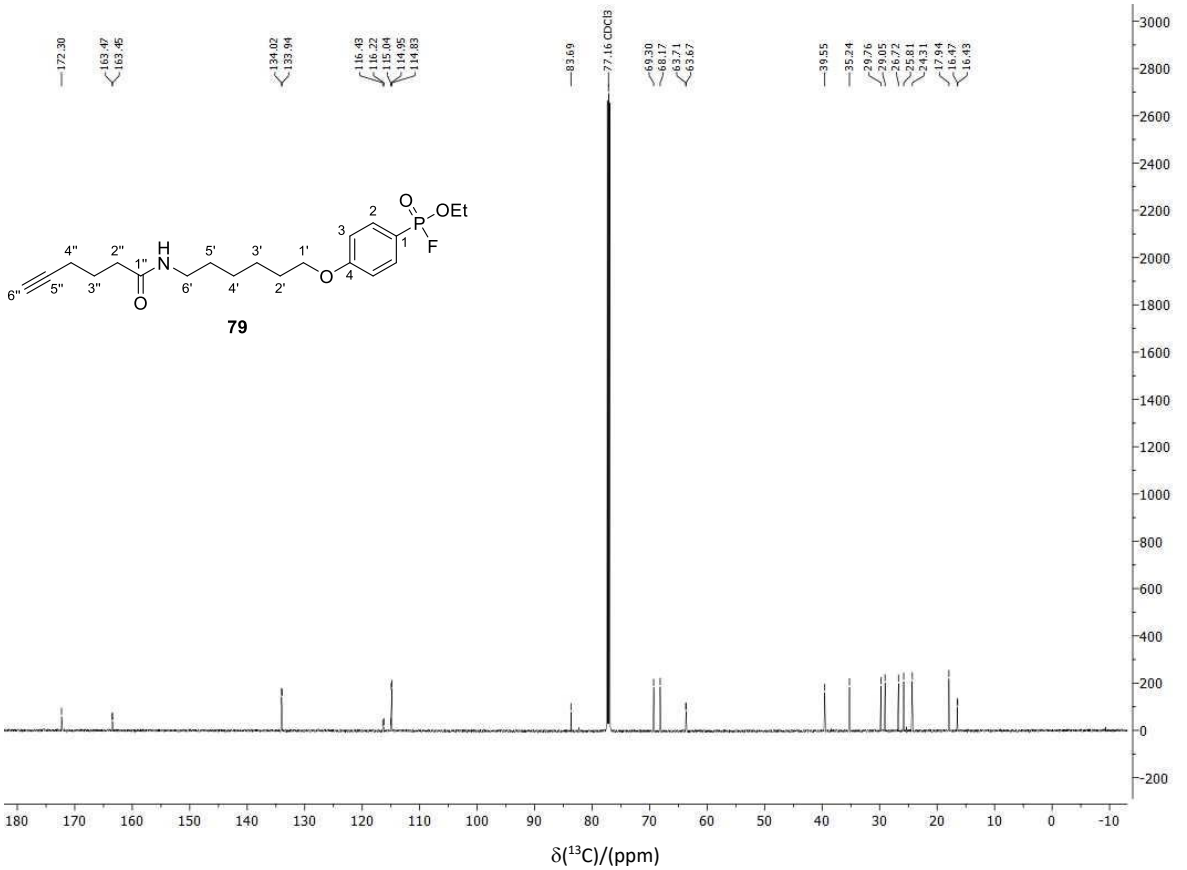
172.30
163.47
163.45
134.02
133.94
116.48
116.22
115.04
114.95
114.83
83.69
77.16 CDCl3
69.30
68.17
63.71
63.67
39.55
35.24
29.76
29.05
26.72
25.81
24.31
17.94
16.47
16.43
δ(13C)/(ppm)

^{31}P NMR (162 MHz, $CDCl_3$)

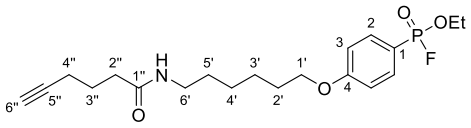

79

^{19}F NMR (376 MHz, $CDCl_3$)

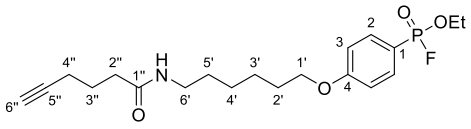

79

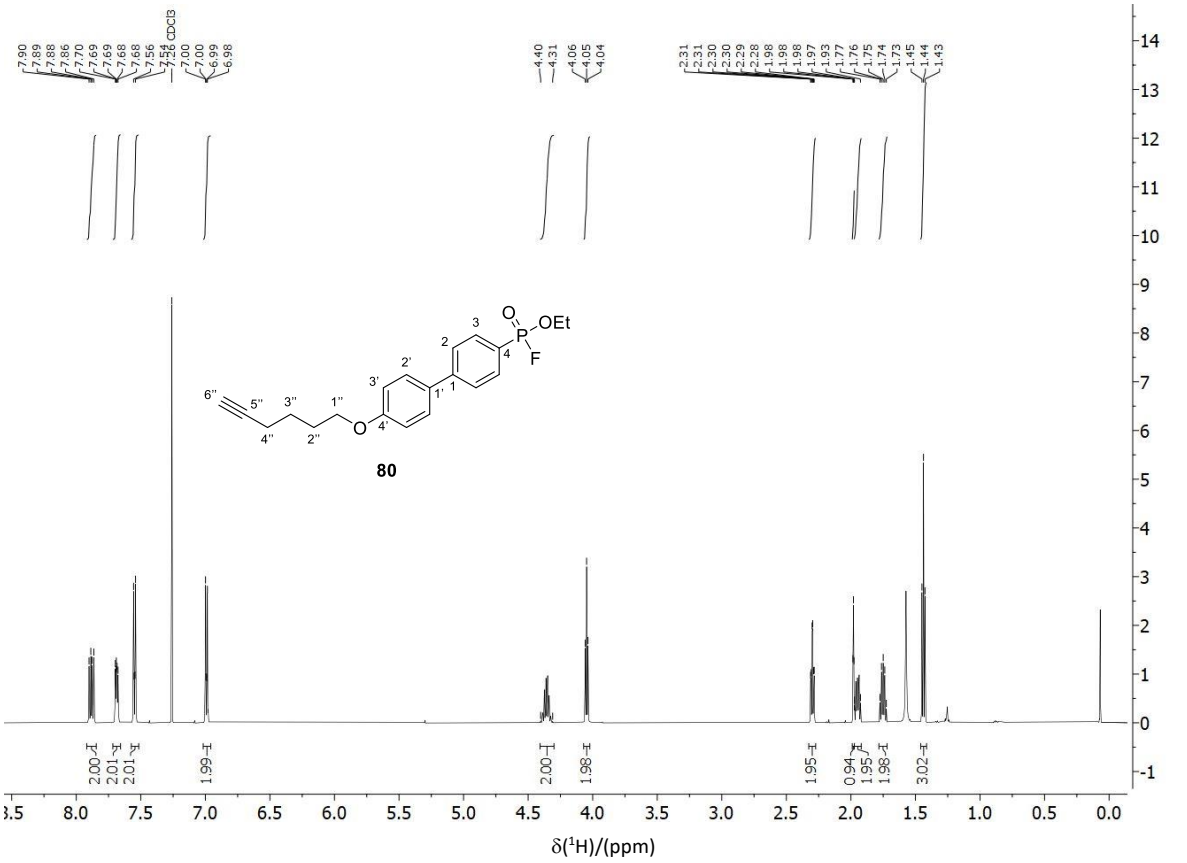
7.90
7.89
7.88
7.86
7.70
7.69
7.69
7.68
7.68
7.56
7.54 CDCl3
7.00
7.00
6.99
6.98
4.40
4.31
4.06
4.05
4.04
2.31
2.31
2.30
2.30
2.29
2.28
1.98
1.98
1.98
1.97
1.93
1.77
1.76
1.75
1.74
1.73
1.45
1.44
1.43
OEt
F
80
2.00
2.01
2.01
1.99
2.00
1.98
1.95
0.94
1.95
1.98
3.02
δ(1H)/(ppm)

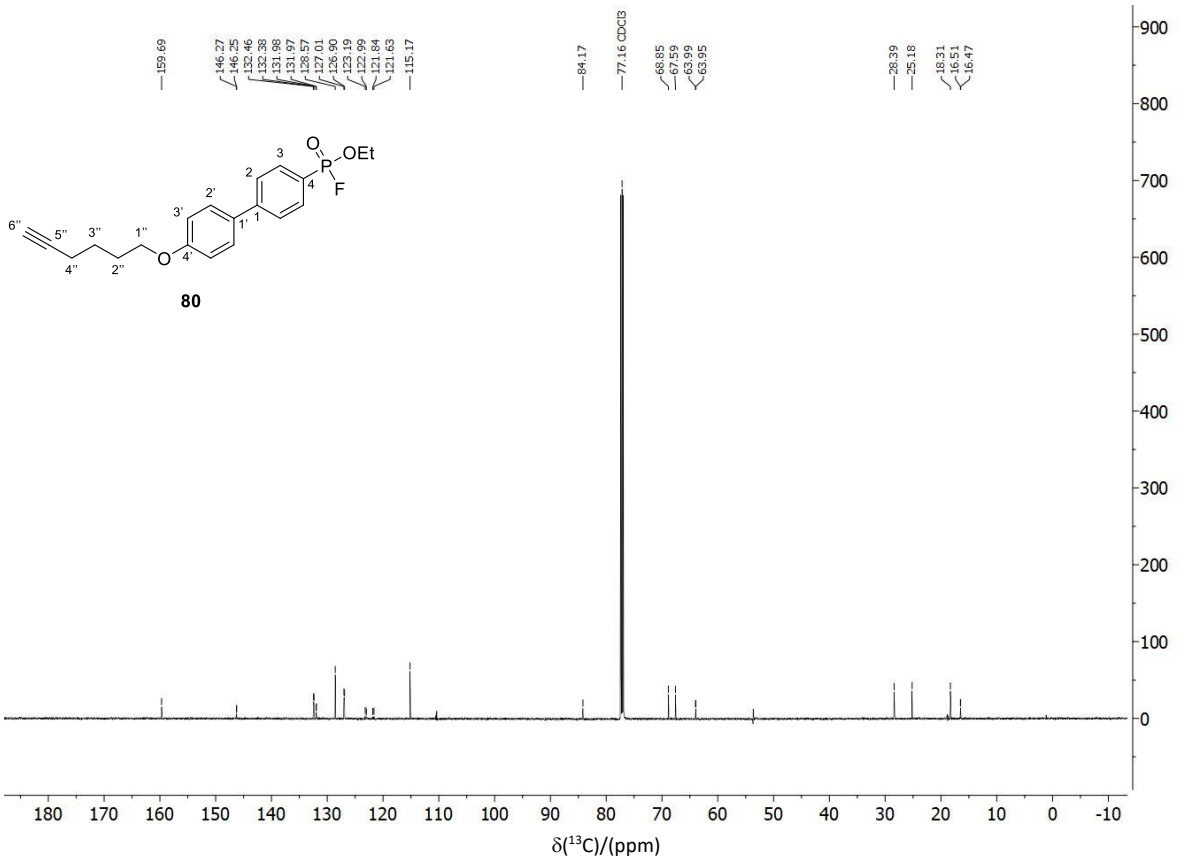
159.69
146.27
146.25
132.46
132.38
131.98
131.97
128.57
127.01
126.90
123.19
122.99
121.84
121.63
115.17
84.17
77.16 CDCl3
68.85
67.59
63.99
63.95
28.39
25.18
18.31
16.51
16.47
OEt
F
80
δ(13C)/(ppm)

^{31}P NMR (162 MHz, $CDCl_3$)

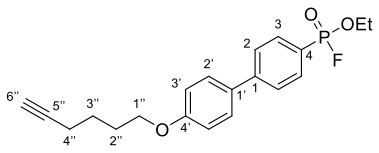

80

^{19}F NMR (376 MHz, $CDCl_3$).

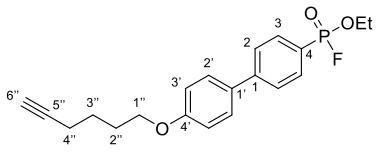

80

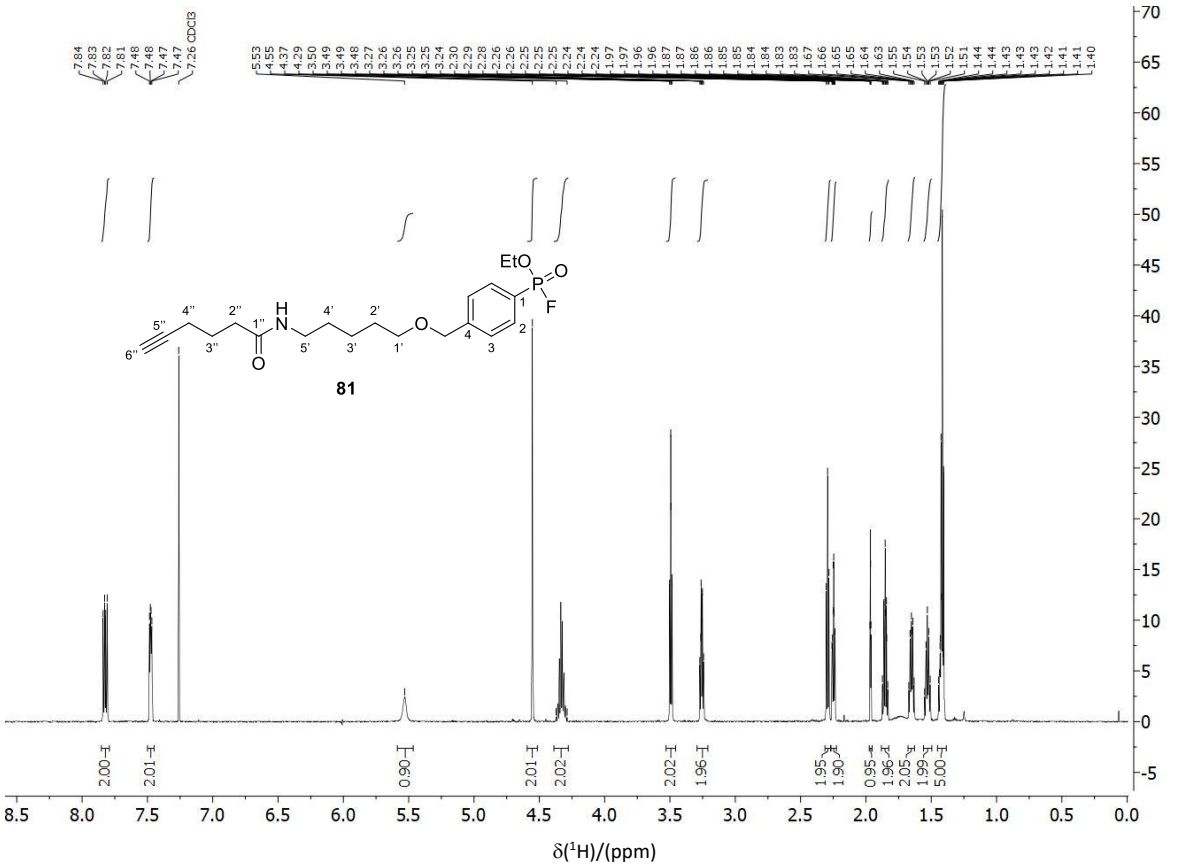
81
δ(1H)/(ppm)

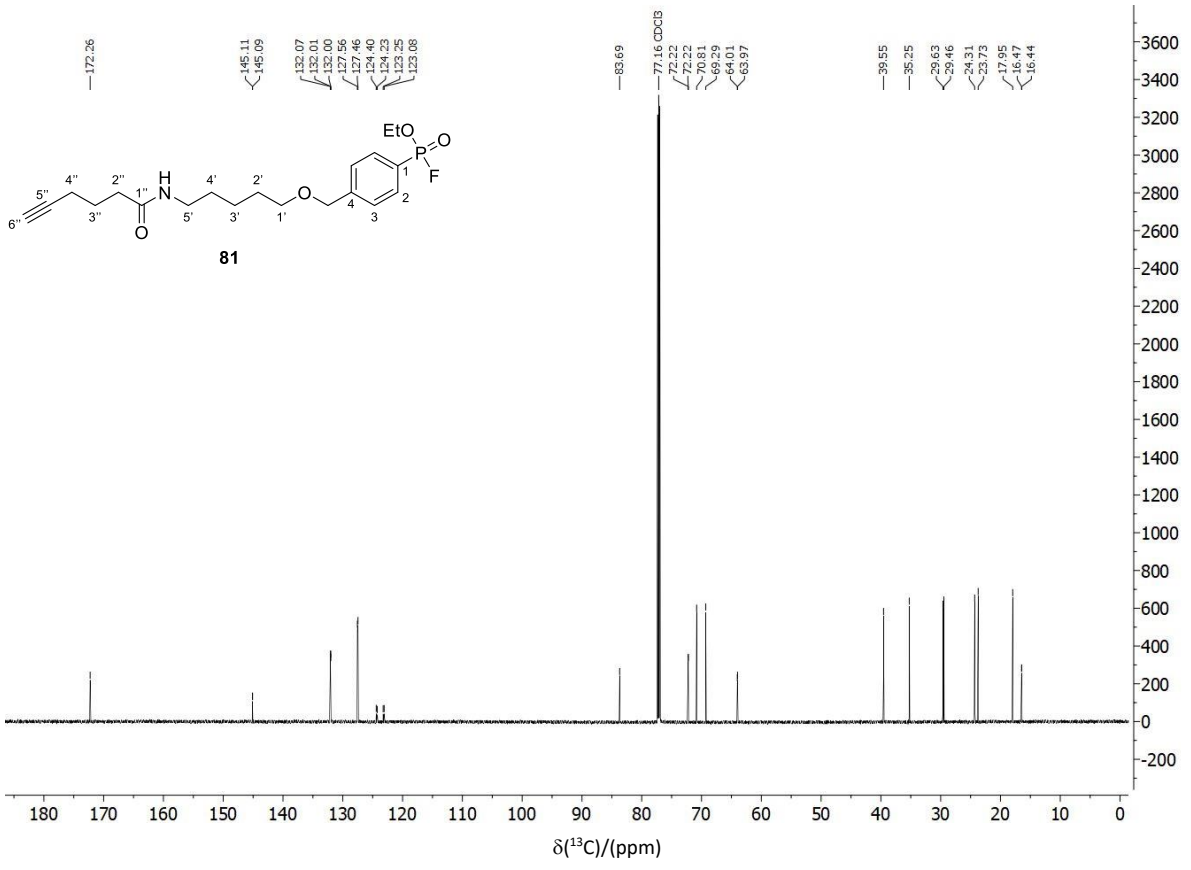
81
δ(13C)/(ppm)

^{31}P NMR (162 MHz, $CDCl_3$)

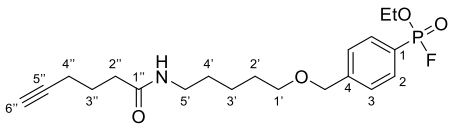

81

^{19}F NMR (376 MHz, $CDCl_3$)

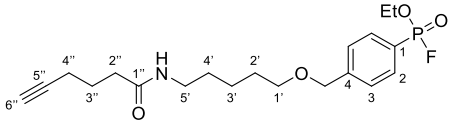

81

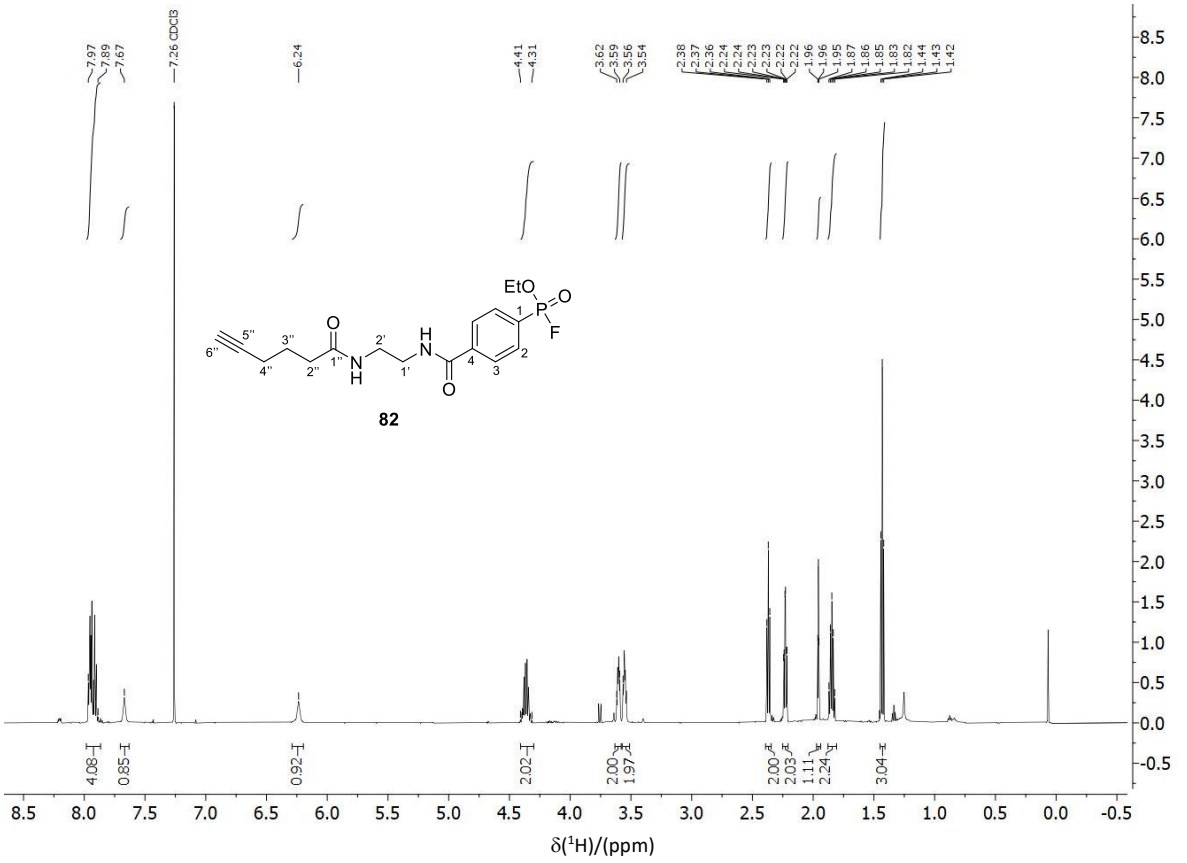
7.97
7.89
7.67
7.26 CDCl3
6.24
4.41
4.31
3.62
3.59
3.56
3.54
2.38
2.37
2.36
2.24
2.24
2.23
2.23
2.22
2.22
1.96
1.96
1.95
1.87
1.86
1.85
1.83
1.82
1.44
1.43
1.42
EtO
P
O
F
O
N
H
N
H
O
82
4.08
0.85
0.92
2.02
2.00
1.97
2.00
2.03
1.11
2.24
3.04
δ(1H)/(ppm)

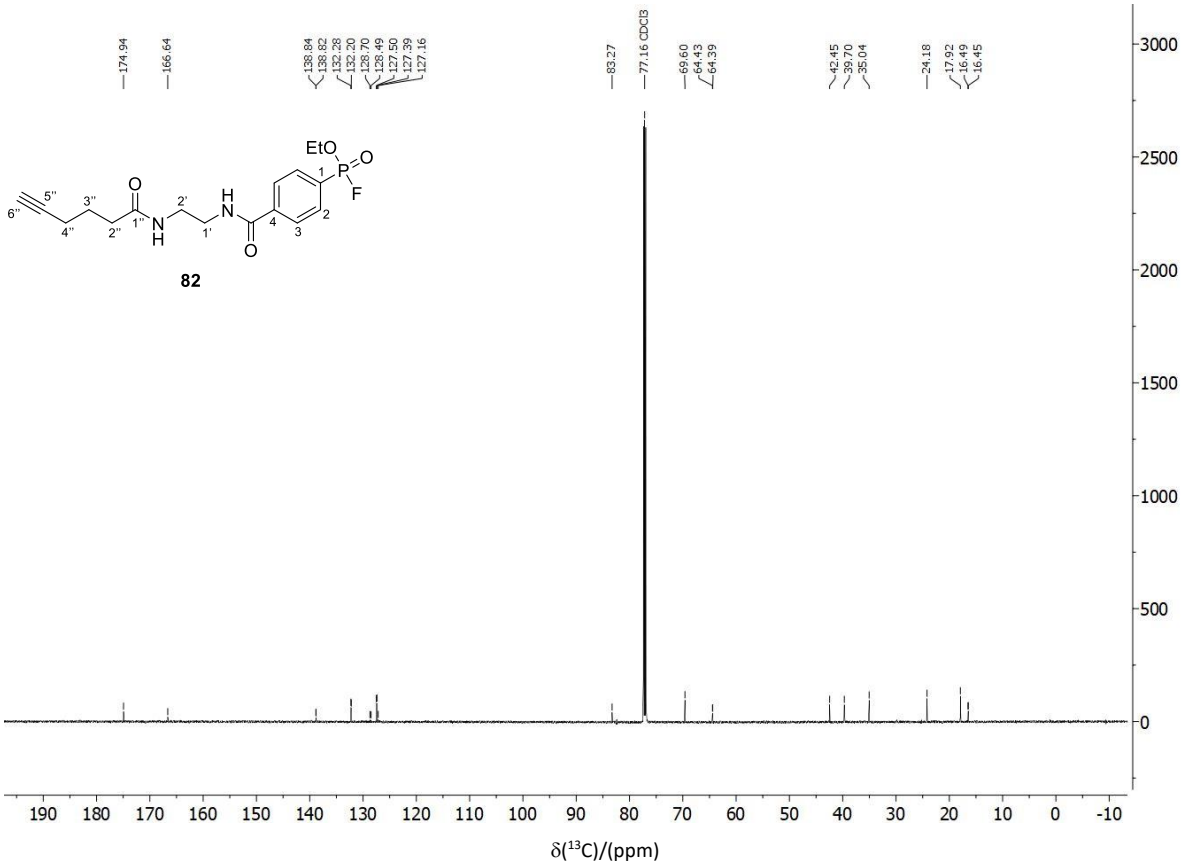
174.94
166.64
138.84
138.82
132.28
132.20
128.70
128.49
127.50
127.39
127.16
83.27
77.16 CDCl3
69.60
64.43
64.39
42.45
39.70
35.04
24.18
17.92
16.49
16.45
EtO
P
O
F
O
N
H
N
H
O
82
δ(13C)/(ppm)

^{31}P NMR (162 MHz, $CDCl_3$)

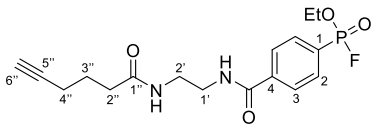

82

^{19}F NMR (376 MHz, None)

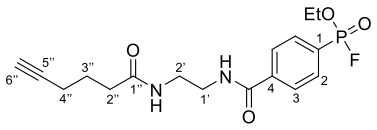

82

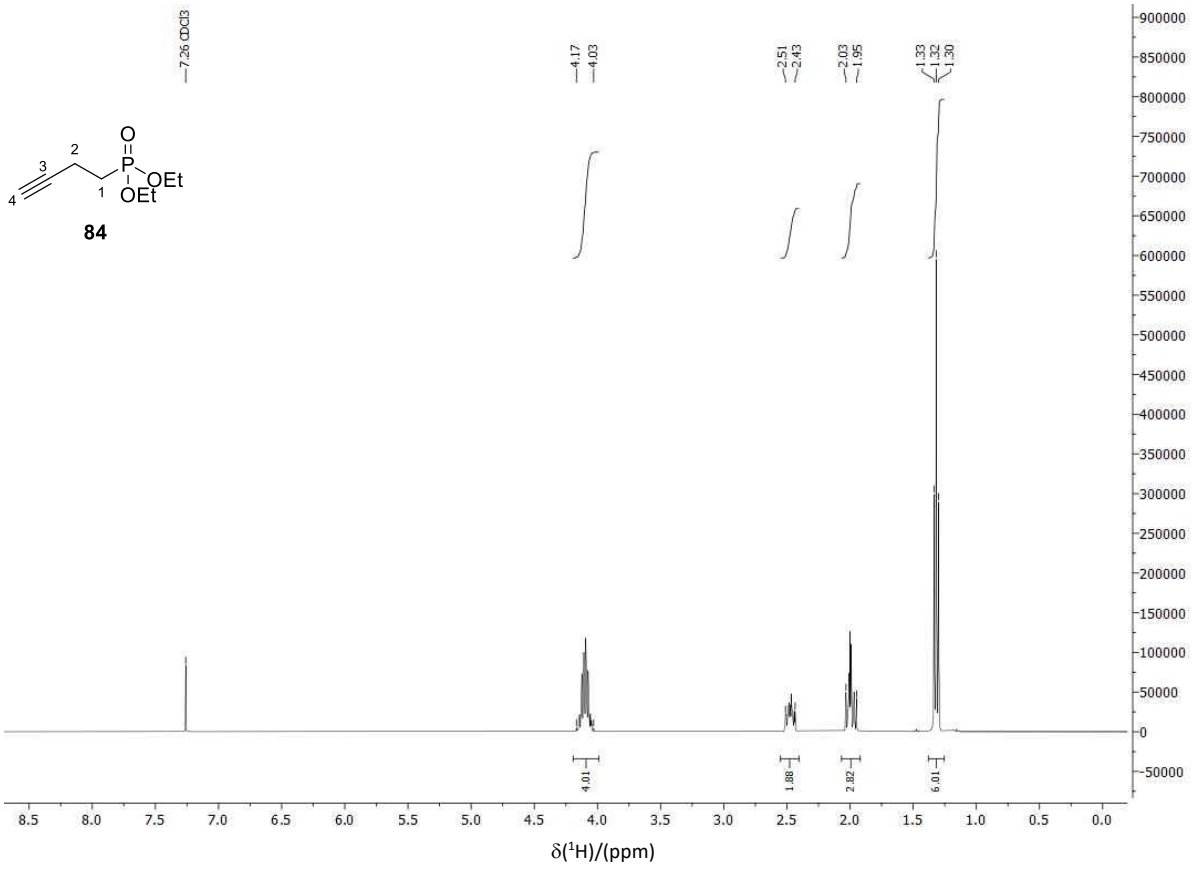
7.26 CDCl3
4.17
4.03
2.51
2.43
2.03
1.95
1.33
1.32
1.30
4.01
1.88
2.82
6.01
δ(1H)/(ppm)

84

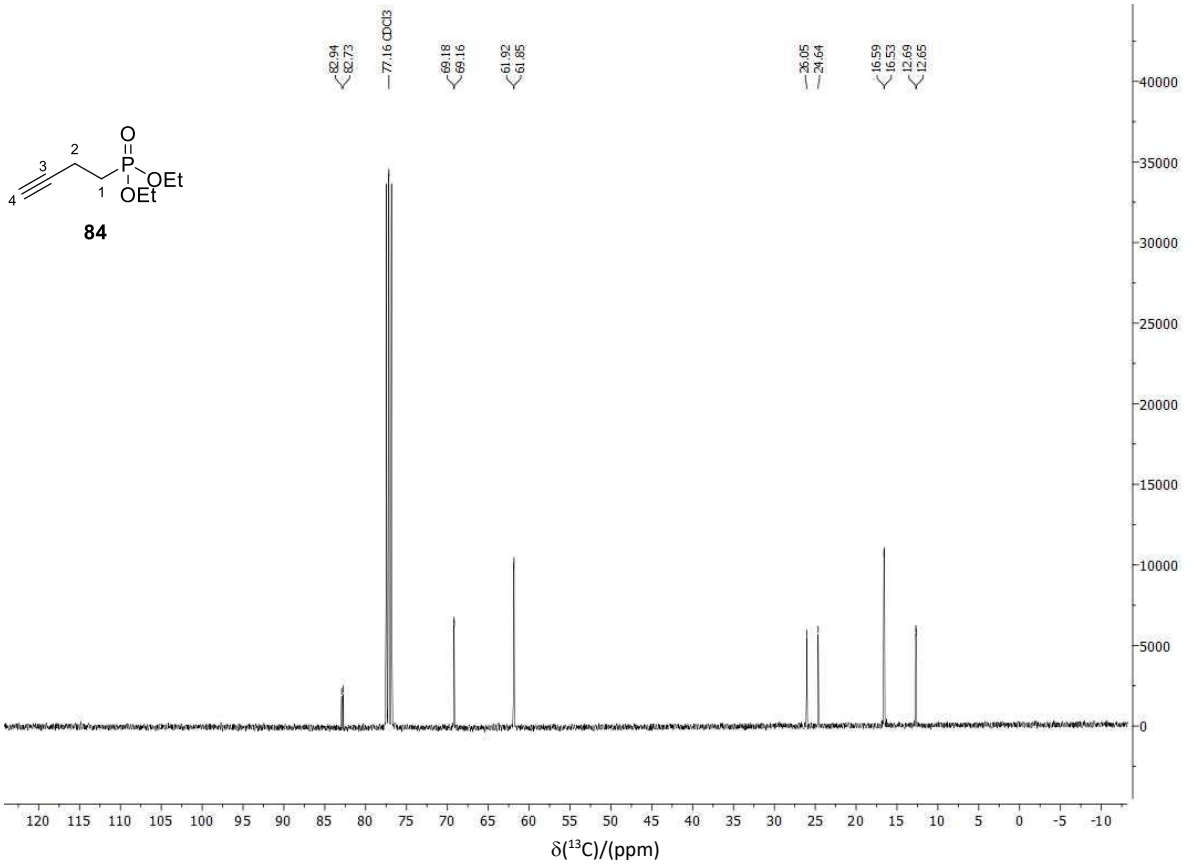
82.94
82.73
77.16 CDCl3
69.18
69.16
61.92
61.85
26.05
24.64
16.59
16.53
12.69
12.65
δ(13C)/(ppm)

84

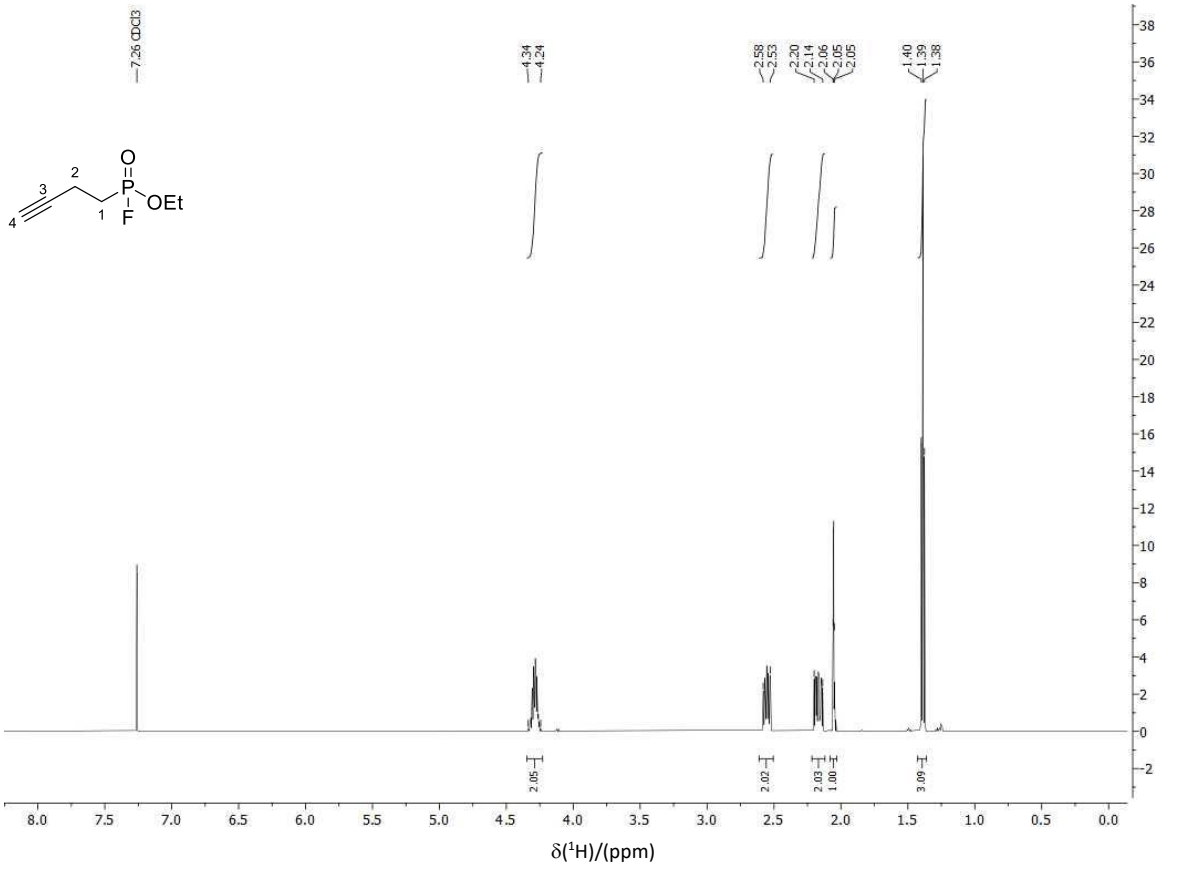
7.26 CDCl3
4.34
4.24
2.58
2.53
2.20
2.14
2.06
2.05
2.05
1.40
1.39
1.38
O
P
F
OEt
1
2
3
4
2.05
2.02
2.03
1.00
3.09
δ(1H)/(ppm)

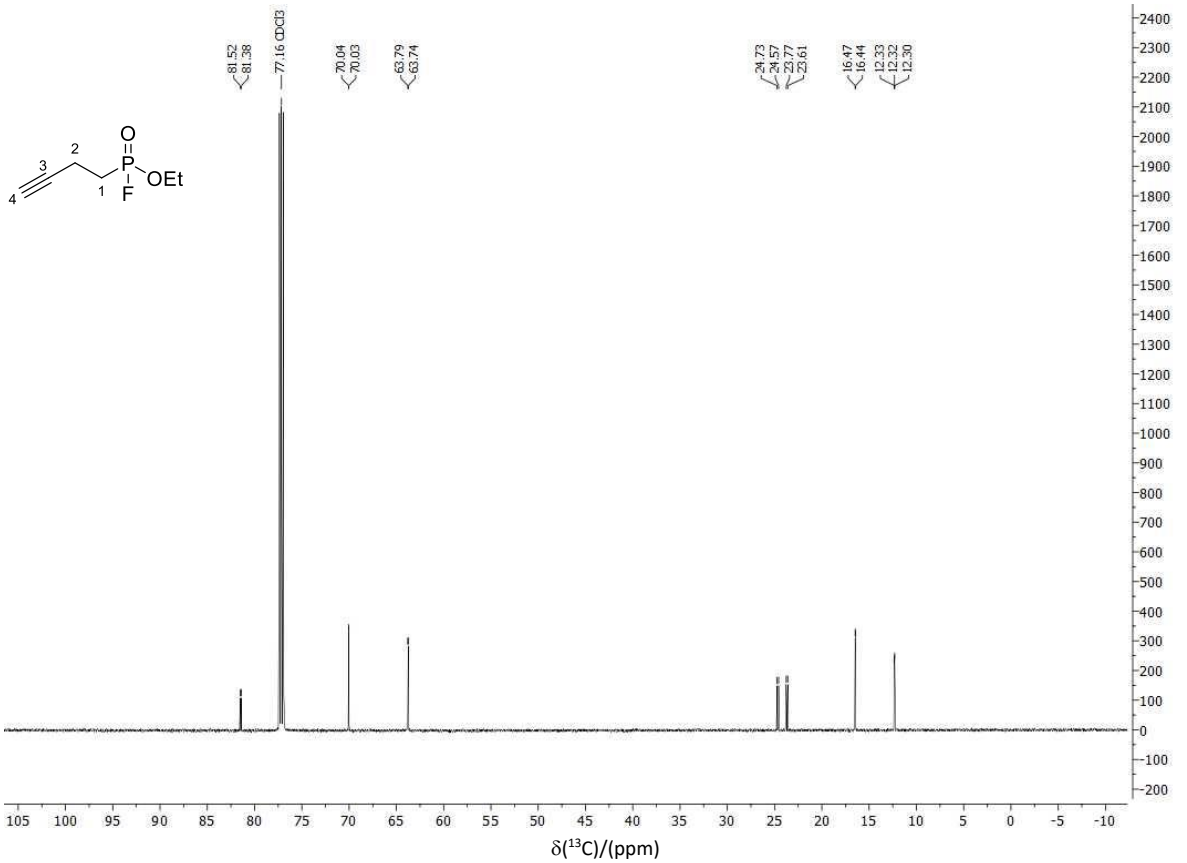
81.52
81.38
77.16 CDCl3
70.04
70.03
63.79
63.74
24.73
24.57
23.77
23.61
16.47
16.44
12.33
12.32
12.30
O
P
F
OEt
1
2
3
4
δ(13C)/(ppm)

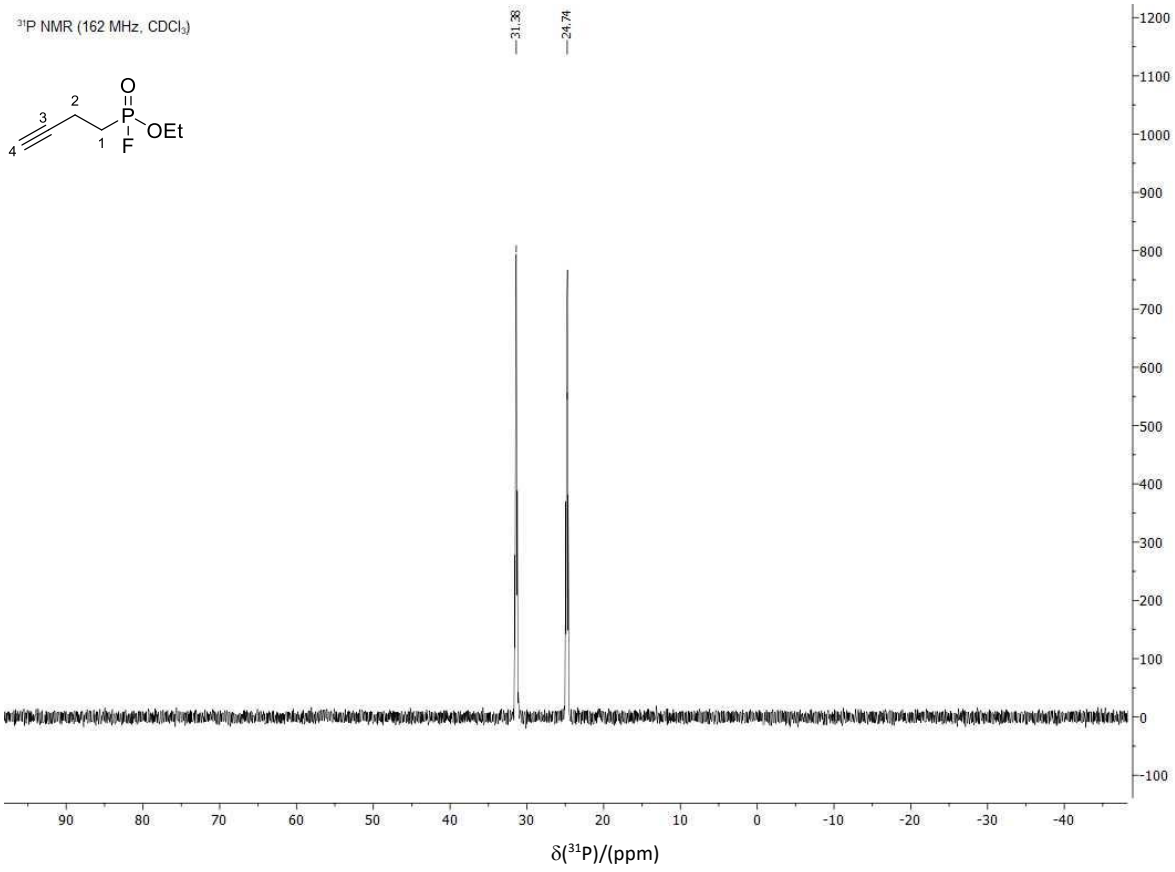
31P NMR (162 MHz, CDCl3)
31.38
24.74
O
P
F
OEt
1
2
3
4
δ(31P)/(ppm)

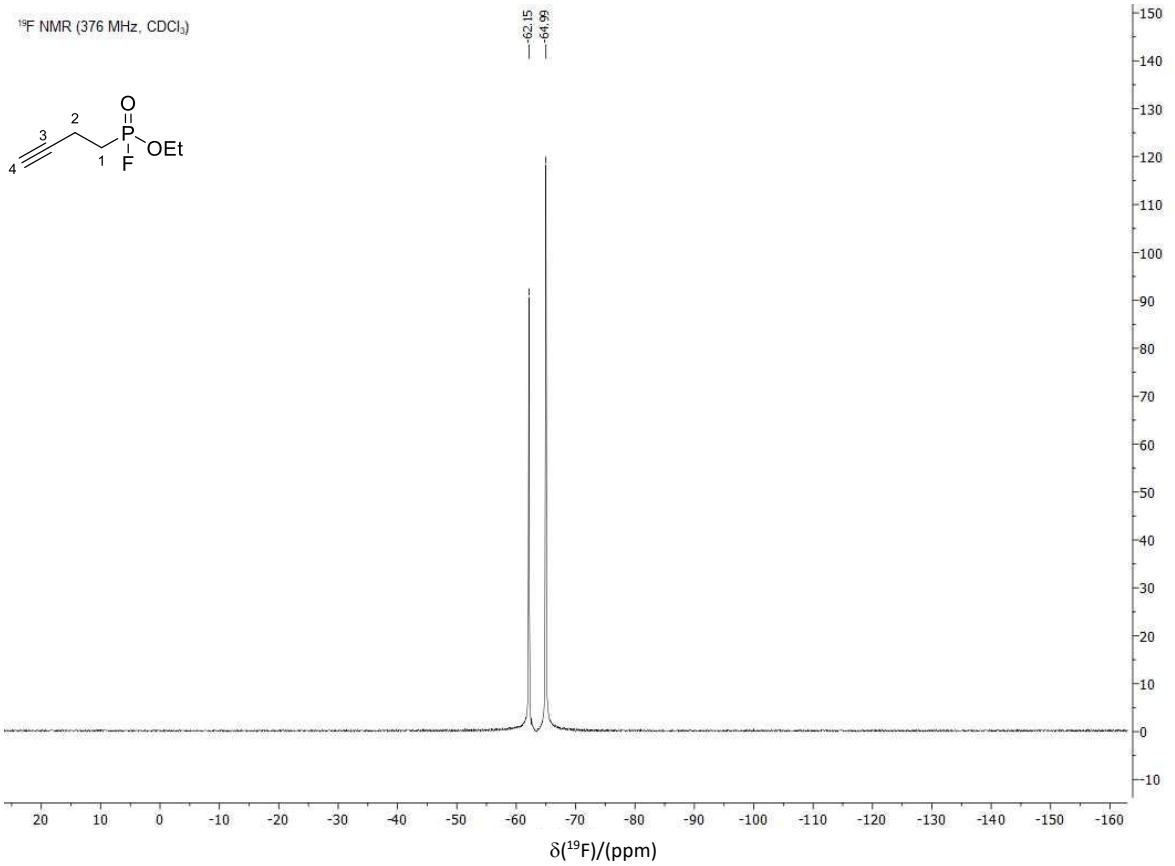
19F NMR (376 MHz, CDCl3)
-62.15
-64.99
O
P
F
OEt
1
2
3
4
δ(19F)/(ppm)

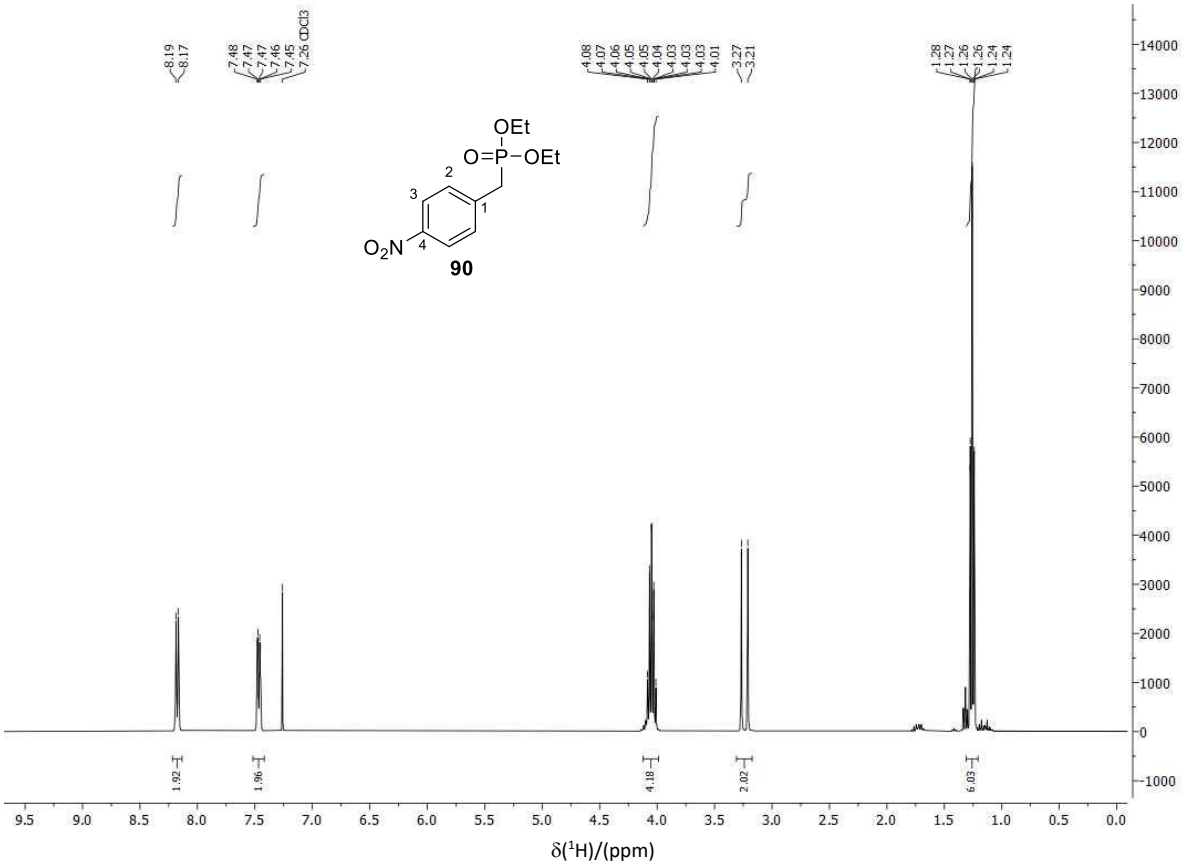
8.19
8.17
7.48
7.47
7.47
7.47
7.46
7.45
7.26 CDCl3
4.08
4.07
4.06
4.05
4.05
4.04
4.03
4.03
4.03
4.01
3.27
3.21
1.28
1.27
1.26
1.26
1.24
1.24
OEt
O=P−OEt
2
3
1
O2N
4
90
1.92
1.96
4.18
2.02
6.03
δ(1H)/(ppm)

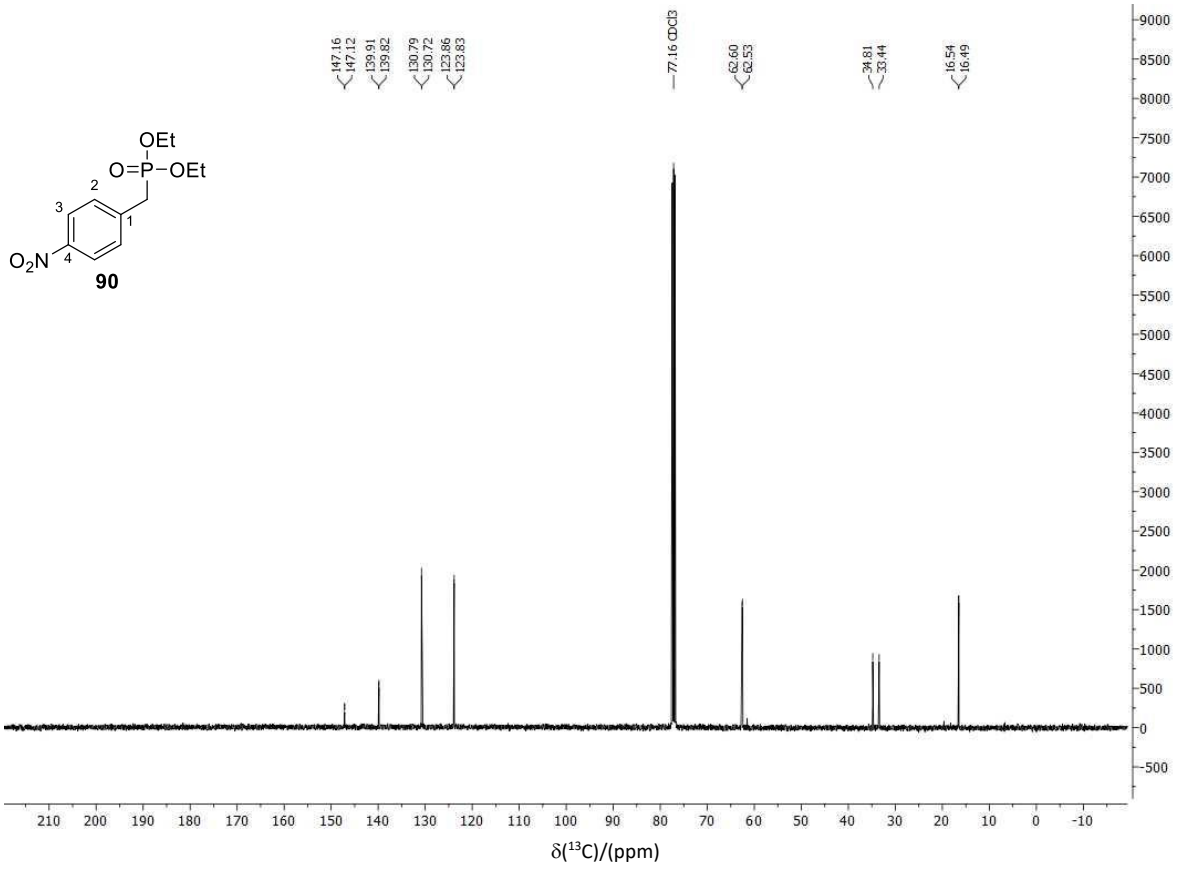
147.16
147.12
139.91
139.82
130.79
130.72
123.86
123.83
77.16 CDCl3
62.60
62.53
34.81
33.44
16.54
16.49
OEt
O=P−OEt
2
3
1
O2N
4
90
δ(13C)/(ppm)

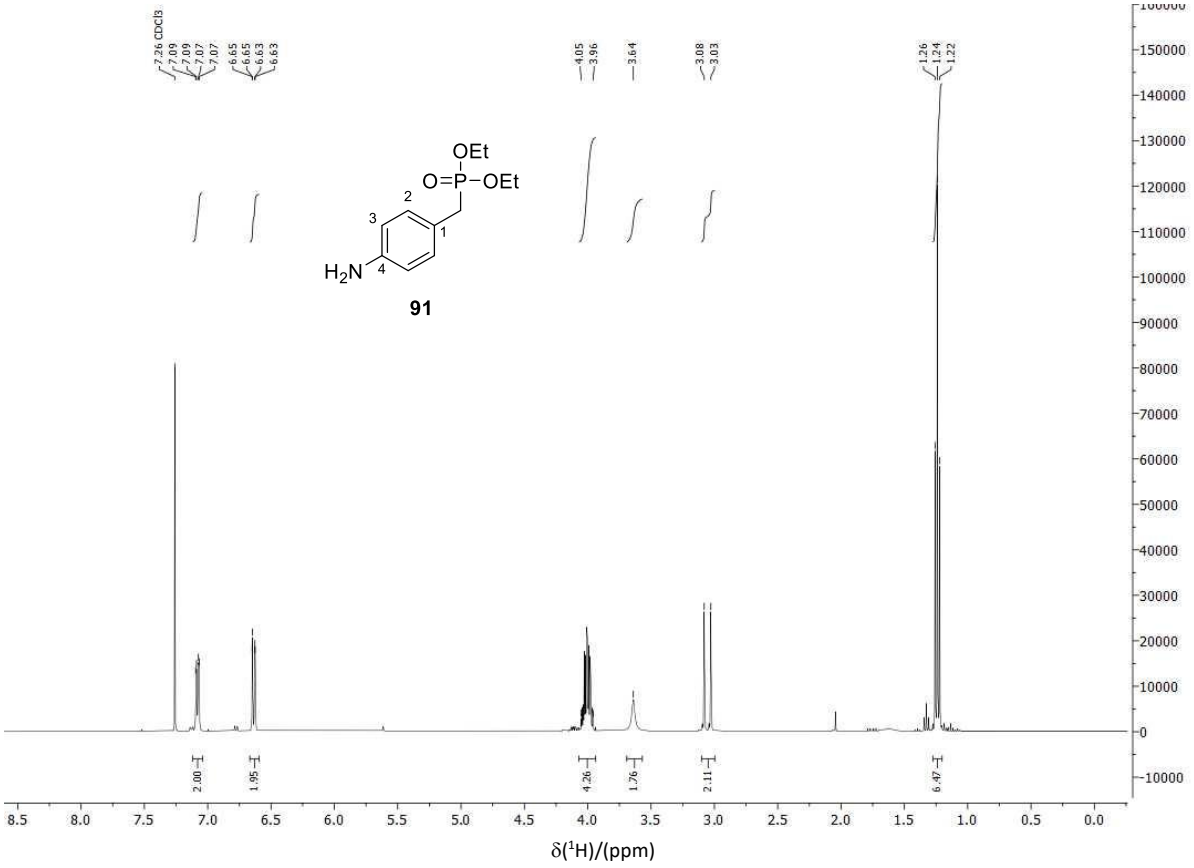
7.26 CDCl3
7.09
7.09
7.07
7.07
6.65
6.65
6.63
6.63
4.05
3.96
3.64
3.08
3.03
1.26
1.24
1.22
OEt
O=P−OEt
2
3
1
H2N
4
91
2.00
1.95
4.26
1.76
2.11
6.47
δ(1H)/(ppm)

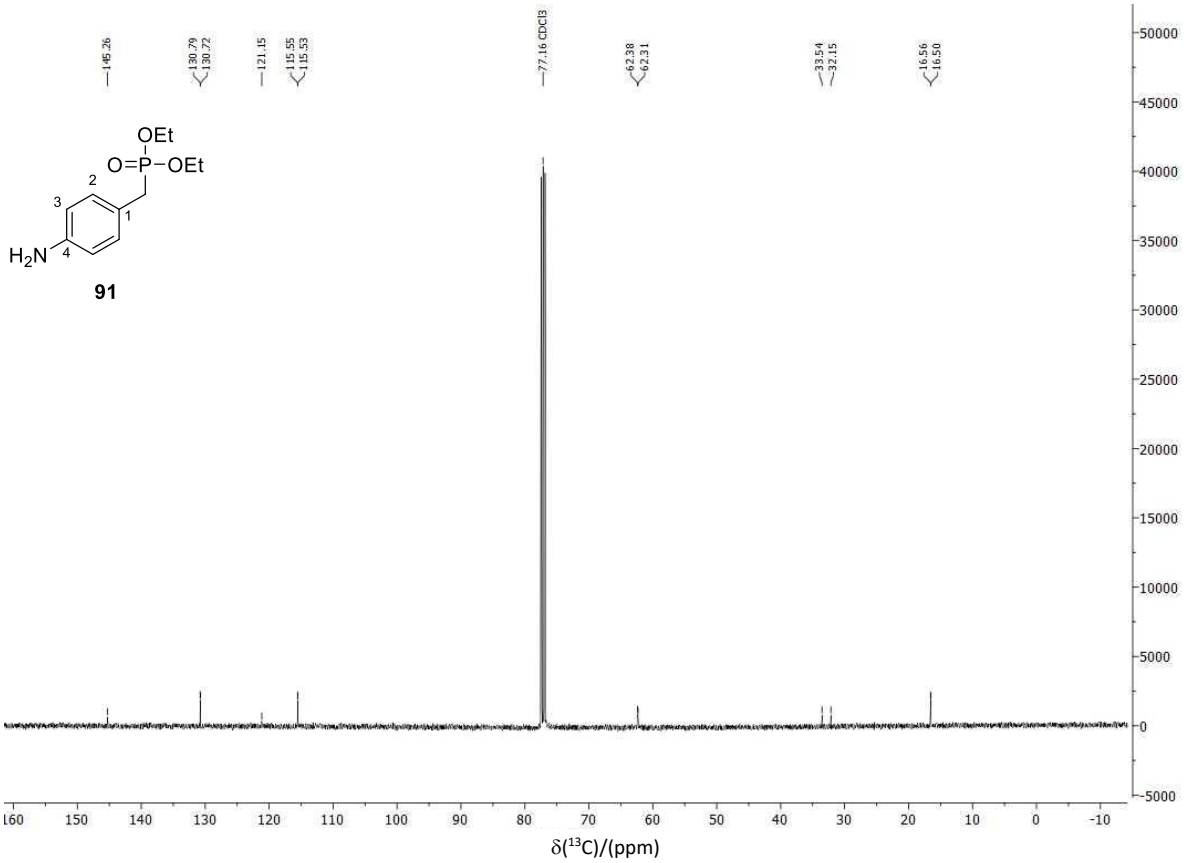
145.26
130.79
130.72
121.15
115.55
115.53
77.16 CDCl3
62.38
62.31
33.54
32.15
16.56
16.50
OEt
O=P−OEt
2
3
1
H2N
4
91
δ(13C)/(ppm)

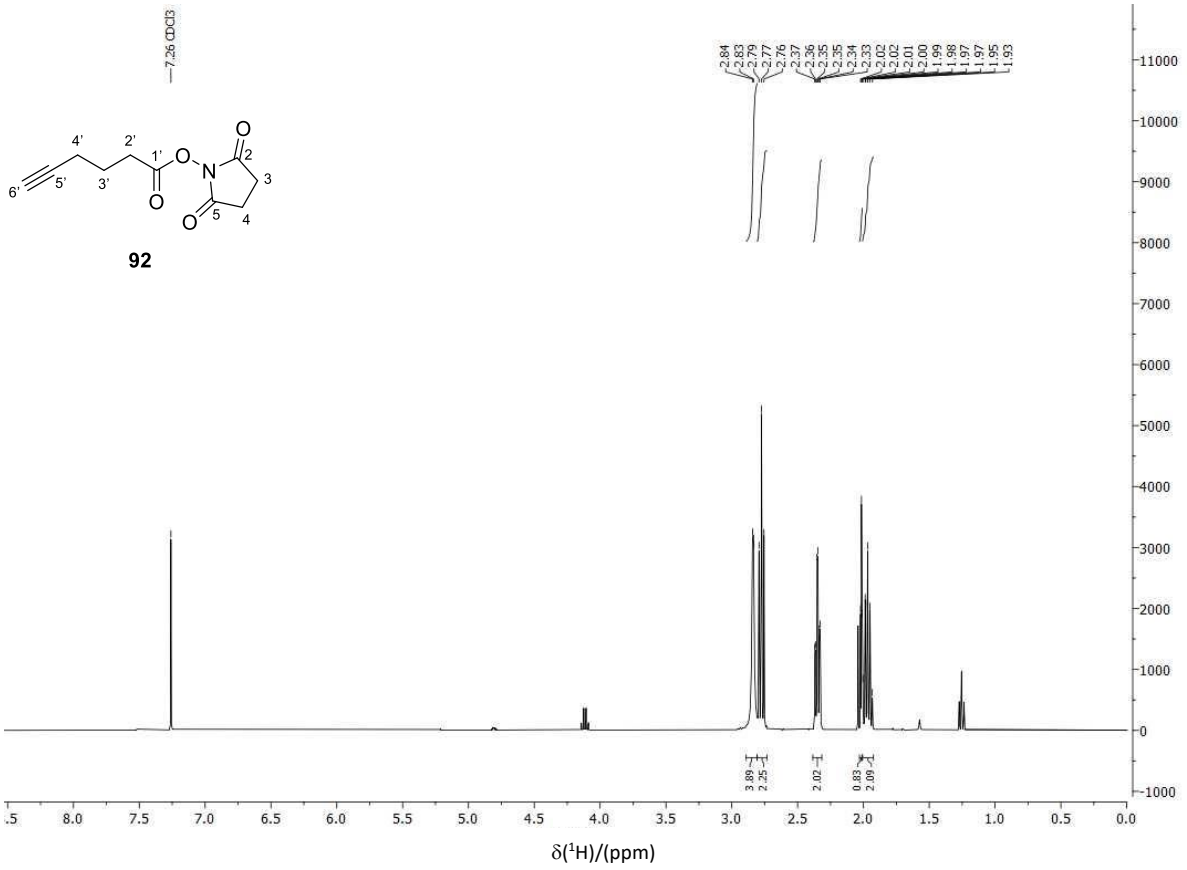
7.26 CDCl3
2.84
2.83
2.79
2.77
2.76
2.37
2.36
2.35
2.35
2.34
2.33
2.02
2.02
2.01
2.00
1.99
1.98
1.97
1.97
1.95
1.93
3.89
2.25
2.02
0.83
2.09
δ(1H)/(ppm)

92

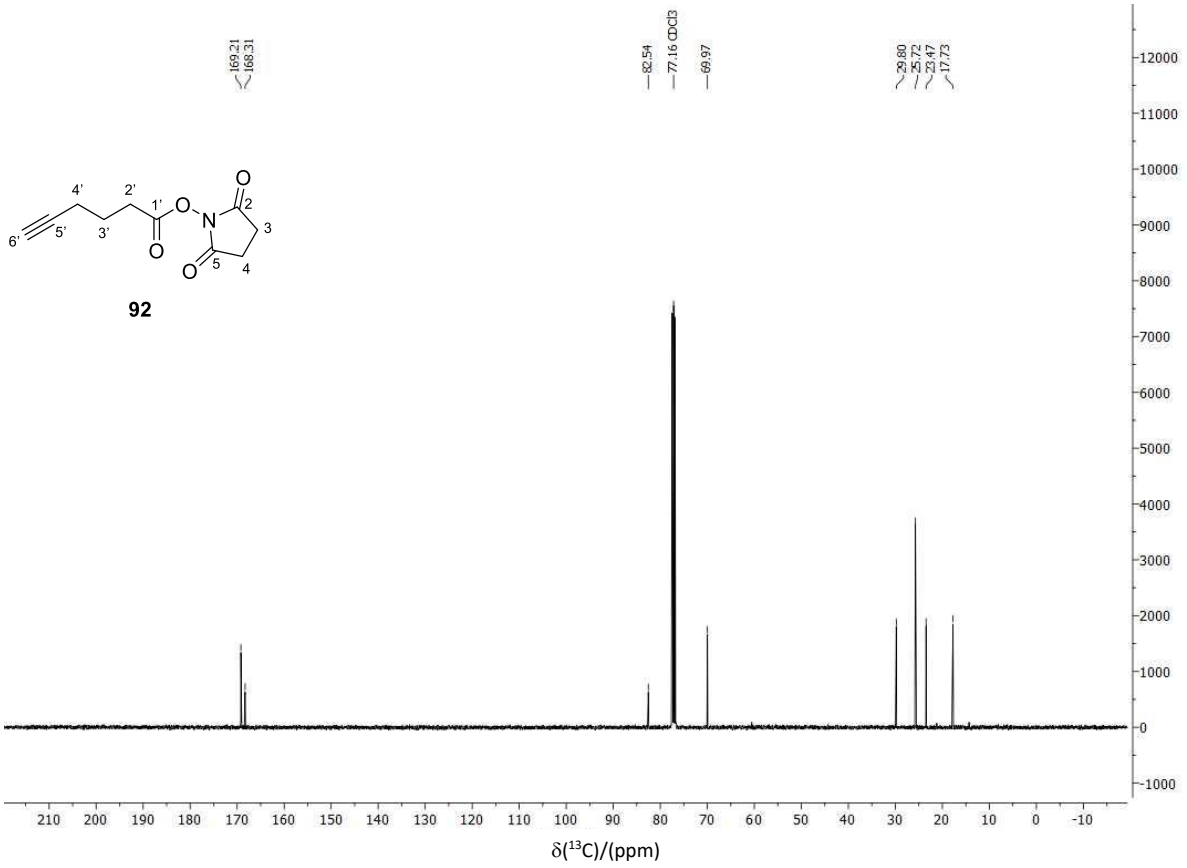
169.21
168.31
82.54
77.16 CDCl3
69.97
29.80
25.72
23.47
17.73
δ(13C)/(ppm)

92

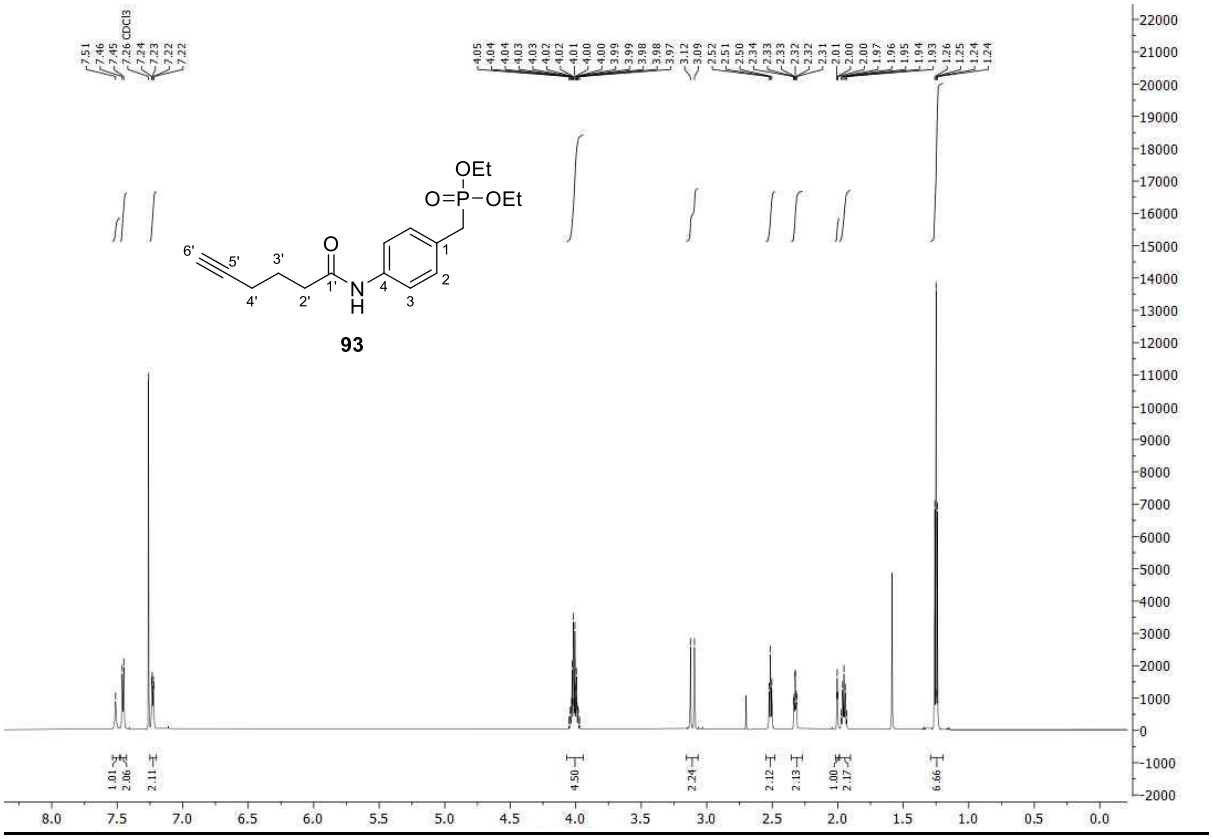

δ(^{1}H)/(ppm)

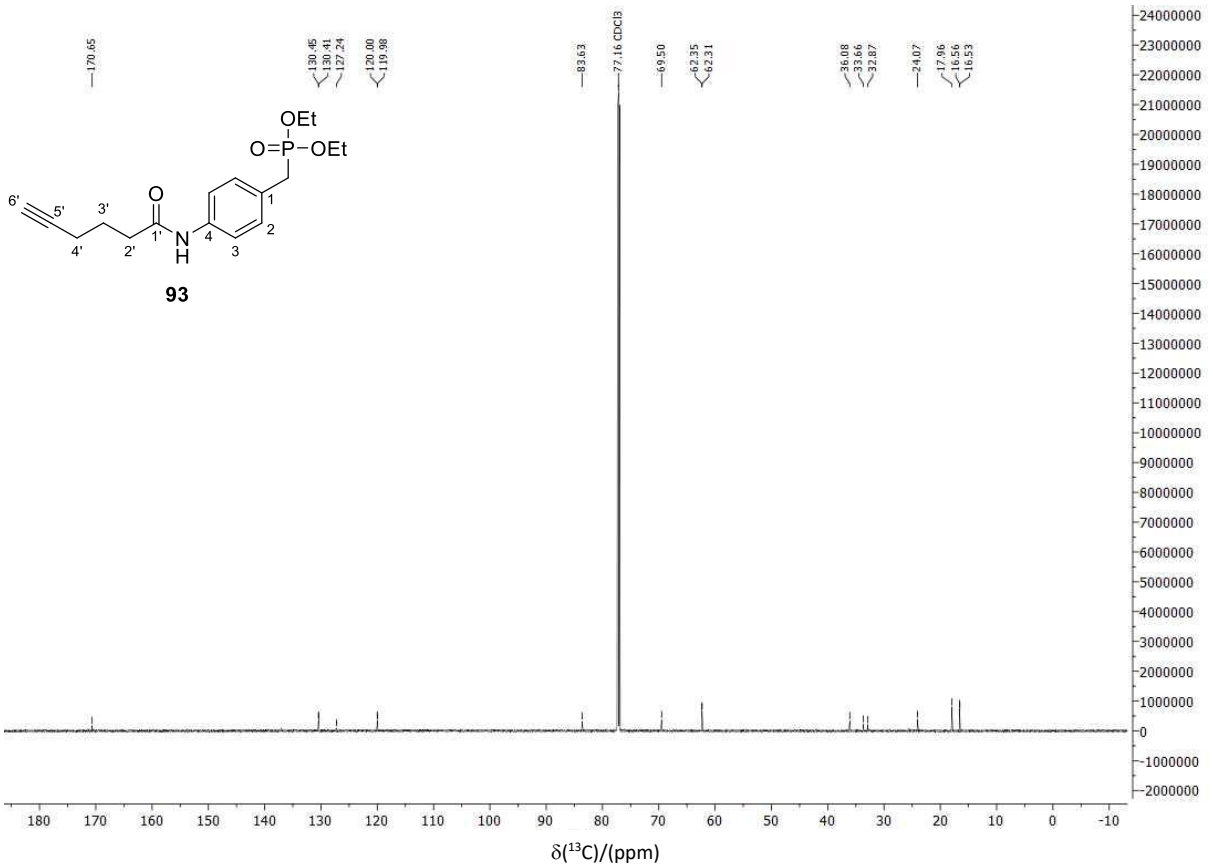

δ(^{13}C)/(ppm)

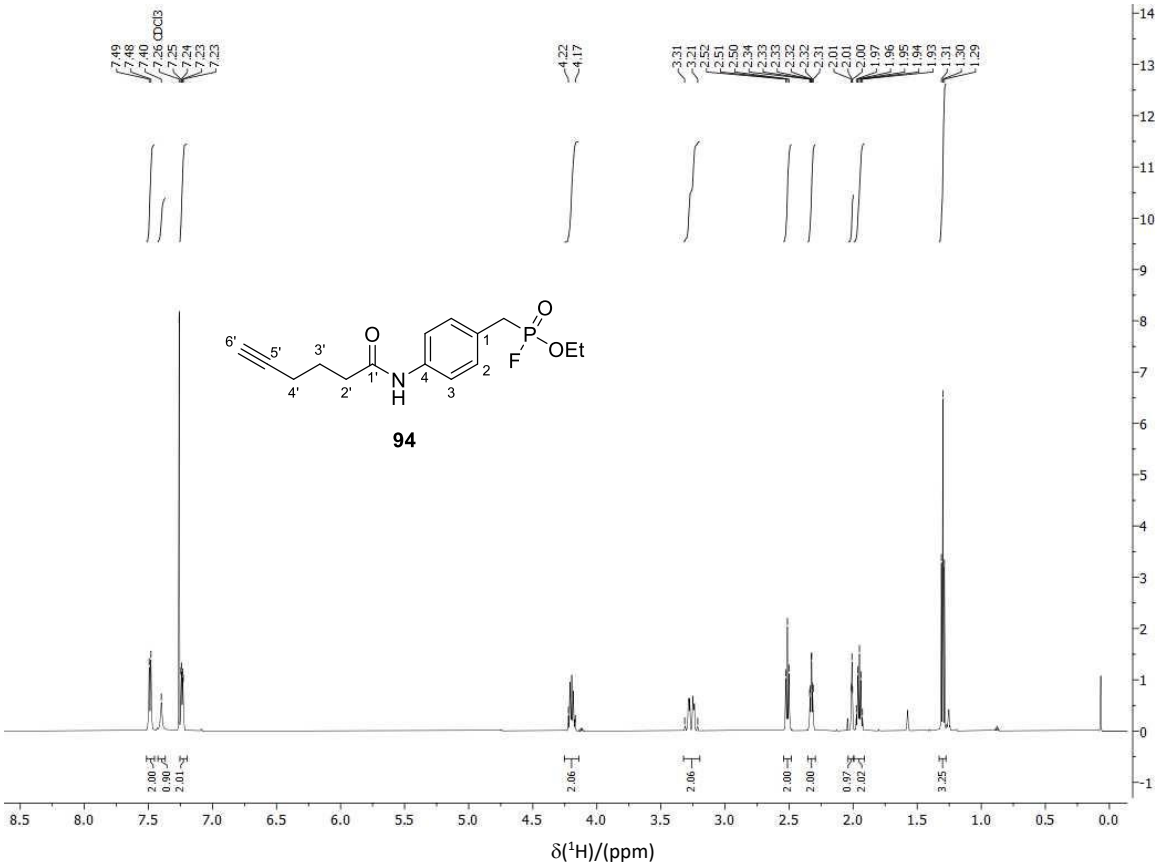
7.49
7.48
7.40
7.26 CDCl3
7.25
7.24
7.23
7.23
4.22
4.17
3.31
3.21
2.52
2.51
2.50
2.34
2.33
2.33
2.32
2.32
2.31
2.01
2.01
2.00
1.97
1.96
1.95
1.94
1.93
1.31
1.30
1.29
2.00
0.90
2.01
2.06
2.06
2.00
2.00
0.97
2.02
3.25
δ(1H)/(ppm)

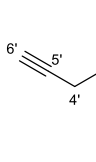
6'
5'
4'
3'
2'
1'
O
N
H
4
1
2
3
P
O
F
OEt

94

170.67
137.55
137.52
130.43
130.39
125.08
125.01
120.25
120.22
83.57
77.16 CDCl3
69.56
64.17
64.12
36.08
32.31
32.15
31.36
31.20
24.03
17.94
16.43
16.40
δ(13C)/(ppm)

^{19}F NMR (376 MHz, $CDCl_3$)

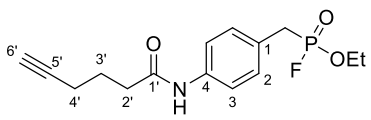

94

^{31}P NMR (162 MHz, $CDCl_3$)

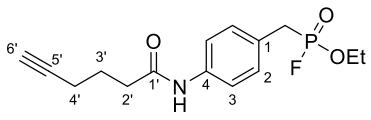

94

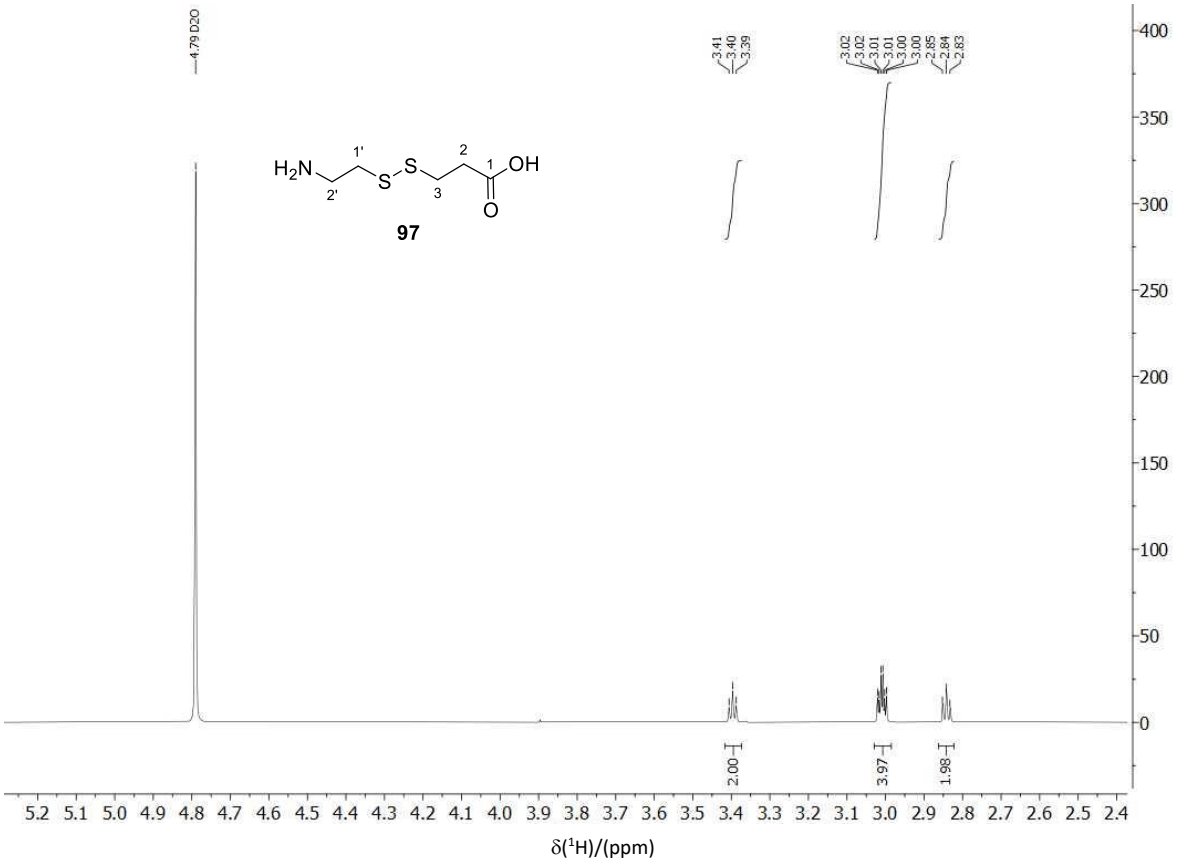
4.79 D2O
3.41
3.40
3.39
3.02
3.02
3.01
3.01
3.00
3.00
2.85
2.84
2.83
2.00
3.97
1.98
δ(¹H)/(ppm)

97

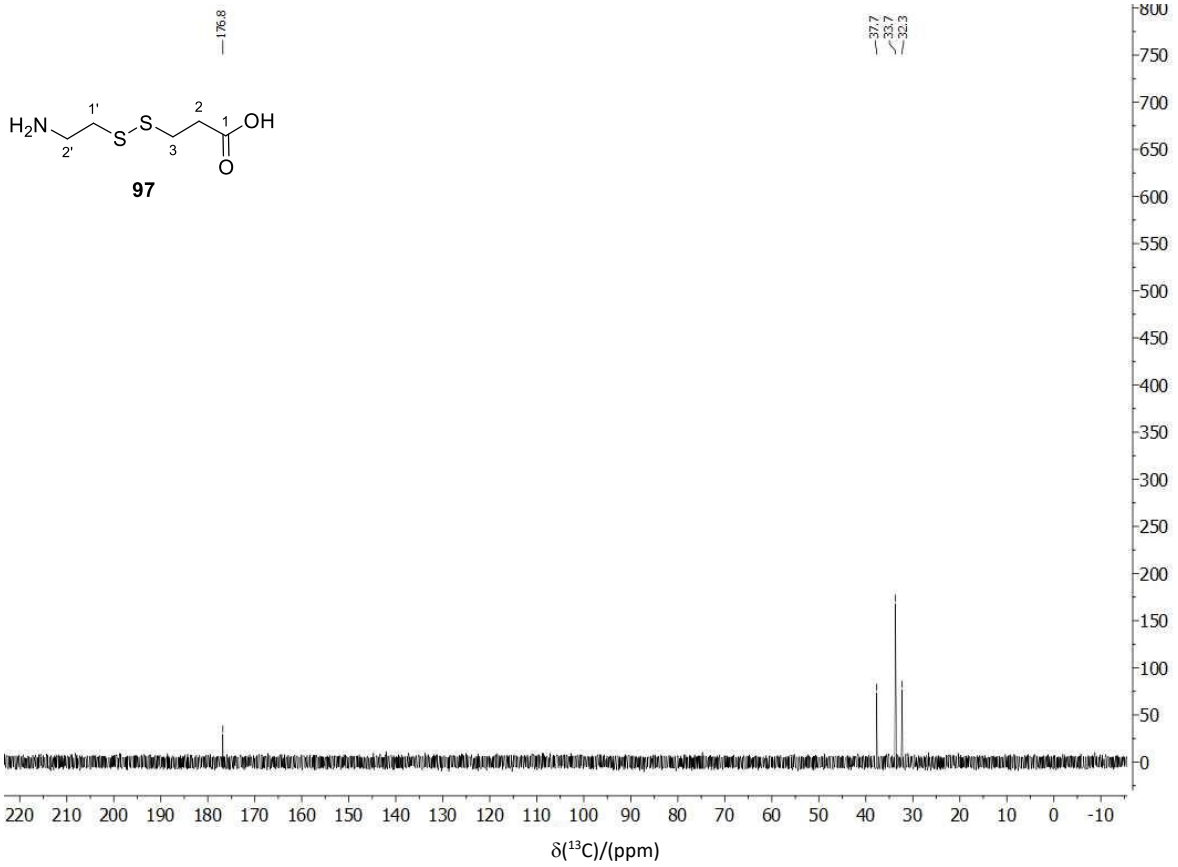
176.8
37.7
33.7
32.3
δ(¹³C)/(ppm)

97

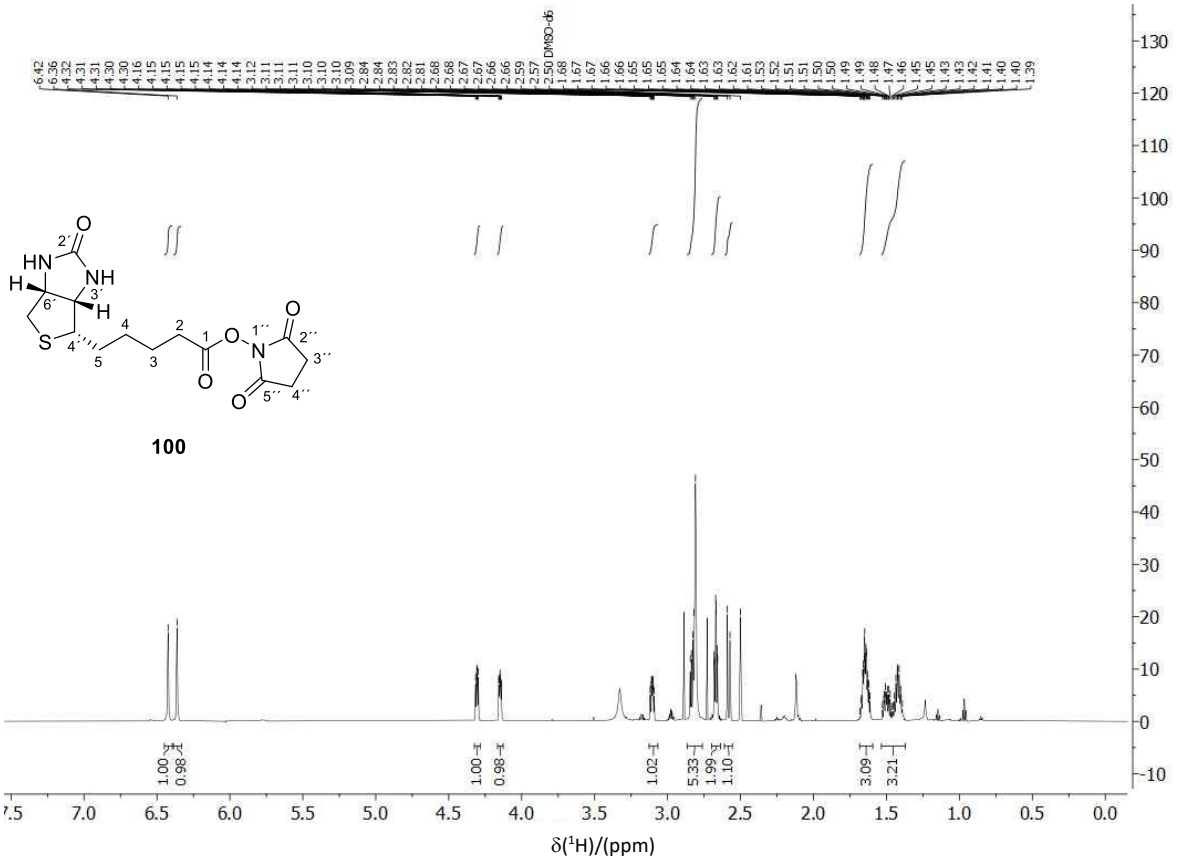

100

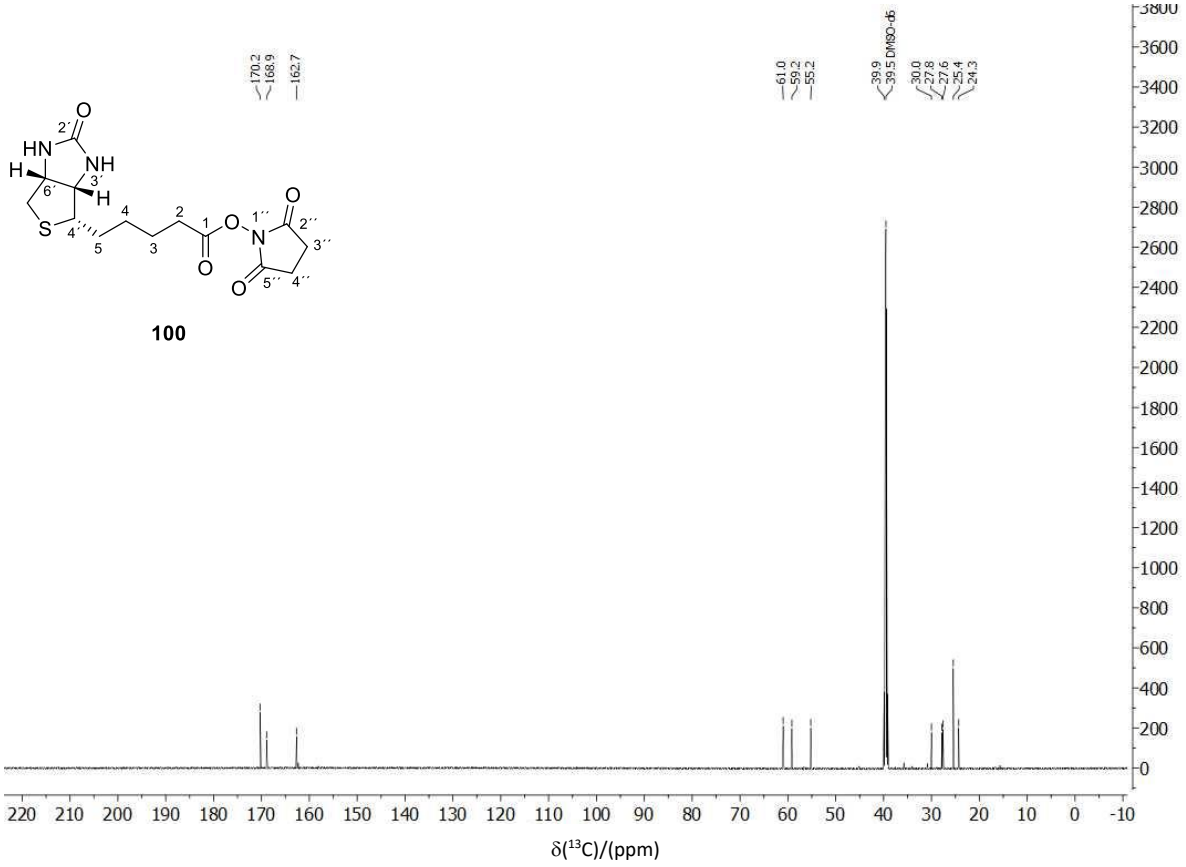

100

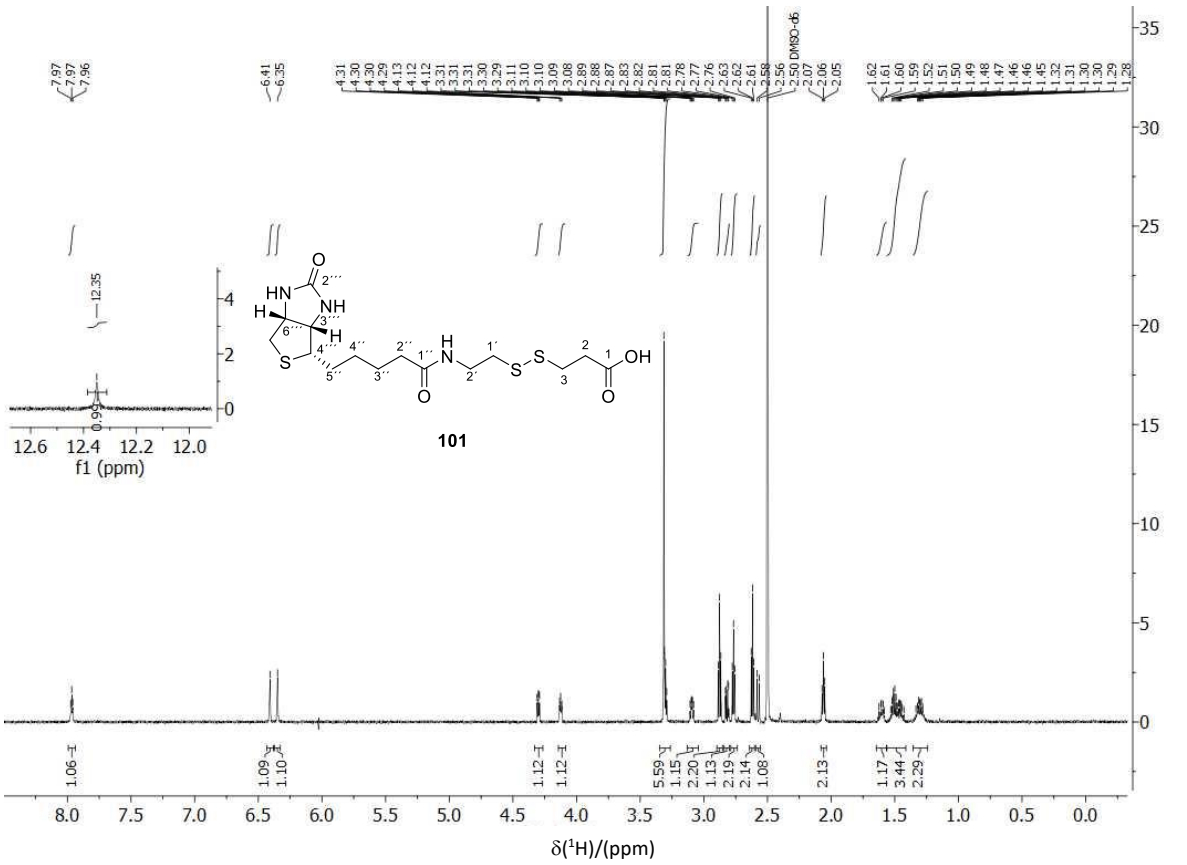
101
δ(¹H)/(ppm)

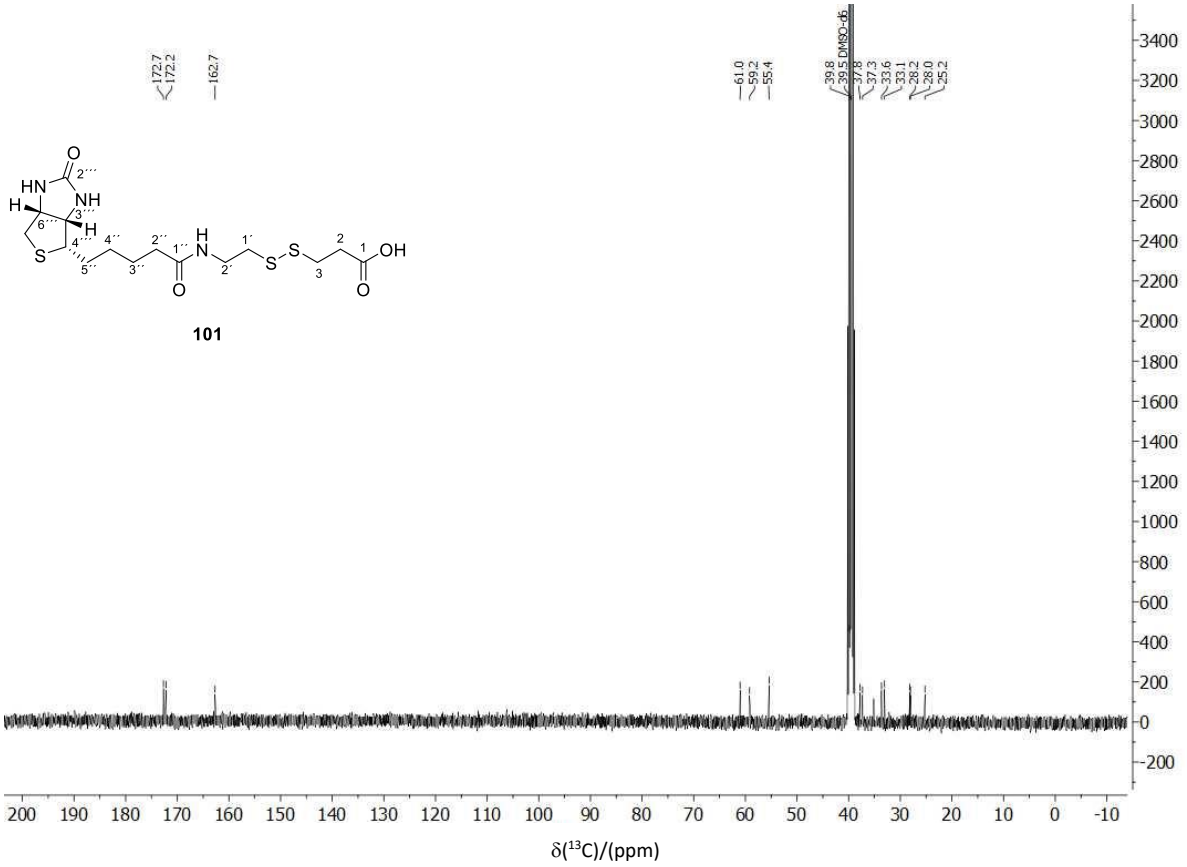
101
δ(¹³C)/(ppm)

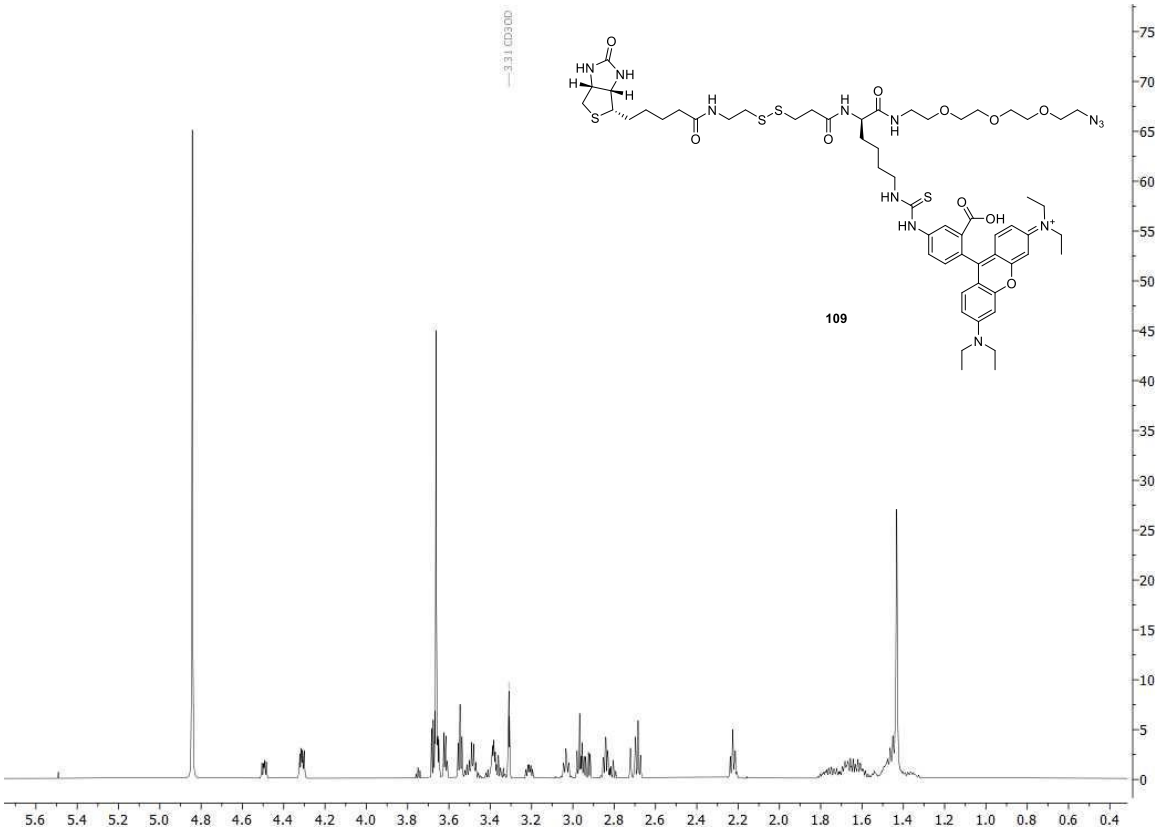
3.31 CD3OD
109
δ(1H)/(ppm)

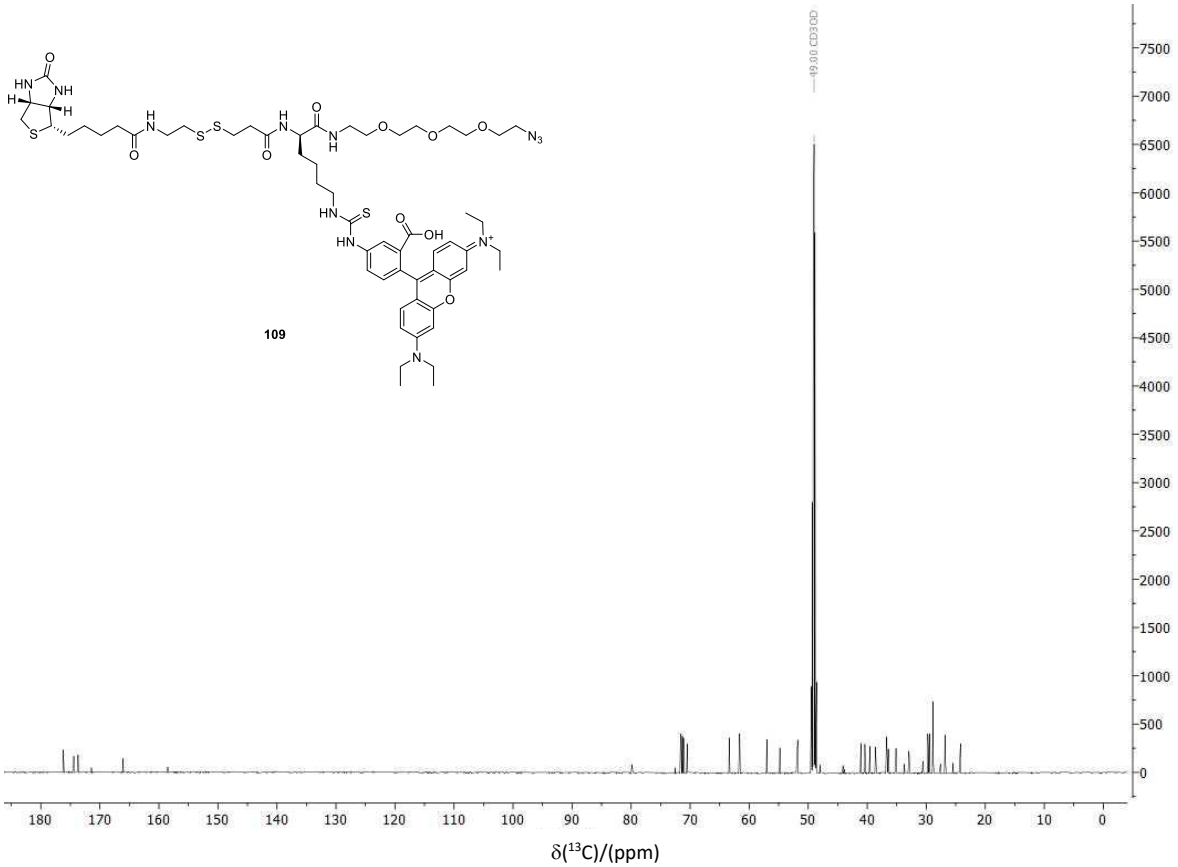
49.00 CD3OD
109
δ(13C)/(ppm)